



Kent Academic Repository

Doyle, Kevin (2022) *Investigating metabolic dysfunction in a *Saccharomyces cerevisiae* model of SOD1-associated amyotrophic lateral sclerosis*. Doctor of Philosophy (PhD) thesis, University of Kent,.

Downloaded from

<https://kar.kent.ac.uk/95966/> The University of Kent's Academic Repository KAR

The version of record is available from

<https://doi.org/10.22024/UniKent/01.02.95966>

This document version

UNSPECIFIED

DOI for this version

Licence for this version

CC BY (Attribution)

Additional information

Versions of research works

Versions of Record

If this version is the version of record, it is the same as the published version available on the publisher's web site. Cite as the published version.

Author Accepted Manuscripts

If this document is identified as the Author Accepted Manuscript it is the version after peer review but before type setting, copy editing or publisher branding. Cite as Surname, Initial. (Year) 'Title of article'. To be published in *Title of Journal*, Volume and issue numbers [peer-reviewed accepted version]. Available at: DOI or URL (Accessed: date).

Enquiries

If you have questions about this document contact ResearchSupport@kent.ac.uk. Please include the URL of the record in KAR. If you believe that your, or a third party's rights have been compromised through this document please see our [Take Down policy](https://www.kent.ac.uk/guides/kar-the-kent-academic-repository#policies) (available from <https://www.kent.ac.uk/guides/kar-the-kent-academic-repository#policies>).

**Investigating metabolic
dysfunction in a *Saccharomyces
cerevisiae* model of *SOD1*-
associated amyotrophic lateral
sclerosis**

Kevin Doyle

2022

A thesis presented for the degree of

Doctor of Philosophy in Cell Biology



School of Biosciences

University of Kent

Declaration

No part of this thesis has been submitted in support of an application for any degree or other qualification of the University of Kent or any other University or Institution of learning.

Kevin Doyle

January, 2022

Acknowledgments

I want to thank my supervisor Dr Campbell Gourlay for all of his constant guidance, ideas, and support throughout this project and for everything that I have been able to learn from him over the years. Without your support this project would not have been possible. I would also like to thank everyone in the Gourlay lab and the Kent Fungal Group for all of their guidance and great company throughout my time in the lab.

I would also like to thank MND Scotland for funding this project.

I would also like to thank my family for their unconditional love and support throughout my studies. Particularly both my parents and my partner who encouraged me and motivated me throughout the project.

Abbreviations

ALS	Amyotrophic lateral sclerosis
ND	Neurodegenerative disease
5-FOA	5-fluoroorotic acid
AD	Autosomal dominant
AID	Autoinhibitory domain
ALD	Alzheimer's disease
ALP	Alkaline phosphatase pathway
AMP	Adenosine monophosphate
AMPA	A-amino-3-hydroxy-5-methyl-4-isoxazolepropionic acid
APP	Amyloid precursor protein
AR	Autosomal recessive
C9orf72	Chromosome 9 open reading frame 72
Cas	CRISPR associated
CCS	Copper chaperone for Sod1
CDM	Canine degenerative myelopathy
CDRE	Calcineurin-dependant response element
CNS	Central nervous system
CRISPR	Clustered regularly interspaced short palindromic repeats
Cu	Copper
Cys	Cysteine
DHFR	Dihydrofolate reductase
DNA	Deoxyribonucleic acid
DPRs	Dipeptide repeat proteins
DSB	Double-stranded break
dsOligo	Double-stranded Oligo
ER	Endoplasmic reticulum
fALS	Familial ALS
FKB12	FK-binding protein 12
FTLD	Frontotemporal dementia
FUS	Fused in sarcoma
GA	Glycine-alanine
GAPDH	Glyceraldehyde phosphate dehydrogenase

gDNA	Genomic DNA
GDP	Guanosine diphosphate
GEF	Guanidine exchange factor
GFP	Green fluorescent protein
GP	Glycine-proline
GR	Glycine-arginine
GRAS	Generally regarded as safe
gRNA	Guide RNA
GSH	Glutathione
GWAS	Genome wide association study
HD	Huntington's disease
His	Histidine
hnRNP	Heterogeneous nuclear ribonucleoprotein
HR	Homologous recombination
IMM	Inner mitochondrial membrane
IMS	Mitochondrial intermembrane space
IP	Immunoprecipitation
IPSC	Induced pluripotent stem cells
LMN	Lower motor neuron
log	Logarithmic
MBR	Metal-binding region
MN	Motor neurons
MND	Motor neuron degeneration
MosCI	Mos1-mediated single copy insertion
mTORC1	Mammalian target of rapamycin complex 1
MTX	Methotrexate
NAB	N-aryl-benzimidazole
NADPH	Nicotinamide adenine dinucleotide phosphate
ND	Neurodegeneration
NHEJ	Non-homologous end joining
NLS	Nuclear localisation sequence
NMDA	<i>N</i> -methyl-D-aspartate
NMJ	Neuromuscular junction
NO	Nitric oxide

ONOO-	Peroxynitrite
oxPPP	Oxidative phase of the pentose pathway
PA	Proline-alanine
PAM	Protospacer adjustment motif
PCA	Protein complementation assay
PD	Parkinson's disease
Pi	Inorganic phosphate
<i>PICALM</i>	Phosphatidylinositol binding clathrin assembly protein
PKA	Protein kinase A
PPI	Protein-protein interaction
PR	Proline-arginine
pre-crRNA	Precursor CRISPR RNA
PTM	Post-translational modification
qPCR	Quantitative PCR
RAN	Repeat-associated non-ATG
RAVE	Regulator of ATPase of vacuoles and endosomes
redox	Reduction–oxidation
RNA	Ribonucleic acid
ROS	Reactive oxygen species
RRMs	RNA recognition motifs
sALS	Sporadic ALS
Ser	Serine
Single-stranded oligo	ssOligo
Sod1	Superoxide dismutase 1
TALEN	Transcription activator-like effector nucleases
TARDBP	TAR DNA binding protein
Thr	Threonine
Trp	Tryptophan
UMN	Upper motor neuron
V-ATPase	Vacuolar-ATPase
WT	Wild type
WTL	Wild type like
X-LD	X-linked dominant

YNB	Yeast nitrogen base
ZFN	Zinc-finger nucleases
Zn	Zinc
α-syn	A-synuclein

Abstract

Superoxide dismutase 1 (Sod1) is an enzyme that converts superoxides into hydrogen peroxide and water. Over 200 mutations in the gene *SOD1* which encodes Sod1, causes familial amyotrophic lateral sclerosis (ALS), a neurodegenerative disease (ND) that involves the progressive death of motor neurons (MNs). The precise mechanism as to how mutations in *SOD1* give rise to ALS is not yet known. Many cellular and animal models of *SOD1*-associated ALS (*SOD1*-ALS) have been developed in organisms ranging from baker's yeast (*Saccharomyces cerevisiae*) to mice (*Mus musculus*) which have led to many discoveries into the function of Sod1.

In recent years, there has been a focus on developing stable single-copy models of ALS, so as to study mutant isoforms of Sod1 when it is expressed at a physiologically relevant level. The first aim of this project was to develop a stable single-copy *SOD1*-ALS model in *S. cerevisiae*. Gateway cloning and CRISPR/Cas9 gene editing techniques were used to generate an integrated plasmid-based model, and a model with the mutations A4V, G37R and H48Q introduced into the endogenous yeast *SOD1* gene. The stable integrated plasmid model was used in this study to carry out phenotypic and genetic screens.

In this thesis, I investigated previous findings that were made using a *S. cerevisiae* model of *SOD1*-ALS. It was found that overexpression of ALS-linked mutant isoforms of Sod1 into *S. cerevisiae* causes cytotoxicity, metabolic dysfunction, and a vacuole acidification defect. Vacuole acidification is mediated by the V-ATPase, a highly conserved proton pump. Using an *in vivo* protein complementation assay (PCA) and *in vitro* V-ATPase assays, I found that Sod1 may interact with the Vma2, Vma4 and Vma8 subunits of the V₁ domain of the V-ATPase. I also found that altering the assembly state of the V-ATPase either by modulating glucose levels, or by deleting Vma2 or Vma4, affected the interaction between Sod1 and the V-ATPase. The interaction between Sod1 and calcineurin was also explored in *S. cerevisiae* using the *in vivo* PCA assay and a flow cytometry based calcineurin activity assay.

In summary, the stable *SOD1*-ALS model that was developed allowed for the study of mutant Sod1 when expressed in the cell at a physiologically low level. A novel interaction between Sod1 and the V-ATPase in *S. cerevisiae* was observed which could potentially be relevant towards ALS pathogenesis. It was found that in *S. cerevisiae*, Sod1 plays a protective role for calcineurin and that cells expressing mutant Sod1 alleles have reduced calcineurin signalling.

Contents

Declaration	2
Acknowledgments	3
Abbreviations	4
Abstract	8
Contents	9
List of figures	18
List of Tables	20
1 Introduction	22
1.1 Amyotrophic Lateral Sclerosis.....	22
1.1.1 Clinical phenotypes and diagnosis	22
1.1.2 Treatments and therapies	22
1.2 Genetic and environmental factors in ALS.....	23
1.2.1 ALS as a multistep process	23
1.2.2 Inheritance of fALS-linked gene variants.....	24
1.2.3 Discovery of fALS-linked gene variants.....	24
1.2.4 <i>FUS</i> , <i>TARDBP</i> and <i>C9orf72</i>	25
1.2.5 Environmental factors contributing to ALS.....	29
1.3 Superoxide dismutase 1	30
1.3.1 Structure and canonical function	30
1.3.2 Maturation of Sod1	31
1.3.3 Roles in the cell.....	32
1.4 <i>SOD1</i> -associated ALS	36
1.4.1 Mutations in <i>SOD1</i> that are associated with fALS	36
1.4.2 Aberrant PTMs that are associated with <i>SOD1</i> -fALS.....	37

Contents

1.4.3	Is <i>SOD1</i> -ALS caused by toxic loss-of function or gain-of function?.....	37
1.5	Animal models of <i>SOD1</i> -associated ALS.....	39
1.5.1	Nematodes.....	39
1.5.2	Flies.....	40
1.5.3	Zebrafish.....	40
1.5.4	Rodents.....	41
1.5.5	Neuronal models: human fibroblast and induced pluripotent stem cell models.....	41
1.5.6	Other models: Dog, Swine and Primate.....	42
1.6	Currently proposed mechanisms of ALS-linked mutant Sod1 toxicity.....	42
1.6.1	Mitochondrial dysfunction.....	42
1.6.2	Aggregation and stability of ALS-linked Sod1 mutants.....	43
1.6.3	Lysosome and autophagy dysfunction in ALS.....	43
1.6.4	Oxidative Stress.....	43
1.6.5	Glutamate excitotoxicity.....	44
1.7	<i>Saccharomyces cerevisiae</i> as a model to study neurodegenerative diseases.....	45
1.7.1	Tools for <i>S. cerevisiae</i> research.....	45
1.7.2	Using <i>S. cerevisiae</i> as a model for neurodegenerative diseases.....	46
1.8	Yeast models of Amyotrophic Lateral Sclerosis.....	48
1.8.1	Modelling <i>TARDBP</i> , <i>FUS</i> and other prion-like domain containing ALS-associated genes.....	48
1.8.2	Modelling <i>C9orf72</i> -associated ALS in <i>S. cerevisiae</i>	50
1.8.3	Modelling <i>SOD1</i> -associated ALS in <i>S. cerevisiae</i>	50
1.9	Project Aims.....	51
	1: To use the integrated model to conduct phenotypic and genetic screens to identify any mechanisms of dysfunction caused by ALS-linked Sod1 mutants.....	51
	2: To develop a stable single-copy model of <i>SOD1</i> -ALS in <i>S. cerevisiae</i>	51
	3: To investigate the interaction between Sod1 and the V-ATPase in <i>S. cerevisiae</i>	51
	4: Investigate the interaction between Sod1 and calcineurin in <i>S. cerevisiae</i>	52

2	Materials and Methods	53
2.1	Media for yeast and bacterial growth	53
2.1.1	Media preparation and growth conditions for <i>Saccharomyces cerevisiae</i> and <i>Escherichia coli</i>	53
2.1.2	Yeast growth media.....	53
2.1.3	Bacterial media.....	54
2.2	Yeast and bacterial strains used in this study	55
2.2.1	<i>E. coli</i> strains	55
2.2.2	<i>S. cerevisiae</i> Strains.....	56
2.2.3	Yeast mating of haploid strains.....	65
2.3	Molecular Biology methods	65
2.3.1	Plasmids used in this study	65
2.3.2	Oligonucleotides.....	68
2.3.3	Preparation of chemically competent <i>E. coli</i> cells.....	74
2.3.4	Bacterial transformation of <i>E. coli</i> cells.....	74
2.3.5	High efficiency yeast transformation using the LiAc/SS carrier DNA/PEG method	74
2.3.6	Quick & easy LiAC/SS carrier DNA/PEG yeast transformation	75
2.3.7	One-step yeast transformation protocol	75
2.3.8	Colony PCR from <i>E. coli</i> cells.	76
2.3.9	Quick genomic DNA extraction from <i>S. cerevisiae</i>	76
2.3.10	LiAc/SDS based genomic DNA extraction from <i>S. cerevisiae</i>	76
2.3.11	Purification of plasmids from <i>E. coli</i>	76
2.3.12	Quantification and purity analysis of DNA	77
2.3.13	DNA gel electrophoresis.....	77
2.3.14	DNA sequencing.....	78
2.3.15	Frozen Glycerol stock preparation of yeast and bacterial strains	78
2.3.16	Polymerase chain reaction using recombinant <i>Taq</i> DNA polymerase.....	78

Contents

2.3.17	Cloning of pAG306-GPD-ccdB chrI I integration vectors using Gateway Technology	80
2.3.18	Cloning of the Cas9-sgRNA expression vector pML104 containing gRNA to target the yeast <i>SOD1</i> gene	83
2.4	Yeast Strain construction.....	85
2.4.1	Integration of pAG306-GPD-ySOD1-chrI vector expressing Sod1 ^{WT} and Sod1 ^{A4V} into BY4741 and BY4741 Δ <i>sod1</i> cells.....	85
2.4.2	Generation of Sod1 ^{A4V} , Sod1 ^{H48Q} and Sod1 ^{G37R} mutants using CRISPR/Cas9 gene editing with pML104 plasmids.....	85
2.4.3	Gene knockout using HR mediated marker replacement	85
2.4.4	Gene C-terminal tagging	86
2.5	Protein methods.....	86
2.5.1	Yeast whole cell protein extraction	86
2.5.2	Native yeast whole cell extracts.....	86
2.5.3	SDS-polyacrylamide gel electrophoresis (SDS-PAGE)	87
2.5.4	Semi-dry transfer	87
2.5.5	Immunoblotting.....	88
2.5.6	Enhanced chemiluminescence (ECL) detection	88
2.5.7	Stripping of PVDF membrane.....	89
2.5.8	Native polyacrylamide gel electrophoresis (Native-PAGE).....	89
2.5.9	In gel Sod activity assay using nitrotetrazolium blue (NBT) chloride.....	90
2.5.10	Purification of yeast vacuoles.....	90
2.5.11	Measurement of V-ATPase ATP-hydrolysis activity using malachite green.....	91
2.5.12	Sample preparation and analysis of amino acids via double-derivatisation and liquid-liquid extraction.....	93
2.5.13	Co-immunoprecipitation	94
2.6	Whole Cell Experimental procedures	95
2.6.1	Measurement of yeast growth in liquid by absorbance.....	95
2.6.2	BIOLOG screen.....	95

Contents

2.6.3	Vacuole knockout library screen.....	97
2.6.4	Measurement of yeast growth by spotting onto agar	97
2.6.5	Quantification of calcineurin activity by flow cytometry.....	98
2.6.6	Fluorescence microscopy.....	98
2.6.7	Analysis of images using ImageJ.....	99
2.6.8	Quinocrine staining.....	99
3	Developing a stable <i>S. cerevisiae</i> model for <i>SOD1</i>-ALS using integration vectors.	100
3.1	Introduction.....	100
3.1.1	Comparison between different models of fALS.....	100
3.1.2	Overexpression models versus stable single-copy expression models of <i>SOD1</i> associated fALS.....	100
3.1.3	Aim of this study	101
3.2	Results.....	101
3.2.1	Testing the effect of Sod1 ^{A4V} expression on activity and abundance of Sod1 in WT and Δ <i>sod1</i> cells	101
3.2.2	Testing the effect of expression of Sod1 ^{A4V} on growth of <i>S. cerevisiae</i> in a WT or Δ <i>sod1</i> background.....	104
3.2.3	Assessment of the effect of expression of Sod1 ^{A4V} on vacuole function in <i>S. cerevisiae</i>	104
3.2.4	Testing the effect of Sod1 ^{A4V} expression in Δ <i>sod1</i> cells on the regulation of Sod1 by Torc1 signalling.....	107
3.2.5	Screening for metabolic defects upon expression of Sod1 ^{A4V} using the BIOLOG phenotypic microarray.....	109
3.2.6	PM6, 7 and 8 testing for dipeptide utilisation as a nitrogen source were repeated.....	113
3.2.7	Further investigation of dipeptide utilisation as a nitrogen source in cells expressing mutant Sod1 isoforms.....	116
3.2.8	Testing the growth of WT and Δ <i>sod1</i> cells expressing Sod1 ^{A4V} in combination with menadione induced oxidative stress.....	117

Contents

3.2.9	Expression of Sod1 ^{A4V} into a library of knockouts related to the function of the vacuole in yeast.	119
3.3	Discussion.....	123
3.3.1	Comparison between the integration vector model and the overexpression model of <i>SOD1</i> -ALS.....	123
3.3.2	Lack of cytotoxicity or vacuole dysfunction in the <i>SOD1</i> -ALS integration model	124
3.3.3	Sod1 ^{A4V} loss of function with the rapamycin resistance phenotype.....	125
3.3.4	Phenotypic screening with the BIOLOG system.....	126
3.3.5	Potential synthetic interactions between Sod1 ^{A4V} and EGO3/ PMC1.....	128
4	Developing CRISPR/Cas9 strategies for generating ALS linked SOD1 mutants in <i>S. cerevisiae</i>.....	130
4.1	Introduction.....	130
4.1.1	Development of genome editing in <i>S. cerevisiae</i>	130
4.1.2	CRISPR/Cas9 system discovery and function.....	131
4.1.3	Utilisation of CRISPR/Cas9 system for genome editing.....	131
4.1.4	Using CRISPR/Cas9 editing to generate a single-copy <i>S. cerevisiae</i> model for <i>SOD1</i> -associated ALS.....	132
4.1.5	Aim of this study.....	132
4.2	Results.....	133
4.2.1	Guide RNA and repair template designs.....	133
4.2.2	Screening colonies for phenotypes previously observed upon overexpression of mutant isoforms of Sod1 in <i>S. cerevisiae</i> failed to identify correct mutants.	135
4.2.3	Increasing concentrations of repair template resulted in improved transformation efficiency.....	136
4.2.4	Generation of Sod1 ^{A4V} , Sod1 ^{G37R} and Sod1 ^{H48Q} mutations using CRISPR-Cas9 genome editing.....	138
4.2.5	Effect of ALS-linked mutations generated by CRISPR/Cas9 on activity and expression of Sod1.....	141

Contents

4.3	Discussion.....	143
4.3.1	Strategy for identifying correct mutants	143
4.3.2	Comparison of gene editing efficiency with other studies	144
4.3.3	Conclusion and future directions.....	146

5 Investigating the interaction between Sod1 and the V-ATPase **147**

5.1	Introduction.....	147
5.1.1	Function of the Vacuole in <i>S. cerevisiae</i>	147
5.1.2	Consequences of loss of vacuole acidification	147
5.1.3	The V-ATPase	148
5.1.4	Regulation of V-ATPase activity by reversible disassembly.....	149
5.1.5	Regulation V-ATPase activity by redox signalling.....	149
5.1.6	Sod1 and the vacuole	150
5.1.7	Aim of this study	150
5.2	Results.....	150
5.2.1	Loss of <i>SOD1</i> leads to phenotypes indicative of vacuole dysfunction	150
5.2.2	$\Delta sod1$ mutants contain increased levels of basic amino acids	152
5.2.3	Sod1 interacts with the V_1 domain of the V-ATPase in a dihydrofolate reductase protein complementation assay.....	153
5.2.4	Extrachromosomal overexpression of <i>SOD1</i> reduced the relative growth of the Sod1 ^{bait} Vma4 ^{prey} diploid.	157
5.2.5	Overexpression of <i>PDE2</i> decreases the interaction between Sod1 and Vma2 DHFR fragments.....	159
5.2.6	Removal of glucose increases the interaction between Sod1 and the V-ATPase .	161
5.2.7	Effect of deletion of <i>VMA2</i> or <i>VMA4</i> on the interaction of Sod1 and the V-ATPase by DHFR-PCA.....	163
5.2.8	DHFR-PCA screening revealed interactions between Sod1/Ego3 and Sod1/Rav1.	166
5.2.9	Effect of <i>SOD1</i> deletion on assembly of the V-ATPase.....	168

Contents

5.2.10	Recombinant bovine Sod1 affects V-ATPase ATP hydrolysis activity in vitro. ...	169
5.2.11	Sod1 was not found to be co-immunoprecipitated along with Vma2, Vma4 and Vma8.....	173
5.2.12	Measurement of the amino acid content of vacuoles from WT and $\Delta sod1$ cells ...	174
5.3	Discussion.....	175
5.3.1	Vacuole dysfunction in cells lacking <i>SOD1</i>	175
5.3.2	Interaction of Sod1 with the V-ATPase.....	176
5.3.3	Effect of Sod1 on V-ATPase activity	179
6	Investigating the interaction between Sod1 and Calcineurin ..	180
6.1	Introduction.....	180
6.1.1	Calcineurin complex.....	180
6.1.2	Calcineurin in <i>S. cerevisiae</i>	180
6.1.3	Calcineurin and ALS	182
6.1.4	Calcineurin and Sod1	182
6.1.5	Aim of this study	183
6.2	Results.....	183
6.2.1	I-TASSER modelling of ALS-linked mutant isoforms of Sod1.....	183
6.2.2	Investigating calcineurin / Sod1 and V-ATPase interactions in vivo	187
6.2.3	Sensitivity of WT and $\Delta sod1$ strains to calcineurin inhibition using FK506.....	190
6.2.4	Measurement of calcineurin activity by flow cytometry in response to $CaCl^{2+}$ treatment in WT and $\Delta sod1$ cells.....	192
6.2.5	Measurement of calcineurin activity by flow cytometry in response to $CaCl^{2+}$ treatment in WT and $\Delta sod1$ cells.....	195
6.2.6	Further investigation of effects of Sod1 on calcineurin activity.....	196
6.2.7	Effect of overexpression of ALS-linked mutant isoforms of <i>SOD1</i> on calcineurin activity.....	198
6.3	Discussion.....	201
6.3.1	<i>SOD1</i> interaction with Calcineurin.....	201

Contents

6.3.2	Effect of Sod1 and ALS-linked Sod1 mutants on calcineurin activity.....	201
6.3.3	Inability of I-TASSER modelling to predict α -helix for Sod1 mutant isoforms...	202
7	Final Discussion	206
7.1	Perspectives.....	206
7.2	Reduced expression of Sod1 ^{A4V} is not toxic to <i>S. cerevisiae</i> in a $\Delta sod1$ background. 206	
7.2.1	Dose-dependent effects of mutant <i>SOD1</i>	206
7.2.2	Differences between expression of yeast <i>SOD1</i> and human <i>SOD1</i> into <i>S. cerevisiae</i> 208	
7.3	Sod1 and V-ATPase interaction.....	209
7.3.1	Perturbed amino acid homeostasis in cells lacking <i>SOD1</i>	210
7.3.2	The role of the V-ATPase in amino acid sensing and Torc1 activation.....	211
7.3.3	Sod1 interacts with calcineurin in yeast and is required for its activation in response to increases in intracellular calcium	214
7.4	Implications for <i>SOD1</i> -associated Amyotrophic Lateral Sclerosis.....	216
7.5	Conclusion.....	218
8	Appendix	221
	Bibliography	227

List of figures

Figure 1.1 Sod1 Structure (PDB:2C9V).....	30
Figure 1.2 Maturation of Sod1 by Ccs.....	32
Figure 1.3 non-canonical roles of Sod1 in the cell.....	35
Figure 1.4 Summary of mechanisms involved in <i>SOD1</i> -ALS.....	45
Figure 2.1 pAG306 ySOD1 chrI vector construction with gateway cloning	82
Figure 2.2 Plasmid map for pML104 Cas9 gRNA expression vector.....	84
Figure 3.1 Testing the effect of the Sod1 ^{A4V} mutation on Sod1 activity and abundance in both WT and Δ <i>sod1</i> backgrounds.	103
Figure 3.2 Effect of expression of Sod1 ^{A4V} in both WT and Δ <i>sod1</i> background on growth in SC media.	104
Figure 3.3 Spotting assay testing zinc sensitivity, sensitivity to alkaline pH and sensitivity to high salt levels.....	105
Figure 3.4 Quinocrine staining of WT and Δ <i>sod1</i> cells expressing Sod1 ^{A4V} or an empty vector control.....	106
Figure 3.5 Effect of the Sod1 ^{A4V} mutation on the interaction between Sod1 and the Torc1 signalling.	108
Figure 3.6 Biolog Screen Workflow.....	111
Figure 3.7 PM1 Carbon source utilisation test between WT and A4V.	112
Figure 3.8 PM6, 7 and 8 screen results of WT and A4V testing for utilisation of dipeptides as a nitrogen source.	114
Figure 3.9 PM7 Dipeptide utilisation as a nitrogen source screen.	115
Figure 3.10 Cells expressing Sod1 ^{A4V} do not have any defects in dipeptide uptake or utilisation.	117
Figure 3.11 Spotting assays investigate growth using different nitrogen sources in combination with menadione induced oxidative stress.	118
Figure 3.12 Spotting assays in different media conditions were carried out to screen for synthetic effects upon expression of Sod1 ^{A4V}	121
Figure 3.13 Fold change between WT and A4V from vacuole knockout library screen in different conditions.	122
Figure 3.14 Synthetic interactions identified in the knockout screen.	123

List of Figures & Tables

Figure 4.1 Nucleotide sequences of the different repair template designs utilised to generate the A4V, G37R and H48Q mutations in <i>SOD1</i>	134
Figure 4.2 Transformation efficiency of CRISPR/Cas9 transformations with varying concentrations of repair template.	137
Figure 4.3 GATC Sanger sequencing results of the <i>SOD1</i> gene amplified from colonies.....	140
Figure 4.4 Amino acid alignment of translated sequences from succesful CRISPR/Cas9 clones	140
Figure 4.5 Effect of Sod1 ^{A4V} mutation on activity of Sod1.	141
Figure 4.6 Effect of Sod1 ^{H48Q} and Sod1 ^{G37R} mutations on Sod1 activity and expression.....	142
Figure 5.1 Deletion of <i>SOD1</i> causes phenotypes linked to vacuole dysfunction in the BY4741 background.....	151
Figure 5.2 Analysis of the Ralser free amino acid measurement dataset.....	153
Figure 5.3 DHFR-PCA assay between Sod1 and the V-ATPase.	156
Figure 5.4 DHFR-PCA competition assay.....	158
Figure 5.5 Effect of overexpression of PDE2 on Sod1/V-ATPase interaction by DHFR-PCA.	160
Figure 5.6 Testing the effect of glucose titration on the Sod1/V-ATPase interaction by DHFR-PCA.	162
Figure 5.7 Interaction of Sod1 with different isoforms of the V-ATPase.....	165
Figure 5.8 PCA assay between Sod1 and V-ATPase in <i>VM42</i> and <i>VM44</i> deletions.	166
Figure 5.9 Further PCA screening of F-ATPsynthase subunits, Ego3 and subunits of the RAVE complex.....	168
Figure 5.10 Reversible disassembly of the V-ATPase in response to glucose deprivation.	169
Figure 5.11 Effect of Sod1 on V-ATPase ATP hydrolysis activity.....	171
Figure 5.12 Western blot of ficoll fractions from vacuole extraction of BY4741.	172
Figure 5.13 V-ATPase activity assay comparing WT and $\Delta sod1$	173
Figure 5.14 Western blots of Co-IP between Sod1 and Vma2, Vma4 and Vma8.	174
Figure 5.15 Amino acid content of vacuoles from WT and $\Delta sod1$ cells	175
Figure 5.16 Interaction of Sod1 with different sub-complexes of the V1 domain of the V-ATPase.....	178
Figure 6.1 Calcineurin in <i>S. cerevisiae</i> . Structure and activation by calmodulin.....	181
Figure 6.2 I-TASSER modelling predicted secondary structures and disorder level.	185
Figure 6.3 I-TASSER predicted solvent accessibility.	186
Figure 6.4 3D model predictions made by I-TASSER.....	186

List of Figures & Tables

Figure 6.5 DHFR PCA assay of Sod1 and Calcineurin.....	188
Figure 6.6 Relative growth calculation from DHFR screen between calcineurin and the V-ATPase.....	189
Figure 6.7 Growth curves of WT and $\Delta sod1$ cells in presence of FK506, a calcineurin inhibitor.....	191
Figure 6.8 AUC calculation from the growth curve of WT and $\Delta sod1$ FK506 experiment.....	192
Figure 6.9 Flow cytometry of a transcriptional reporter for calcineurin activity of WT and $\Delta sod1$ cells before and after $CaCl_2^{2+}$ treatment.....	194
Figure 6.10 Effect of deletion of <i>CCS1</i> on calcineurin activity.....	196
Figure 6.11 Calcineurin activity of V-ATPase deletions and casein kinase deletions.....	197
Figure 6.12 Effect of expression of ALS-linked mutant isoforms and fragments of <i>SOD1</i> into a $\Delta sod1$ background on calcineurin activity.....	199
Figure 6.13 Effect of overexpression of various Sod1 isoforms in a WT background on calcineurin activity.....	200
Figure 6.14 Visual model of the function of Calcineurin in <i>S. cerevisiae</i> and the effect of Sod1 on its function.....	204
Figure 7.1 Amino acid homeostasis in yeast.....	213
Figure 7.2 Redox control of calcineurin activity.....	215
Figure 7.3 Implications for the Sod1 / V-ATPase & Sod1 / Calcineurin interactions in motor neurons.....	217
Figure 7.4 Implications for the Sod1 / V-ATPase and Sod1 / Calcineurin interactions in <i>S. cerevisiae</i>	220
Figure 8.1 PM 3 and 4 AUC heatmap.....	221
Figure 8.2 PM 5 and 9 AUC heatmaps.....	222
Figure 8.3 PM 10 AUC heatmap.....	223
Figure 8.4 Calcineurin activity of WT cells in response to calcium with FK506.....	224
Figure 8.5 SOD1-ALS CRISPR strain liquid growth curves.....	224
Figure 8.6 CRISPR <i>SOD1</i> -ALS model menadione sensitivity spotting assay.....	225
Figure 8.7 CRISPR <i>SOD1</i> -ALS model VMA spotting assay.....	226

List of Tables

Table 1.1 Genes associated with fALS.....	27
Table 2.1 YPD media components.....	53

List of Figures & Tables

Table 2.2 SC media components.....	54
Table 2.3 W/V percentage of CSM amino acid drop-out mixture required.	54
Table 2.4 LB media components.	54
Table 2.5 Antibiotics used for plasmid selection in bacteria.	55
Table 2.6 Bacterial strains used in this study.....	55
Table 2.7 Haploid Strains.	56
Table 2.8 Diploid Strains.	60
Table 2.9 Plasmids used in this study.	65
Table 2.10 Oligonucleotides used in this study.....	68
Table 2.11 LiAc/SSDNA/PEG transformation mix.	75
Table 2.12 One-step transformation mix.....	75
Table 2.13 Mix for sanger sequencing of plasmid DNA.	78
Table 2.14 PCR reaction mix.	79
Table 2.15 <i>Taq</i> Polymerase thermocycler steps.	79
Table 2.16 LR reaction mix.	80
Table 2.17 Hybridized oligonucleotide and <i>Swa</i> I, <i>Bcl</i> I digested pML104 vector ligation reaction.	84
Table 2.18 SDS-PAGE reagent components.....	87
Table 2.19 ECL solution reagents.	88
Table 2.20 Primary and secondary antibodies used for immunoblotting in this study.....	88
Table 2.21 Native-PAGE reagent components.....	90
Table 2.22 ATP hydrolysis assay reagent mix.	92
Table 2.23 Recipe for 48× Yeast Nutrient Supplement (NS) for BIOLOG.....	96
Table 2.24 Recipe for PM additive (12×) solutions for BIOLOG.	96
Table 2.25 Recipe for inoculating PM plates for BIOLOG.	96
Table 3.1 Summary of Biolog plates.....	109
Table 4.1 Summary of characteristics of different ssOligo repair templates used.....	135
Table 5.1 Summary of subunits of the V-ATPase in <i>S. cerevisiae</i>	155
Table 6.1 Consensus prediction of Go-Terms from I-TASSER modelling.....	187

1 Introduction

1.1 Amyotrophic Lateral Sclerosis

1.1.1 Clinical phenotypes and diagnosis

Amyotrophic lateral sclerosis (ALS), also known as Lou Gehrig's disease, is a neurodegenerative disease (ND) that involves the progressive death of motor neurons (MNs) in the brain and spinal cord. ALS comes in two forms, sporadic (sALS) and familial (fALS) that are pathologically indistinguishable from one another. 90% of cases are sporadic, meaning they possess no obvious genetically inherited component. 10% are familial, as they have an associated genetic dominant inheritance factor. On average, first onset of symptoms comes between the ages of 50–65 [1]. Median survival upon onset is variable depending on the region, with it being 24 months in Europe and 48 months in Central Asia [2].

In both sALS and fALS, progressive MN death leads to muscle weakness, twitching and cramping, eventually leading to difficulty breathing known as dyspnoea. 70% of ALS cases are classed as limb onset cases (combination of upper motor neuron (UMN) and lower motor neuron (LMN) degeneration signs in the limbs), 25% of cases are bulbar onset (speech and swallowing difficulties present prior to any degeneration signs in the limbs). 5% of cases have an initial involvement in the torso or respiratory system. The most common cause of death in ALS is failure to respire due to complications with the pulmonary system [3]. Other common symptoms associated with ALS include increased fatigue and a reduced capacity to do exercise.

Despite motor function being by far the main defect that arises from ALS, ~50% of patients present with some form of cognitive impairment. 13% of ALS cases also have a disorder known as frontotemporal dementia (FTLD). ALS is a highly heterogeneous condition and it is widely becoming understood that ALS exists on a spectrum with other NDs conditions such as FTLD.

1.1.2 Treatments and therapies

Currently, treatment and therapy options for ALS remain limited. Over 50 drugs and their effects on ALS have been studied, however to this day only two, Riluzole and Edaravone have been approved by the FDA (Edaravone is not approved in Europe by the EMA). Riluzole reduces glutamatergic excitability by blocking voltage gated sodium channels. Riluzole prolongs life of ALS patients by ~3 months [4]. Edaravone is thought to have antioxidant properties and slows disease progression in certain cohorts of patients [5]. There are currently 29 active clinical trials

ongoing or recruiting patients for the intervention of various forms of ALS. Treatments in clinical trials range from stem cell therapy (NeuroNata-R) to combination therapy targeting both mitochondrial neuron degeneration pathways and endoplasmic reticulum (ER) stress (AMX0035) to a compound that slows calcium release from sarcomeres (Reldesemtiv). Antisense oligonucleotide treatment targeting both superoxide dismutase 1 (Sod1) and chromosome 9 open reading frame 72 (*C9orf72*) are currently being developed as well. Current and past clinical trial information can be found on the website www.clinicaltrials.gov. The lack of success of clinical trials and drug development in ALS is thought to be partly due to the high heterogeneity in ALS cases and the low incidence of the disease, making it difficult to design effective patient cohorts for the trials. Another factor is thought to be large quantity of different mechanisms that have been identified in which the disease develops.

Management of symptoms and disease course in patients will not be discussed in depth in this introduction as this study is focussed on the fundamental biological mechanisms that underly cellular dysfunction in ALS rather than the development of the physiological condition in patients. Management of ALS in patients has improved dramatically in the last 25 years due to the multidisciplinary approach that is now more often being taken in treating patients. Patients with ALS receive treatment from neurologists, physical therapists, speech, therapists, nutritionists, and specialised care nurses. This approach to patient care has been shown to prolong survival of the patient and increase their quality of life both physically and mentally [6].

1.2 Genetic and environmental factors in ALS

1.2.1 ALS as a multistep process

Population modelling studies have demonstrated that the development of ALS in patients is a multistep process requiring six steps. This means that various genetic and environmental factors need to occur in order for ALS to develop. Mutations in strongly linked fALS genes that are said to have high-penetrance such as *SOD1*, *C9orf72*, fused in sarcoma (*FUS*) or TAR-DNA binding protein (*TARDBP*) are estimated to make up to four steps [7]. Low-penetrance mutations that are less strongly linked could take up fewer steps [8]. This would explain why patients that are born with an fALS linked mutant gene, may grow old and never develop ALS, or why the onset of disease is between 50–60 years old. This model could also explain the pleiotropic nature of the disease in which individuals with the same *C9orf72* mutation may develop ALS, FTLN, ALS/FTLD or no disease at all.

1.2.2 Inheritance of fALS-linked gene variants

fALS cases constitute 10–20% of all ALS cases, as they are passed down in the family, usually by a gene variant that is passed down in a mendelian fashion. The mode of inheritance is most often autosomal dominant (AD) (24 out of 29 fALS genes) meaning that the mutations occur on a chromosome other than the X or Y chromosome and that only one copy of the mutant allele is required for the disease to present itself. Autosomal recessive (AR) inheritance has also been observed in seven out of 29 fALS genes. In autosomal recessive inheritance, one copy of the mutant gene alone is not enough for the disease to develop. In one case with *UBQLN2*, the mode of inheritance is X-linked dominant (X-LD) [9]. X-LD inheritance is where a mutation in a gene on the X-chromosome is passed down and only one copy of the mutated gene is required to cause disease (Table 1.1).

1.2.3 Discovery of fALS-linked gene variants

The majority of gene variants that are understood to cause fALS have been discovered through linkage analysis (15 out of 29) (Table 1.1). Linkage analysis is where the progression disease is followed in a family over generations and chromosome segregation is followed in order to identify candidate genes that could be causing the disease phenotype. Mutations in *SOD1* were the first fALS mutations to be identified via linkage analysis [10]. Most of the high penetrance fALS gene mutations have been discovered by linkage analysis, including the hexanucleotide repeat in *C9orf72* [11], mutations in *FUS* [12] and mutations in *TARDBP* [13].

A number of fALS genes have been discovered due to being a candidate gene. Genes become candidates for fALS due to studies in animal models and if they are associated with any other similar neurodegenerative diseases. For example, polyQ repeats in the gene *ATXN2* were discovered to be significantly associated with fALS. The *S. cerevisiae* homologue of *ATXN2*, poly(A) binding protein (*PBP1*) was initially identified in a *S. cerevisiae* overexpression screen for modulators of TDP-43 toxicity [14]. *ATXN2* was then found to modify TDP-43 toxicity in flies. A physical interaction between Ataxin-2 and TDP-43 was identified in the cytoplasm and was found to depend on RNA binding. Ataxin-2 was then shown to be mis-localised in spinal cord MNs in ALS patients compared to control individuals. By analysing the *ATXN2* gene in 915 ALS patients and 980 control individuals, it was found that polyQ repeats in *ATXN2* were significantly associated with ALS [14]. 7 out of 29 fALS genes have been identified in this way, in which knowledge from animal model studies have led to a gene becoming a likely candidate for association with ALS.

In recent years, advances in next-generation sequencing techniques have allowed for the discovery of further fALS genes such as *TUBA4A* [15], *ANXA11* [16]. Whole genomes or whole exomes of families that have a history of ALS were assayed and then genes that have similar variants were compared. A genome wide association study (GWAS) was used to identify *KIF5A* as an fALS gene [17]. GWAS is an approach in which the genomes of a disease population and a control population and variants that cause susceptibility to the disease are thought to be overrepresented in the disease population. Therefore, any gene variants that are in over 1% of the disease population, could potentially increase susceptibility to the disease.

Simply separating ALS cases into strictly fALS or sALS cases is not necessarily the most accurate way to group cases. This is because some sALS cases have evidence of genetic inheritance that may have not yet been discovered, and many fALS cases are said to have pleiotropic inheritance in which a single gene variant may present with many different phenotypes. In some cases of fALS, it is said to be caused by an oligogenic inheritance, in which a number of gene variants contribute towards the disease phenotype.

1.2.4 *FUS*, *TARDBP* and *C9orf72*

A few genes make up the majority of fALS cases, these being *SOD1*, *C9orf72*, *TARDBP*, and *FUS*. *SOD1* encodes Sod1 and will be discussed in depth later on. *C9orf72* encodes C9orf72, *TARDBP* encodes TDP-43 and *FUS* encodes FUS. In total ~30 genes are thought to cause ~70% of all fALS cases (Table 1.1).

C9orf72 encodes a protein that has predicted guanyl nucleotide exchange activity and regulates endosomal trafficking and autophagy in neurons [18]. *C9orf72*-associated fALS is the most common cause of fALS. *C9orf72* contains a polymorphic hexanucleotide repeat 'GGGGCC' that can be expanded to many hundreds of repeats [23]. Repeat-associated non-ATG (RAN) translation of these hexanucleotide repeats can then occur. RAN translation occurs in both sense and anti-sense direction and occurs in all reading frames. This results in the production of dipeptide repeat proteins (DPRs). DPRs are polymers of dipeptides. In *C9orf72*-ALS, the predicted DPRs that are produced are glycine-alanine (GA), glycine-proline (GP), proline-alanine (PA), glycine-arginine (GR), and proline-arginine (PR). DPRs have a propensity to aggregate and accumulate in the central nervous system (CNS) in ALS patients with *C9orf72* mutations [23].

The arginine rich GR and PR-DPRs have been suggested to be the most toxic. Another suggested mechanism of toxicity for *C9orf72*-ALS is that the many hexanucleotide repeats impair the normal functioning of the enzyme in endosomal trafficking and autophagy, leading to lysosomal defects. It has been shown that normally C9ORF72 interacts with SMCR8 and

localises to the lysosome membrane when amino acid levels are low and is required for the activation of mTORC1. This study also showed that in cells lacking *C9orf72*, lysosome morphology is abnormal [19]. In summary, it is thought that toxic loss and gain-of functions play a role in *C9orf72*-ALS with aggregation of toxic DPRs and possibly accumulation of RNA in the nucleus and cytosol causing toxic gain of functions and lysosome / autophagic dysfunction causing a toxic loss-of function.

Fused in sarcoma, encoded by *FUS* is an RNA binding protein that functions in transcriptional activation and also in the deoxyribonucleic acid (DNA) damage repair response via a direct interaction with histone deacetylase 1 (HDAC1) [20]. Mutations in *FUS* are associated with fALS [12]. Currently, the exact mechanism of how mutations in *FUS* cause ALS is not known, however it is thought to be via a combination of a toxic gain-of function and a toxic loss-of function of the FUS protein. Neurons that contain ALS-linked mutant isoforms of FUS show increased sensitivity to DNA damage and a reduced interaction between FUS and HDAC1. It is thought that decreased capacity for DNA damage repair plays apart in the loss-of function pathogenesis of *FUS*-ALS. Aggregation of mutant forms of FUS into the cytosol results in a loss or reduction of its function in the nucleus [20]. There are certain variants of *FUS* that cause fALS but do not show aggregation in the cytosol, suggesting a toxic gain-of function in the nucleus as well. The formation of dysfunctional paraspeckles in cells expressing mutant isoforms of FUS has been suggested to be a toxic gain-of function that occurs in the nucleus [21].

TARDBP encodes TDP-43, a DNA/RNA binding protein that localises to the nucleus and can shuttle between the nucleus and cytosol. TDP-43 is part of the heterogeneous nuclear ribonucleoprotein (hnRNP) family of DNA/RNA binding proteins that contain highly specific RNA recognition motifs (RRMs). TDP-43 regulates mRNAs that are important in neuronal development [22]. Insoluble and ubiquitinated inclusions of TDP-43 are found in 97% of all ALS cases and 45% of the FTLN cases, suggesting that its aggregation is an important part of the pathogenesis of ALS. Whether the aggregation of TDP-43 is a cause of neuronal death, or a consequence of earlier events is still not fully understood. Most of the ALS-linked mutations that occur in *TARDBP* are located in the c-terminal glycine rich region. Mutations in this region are linked to an increased propensity of the protein to aggregate [23]. Localisation of mutant TDP-43 in the cytosol results in its depletion in the nucleus. Loss of TDP-43 in the nucleus causes defects in RNA metabolism, whereas increase in localisation in the cytosol leads to its interaction with RACK1 on polyribosomes and the repression of global protein synthesis [24][25]. In summary, both toxic loss and gain-of functions are implicated in the development of *TARDBP*-ALS.

Table 1.1 Genes associated with fALS

Genes associated with fALS, sorted by their frequency rate in fALS cases. Type is based on the type given in the Online mendelian inheritance in man (OMIM) database. FTLN-ALS means cases with FTLN and ALS. For the inheritance, AD stands for autosomal dominant, AR is autosomal recessive, X-LD is X-linked dominant.

Type	Gene	Protein	Locus	Inheritance	Frequency (% of fALS cases)	Ref	Method of discovery	Implicated pathway
FTD-ALS1	<i>C9orf72</i>	C9orf72	9p21.2	AD	40–45%	[11]	Linkage analysis	RNA metabolism
ALS1	<i>SOD1</i>	Superoxide dismutase 1	21q22.1	AD, AR	15–20%	[10]	Linkage analysis	Redox Signalling Mitochondrial dysfunction
ALS10	<i>TARDBP</i>	TDP43	1p36.2	AD	10%	[13]	Linkage analysis	RNA metabolism
ALS6	<i>FUS</i>	fused in sarcoma	16p11.2	AD, AR	5%	[12]	Linkage analysis	RNA metabolism
FTD-ALS2	<i>CHCHD10</i>	Coiled-coil-helix-coiled-coil-helix domain-containing protein 10	22q11.23	AD	2%	[26]	Linkage analysis	Mitochondria
ALS22	<i>TUBA4A</i>	Tubulin alpha-4A chain	2q35	AD	1%	[15]	Exome sequencing	Cytoskeleton
ALS23	<i>ANXA11</i>	Annexin A11	10q22,3	AD	1%	[16]	Whole exome sequencing	RNA binding, Calcium dependant protein binding
ALS2	<i>ALS2</i>	Alsin	2q33.1	AR	<1%	[27]	Linkage analysis	Endosomal trafficking

Chapter 1. Introduction

ALS3	<i>Unknown</i>	Unknown	18q21	AD, AR	<1%	[28]	Linkage analysis	Unknown
ALS4	<i>SETX</i>	Senataxin	9q34.13	AD	<1%	[29]	Linkage analysis	DNA & RNA metabolism
ALS5	<i>SPG11</i>	Spatascin	15q21.1	AR	<1%	[30]	Linkage analysis	Cytoskeleton stability Synaptic vesicle transport
ALS7	<i>Unknown</i>	Unknown	20p13	AD	<1%	[31]	Linkage analysis	Unknown
ALS8	<i>VAPB</i>	Vesicle-associated membrane protein-associated protein B/C	20q13.3	AD	<1%	[32]	Linkage analysis	ER Stress Calcium homeostasis
ALS9	<i>ANG</i>	Angiogenin	14q11.2	AD	<1%	[33]	Candidate gene	RNA metabolism
ALS11	<i>FIG4</i>	SAC domain-containing protein 3 (Sac3)	6q21	AD	<1%	[34]	Candidate gene	Endosomal trafficking PI metabolism
ALS12	<i>OPTN</i>	Optineurin	10p13	AD, AR	<1%	[35]	Homozygosity mapping	Autophagy
ALS13	<i>ATXN2</i>	Ataxin-2	12q24.12	AD	<1%	[14]	Candidate gene	RNA metabolism
ALS14	<i>VCP</i>	Valosin-containing protein	9p13.3	AD	<1%	[36]	Candidate gene	Autophagy
ALS15	<i>UBQLN2</i>	Ubiquilin-2	Xp11.21	X-LD	<1%	[9]	Linkage analysis	Autophagy Protein degradation pathways
ALS16	<i>SIGMAR1</i>	Sigma-1 receptor	9p13.3	AR	<1%	[37]	Candidate gene	Autophagy

Chapter 1. Introduction

ALS17	<i>CHMP2B</i>	Charged multivesicular body protein 2b	3p11.2	AD	<1%	[38]	Candidate gene	Endosomal trafficking
ALS18	<i>PFN1</i>	Profilin 1	17p13.2	AD	<1%	[39]	Exome sequencing	Cytoskeleton organisation
ALS19	<i>ERBB4</i>	Receptor tyrosine-protein kinase erbB-4	2q34	AD	<1%	[40]	Linkage analysis	Development of neurons
ALS20	<i>HNRNP A1</i>	Heterogeneous nuclear ribonucleoprotein in A1	12q13.13	AD	<1%	[41]	Linkage analysis	RNA metabolism
ALS21	<i>MATR3</i>	Matrin-3	5q31.2	AD	<1%	[42]	Linkage analysis	DNA & RNA metabolism
ALS24	<i>NEK1</i>	NIMA-related kinase 1	4q33	Unknown	<1%	[43]	Exome sequencing	DNA damage repair
ALS25	<i>KIF5A</i>	Kinesin heavy chain isoform 5A	12q13.3	AD	<1%	[17]	Genome wide association	Cytoskeleton organisation, Golgi-ER transport
FTD-ALS3	<i>SQSTM1</i>	Sequestosome 1	5q35.3	AD	<1%	[44]	Candidate gene	Autophagy
FTD-ALS4	<i>TBK1</i>	TANK-binding kinase 1	12q14.2	AD	<1%	[45]	Whole exome sequencing	Autophagy, Inflammatory response

1.2.5 Environmental factors contributing to ALS

As it has been widely suggested that the development ALS is a six-step process, and that some high penetrance genes such as *SOD1*, *TARDBP* or *FUS* may contribute to up to four of those six steps, studies have been carried out with the aim of trying to identify environmental factors that may contribute to an increased susceptibility to develop the disease. Due to how rare ALS is as a disease in the general population, it has been difficult to conduct studies with enough of a sample to identify many environmental factors. Factors that have been suggested as risk factors towards ALS include, previous exposure to heavy metals or organic chemicals, a history of

physical trauma or injury, smoking, a history of electro-shock, or participation in professional sports [46].

1.3 Superoxide dismutase 1

1.3.1 Structure and canonical function

SOD1 encodes a highly conserved 32kDa homodimeric copper/zinc (Cu/Zn) metalloenzyme called Sod1. Sod1 was first discovered and characterised in 1969 [47](Figure 1.1). Sod1 catalyses the conversion of superoxide anions (O_2^-) into hydrogen peroxide (H_2O_2) and water (H_2O). O_2^- is oxidised by the Cu^{2+} ion in the Sod1 active site to produce oxygen (O_2). A second O_2^- anion is then oxidised by Cu^+ to produce O_2 . This reaction is carried out in the presence of two H^+ protons and the final result is the production of H_2O_2 . H_2O_2 is then broken down by catalase into H_2O and O_2 . In *S. cerevisiae*, the main sources of cytoplasmic O_2^- come from the mitochondria [48][49], nicotinamide adenine dinucleotide phosphate (NADPH) oxygenases (Yno1) [50] and other redox reactions in the cytosol. Cells lacking *SOD1* are vulnerable to oxidative stress, possess elevated endogenous levels of oxidative stress and display signs of metabolic and vacuolar dysfunction.

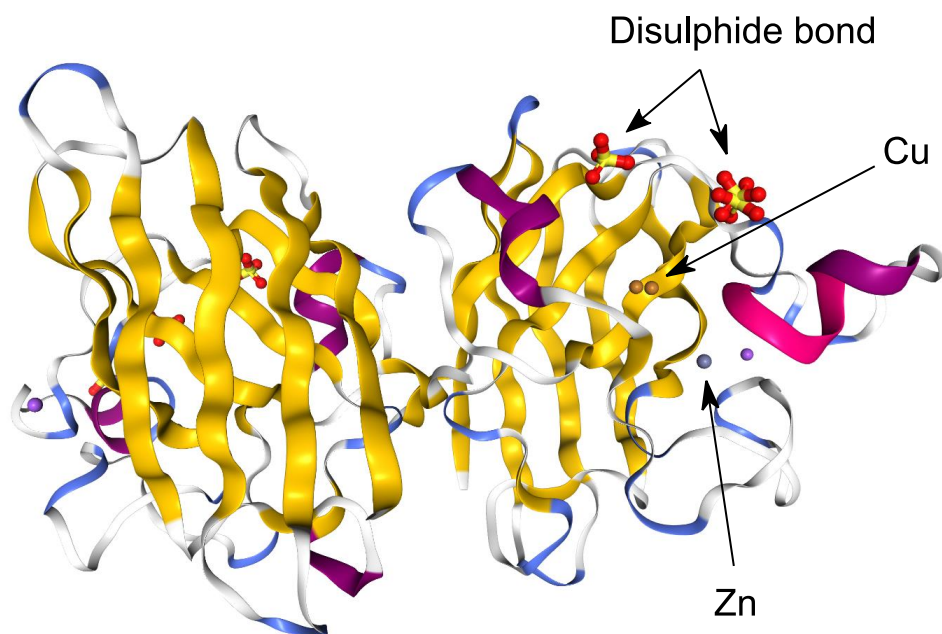


Figure 1.1 Sod1 Structure (PDB:2C9V).

Atomic resolution of the crystal structure of human Sod1 homodimer with its Cu/Zn ligands [51] (PDB ID : 2C9V).3D view was rendered using NGL viewer [52]. The intra-subunit disulphide bond that is formed between Cys57 and Cys146 is illustrated by the yellow and red symbols. Yellow denotes beta strands. Blue denotes beta turns. Pink denotes alpha helix. Light purple denotes 3/10 helix. Dark Purple denotes pi helix. The colour coding was coded by secondary structure (<https://www.rcsb.org/docs/3d-viewers/ngl#structure-view>).

The active site and the channel that leads to it are positively charged, whereas the rest of the enzyme is negatively charged. This gradient naturally guides O_2^- anions to the active site. Sod1 is primarily localised in the cytosol, although it is also found in the mitochondria, lysosomes (in mammalian cells), vacuoles (in yeast), nucleus, and ER. Apo-Sod1 has been shown to localise to the mitochondrial intermembrane space (IMS) along with copper chaperone for Sod1 (CCS) whereupon it becomes metalated and fully matured in response to elevated mitochondrial oxidative stress caused by the electron transport chain. Import of Sod1 into the IMS is mediated by the TOM translocase and a disulphide relay system involving Mia40 and Erv1 [53]

1.3.2 Maturation of Sod1

The fully mature human Sod1 homodimer contains one Cu ion and one Zn ion per monomer and an intra-subunit disulphide bond (between Cys57 and Cys146). Fully mature holo-Sod1 is a highly stable enzyme, with a melting temperature of $\sim 90^\circ\text{C}$ [54] (depending on the buffer). In contrast, the melting temperature of apo-Sod1 is 42.9°C . Mutations or post-translational modifications (PTMs) such as oxidation of cysteine or histidine residues on apo-Sod1 can further decrease the melting temperature to below 37°C , leading to potential unfolding of the enzyme in physiological scenarios. Sod1 without its metal ligands or disulphide bridge contains many highly disordered regions. The Cu and Zn ions, along with the disulphide bond provide stability due to their hydrogen bond networks [55].

The first step of Sod1 maturation is insertion of the Zn ion into an apo-Sod1 monomer. It is thought that Zn is delivered to Sod1 via the Ccs-Cu-Ctr1 complex. An apo-Sod1 monomer forms a dimer with a Zn bound Ccs-Cu-Ctr1 complex at the plasma membrane. Zn is then transferred to the apo-Sod1 monomer. Once Zn is bound to Sod1, the Cu ion can be inserted, and the disulphide bond can be created. The fully metalated apo-Sod1 monomer can then form a homodimer with another holo-Sod1 monomer. Sod1 can also be matured in a Ccs independent fashion. Studies suggest that reduced glutathione (GSH) and protein deglycase DJ-1 may play roles in CCS independent Sod1 maturation (Figure 1.2).

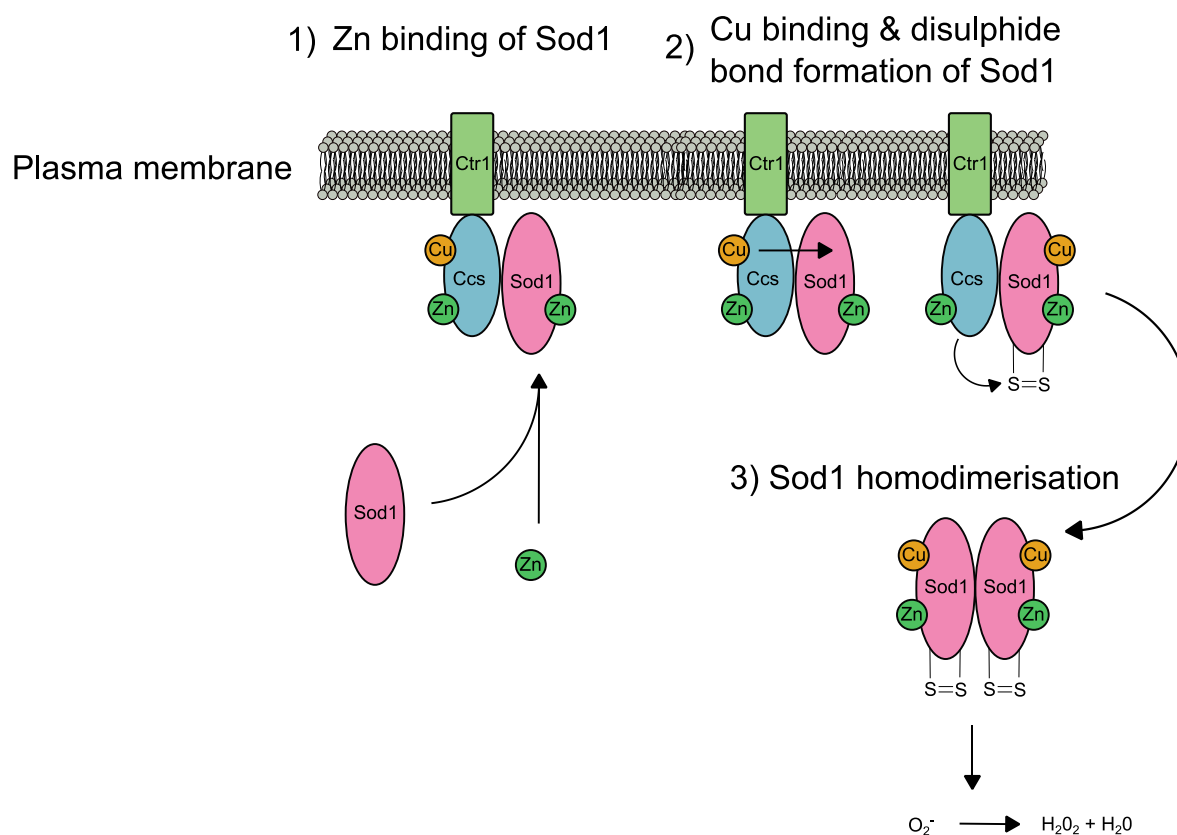


Figure 1.2 Maturation of Sod1 by Ccs.

1) Apo-Sod1 monomer associates with the Ccs-Ctr1-Cu complex at the plasma membrane. Ccs facilitates the binding of a Zn ion to the apo-Sod1 monomer. 2) After Zn binding, Ccs transfers its Cu ion to the apo-Sod1 monomer and creates a disulphide bond between Cys57 and Cys146 on Sod1. 3) Fully metalated apo-Sod1 is then released by Ccs whereby it forms homodimers with other fully metalated apo-Sod1 monomers to form the fully mature Sod1 homodimer.

1.3.3 Roles in the cell

In *S. cerevisiae*, less than 1% of the total pool of Sod1 in the cell is required to protect the cells from oxidative stress. The rest of the Sod1 pool, which was mainly based in the cytosol is not required for protection against oxidative stress but is thought to be important for regulating redox signalling [56]. Sod1 is highly abundant making up ~1% of the total protein content of the cell [57].

More and more non-canonical functions of Sod1 are being discovered, demonstrating the versatility of this enzyme and the important part it plays in regulating metabolism and cell survival in response to nutrient signals or redox signals.

In *S. cerevisiae* and mammalian cells, Sod1 has been shown to act as a transcription factor in response to elevated levels of oxidative stress, translocating to the nucleus and regulating the expression of 123 genes that are involved in defence against reactive oxygen species (ROS),

defence against DNA damage and cell survival [58] (Figure 1.3 A)). ATM/Mec1 through its effector kinase Dun1/Cds1 kinase phosphorylates Sod1 at Ser60 and Ser99. Nuclear translocation of Sod1 also has been shown to depend on the palmitoylation of the C6 residue of Sod1 [59]. Palmitoylation of Sod1 could be a PTM that guides Sod1 to other organelles in order for it to participate in various interactions in the cell..

In mice and human cells, Sod1 has been shown to play a role in NADPH oxygenase (Nox2) signalling through its interaction with a protein called Rac1 (Figure 1.3 B)). Nox2 produces O_2^- , which is then converted into H_2O_2 by Sod1. Rac1 activates Nox2. When bound to Sod1, Rac1 becomes stabilised and is able to promote Nox2 activity, thereby producing more O_2^- . The interaction between Sod1 and Rac1 is inhibited by H_2O_2 because H_2O_2 oxidises Rac1 and leads to it dissociating from Sod1. When dissociated from Sod1, Rac1 is in the guanosine diphosphate (GDP) bound state and no longer promotes Nox2 activity. This suggests that Sod1, Rac1 and Nox2 are involved in a feedback loop that senses O_2^- and H_2O_2 levels to maintain an appropriate redox balance in the cell [60].

Sod1 plays an important role in repressing respiration in response to nutrient signals via its interaction with the yeast casein kinases Yck1 and Yck2. Sod1 binds a C-terminal degron in Yck1 and Yck2 and promotes their stability via its local production of H_2O_2 . This interaction was observed in *S. cerevisiae* and mammalian cells. Sod1 utilises the O_2^- generated by growth in the presence of glucose and O_2 to stabilise the yeast casein kinases. In this interaction with Yck1/Yck2, Sod1 can regulate nutrient sensing by the amount of glucose or oxygen present [61] (Figure 1.3 D)).

A study showed that Sod1 interacts with glyceraldehyde phosphate dehydrogenase (GAPDH) by oxidatively modifying a Cys150 residue with the local production of H_2O_2 . Sod1 uses the O_2^- produced by mitochondrial respiration and NADPH oxidase activity to inactivate GAPDH and thereby push the cells from using glycolysis to the oxidative phase of the pentose pathway (oxPPP) [50] (Figure 1.3 C)). Rerouting metabolism to the oxPPP pathway results in increased NADPH. The production of NADPH is important for aerobic growth. This interaction between Sod1 and GAPDH was also observed in human cells. In the same study, a screen was carried out in order to identify proteins that had Sod1-dependant oxidative modifications to cysteine residues. A second screen was carried out to identify proteins that had altered cellular abundances in WT or $\Delta sod1$ cells. Out of 4409 proteins tested, 373 had significantly altered abundances between WT and $\Delta sod1$ cells. GO enrichment analysis of the 373 significantly altered proteins revealed enrichment in the glycolytic pathway, oxPPP and amino acid biosynthesis. Out

Chapter 1. Introduction

of 2077 cys residues that were screened, 99 had significant changes in oxidation between WT and $\Delta sod1$. Oxidation of cys residues was decreased in $\Delta sod1$ cells compared to the WT, suggesting that cys residues are being oxidised due to H_2O_2 production by Sod1 rather than elevated endogenous oxidative stress in $\Delta sod1$ cells. There was a significant enrichment in cys residues belonging to proteins involved in metabolism and amino acid biosynthesis [50].

In *S. cerevisiae* and mammalian cells, Sod1 enzymatic activity is inhibited by mammalian target of rapamycin complex 1 (mTORC1) signalling (Figure 1.3 E)). In the presence of nutrient rich conditions (glucose present), Sod1 is phosphorylated by mTORC1 at Thr39. Phosphorylation at Thr39 induces a conformational change in Sod1 that inhibits its activity by making the active site less accessible to substrates. In poor nutrient conditions (glycerol present), mTORC1 is inhibited and Sod1 is not phosphorylated. In its unphosphorylated state, Sod1 is more active and is important in the starvation response in the cell [62].

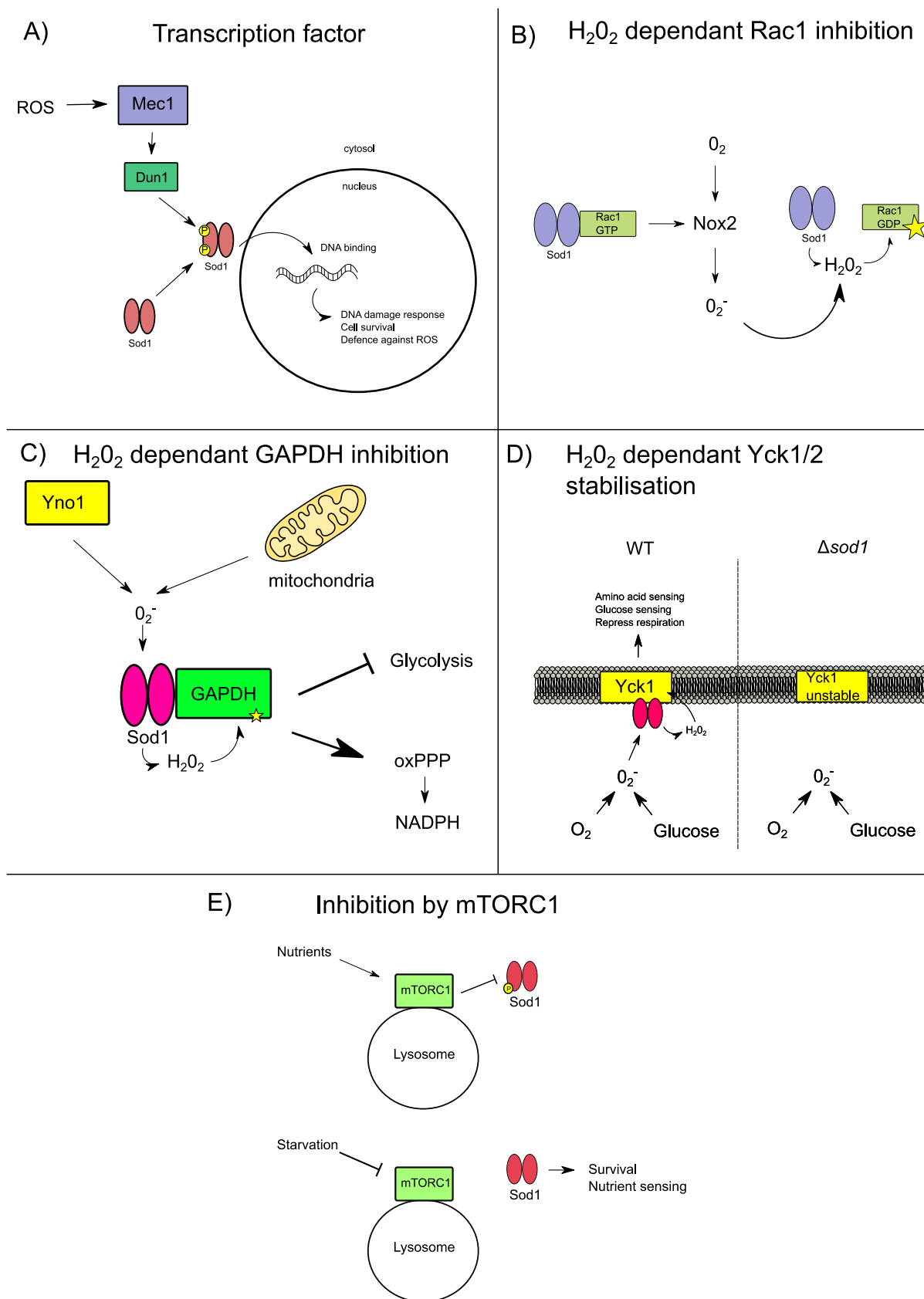


Figure 1.3 non-canonical roles of Sod1 in the cell.

A) Elevated levels of ROS result in Mec1 activating Dun1 kinase, which then phosphorylates Sod1 at S60 and S99. Once phosphorylated, Sod1 translocates into the nucleus and acts as a transcription factor for genes related to DNA damage response,

cellular survival, and ROS protection. B) Nox2, Sod1 and Rac1 exist in a feedback loop to balance redox levels in the cell. Sod1 interacts with Rac1 and promotes its activity. When active, Rac1 promotes the activity of Nox2. Nox2 produces O_2^- from O_2 . Sod1 converts O_2^- to H_2O_2 . H_2O_2 oxidatively modifies Rac1, changing its conformation such that it no longer interacts with Sod1. When Rac1 is no longer interacting with Sod1 it is in its GDP bound state and no longer promotes Nox2 activity. C) Sod1 converts cytosolic O_2^- (that are produced by Yno1 and the mitochondria), into H_2O_2 . Sod1 interacts with GAPDH and inactivates it due to the local production of H_2O_2 . When GAPDH is inactive, metabolism is rerouted from glycolysis to oxPPP which produces NADPH. D) Sod1 senses O_2 and glucose (via O_2^- production) to stabilise the yeast casein kinases Yck1 and Yck2 via its local production of H_2O_2 . Yck1 and Yck2 promote amino acid sensing, glucose sensing and the repression of respiration. E) When active (when nutrients are present), mTORC1 inhibits Sod1 by phosphorylating it at Thr39. When inactive (during starvation), Sod1 is no longer inhibited and promotes cell survival and nutrient sensing.

1.4 SOD1-associated ALS

1.4.1 Mutations in SOD1 that are associated with fALS

SOD1 was the first gene that was found to be linked to ALS back in 1993 [10]. *SOD1* is located on chromosome 21 at position 31.66 mb to 31.67 mb in humans. Since the first discovery, up to 217 mutations spanning the whole length of the gene have been linked with fALS. A list of all ALS-linked variants of *SOD1* that have been discovered can be found in the ALS online database (ALSod: <https://alsod.ac.uk/>). These mutations span all five exons of the gene and consist of point mutations, truncations, deletions, and substitutions.

The most common fALS-linked variants of human *SOD1* are the D90A, A4V and G93A mutations. The D90A mutation is the most common one found around the world, whereas the A4V mutation is the most common mutation found in the US. The G93A mutation is less common, however it is by far the most studied and well characterised due to the first transgenic *SOD1*-ALS model in mice being based on this mutation [63]. The fALS-linked mutations in human *SOD1* can be divided into two groups, metal-binding region mutants (MBR) and WT-like (WTL) mutants. MBR mutants with mutations such as H48R, H48Q, G85R, D124V, S134N and C146R have impaired metal binding and a diminished sod activity of the enzyme. WTL mutants with mutations such as A4V, G37R, D90A, G93A and N139K possess metal binding affinities and structures that are closer to that of human Sod1^{WT}. MBR mutations impair the formation of fully-mature human holo-Sod1 *in vitro* [64] and increase the propensity for the enzyme to aggregate in mice [65] and in purified Sod1 from human erythrocytes [66] in response to cellular stresses. WTL mutations reduce the ability of apo-Sod1 monomers to form dimers and increase the rate of unfolding at physiological temperature [67]. In summary, a universal theme of both WTL and MBR mutations is that they increase the tendency of human Sod1 to exist in the apo-

monomeric state, where it is intrinsically more aggregation prone. Despite this common feature, some fALS-linked human *SOD1* mutations such as H46R, D101N, D124V, D125H, S134N and V148I do not increase the instability of apo-Sod1 monomers *in vitro*. It could be that in a more complex environment such as the human body, the effects of these mutations on monomer stability may be more apparent than in a controlled *in vitro* system [64], [67].

1.4.2 Aberrant PTMs that are associated with *SOD1*-fALS

Several PTMs are required for the normal functioning of yeast and mammalian Sod1. The PTMS for Sod1 include the disulphide bridge between residues (Cys57 and Cys146) [68], phosphorylation of Ser60 and Ser99 by Dun1 to regulate nuclear translocation [58], ubiquitylation at Lys63 to regulate degradation, phosphorylation at Thr39 by mTORC1 to regulate activity [69]. Other PTMs include acetylation, succinylation and glycation [70].

In vitro studies with human erythrocyte Sod1 demonstrated that fully mature holo-Sod1 is highly stable, with many of the important residues being buried. fALS-linked Sod1 mutations can lead to buried residues becoming more solvent accessible and thereby more vulnerable to aberrant modifications [71]. Findings from *in silico* molecular dynamics simulations suggested that oxidative modifications in the dimer interface of human Sod1 drastically affected the stability of the Sod1 homodimer [72]. Oxidation of the Trp32 residue and glutathionylation of the Cys11 residue are two PTMs that have been shown to lead to dissociation of the human Sod1 homodimer and subsequent aggregate formation [73]. Histidine residues (His40, His63, His71, His80 and His20) that are important for metal ion coordination in the human Sod1 protein are vulnerable to oxidative modification from H₂O₂ [71].

In summary, aberrant PTMS are associated with misfolding and aggregation of Sod1. Deleterious PTMs may provide a mechanism for how Sod1^{WT} can play a role in the development of sALS. It is thought that fALS-linked mutant isoforms of Sod1 are more vulnerable to aberrant PTM due to key residues being more exposed.

1.4.3 Is *SOD1*-ALS caused by toxic loss-of function or gain-of function?

Initially it was widely accepted that the toxicity conferred by ALS-linked mutant isoforms of Sod1 is caused by a gain-of function of the enzyme, rather than a loss-of function. This due to the fact that the deletion of *SOD1* in mice does not cause the loss of MNs at six, nine, and 17 months respectively [74]. Furthermore, numerous ALS-linked human Sod1 mutants expressed in transgenic mice exhibit similar or partial levels of sod activity to that of Sod1^{WT}, suggesting that a loss of sod activity is not the main driver of toxicity [75].

Chapter 1. Introduction

Proposed gain-of functions of ALS-linked human Sod1 mutant isoforms include an increased propensity to aggregate, misfolding and the ability to induce misfolding of the Sod1^{WT} isoform [76]. Zn binding is thought not to be as important for sod activity as Cu binding, however it is important for stability of the enzyme. ALS-linked human Sod1 mutations are associated with an incomplete metalation of the enzyme [77].

Differences in the catalytic activity of Sod1 mutant isoforms compared to the WT have been reported. One study suggested that a gained function could be an increase in H₂O₂ mediated oxidation of small anionic molecules such as formate or glutamate (that may be able to fit into the active site of Sod1 where H₂O₂ mediated oxidation may occur), due to the 3D structure of Sod1 being more open, thus leading to the active site becoming more easily accessible [78]. Another possible gain-of function that has been proposed is that Sod1 mutants with less affinity for Zn, or no affinity for Zn at all, a Cu¹⁺ ion that is bound to Sod1 reduces O₂ to form O₂⁻. O₂⁻ then reacts with nitric oxide (NO) to form peroxynitrite(ONOO⁻). With ONOO⁻, Sod1 can then catalyse the nitration of protein bound tyrosine residues, a permanent modification that can affect protein function [79]. Finally, another key gain-of function that is thought to be acquired by ALS-linked mutant isoforms of Sod1 is the increased propensity to misfold and form aggregates, which can have toxic effects on MNs. This will be further discussed in the next section.

Further investigation has showed that *SOD1* null mice display phenotypes such as early locomotor defects [80] and signs of axon degeneration which are signs of motor neuron degeneration (MND) [94], suggesting that loss-of function may also play a part in the disease as well. MNs in *SOD1* null mice were more sensitive to damage compared to WT mice. As there has been an association reported between trauma and ALS, it could be that the loss-of function of Sod1 plays a role in this [81].

In summary, it is becoming clear that toxicity from ALS-linked mutant isoforms of Sod1 does not stem completely from a gain-of function, or a loss-of function. It is most likely that both gain-of and loss-of functions contribute towards disease progression. Loss-of function of the ALS-linked Sod1 mutant isoforms allows the gain-of function, such as protein aggregation and aberrant redox chemistry to occur. Gained functions then lead to an increased loss of function in the Sod1 enzyme. Interestingly in some sALS cases in which patients do not have any ALS-linked Sod1 mutations, Sod1^{WT} is found to form aggregates and adopted misfolded conformations resembling that of mutant isoforms [82].

1.5 Animal models of *SOD1*-associated ALS

To study *SOD1*-ALS, animal models have been created in a range of organisms from, yeast, worms, flies, zebrafish, rodents, induced pluripotent stem cells (iPSC) differentiated into MNs and more. Each animal model has their advantages and disadvantages (discussed in Chapter 3.1 Introduction). There is a trade-off between fast, cheap, and high-throughput models, and models that are physiologically more relevant to human MNs. As *S. cerevisiae* models of *SOD1*-ALS will be discussed in greater detail (section 1.8)), they will not be discussed in this section. Animal models of other fALS genes have been generated as well and have been important in providing key insights into the understanding of ALS pathogenesis [83], however for this section only *SOD1*-ALS models will be discussed.

1.5.1 Nematodes

Caenorhabditis elegans (*C. elegans*) are a widely used model organism to study neurons and ageing in whole organisms. ALS-linked proteins can be expressed transgenically and due to the transparency of the worms, localisation of the protein in the whole organism can be assessed using fluorescent reporters. Specific neurons can be visualised using fluorescent reporter tags, allowing for assessment of neurodegeneration of different neuron types. In *C. elegans*, ALS-linked proteins are expressed transgenically, and different promoters can be used to allow for specific expression in different neuron types.

Overexpression models of *SOD1*-ALS have been developed in *C. elegans* in which the fALS-linked mutant human isoforms of Sod1, Sod1^{G85R}, Sod1^{H46R} and Sod1^{H48Q} were pan-neuronally expressed into *C. elegans* using the synaptobrevin (*snb-1*) promoter [84]. Locomotor defects and Sod1 aggregation was observed. Interestingly, no increase in MND was observed in worms expressing mutant isoforms of Sod1. An RNAi screen for genes that modified aggregation of Sod1^{G85R} identified many genes with protein-chaperone, and quality control functions. Another model was developed in which either human Sod1^{WT} or human Sod1^{G93A} was overexpressed in D-type MNs in *C. elegans*. Age-dependant locomotor defects and MND were observed in worms expressing both human Sod1^{WT} and human Sod1^{G93A}. This suggests deleterious effects of Sod1^{WT} when overexpressed in certain conditions [85].

Recently a stable single-copy model of *SOD1*-ALS has been developed in *C. elegans* using clustered regularly interspaced short palindromic repeats (CRISPR)/Cas9 gene editing and also Mos1-mediated single copy insertion (MosCI). The A4V, H71Y, L84V, G85R and G93A mutations were introduced into *SOD1* [86]. Aggregation of Sod1 into puncta and MND of cholinergic neurons after oxidative stress was observed in worms with the A4V, H71Y, G85R

and G93A mutations. Glutamatergic MND was observed in worms with the H71Y, L84V and G85R mutations. Dopaminergic and serotonergic neurons were not affected in this *SOD1*-ALS model, which is consistent with ALS pathology.

1.5.2 Flies

Drosophila melanogaster (*D. melanogaster*) is another powerful organism for the study of ageing and the nervous system. In particular the UAS/Gal4 expression system allows for tissue specific and cell specific overexpression of human disease linked genes into flies [87]. In flies, loss of *SOD1* had severe effects on lifespan and locomotion. Expression of human Sod1^{WT} fully rescued the phenotypes of *SOD1* null flies, whereas expression of human ALS-linked Sod1 mutants only partially rescued the same phenotype [88]. Using the UAS/Gal4 expression system, a *SOD1*-ALS model was developed in flies whereby ALS-linked Sod1 isoforms were overexpressed into the MNs. Flies overexpressing ALS-linked isoforms of Sod1 into MNs did not have any lifespan defects, however they did show locomotory defects. In this model, mutant isoforms of Sod1 were not found to aggregate, suggesting that MN deficits were caused by a soluble form of the protein [89]. A stable single-copy model of *SOD1*-ALS was constructed in *D. melanogaster* using ends out homologous recombination (HR). ALS-linked mutations G37R, H48R, H71Y, and G85R were introduced into the endogenous *SOD1* locus. Reductions in lifespan, locomotory defect and MND was observed in flies with the G85R, H48R and H71Y mutations (which all exhibited no sod activity) whereas flies with the G37R mutation were identical to the control [90].

1.5.3 Zebrafish

Danio rerio (*D. rerio*) are ideal models for human disease as they exhibit a high degree of genetic homology to humans with most human genes having a zebrafish homolog. They are amenable to drug screening and genes can be overexpressed or knocked down by injecting RNA or anti-sense RNA (morpholinos) into embryos [91]. A model of *SOD1*-ALS was developed by overexpressing ALS-linked human Sod1 isoforms into zebrafish embryos. It was found that expression of ALS-linked human Sod1 isoforms produced a motor axonopathy and the severity of the phenotypes depended on the degree of expression of Sod1 [92]. Subsequently, a stable model for *SOD1*-ALS was developed using TILLING (targeting induced local lesions in the genome) in which the zebrafish lines expressing Sod1 with the ALS-linked mutations T70I and G93A were generated. These ALS-models express Sod1 at a physiological level and recapitulate many aspects of ALS pathology including neuromuscular junction (NMJ) defects, shortened lifespans and motor defects [93].

1.5.4 Rodents

The first and most well characterised animal model of *SOD1*-ALS was the transgenic mouse line overexpressing human Sod1^{G93A} [77]. This model has been studied extensively over the years, recapitulates key aspects of ALS disease progression (paralysis, MND and shortened lifespan) and has been used in preclinical trials to test for the effectiveness of drugs against ALS. A study demonstrated that overexpression of WT human Sod1 into mice also causes an ALS-like phenotype, albeit less severe than that found in the Sod1^{G93A} mouse model. This has cast doubt over whether the effects observed in the Sod1^{G93A} model are entirely caused by the mutation [78]. Mouse models expressing other mutant Sod1 isoforms were developed for the Sod1^{G37R}, Sod1^{G86R}, and Sod1^{G85R} isoforms [79][80][81]. These mouse models all recapitulate elements of ALS pathology such as paralysis, reduced lifespan, and MN loss, however they differed on the time of onset, speed of disease progression and time of death. Rat models of *SOD1*-ALS have been developed with the overexpression of Sod1^{G94A} and Sod1^{H46R} isoforms. Similar to mice, these overexpression models recapitulate aspects of ALS, and the toxicity appears to correlate with the level of gene expression.

1.5.5 Neuronal models: human fibroblast and induced pluripotent stem cell models

Skin fibroblast models from patients harbouring ALS-linked mutations have been developed in order to model the disease [94]. The advantages of using ALS-patient fibroblast models are that they are highly physiologically relevant to the human condition. Furthermore, the ALS-linked genes are expressed under their native promoter in their original genetic locus. Increased aggregation and misfolding of mutant Sod1 isoforms was observed in this model [94].

ALS patient derived induced pluripotent stem cells (iPSCs) are powerful tools to model ALS. iPSCs can be differentiated into many cell types, including MNs and glial cells. Challenges of iPSCs include the cost and the difficulty to culture and differentiate the cells into mature MNs. Furthermore, iPSCs between different patients are quite variable with disease severity. A study developed models of *SOD1*-ALS with the A4V and D90A mutations. Transcription activator-like effector nucleases (TALEN) based HR was used to correct the ALS mutations back to the WT sequence in order to generate appropriate controls. This study revealed that iPSCs from patients differentiated into MNs, showed MND, aggregation of neurofilament and small aggregates Sod1 in the cytoplasm and nucleus and neurites [95].

1.5.6 Other models: Dog, Swine and Primate

Other animal models of *SOD1*-ALS include those in dogs, swine, and primates. A specific breed of dogs can suffer from a condition known as canine degenerative myelopathy (CDM) which involves adult-onset MND leading to a progressive loss of motor functions. The mutations in *SOD1*, T18S and E40K have been shown to cause a recessive form of CDM in canines, with Sod1 aggregation being a hallmark of the condition [96]. A swine model of *SOD1*-ALS was developed by transfecting porcine adult make fibroblasts with a vector expressing Sod1^{G93A}. Sod1^{G93A} embryos were then developed and transferred to a recipient sow. Eventually five piglets were born expressing Sod1^{G93A} transgenically [97]. This swine *SOD1*-ALS model successfully recapitulated aspects of ALS pathology including MND and Sod1 aggregation [98]. A primate model has been developed for TDP-43-ALS but not for *SOD1*-ALS. This primate model recapitulated aspects of ALS pathology [99]. Primate models have been used to test for safety of an artificial microRNA to silence Sod1 with the aim of treating ALS patients with *SOD1* mutations [100].

1.6 Currently proposed mechanisms of ALS-linked mutant Sod1 toxicity

The use of animal models to model *SOD1*-ALS over the years has led to the proposal of a number of mechanisms of toxicity that mutant isoforms of Sod1 are linked with including, mitochondrial dysfunction, glutamate excitotoxicity, oxidative stress, protein aggregation and misfolding and metabolic dysfunction.

1.6.1 Mitochondrial dysfunction

The mitochondria are organelles that generate energy in the cell in the form of adenosine triphosphate (ATP) by oxidative phosphorylation. Mitochondria are associated with apoptosis through outer-membrane proteins called Bcl2 and Vdac [101]. ALS-linked Sod1 mutants have been shown to associate with the outer mitochondrial membrane at the cytoplasmic face [102]. Mutant Sod1 has been found to interact with Bcl2 in spinal cord mitochondria and induces a conformational change exposing the toxic BH3 (Bcl-2 homology) domain. When Bcl-2 is in this toxic conformation, cytochrome c is released and apoptosis is promoted [103]

Degraded mitochondria were observed in vacuole-like structures in a mouse model of *SOD1*-ALS overexpressing Sod1^{G93A} [104]. Increases in activity of complex I, II and III from the mitochondrial electron transport chain were observed in *SOD1*-ALS patients and also in the Sod1^{G93A} mouse model [105].

1.6.2 Aggregation and stability of ALS-linked Sod1 mutants

Originally it was thought that aggregation of Sod1 led to fALS development by causing a loss of function. Aggregation of Sod1 was observed in spinal cord and brain samples from ALS patients. These aggregates have been shown to spread from cell–cell in a prion-like manner [106]. In a mouse model of *SOD1*-ALS, overexpression of Sod1^{WT} inhibited protein aggregate formation of mutant Sod1 isoforms. When protein aggregation was inhibited, progression of the disease was accelerated, suggesting that soluble misfolded mutant Sod1 isoforms are the toxic agent [107]. Furthermore, it was observed that Sod1^{WT} can become oxidised, giving it a conformational epitope that is also found in mutant Sod1 protein and not the unoxidized Sod1^{WT} protein [108]. In summary, it could be that aggregation of Sod1 is a protective mechanism in the cell to defend against soluble misfolded toxic Sod1.

1.6.3 Lysosome and autophagy dysfunction in ALS

Lysosomes are organelles that contain hydrolytic enzymes that function to break down proteins. They play crucial roles in protein sorting, amino acid storage, ion storage, autophagy, and stress responses in the cell. Lysosomal defects have been associated with the pathogenesis of a range of NDs that involve protein misfolding, such as Alzheimer's disease (AD), Parkinson's disease (PD), Huntington's disease (HD), and ALS. Disruption in autophagy worsens survival of MNs [109], however knocking out autophagy in mice was not enough to cause ALS [110]. Studies have investigated the effects of compounds that promote autophagy on survival in different *SOD1*-ALS models, with mixed results. Trehalose, an autophagic inducer independent of mTORC1 signalling has been shown to improve MND in mouse models of ALS [111]. Lithium was found to slow disease progression in humans and protect against MND in mouse models of ALS [112]. Studies involving rapamycin, an mTORC1-dependant activator of autophagy found that it increased MN loss and reduced survival in the Sod1^{G93A} mouse model, however it increased survival in an immunodeficient ALS mouse model [113][114].

A link has been found between overexpression of ALS-linked Sod1 mutants and vacuole dysfunction in *S. cerevisiae*. In *S. cerevisiae*, the vacuole shares many functional similarities to the mammalian lysosome and has been shown to be a good model to study aspects of lysosomal function, It was shown that overexpression of ALS-linked Sod1 mutants in *S. cerevisiae* led to a defect in vacuole acidification and a decrease in autophagy [115].

1.6.4 Oxidative Stress

When the initial link between mutations in *SOD1* and fALS was established, it was hypothesised that mutations in *SOD1* would cause a decrease in sod activity, resulting in elevated levels of

oxidative stress in MNs due to the reduced ability of mutant Sod1 to convert O_2^- into H_2O_2 and H_2O . This is the free radical theory of ALS. A small pool of Sod1 has been shown to localise to the inner mitochondrial membrane (IMM) where it detoxifies the O_2^- generated from the electron transfer chain. Oxidative damage of a protein involved in glutamate transport, EAAT2 by 4-hydroxynonenal, (a reactive aldehyde product of lipid peroxidation as a result of increase oxidative stress) has been observed in ALS patients. This was suggested to result in defects in glutamate transport and excitatory MND [116]. Oxidative damage to proteins was also found in a *SOD1*-ALS mouse model in which increased hydroxyl production caused extensive damage to proteins along with damage to Sod1 itself, further compromising its antioxidant function [117].

Although it is clear that oxidative stress plays a part in the development of ALS and that the role of Sod1 in catalysing the dismutation of O_2^- into H_2O_2 and H_2O is important, there are additional mechanisms of dysfunction that are caused by mutant Sod1 that are independent of general oxidative stress damage. This is highlighted by the fact that multiple mutant alleles of *SOD1* possess partial or full Sod activity and yet still give rise to fALS [64].

1.6.5 Glutamate excitotoxicity

MNs become damaged when the levels of neurotransmitters become elevated, resulting in excessive stimulation of certain receptors. This is known as excitotoxicity. Glutamate excitotoxicity is a mechanism of dysfunction that is associated with *SOD1*-ALS. Upon elevation of glutamate levels, glutamate receptors such as the α -amino-3-hydroxy-5-methyl-4-isoxazolepropionic acid (AMPA) and *N*-methyl-D-aspartate (NMDA) receptors become overly stimulated. This results in an excessive level of Ca^{2+} being imported into the cell. Elevated intracellular Ca^{2+} levels act as a signal for cellular stress and promotes apoptosis [118].

AMPA receptors are made up of four subunits, GluR1 – GluR4. In MNs, the AMPA receptors lack the GluR2 subunit and are therefore highly permeable to Ca^{2+} compared to other neuron types. Increased permeability to Ca^{2+} makes MNs inherently more vulnerable to glutamate excitotoxicity. Increased levels of neuronal calcium have been detected in ALS [119]. Up to 90% loss of the glutamate transporter EAAT2 was observed in the Sod1^{G93A} mouse model [120]. Transgenic expression of the GluR2 subunit in the Sod1^{G93A} mouse model to reduce the Ca^{2+} permeability in MNs delayed onset of the disease phenotype and slowed progression [121].

Elevated intracellular Ca^{2+} levels caused by glutamate excitotoxicity in MNs promotes mitochondrial apoptotic pathways and protein misfolding pathways.

Many more mechanisms for *SOD1*-ALS toxicity have been identified and proposed, including ER stress and defects in the ubiquitin-proteasome system. It is difficult to determine which dysfunction mechanisms are early events or late events in the development of the disease.

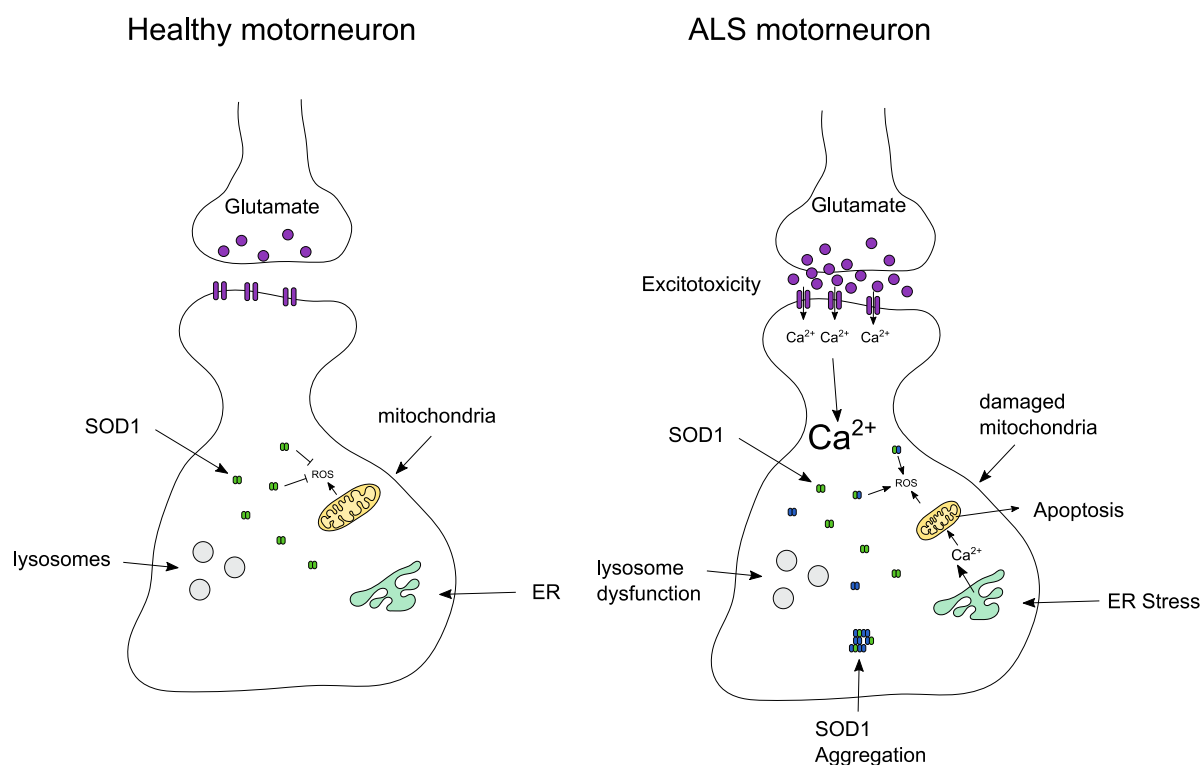


Figure 1.4 Summary of mechanisms involved in *SOD1*-ALS.

In healthy MNs, glutamate signalling, mitochondrial function, ER function, lysosome function and autophagic function all function correctly to ensure that the high energetic demands of the cells are met. Sod1 is not abnormally aggregated or misfolded, it detoxifies O_2^- in the cytosol and carries out its many roles in the cell. In a diseased ALS MN, glutamate excitotoxicity is observed, which results in excess Ca^{2+} importation into the cytosol. Elevated cytosolic Ca^{2+} leads to increased ROS, protein misfolding, ER stress and damaged mitochondria. Ca^{2+} is depleted from the ER and is imported into the mitochondria. Influx of Ca^{2+} into the mitochondria combined with the aberrant interaction of mutant Sod1 with Bcl-2 promotes apoptosis. Misfolded mutant Sod1 aggregates are found.

1.7 *Saccharomyces cerevisiae* as a model to study neurodegenerative diseases

1.7.1 Tools for *S. cerevisiae* research

S. cerevisiae is an excellent, simple model for the study of human disease as it is a well characterised, highly tractable genetic tool that is amenable to high-throughput experimentation. Many key biochemical and signalling pathways that are involved in human disease are highly conserved in *S. cerevisiae*. Furthermore, *S. cerevisiae* is simple and inexpensive to grow and maintain, can be stored long term, has relatively simple requirements for sterility, and is recognised as a generally regarded as safe (GRAS) organism. *S. cerevisiae* cells also have a rapid cell

cycle and a limited replicative lifespan making them an excellent model for research into cell ageing.

Powerful genetic tools have been developed in *S. cerevisiae* including the ability to knock-in, knock-out, mutate, or tag genes using HR-based and CRISPR/Cas9 technology. Libraries have been developed in which every non-essential gene has been deleted [122] and essential genes placed under regulatable promoters [123]. A green fluorescent protein (GFP) library has been developed in which every gene has been C-terminally tagged with GFP to enable localisation studies of every protein in the cell [124]. Genome-wide libraries to study protein-protein interactions (PPIs) have also been developed [125].

The *Saccharomyces* Genome Database (SGD) website (<https://www.yeastgenome.org/>) is a fantastic, curated resource for *S. cerevisiae* research. It contains a wealth of information on the large number of *S. cerevisiae* genomes sequenced to date as well as powerful tools to analyse gene function, genetic interactions, and gene expression data.

1.7.2 Using *S. cerevisiae* as a model for neurodegenerative diseases

Over the last decade, *S. cerevisiae* has emerged as a powerful tool to model NDs. ~6000 human genes and 500 human disease genes have homologues in *S. cerevisiae* [126]. NDs are understood to be caused by a combination of genetic and environmental factors. *S. cerevisiae* is used to model NDs due to the ease with which it can be genetically modified, and the fact that key cellular processes including mitochondrial function, vesicular trafficking and protein quality and control pathways are highly evolutionarily conserved. The use of *S. cerevisiae* as a model has led to the generation of key discoveries into aspects of MND which have led to the development of therapies. Examples from ALD, HD, PD and ALS are given below.

There are a number of approaches when it comes to modelling NDs that are caused by mutations in a gene. Firstly, when no homologue exists in *S. cerevisiae*, the human gene can be expressed into the cell in order to investigate what effect its expression will have.. Secondly, if a homologue, or an orthologue does exist, then the function of that gene can be investigated by knocking it out, or modulating expression levels, so as to learn what cellular functions it is important for. The endogenous gene can also be edited so that it contains the equivalent mutations that are linked with the human disease. Edited genes can be expressed from a plasmid, allowing for control over the degree of expression. It can then be investigated whether the expression of the disease linked gene causes any changes to the *S. cerevisiae* cells, possibly by affecting growth or viability. Localisation and / or aggregation of the protein can also be assessed by tagging with a fluorescent protein and visualising by fluorescence microscopy.

PD is a ND disorder of the brain that causes stiffness, shaking, difficulty balancing and walking. It involves the progressive loss of dopamine producing neurons in the base ganglia. Aggregation of misfolded α -synuclein (α -syn) into Lewy bodies is thought to cause neuron death by disrupting cellular processes. The establishment of a *S. cerevisiae* model of α -syn-associated PD has led to numerous findings that have been recapitulated in mammalian cells. Expression of α -syn in *S. cerevisiae* successfully recapitulated aspects of PD, including formation of α -syn aggregates, toxicity and, defects in vesicular trafficking. Toxicity caused by α -syn to *S. cerevisiae* was observed to be dose-dependent [127]. *S. cerevisiae* cells are highly amenable to high-throughput experimentation. This factor was exploited in a study in which 190,000 compounds were screened in *S. cerevisiae* for their effects on ameliorating the toxicity from the expression of α -syn, TDP-43, FUS and amyloid beta ($A\beta$) [128]. A compound called N-Aryl-Benzimidazole (NAB) was found to reverse the toxicity of α -syn, including the formation of α -syn foci in vesicles, nitration of proteins, the block of ER–Golgi traffic and the accumulation of ROS. NAB was then tested in nematode, mouse and patient derived iPSCs models of PD and was found to improve α -syn toxicity in all of them [129][130]. The mechanism of action of NAB rescue of α -syn toxicity was investigated using an overexpression screen of ~ 5800 genes. As high concentrations of NAB reduced growth in WT cells, the overexpression screen was carried out to screen for genes which either enhanced or suppressed this phenotype. This approach identified the gene *RSP5*, which encodes an E3 ubiquitin ligase that promotes endosomal trafficking. This approach, involving an unbiased high-throughput chemical screen combined with overexpression screening. Using this approach, the compound NAB was found to rescue α -syn toxicity by promoting Rsp5 dependant endosomal trafficking [131].

ALD is a ND that involves the gradual loss of memory and cognitive skills. This is caused by the progressive loss of neurons in the hippocampus and cerebral cortex. Neuron death is heavily associated with aggregation of $A\beta$ protein into extracellular plaques and intracellular inclusions, as well as intracellular aggregation of Tau protein. Defective processing of an aggregation prone form of $A\beta$ called $A\beta_{42}$ impairs endocytic sorting and synaptic transmission. In neurons, $A\beta_{42}$ is processed by the amyloid precursor protein (APP), a transmembrane protein found in the plasma membrane. After processing it is trafficked to the trans-Golgi network, endosomal compartments, and the plasma membrane. Once at the plasma membrane, it is endocytosed. A *S. cerevisiae* model of ALD was difficult to construct as *S. cerevisiae* do not have a homologue for $A\beta$ or APP and they do not secrete neurotransmitters in synaptic vesicles. A *S. cerevisiae* model of ALD was developed in which the $A\beta_{42}$ fragment was expressed with an N-terminal ER signal sequence in order to target it to the yeast secretory pathway. The aim of this was to mimic the

way in which A β is secreted and then endocytosed in neurons. Once the A β was secreted from the *S. cerevisiae* cells, it would be blocked at the cell wall and would then be endocytosed. This model recapitulated the toxicity and oligomerisation of the A β peptide that is thought to be a hallmark of the disease. Genome wide overexpression screens using this model identified a number of suppressors and enhancers of A β toxicity, with one of the key hits being *YAP1802* which is the *S. cerevisiae* homologue of phosphatidylinositol binding clathrin assembly protein (*PICALM*). *PICALM* is a protein involved in clathrin-mediated endocytosis and is a known risk factor for ALD [132]. The study also identified other genes that suppressed A β 42 toxicity when overexpressed such as *INP52/SYNJ1* and *SLA1/SH3KBP1*. Both genes encode proteins that are involved in endocytosis and interact with known risk factors of ALD. This ALD model in *S. cerevisiae* took advantage of the ease with which *S. cerevisiae* can be genetically modified to mimic A β trafficking through the secretory system in neurons. Furthermore, this study showed how *S. cerevisiae* can be used to screen large numbers of genes to test for suppression or enhancement of toxicity.

Both of these examples from a PD model and an AD model in *S. cerevisiae* demonstrate the power of the *S. cerevisiae* system to create models of ND that recapitulate elements of each disease. Due to the ability to carry out high-throughput experiments, these studies demonstrated the suitability of *S. cerevisiae* to screen for large libraries of compounds, or large libraries of genes that suppress toxicity of the disease. These results have then been validated in either patient derived iPSC cells or mouse models and have generated important findings in terms of the development of therapies in the future. *S. cerevisiae* has also been used as a model for Huntington's disease (HD), Batten's disease, Friedreich's Ataxia, Ataxia-telangiectasia, Niemann-Pick disease, Hereditary spastic paraplegia, Creutzfeldt-Jakob disease and ALS [133].

1.8 Yeast models of Amyotrophic Lateral Sclerosis

1.8.1 Modelling *TARDBP*, *FUS* and other prion-like domain containing ALS-associated genes

No homologue for *FUS* exists in *S. cerevisiae*. Expression of human WT *FUS* into *S. cerevisiae* causes aggregate formation and cytotoxicity. Furthermore, expression of *FUS* with the ALS-linked mutations R524S and P524L increased cytotoxicity under certain conditions [134].

Interestingly, expression of certain shorter fragments of *FUS* led to aggregation, but no cytotoxicity. Two similar *FUS*-ALS models were generated in *S. cerevisiae* [135][136]. Both studies carried out genome-wide screens to identify modifiers of *FUS* toxicity in *S. cerevisiae*. In both studies, the genes *UPF1*, *NAM8* and *SBP1* were found to suppress *FUS* toxicity when

overexpressed. All three genes are involved in RNA metabolism, a key point of dysfunction in *FUS*-ALS. Key regions in the *FUS* gene that are important for toxicity and aggregation were also identified in this study. By replacing four phenylalanine residues (Phe305, Phe341, Phe359 and Phe368) required for RNA binding of FUS with leucine, it was demonstrated that abolishing RNA binding rescued the toxicity of *FUS* proteins [135]. Additionally, driving nuclear localisation of FUS using a *S. cerevisiae* *HRP1* nuclear localisation sequence (NLS), it was shown that FUS is more toxic when aberrantly localised to the cytosol where it forms aggregates in stress granules [136].

There are no *S. cerevisiae* homologues for *TARDBP*, the gene that encodes TDP-43, a nuclear protein that plays a role in RNA trafficking. In the cell TDP-43 is constantly shuttling between the nucleus and the cytosol [137]. Most ALS-linked mutations in *TARDBP* are in its glycine-rich region. A *S. cerevisiae* model of TDP-43-ALS was developed in which a single copy of human TDP-43-GFP fusion was expressed from an integrated plasmid. In this strain, TDP-43 was found to be predominantly localised to the nucleus. When TDP-43-GFP was expressed from a high copy 2 μ plasmid, the protein became predominantly localised to the cytosol in aggregates [138]. In this study it was also observed through expressing truncated forms of TDP-43, that one of the RNA recognition motifs, RRM2 and the glycine rich C-terminal domain were required for toxicity of TDP-43. Furthermore it was shown that the C-terminal domain was required for aggregation, whereas the N-terminal domain (containing the NLS) was required for nuclear localisation [138]. Further studies revealed that several ALS-linked mutant isoforms of TDP-43, increased aggregation and toxicity in *S. cerevisiae* cells compared to the WT form of TDP-43 [23].

Other prion like ALS-linked proteins that have been modelled in *S. cerevisiae* include hnRNPA2, TAF-15, and EWSR1. hnRNPA2 is a protein that functions in mRNA metabolism and is aggregation prone and often found in cytoplasmic aggregates in neurons. ALS-linked mutations in the hnRNPA2 C-terminal prion-like domain accelerated aggregation by strengthening a steric zipper like domain [41]. *S. cerevisiae* has been used as a model to assess the effect of different amino acid substitutions in the prion-like domain of hnRNPA2 on the propensity of the protein to aggregate. The study found that large aliphatic residues promoted degradation of the protein, whereas aromatic residues promoted aggregation [139]. TAF-15 is very similar to FUS and when human TAF-15 was expressed into *S. cerevisiae*, cytosolic aggregation and toxicity was observed [140]. *EWSR1* encodes a protein called EWS which is similar to both FUS and TAF-15 and when overexpressed in *S. cerevisiae*, aggregates in the cytosol and has cytotoxic effects as well [141].

1.8.2 Modelling *C9orf72*-associated ALS in *S. cerevisiae*

A *S. cerevisiae* model of *C9orf72*-ALS was developed in which 50 repeats of four of the different DPRs were expressed under an inducible galactose promoter. 50 repeats of the arginine rich PR-DPR was found to be the most toxic in *S. cerevisiae*. In this study, genome-wide overexpression screens and non-essential gene deletion screen were carried out on cells expressing 50-PR in order to identify enhancers or suppressors of toxicity in *S. cerevisiae*. In total, 27 genes that suppress toxicity and 35 genes that enhance toxicity when overexpressed were identified. The non-essential gene deletion screen identified 16 genes that suppressed toxicity when deleted. Combined results of both screens revealed an enrichment in genes that function in nucleocytoplasmic transport. In particular genes that encode nuclear import proteins from the karyopherin family were identified [142]. A drug called BIIB100 that inhibits Exportin-1 (XPO1) is currently in phase 1 clinical trials for the treatment of sALS. The aim of the treatment is to ameliorate defective nucleocytoplasmic transport.

1.8.3 Modelling *SOD1*-associated ALS in *S. cerevisiae*

The first *SOD1*-ALS model in *S. cerevisiae* involved the expression of either WT or mutant human Sod1 isoforms into a *S. cerevisiae* strain lacking *SOD1*. The mutant isoforms Sod1^{A4V}, Sod1^{G93A}, Sod1^{G93C} and Sod1^{L38V} were expressed. It was found that the human mutant Sod1 isoforms were able to rescue the phenotype of the *SOD1* deletion, restoring resistance to paraquat and the ability to grow in 100% O₂ (hypoxic condition). Many human mutant isoforms showed normal levels of sod activity as well. In this study, human *SOD1* was expressed under the *S. cerevisiae* *SOD1* promoter from a multicopy plasmid. The results from this study demonstrated that many ALS-linked Sod1 mutants isoforms were enzymatically active, and that the disease may not be caused by a loss-of function of the enzyme [143].

A *SOD1*-ALS model was developed in *S. cerevisiae* where the ALS-linked mutations Sod1^{A4V}, Sod1^{G37R}, Sod1^{H48Q}, Sod1^{G93A} and Sod1^{S134N} were introduced into the endogenous *SOD1* via site-directed mutagenesis. These ALS-linked yeast Sod1 mutant isoforms were overexpressed into *S. cerevisiae* under a constitutive GPD promoter from a high copy 2 μ plasmid. The study demonstrated that these *S. cerevisiae* mutant Sod1 isoforms were unstable and possessed markedly reduced Sod activity compared to the WT yeast Sod1 protein. Overexpression of the *S. cerevisiae* mutant isoforms in cells lacking *SOD1* resulted in strong growth defects, reductions in viability, and defects in vacuole function [115]. No aggregation of these ALS-linked mutant isoforms was observed suggesting that toxicity was being caused by soluble misfolded isoforms of Sod1, rather than large aggregates. This study suggested that ALS-linked mutations in the *S. cerevisiae* *SOD1*

gene caused metabolic dysfunction due to defects in vacuole acidification. This study also highlighted the effectiveness of introducing the equivalent disease linked mutations into the endogenous gene of the organism that is being used to model the disease.

1.9 Project Aims

1: To use the integrated model to conduct phenotypic and genetic screens to identify any mechanisms of dysfunction caused by ALS-linked Sod1 mutants

The integrated model of *SOD1-ALS* was constructed in the following way. Using gateway cloning technology, the inserts from the plasmids used in the overexpression yeast *SOD1-ALS* model [115] were cloned into an integration vector that integrates into an empty region of chromosome I in *S. cerevisiae* [144]. Phenotypic screens were carried out in BY4741 cells expressing either Sod1^{A4V} from an integration vector or an empty vector control. Phenotypic screens were carried out using the BIOLOG system, testing for the ability of *S. cerevisiae* cells to use carbon, nitrogen, phosphate, and sulphate sources along with the sensitivity of *S. cerevisiae* cells to salt stress and pH stress.

The genetic screen involved selecting a library of knockout strains from the MATa non-essential knockout collection. Genes that were involved in metabolic functions at the vacuole were selected. The vector expressing Sod1^{A4V} was integrated into each knockout strain and strains were screened for synthetic growth defects in various media conditions.

2: To develop a stable single-copy model of SOD1-ALS in S. cerevisiae

A stable single-copy model of *SOD1-ALS* was developed and characterised in *S. cerevisiae* in the following way. ALS-linked mutations were introduced into the endogenous *SOD1* genes using CRISPR/Cas9 gene editing. Characterisation of these models suggested that the phenotypes were much less severe than those observed in the overexpression model.

3: To investigate the interaction between Sod1 and the V-ATPase in S. cerevisiae

Previous research using the overexpression model of *SOD1-ALS* in *S. cerevisiae* implicated vacuole dysfunction as an important factor in the toxicity observed. Specifically, a loss of vacuolar acidification was observed. Vacuolar acidification is mediated by the evolutionarily conserved vacuolar-ATPase (V-ATPase) enzyme in *S. cerevisiae*. The aim was to explore whether Sod1 interacts with the V-ATPase in *S. cerevisiae*. This was done using an *in vivo* protein

complementation assay (PCA), using Sod1 as the bait and various subunits of the V-ATPase as the prey. The nature of this interaction between Sod1 and the V-ATPase was then explored.

4: Investigate the interaction between Sod1 and calcineurin in *S. cerevisiae*

Decreased calcineurin activity has been documented in ALS patients, and Sod1 has been shown to interact with calcineurin and carry out a protective role. This interaction hasn't been studied in *S. cerevisiae* so far. The aim of this study was to test whether Sod1 interacts with calcineurin in *S. cerevisiae*, and to use the *S. cerevisiae* system to explore the nature of this interaction. This was achieved using the same PCA assay to check for PPI with Sod1 as the bait and various subunits of the calcineurin complex as the prey. A fluorescence based transcriptional reporter (4×-CDRE-GFP) of calcineurin activity was also used to measure the effect of loss of *SOD1* and expression of ALS-linked mutant isoforms of Sod1 on calcineurin activity in *S. cerevisiae*.

2 Materials and Methods

2.1 Media for yeast and bacterial growth

2.1.1 Media preparation and growth conditions for *Saccharomyces cerevisiae* and *Escherichia coli*

All components of the media were mixed in to deionised distilled water prior to autoclaving unless specifically stated otherwise. Media was heat-sterilised by autoclaving at 121 °C for 20 min. For all solid-media, 2% w/v granulated agar was added prior to autoclaving. Liquid growth of *S. cerevisiae* was carried out at 30 °C with constant shaking at 180 rpm in 5 ml of growth media in a sterile boiling tube (unless stated otherwise). Liquid growth of *E. coli* was carried out at 37 °C with constant shaking at 180rpm in 5 ml of bacterial growth media in a sterile boiling tube (unless stated otherwise). For growth on solid media, *S. cerevisiae* was grown at 30 °C and *E. coli* was grown at 37 °C.

2.1.2 Yeast growth media

YPD (yeast extract, peptone, dextrose) media

Table 2.1 YPD media components.

W/V (%)	Component	Manufacturer
2 %	D-glucose	Fisher Scientific UK Limited (CAT no: BG05002)
1 %	Yeast Extract	Scientific Laboratory Supplies (CAT no: B0127179500)
2 %	Bactopeptone	Scientific Laboratory Supplies (CAT no: B0118170500)

Synthetic complete (SC) media

For auxotrophic selection of yeast mutants, synthetic complete media lacking specific amino acids was prepared with the following components (Table 2.2).

Table 2.2 SC media components.

W/V (%)	Component	Manufacturer
2 %	D-glucose	Fisher Scientific UK Limited (CAT no: BG05002)
0.67 %	Yeast nitrogen base without amino acids, with ammonium sulphate	Formedium (SKU: CYN0402)
Variable	Complete supplement mixture (CSM) drop-out	Formedium

Table 2.3 W/V percentage of CSM amino acid drop-out mixture required.

W/V (%)	Amino acid drop-out	Manufacturer
0.164	Leucine	Formedium (SKU: DCS0091)
0.19	Uracil	Formedium (SKU: DCS0161)
0.193	Histidine	Formedium (DCS0071)
0.174	Leucine and uracil	Formedium (DCS0581)

2.1.3 Bacterial media

Luria Bertani (LB) media.

LB media was used for liquid and solid growth of *E. coli* strains used in this study (Table 2.4). To select for *E. coli* cells harbouring a plasmid, appropriate antibiotics were added to the media. Antibiotics were added from a 1000× stock solution to the final concentration stated below (Table 2.5). Antibiotics were added to the LB media after autoclaving, once the media had cooled to 50–55 °C.

Table 2.4 LB media components.

W/V (%)	Component	Manufacturer
0.5 %	Yeast extract	Scientific Laboratory Supplies (CAT no: B0127179500)
1%	Bacto-tryptone	Scientific Laboratory Supplies (CAT no: B0123173500)
1%	Sodium chloride (NaCl)	Fisher Scientific UK Limited (CAT no: BS31601)
If required	Antibiotic	

Table 2.5 Antibiotics used for plasmid selection in bacteria.

Concentration ($\mu\text{g/ml}$)	Antibiotic	Manufacturer
100	Ampicillin	Melford (CAT no: AO104)
50	Kanamycin	

2.2 Yeast and bacterial strains used in this study

2.2.1 *E. coli* strains

Table 2.6 Bacterial strains used in this study.

Name	Genotype	Source
DH5- α	<i>F</i> - <i>deoR endA1 recA1 relA1</i> <i>gyrA96 hsdR17(rk</i> <i>- , mk +) supE44 thi-</i> <i>1 phoA Δ(lacZYA-argF)U169</i> <i>Φ80lacZΔM15 λ-</i>	Bioline

DB3.1	<i>F- gyrA462 endA1 glnV44</i> <i>Δ(sr1-recA) mcrB mrr</i> <i>hsdS20(rB</i> <i>- -, mB</i> <i>) ara14 galK2 lacY1 proA2</i> <i>rpsL20(Smr) xyl5 Δleu mtl1</i>	Addgene
-------	--------------------------------------------------------------------------------------------------------------------------------------------------------------------------------------	---------

2.2.2 *S. cerevisiae* Strains

Table 2.7 Haploid Strains.

Strain	Genotype	Source
BY4741	<i>MATa his3Δ1 leu2Δ0</i> <i>met15Δ0 ura3Δ0</i>	CGY424 [145]
BY4741 Δsod1	<i>MATa his3Δ1 leu2Δ0</i> <i>met15Δ0 ura3Δ0 sod1::HIS5</i>	MFT Collection [115]
BY4741 Δsod1 no marker	<i>MATa his3Δ1 leu2Δ0</i> <i>met15Δ0 ura3Δ0 sod1::loxP</i>	KD16.2 (This study)
BY4741 Sod1 ^{A4V} CRISPR	<i>BY4741 (MATa his3Δ1</i> <i>leu2Δ0 met15Δ0 ura3Δ0)</i> <i>Sod1^{A4V}-CRISPR</i>	KD65.1 (This study)
BY4741 Sod1 ^{G37R} CRISPR	<i>BY4741 (MATa his3Δ1</i> <i>leu2Δ0 met15Δ0 ura3Δ0)</i> <i>Sod1^{G37R}-CRISPR</i>	KD41.1 (This study)
BY4741 Sod1 ^{H48Q} CRISPR	<i>BY4741 (MATa his3Δ1</i> <i>leu2Δ0 met15Δ0 ura3Δ0)</i> <i>Sod1^{H48Q}-CRISPR</i>	KD44.1 (This study)
SOD1-3HA:HIS3MX (CO-IP)	<i>BY4741 (MATa his3Δ1 leu2Δ0</i> <i>met15Δ0 ura3Δ0) SOD1-</i> <i>3HA::HIS3MX</i>	KD67.1 (This study)
VMA2-3HA::HIS3MX (CO-IP)	<i>BY4741 (MATa his3Δ1 leu2Δ0</i> <i>met15Δ0 ura3Δ0) VMA2-</i> <i>3HA::HIS3MX</i>	KD68.1 (This study)
VMA4-3HA::HIS3MX (CO-IP)	<i>BY4741 (MATa his3Δ1</i> <i>leu2Δ0 met15Δ0 ura3Δ0)</i> <i>VMA4-3HA::HIS3MX</i>	KD69.1 (This study)
VMA8-3HA::HIS3MX (CO-IP)	<i>BY4741 (MATa his3Δ1</i> <i>leu2Δ0 met15Δ0 ura3Δ0)</i> <i>VMA8-3HA::HIS3MX</i>	KD70.1 (This study)

CNB1-3HA::HIS3MX (CO-IP)	BY4741 (<i>MATa his3Δ1 leu2Δ0 met15Δ0 ura3Δ0</i>) <i>CNB1-3HA::HIS3MX</i>	KD71.1 (This study)
ΔSOD1::loxP VPH1-GFP:HIS3 VMA5-RFP::KAN	BY4741 (<i>MATa his3Δ1 leu2Δ0 met15Δ0 ura3Δ0</i>) <i>sod1Δ::loxP VPH1-GFP::HIS3 VMA5-RFP::KAN</i>	KD10.2 (This study)
BY4741 VPH1-GFP:HIS3 VMA5-RFP::KAN	BY4741 (<i>MATa his3Δ1 leu2Δ0 met15Δ0 ura3Δ0</i>) <i>VPH1-GFP::HIS3 VMA5-RFP::KAN</i>	KD14.2 (This study)
VMA9 Prey (DHFR)	BY4742 (<i>MATa his3Δ1 leu2Δ0 lys2Δ0 ura3Δ0</i>) <i>VMA9-DHFR[F3]::HPH</i>	KD1.1 [125]
TFP1 Prey (DHFR)	BY4742 (<i>MATa his3Δ1 leu2Δ0 lys2Δ0 ura3Δ0</i>) <i>TFP1-DHFR[F3]::HPH</i>	KD2.1 [125]
PPA1 Prey (DHFR)	BY4742 (<i>MATa his3Δ1 leu2Δ0 lys2Δ0 ura3Δ0</i>) <i>PPA1-DHFR[F3]::HPH</i>	KD3.1 [125]
VMA6 Prey (DHFR)	BY4742 (<i>MATa his3Δ1 leu2Δ0 lys2Δ0 ura3Δ0</i>) <i>VMA6-DHFR[F3]::HPH</i>	KD4.1 [125]
VPH1 Prey (DHFR)	BY4742 (<i>MATa his3Δ1 leu2Δ0 lys2Δ0 ura3Δ0</i>) <i>VPH1-DHFR[F3]::HPH</i>	KD5.1 [125]
VMA13 Prey (DHFR)	BY4742 (<i>MATa his3Δ1 leu2Δ0 lys2Δ0 ura3Δ0</i>) <i>VMA13-DHFR[F3]::HPH</i>	KD6.1 [125]
VMA5 Prey (DHFR)	BY4742 (<i>MATa his3Δ1 leu2Δ0 lys2Δ0 ura3Δ0</i>) <i>VMA5-DHFR[F3]::HPH</i>	KD7.1 [125]
TFP3 Prey (DHFR)	BY4742 (<i>MATa his3Δ1 leu2Δ0 lys2Δ0 ura3Δ0</i>) <i>TFP3-DHFR[F3]::HPH</i>	KD8.1 [125]
VMA10 Prey (DHFR)	BY4742 (<i>MATa his3Δ1 leu2Δ0 lys2Δ0 ura3Δ0</i>) <i>VMA10-DHFR[F3]::HPH</i>	KD9.1 [125]
VMA7 Prey (DHFR)	BY4742 (<i>MATa his3Δ1 leu2Δ0 lys2Δ0 ura3Δ0</i>) <i>VMA7-DHFR[F3]::HPH</i>	KD11.1 [125]

Chapter 2. Materials and Methods

VMA8 Prey (DHFR)	<i>BY4742 (MATa his3Δ1 leu2Δ0 lys2Δ0 ura3Δ0) VMA8-DHFR[F3]::HPH</i>	KD12.1 [125]
SOD1 Bait (DHFR)	<i>BY4741 (MATa his3Δ1 leu2Δ0 met15Δ0 ura3Δ0) SOD1-DHFR[F1,2]::NAT</i>	KD13.1 [125]
VMA2 Prey (DHFR)	<i>BY4742 (MATa his3Δ1 leu2Δ0 lys2Δ0 ura3Δ0) VMA2-DHFR[F3]::HPH</i>	KD14.1 [125]
VMA4 Prey (DHFR)	<i>BY4742 (MATa his3Δ1 leu2Δ0 lys2Δ0 ura3Δ0) VMA4-DHFR[F3]::HPH</i>	KD15.1 [125]
STV1 Prey (DHFR)	<i>BY4742 (MATa his3Δ1 leu2Δ0 lys2Δ0 ura3Δ0) STV1=DHFR[F3]::HPH</i>	KD16.1 [125]
VMA4 Prey Δvph1::URA3 (DHFR)	<i>BY4742 (MATa his3Δ1 leu2Δ0 lys2Δ0 ura3Δ0) VMA4-DHFR[F3]::HPH vph1Δ::URA3</i>	KD40.1 (This study)
VMA4 Prey ΔVMA2::URA3 (DHFR)	<i>BY4742 (MATa his3Δ1 leu2Δ0 lys2Δ0 ura3Δ0) VMA4-DHFR[F3]::HPH vma2Δ::URA3</i>	KD54.1 (This study)
VMA8 Prey (DHFR) ΔVMA2::URA3	<i>BY4742 (MATa his3Δ1 leu2Δ0 lys2Δ0 ura3Δ0) VMA8-DHFR[F3]::HPH vma2Δ::URA3</i>	KD56.1 (This study)
SOD1 Bait (DHFR) ΔVMA2::URA3	<i>BY4741 (MATa his3Δ1 leu2Δ0 met15Δ0 ura3Δ0) SOD1-DHFR[F1,2]::NAT vma2Δ::URA3</i>	KD57.1 (This study)
VMA2 Prey (DHFR) ΔVMA4::URA3	<i>BY4742 (MATa his3Δ1 leu2Δ0 lys2Δ0 ura3Δ0) VMA2-DHFR[F3]::HPH vma4Δ::URA3</i>	KD58.1 (This study)
SOD1 Bait (DHFR) ΔVMA4::URA3	<i>BY4741 (MATa his3Δ1 leu2Δ0 met15Δ0 ura3Δ0) SOD1-DHFR[F1,2]::NAT vma4Δ::URA3</i>	KD59.1 (This study)
VMA2 Prey (DHFR) ΔVPH1::URA3	<i>BY4742 (MATa his3Δ1 leu2Δ0 lys2Δ0 ura3Δ0) VMA2-DHFR[F3]::HPH vph1Δ::URA3</i>	KD21.2 (This study)

SOD1 Bait ΔVPH1::URA3 (DHFR)	<i>BY4741 (MATa his3Δ1 leu2Δ0 met15Δ0 ura3Δ0) SOD1-DHFR[F1,2]::NAT vpb1Δ::URA3</i>	KD32.2 (This study)
VMA8 Prey ΔVPH1::URA3 (DHFR)	<i>BY4741 (MATa his3Δ1 leu2Δ0 met15Δ0 ura3Δ0) VMA8-DHFR[F1,2]::HPH vpb1Δ::URA3</i>	KD33.2 (This study)
CNB1 Prey (DHFR)	<i>BY4742 (MATa his3Δ1 leu2Δ0 lys2Δ0 ura3Δ0) CNB1-DHFR[F3]::HPH</i>	Yeast Protein Interactome [125]
CMP2 Bait (DHFR)	<i>BY4741 (MATa his3Δ1 leu2Δ0 met15Δ0 ura3Δ0) CMP2-DHFR[F1,2]::NAT</i>	Yeast Protein Interactome [125]
CNA1 BAIT (DHFR)	<i>BY4741 (MATa his3Δ1 leu2Δ0 met15Δ0 ura3Δ0) CNA1-DHFR[F1,2]::NAT</i>	Yeast Protein Interactome [125]
CMP2 Prey (DHFR)	<i>BY4742 (MATa his3Δ1 leu2Δ0 lys2Δ0 ura3Δ0) CMP2-DHFR[F3]::HPH</i>	Yeast Protein Interactome [125]
CNA1 Prey (DHFR)	<i>BY4742 (MATa his3Δ1 leu2Δ0 lys2Δ0 ura3Δ0) CNA1-DHFR[F3]::HPH</i>	Yeast Protein Interactome [125]
EGO3 Prey (DHFR)	<i>BY4742 (MATa his3Δ1 leu2Δ0 lys2Δ0 ura3Δ0) EGO3-DHFR[F3]::HPH</i>	Yeast Protein Interactome [125]
ATP16 Prey (DHFR)	<i>BY4742 (MATa his3Δ1 leu2Δ0 lys2Δ0 ura3Δ0) ATP16-DHFR[F3]::HPH</i>	Yeast Protein Interactome [125]
ATP15 Prey (DHFR)	<i>BY4742 (MATa his3Δ1 leu2Δ0 lys2Δ0 ura3Δ0) ATP15-DHFR[F3]::HPH</i>	Yeast Protein Interactome [125]
ATP14 Prey (DHFR)	<i>BY4742 (MATa his3Δ1 leu2Δ0 lys2Δ0 ura3Δ0) ATP14-DHFR[F3]::HPH</i>	Yeast Protein Interactome [125]
ATP3 Prey (DHFR)	<i>BY4742 (MATa his3Δ1 leu2Δ0 lys2Δ0 ura3Δ0) ATP3-DHFR[F3]::HPH</i>	Yeast Protein Interactome [125]
ATP7 Prey (DHFR)	<i>BY4742 (MATa his3Δ1 leu2Δ0 lys2Δ0 ura3Δ0) ATP7-DHFR[F3]::HPH</i>	Yeast Protein Interactome [125]

RAV1 Prey (DHFR)	<i>BY4742 (MATa his3Δ1 leu2Δ0 lys2Δ0 ura3Δ0) RAV1-DHFR[F3]::HPH</i>	Yeast Protein Interactome [125]
SKP1 Prey (DHFR)	<i>BY4742 (MATa his3Δ1 leu2Δ0 lys2Δ0 ura3Δ0) SKP1-DHFR[F3]::HPH</i>	Yeast Protein Interactome [125]
RAV2 Prey (DHFR)	<i>BY4742 (MATa his3Δ1 leu2Δ0 lys2Δ0 ura3Δ0) RAV2-DHFR[F3]::HPH</i>	Yeast Protein Interactome [125]

Table 2.8 Diploid Strains.

Diploid strains in this table were constructed by mating haploid MAT α and MAT α cells together (2.2.3).

Strain	Genotype		Source
	MATα	MATα	
BY4743	<i>his3Δ1 leu2Δ0 LYS2 met15Δ0 ura3Δ0</i>	<i>his3Δ1 leu2Δ0 lys2Δ0 MET15 ura3Δ0</i>	CGY941 [145]
SOD1 Bait VMA8 Prey Δ stv1::URA3 (DHFR)	<i>(his3Δ1 leu2Δ0 LYS2 met15Δ0 ura3Δ0) SOD1-DHFR[F1,2]::NAT stv1Δ::URA3</i>	<i>(his3Δ1 leu2Δ0 lys2Δ0 MET15 ura3Δ0) VMA8-DHFR[F3]::HPH stv1Δ::URA3</i>	KD17.1 (This study)
SOD1 Bait VMA4 Prey Δ stv1::URA3 (DHFR)	<i>(his3Δ1 leu2Δ0 LYS2 met15Δ0 ura3Δ0) SOD1-DHFR[F1,2]::NAT stv1Δ::URA3</i>	<i>(his3Δ1 leu2Δ0 lys2Δ0 MET15 ura3Δ0) VMA4-DHFR[F3]::HPH stv1Δ::URA3</i>	KD18.1 (This study)
SOD1 Bait VMA2 Prey Δ stv1::URA3 (DHFR)	<i>(his3Δ1 leu2Δ0 LYS2 met15Δ0 ura3Δ0) SOD1-DHFR[F1,2]::NAT stv1Δ::URA3</i>	<i>(his3Δ1 leu2Δ0 lys2Δ0 MET15 ura3Δ0) VMA2-DHFR[F3]::HPH stv1Δ::URA3</i>	KD19.1 (This study)
SOD1 Bait VPH1 Prey (DHFR)	<i>(his3Δ1 leu2Δ0 LYS2 met15Δ0 ura3Δ0) SOD1-DHFR[F1,2]::NAT</i>	<i>(his3Δ1 leu2Δ0 lys2Δ0 MET15 ura3Δ0) VPH1-DHFR[F3]::HPH</i>	KD26.1 (This study)
SOD1 Bait TFP1 Prey (DHFR)	<i>(his3Δ1 leu2Δ0 LYS2 met15Δ0 ura3Δ0) SOD1-DHFR[F1,2]::NAT</i>	<i>(his3Δ1 leu2Δ0 lys2Δ0 MET15 ura3Δ0) TFP1-DHFR[F3]::HPH</i>	KD27.1 (This study)

SOD1 Bait TFP3 Prey (DHFR)	<i>(his3Δ1 leu2Δ0 LYS2 met15Δ0 ura3Δ0) SOD1-DHFR[F1,2]::NAT</i>	<i>(his3Δ1 leu2Δ0 lys2Δ0 MET15 ura3Δ0) TFP3-DHFR[F3]::HPH</i>	KD28.1 (This study)
SOD1 Bait PPA1 Prey (DHFR)	<i>(his3Δ1 leu2Δ0 LYS2 met15Δ0 ura3Δ0) SOD1-DHFR[F1,2]::NAT</i>	<i>(his3Δ1 leu2Δ0 lys2Δ0 MET15 ura3Δ0) PPA1-DHFR[F3]::HPH</i>	KD29.1 (This study)
SOD1 Bait VMA5 Prey (DHFR)	<i>(his3Δ1 leu2Δ0 LYS2 met15Δ0 ura3Δ0) SOD1-DHFR[F1,2]::NAT</i>	<i>(his3Δ1 leu2Δ0 lys2Δ0 MET15 ura3Δ0) VMA5-DHFR[F3]::HPH</i>	KD30.1 (This study)
SOD1 Bait VMA6 Prey (DHFR)	<i>(his3Δ1 leu2Δ0 LYS2 met15Δ0 ura3Δ0) SOD1-DHFR[F1,2]::NAT</i>	<i>(his3Δ1 leu2Δ0 lys2Δ0 MET15 ura3Δ0) VMA6-DHFR[F3]::HPH</i>	KD31.1 (This study)
SOD1 Bait VMA10 Prey (DHFR)	<i>(his3Δ1 leu2Δ0 LYS2 met15Δ0 ura3Δ0) SOD1-DHFR[F1,2]::NAT</i>	<i>(his3Δ1 leu2Δ0 lys2Δ0 MET15 ura3Δ0) VMA10-DHFR[F3]::HPH</i>	KD32.1 (This study)
SOD1 Bait VMA9 Prey (DHFR)	<i>(his3Δ1 leu2Δ0 LYS2 met15Δ0 ura3Δ0) SOD1-DHFR[F1,2]::NAT</i>	<i>(his3Δ1 leu2Δ0 lys2Δ0 MET15 ura3Δ0) VMA9-DHFR[F3]::HPH</i>	KD33.1 (This study)
SOD1 Bait VMA13 Prey (DHFR)	<i>(his3Δ1 leu2Δ0 LYS2 met15Δ0 ura3Δ0) SOD1-DHFR[F1,2]::NAT</i>	<i>(his3Δ1 leu2Δ0 lys2Δ0 MET15 ura3Δ0) VMA13-DHFR[F3]::HPH</i>	KD34.1 (This study)
SOD1 Bait STV1 Prey (DHFR)	<i>(his3Δ1 leu2Δ0 LYS2 met15Δ0 ura3Δ0) SOD1-DHFR[F1,2]::NAT</i>	<i>(his3Δ1 leu2Δ0 lys2Δ0 MET15 ura3Δ0) STV1-DHFR[F3]::HPH</i>	KD35.1 (This study)
SOD1 Bait VMA7 Prey (DHFR)	<i>(his3Δ1 leu2Δ0 LYS2 met15Δ0 ura3Δ0) SOD1-DHFR[F1,2]::NAT</i>	<i>(his3Δ1 leu2Δ0 lys2Δ0 MET15 ura3Δ0) VMA7-DHFR[F3]::HPH</i>	KD36.1 (This study)
SOD1 Bait VMA4 Prey Δvph1::URA3 (DHFR)	<i>(his3Δ1 leu2Δ0 LYS2 met15Δ0 ura3Δ0) SOD1-DHFR[F1,2]::NAT vph1Δ::URA3</i>	<i>(his3Δ1 leu2Δ0 lys2Δ0 MET15 ura3Δ0) VMA4-DHFR[F3]::HPH vph1Δ::URA3</i>	KD37.1 (This study)

SOD1 Bait VMA8 Prey Δvph1::URA3 (DHFR)	<i>(his3Δ1 leu2Δ0 LYS2 met15Δ0 ura3Δ0) SOD1- DHFR[F1,2]::NAT vph1Δ::URA3</i>	<i>(his3Δ1 leu2Δ0 lys2Δ0 MET15 ura3Δ0) VMA8- DHFR[F3]::HPH vph1Δ::URA3</i>	KD38.1 (This study)
SOD1 Bait VMA2 Prey Δvph1::URA3 (DHFR)	<i>(his3Δ1 leu2Δ0 LYS2 met15Δ0 ura3Δ0) SOD1- DHFR[F1,2]::NAT vph1Δ::URA3</i>	<i>(his3Δ1 leu2Δ0 lys2Δ0 MET15 ura3Δ0) VMA2- DHFR[F3]::HPH vph1Δ::URA3</i>	KD39.1 (This study)
SOD1 Bait VMA2 Prey Δvma4::URA3 (DHFR)	<i>(his3Δ1 leu2Δ0 LYS2 met15Δ0 ura3Δ0) SOD1- DHFR[F1,2]::NAT vma4Δ::URA3</i>	<i>(his3Δ1 leu2Δ0 lys2Δ0 MET15 ura3Δ0) VMA2- DHFR[F3]::HPH vma4Δ::URA3</i>	KD45.1 (This study)
SOD1 Bait VMA4 Prey Δvma2::URA3 (DHFR)	<i>(his3Δ1 leu2Δ0 LYS2 met15Δ0 ura3Δ0) SOD1- DHFR[F1,2]::NAT vma2Δ::URA3</i>	<i>(his3Δ1 leu2Δ0 lys2Δ0 MET15 ura3Δ0) VMA4- DHFR[F3]::HPH vma2Δ::URA3</i>	KD46.1 (This study)
SOD1 Bait VMA8 Prey Δvma2::URA3 (DHFR)	<i>(his3Δ1 leu2Δ0 LYS2 met15Δ0 ura3Δ0) SOD1- DHFR[F1,2]::NAT vma2Δ::URA3</i>	<i>(his3Δ1 leu2Δ0 lys2Δ0 MET15 ura3Δ0) VMA8- DHFR[F3]::HPH vma2Δ::URA3</i>	KD47.1 (This study)
SOD1 Bait VMA4 Prey (DHFR)	<i>(his3Δ1 leu2Δ0 LYS2 met15Δ0 ura3Δ0) SOD1- DHFR[F1,2]::NAT</i>	<i>(his3Δ1 leu2Δ0 lys2Δ0 MET15 ura3Δ0) VMA4- DHFR[F3]::HPH</i>	KD23.2 (This study)
SOD1 Bait VMA8 Prey (DHFR)	<i>(his3Δ1 leu2Δ0 LYS2 met15Δ0 ura3Δ0) SOD1- DHFR[F1,2]::NAT</i>	<i>(his3Δ1 leu2Δ0 lys2Δ0 MET15 ura3Δ0) VMA8- DHFR[F3]::HPH</i>	KD24.2 (This study)
SOD1 Bait VMA2 Prey (DHFR)	<i>(his3Δ1 leu2Δ0 LYS2 met15Δ0 ura3Δ0) SOD1- DHFR[F1,2]::NAT</i>	<i>(his3Δ1 leu2Δ0 lys2Δ0 MET15 ura3Δ0) VMA2- DHFR[F3]::HPH</i>	KD25.2 (This study)
CMP2 Bait CNB1 Prey (DHFR)	<i>(his3Δ1 leu2Δ0 LYS2 met15Δ0 ura3Δ0) CMP2- DHFR[F1,2]::NAT</i>	<i>(his3Δ1 leu2Δ0 lys2Δ0 MET15 ura3Δ0) CNB1- DHFR[F3]::HPH</i>	(This study)
CNA1 Bait CNB1 Prey (DHFR)	<i>(his3Δ1 leu2Δ0 LYS2 met15Δ0 ura3Δ0) CNA1- DHFR[F1,2]::NAT</i>	<i>(his3Δ1 leu2Δ0 lys2Δ0 MET15 ura3Δ0) CNB1- DHFR[F3]::HPH</i>	(This study)

SOD1 Bait CNB1 Prey	<i>(his3Δ1 leu2Δ0 LYS2 met15Δ0 ura3Δ0) SOD1-DHFR[F1,2]::NAT</i>	<i>(his3Δ1 leu2Δ0 lys2Δ0 MET15 ura3Δ0) CNB1-DHFR[F3]::HPH</i>	(This study)
SOD1 Bait CMP2 Prey	<i>(his3Δ1 leu2Δ0 LYS2 met15Δ0 ura3Δ0) SOD1-DHFR[F1,2]::NAT</i>	<i>(his3Δ1 leu2Δ0 lys2Δ0 MET15 ura3Δ0) CMP2-DHFR[F3]::HPH</i>	(This study)
SOD1 Bait CNA1 Prey	<i>(his3Δ1 leu2Δ0 LYS2 met15Δ0 ura3Δ0) SOD1-DHFR[F1,2]::NAT</i>	<i>(his3Δ1 leu2Δ0 lys2Δ0 MET15 ura3Δ0) CNA1-DHFR[F3]::HPH</i>	(This study)
SOD1 Bait EGO3 Prey	<i>(his3Δ1 leu2Δ0 LYS2 met15Δ0 ura3Δ0) SOD1-DHFR[F1,2]::NAT</i>	<i>(his3Δ1 leu2Δ0 lys2Δ0 MET15 ura3Δ0) EGO3-DHFR[F3]::HPH</i>	(This study)
SOD1 BAIT ATP16 Prey	<i>(his3Δ1 leu2Δ0 LYS2 met15Δ0 ura3Δ0) SOD1-DHFR[F1,2]::NAT</i>	<i>(his3Δ1 leu2Δ0 lys2Δ0 MET15 ura3Δ0) ATP16-DHFR[F3]::HPH</i>	(This study)
CNB1 Bait VMA2 Prey	<i>(his3Δ1 leu2Δ0 LYS2 met15Δ0 ura3Δ0) CNB1-DHFR[F1,2]::NAT</i>	<i>(his3Δ1 leu2Δ0 lys2Δ0 MET15 ura3Δ0) VMA2-DHFR[F3]::HPH</i>	(This study)
CMP2 Bait VMA2 Prey	<i>(his3Δ1 leu2Δ0 LYS2 met15Δ0 ura3Δ0) CMP2-DHFR[F1,2]::NAT</i>	<i>(his3Δ1 leu2Δ0 lys2Δ0 MET15 ura3Δ0) VMA2-DHFR[F3]::HPH</i>	(This study)
CNA1 Bait VMA2 Prey	<i>(his3Δ1 leu2Δ0 LYS2 met15Δ0 ura3Δ0) CNA1-DHFR[F1,2]::NAT</i>	<i>(his3Δ1 leu2Δ0 lys2Δ0 MET15 ura3Δ0) VMA2-DHFR[F3]::HPH</i>	(This study)
CNB1 Bait VMA4 Prey	<i>(his3Δ1 leu2Δ0 LYS2 met15Δ0 ura3Δ0) CNB1-DHFR[F1,2]::NAT</i>	<i>(his3Δ1 leu2Δ0 lys2Δ0 MET15 ura3Δ0) VMA4-DHFR[F3]::HPH</i>	(This study)
CMP2 Bait VMA4 Prey	<i>(his3Δ1 leu2Δ0 LYS2 met15Δ0 ura3Δ0) CMP2-DHFR[F1,2]::NAT</i>	<i>(his3Δ1 leu2Δ0 lys2Δ0 MET15 ura3Δ0) VMA4-DHFR[F3]::HPH</i>	(This study)
CNA1 Bait VMA4 Prey	<i>(his3Δ1 leu2Δ0 LYS2 met15Δ0 ura3Δ0) CNA1-DHFR[F1,2]::NAT</i>	<i>(his3Δ1 leu2Δ0 lys2Δ0 MET15 ura3Δ0) VMA4-DHFR[F3]::HPH</i>	(This study)

Chapter 2. Materials and Methods

CNB1 Bait VMA8 Prey	<i>(his3Δ1 leu2Δ0 LYS2 met15Δ0 ura3Δ0) CNB1-DHFR[F1,2]::NAT</i>	<i>(his3Δ1 leu2Δ0 lys2Δ0 MET15 ura3Δ0) VMA8-DHFR[F3]::HPH</i>	(This study)
CMP2 Bait VMA8 Prey	<i>(his3Δ1 leu2Δ0 LYS2 met15Δ0 ura3Δ0) CMP2-DHFR[F1,2]::NAT</i>	<i>(his3Δ1 leu2Δ0 lys2Δ0 MET15 ura3Δ0) VMA8-DHFR[F3]::HPH</i>	(This study)
CNA1 Bait VMA8 Prey	<i>(his3Δ1 leu2Δ0 LYS2 met15Δ0 ura3Δ0) CNA1-DHFR[F1,2]::NAT</i>	<i>(his3Δ1 leu2Δ0 lys2Δ0 MET15 ura3Δ0) VMA8-DHFR[F3]::HPH</i>	(This study)
SOD1 Bait ATP15 Prey	<i>(his3Δ1 leu2Δ0 LYS2 met15Δ0 ura3Δ0) SOD1-DHFR[F1,2]::NAT</i>	<i>(his3Δ1 leu2Δ0 lys2Δ0 MET15 ura3Δ0) ATP15-DHFR[F3]::HPH</i>	(This study)
SOD1 Bait ATP14 Prey	<i>(his3Δ1 leu2Δ0 LYS2 met15Δ0 ura3Δ0) SOD1-DHFR[F1,2]::NAT</i>	<i>(his3Δ1 leu2Δ0 lys2Δ0 MET15 ura3Δ0) ATP14-DHFR[F3]::HPH</i>	(This study)
SOD1 Bait ATP13 Prey	<i>(his3Δ1 leu2Δ0 LYS2 met15Δ0 ura3Δ0) SOD1-DHFR[F1,2]::NAT</i>	<i>(his3Δ1 leu2Δ0 lys2Δ0 MET15 ura3Δ0) ATP3-DHFR[F3]::HPH</i>	(This study)
SOD1 Bait ATP7 Prey	<i>(his3Δ1 leu2Δ0 LYS2 met15Δ0 ura3Δ0) SOD1-DHFR[F1,2]::NAT</i>	<i>(his3Δ1 leu2Δ0 lys2Δ0 MET15 ura3Δ0) ATP7-DHFR[F3]::HPH</i>	(This study)
SOD1 Bait RAV1 Prey	<i>(his3Δ1 leu2Δ0 LYS2 met15Δ0 ura3Δ0) SOD1-DHFR[F1,2]::NAT</i>	<i>(his3Δ1 leu2Δ0 lys2Δ0 MET15 ura3Δ0) RAV1-DHFR[F3]::HPH</i>	(This study)
SOD1 Bait SKP1 Prey	<i>(his3Δ1 leu2Δ0 LYS2 met15Δ0 ura3Δ0) SOD1-DHFR[F1,2]::NAT</i>	<i>(his3Δ1 leu2Δ0 lys2Δ0 MET15 ura3Δ0) SKP1-DHFR[F3]::HPH</i>	(This study)
SOD1 Bait RAV2 Prey	<i>(his3Δ1 leu2Δ0 LYS2 met15Δ0 ura3Δ0) SOD1-DHFR[F1,2]::NAT</i>	<i>(his3Δ1 leu2Δ0 lys2Δ0 MET15 ura3Δ0) RAV2-DHFR[F3]::HPH</i>	(This study)

2.2.3 Yeast mating of haploid strains

To construct the diploid strains used in this study (Table 2.8), simple mating of *MATa* and *MAT α* cells was performed. A colony of *MATa* cells was dotted onto a YPD-agar plate and then a colony of *MAT α* cells was dotted onto the YPD agar plate where the *MATa* cells were and both cells were mixed together. The YPD-agar plate was incubated overnight at 30 °C. The following day, cells were streaked onto appropriate selective agar media (to select for diploids) and incubated for 2–3 d at 30 °C.

2.3 Molecular Biology methods

2.3.1 Plasmids used in this study

Table 2.9 Plasmids used in this study.

Name	Backbone	Function	Insert	Yeast selective marker	Source
pUKC2803	pDONR201	Entry Vector	Yeast SOD1	NA	pUKC collection [115]
pUKC 2804	pDONR201	Entry Vector	Yeast SOD1-A4V	NA	pUKC collection [115]
pUKC 2805	pDONR201	Entry Vector	Yeast SOD1-G37R	NA	pUKC collection [115]
pUKC 2806	pDONR201	Entry Vector	Yeast SOD1-H48Q	NA	pUKC collection [115]
pUKC 2807	pDONR201	Entry Vector	Yeast SOD1-G93A	NA	pUKC collection [115]
pUKC 2808	pDONR201	Entry Vector	Yeast SOD1-S134N	NA	pUKC collection [115]
pUKC 2809	pAG425	Expression Vector	Yeast SOD1	<i>LEU2</i>	pUKC collection [115]
pUKC 2810	pAG425	Expression Vector	Yeast SOD1-A4V	<i>LEU2</i>	pUKC collection [115]

pUKC 2812	pAG425	Expression Vector	Yeast SOD1-H48Q	<i>LEU2</i>	pUKC collection [115]
pUKC 2813	pAG425	Expression Vector	Yeast-SOD1-G93A	<i>LEU2</i>	pUKC collection [115]
pUKC 3219	pAG425	Expression Vector	Yeast SOD1 fragment 1-115	<i>LEU2</i>	pUKC collection [115]
pUKC 3220	pAG425	Expression Vector	Yeast SOD1 fragment 1-125	<i>LEU2</i>	pUKC collection [115]
pAG306-GPD-ccdB chrI	pAG306	Destination vector	ccdB	<i>URA3</i>	Addgene[144]
pAG306-GPD-SOD1- chr I	pAG306	Expression Vector	Yeast Sod1	<i>URA3</i>	Constructed in this study
pAG306-GPD-SOD1-G37R chr I	pAG306	Expression Vector	Yeast Sod1 G37R	<i>URA3</i>	Constructed in this study
pAG306-GPD-SOD1-S134N chr I	pAG306	Expression Vector	Yeast Sod1 S134N	<i>URA3</i>	Constructed in this study
pAG306-GPD-SOD1-H48Q chr I	pAG306	Expression Vector	Yeast Sod1 H48Q	<i>URA3</i>	Constructed in this study
pAG306-GPD-SOD1-G93A chr I	pAG306	Expression Vector	Yeast Sod1 G93A	<i>URA3</i>	Constructed in this study
pAG306-GPD-SOD1-A4V chr I	pAG306	Expression Vector	Yeast Sod1 A4V	<i>URA3</i>	Constructed in this study
pAG306-GPD-SOD1-Empty chr I	pAG306	Expression Vector	Empty	<i>URA3</i>	Addgene [144]
pML104 (CRISPR)	pRSII426	Expression Vector	Cas9	<i>URA3</i>	Gift from Dr Tobias von der Haar [146]

pML104-SOD1-G37R (CRISPR)	pRSII426	Expression Vector	Cas9 & sgRNA (targeting G37R)	<i>URA3</i>	Constructed in this study
pML104-SOD1-H48Q (CRISPR)	pRSII426	Expression Vector	Cas9 & sgRNA (targeting H48Q)	<i>URA3</i>	Constructed in this study
pML104-SOD1-A4V (CRISPR)	pRSII426	Expression Vector	Cas9 & sgRNA (targeting A4V)	<i>URA3</i>	Constructed in this study
pAMs366 4x-CDRE-GFP-URA3	pAMS366	Yeast Reporter Plasmid	4xCDRE-CYC1(PM)-yeGFP	<i>URA3</i>	Addgene [147]
pKA150 pFA6-3xHA-HIS3MX6	pFA6a	Yeast Genomic Targeting (3×HA)	His3	<i>HIS3</i>	CWG plasmid collection [148]
pKA149 pFA6-GFP(S65T)-HIS3MX6	pFA6a	Yeast Genomic Targeting (GFP(S65T))	His3	<i>HIS3</i>	CWG plasmid collection [148]
pUG27	pFA6a	loxP flanked marker gene deletion cassette	His5	<i>HIS5</i>	CWG plasmid collection [149]
pUG72	pFA6a	loxP flanked marker gene deletion cassette	Ura3	<i>URA3</i>	CWG plasmid collection [149]
pUG73	pFA6a	loxP flanked marker gene deletion cassette	Leu2	<i>LEU2</i>	CWG plasmid collection [149]
pSH47	p416	Cre recombinase expression vector	<i>GAL1-cre</i>	<i>URA3</i>	CWG plasmid collection [149]
pKA449	YEP13	Expression Vector	PDE2 + promoter	<i>LEU2</i>	CWG plasmid collection [150]

2.3.2 Oligonucleotides

Table 2.10 Oligonucleotides used in this study.

Name	Sequence (5'–3')	Function
KDOligoF1	GATCTCAAGCAGTCGCA GTGTTAAGTTTTAGAGC TAG	Cloning of A4V sgRNA sequence in pML104
KDOligoR1	CTAGCTCTAAAACCTTAA CACTGCGACTGCTTGA	Cloning of A4V sgRNA sequence in pML104
KDg104check1	CGCCACCCTCATCCACC AGAGCATC	Use in combination with Forward primer for pML104 sgRNA cloning for PCR confirmation
KDRepairtemp01	AAAACATAATTAATTTA TAATGGTTCAAGTAGTC GCAGTGTTAAAAGGTG ATGCCGGTGTCTCTGGT GTTGTCAAGTTCGAACA GGCTTCC	Repair template designed to introduce the A4V mutation in yeast SOD1
KDrepairtemp3	CAATCGCGCAAACAAAT AAAACATAATTAATTTA TAATGGTTCAAGTAGTA GCCGUCTTGAAGGGTG ATGCCGGTGTCTCTGGT GTTGTCAAGTTCGAACA GGCTTCCG	Repair template designed to introduce the A4V mutation in yeast <i>SOD1</i>
G37R g1 fwd	GATCACAGTCCTAACGC AGAACGTGTTTAGAGC TAG	Cloning of G37R sgRNA sequence in pML104
G37R g1 rev	CTAGCTCTAAAACACGT TCTGCGTTAGGACTGT	Cloning of G37R sgRNA sequence in pML104

G37R repair 1	TTCGAACAGGCTTCCGA ATCCGAGCCAACCACTG TCTCTTACGAGATCGCT CGAAACAGTCCTAACGC AGAACGTGGCTTCCACA TTCATGAGTTTGGAGAT GCC	Repair template designed to introduce the G37R mutation in yeast <i>SOD1</i>
H48R g1 fwd	GATCGAGTTTGGAGAT GCCACCAAGTTTATAGAG CTAG	Cloning of H48R sgRNA sequence in pML104
H48R g1 rev	CTAGCTCTAAAACCTTGG TGGCATCTCCAAACTC	Cloning of H48R sgRNA sequence in pML104
H48R repair 1	TCTTACGAGATCGCTGG TAACAGTCCTAACGCAG AACGTGGGTTCACATT CAGGAGTTTGGCGATG CAACCAATGGTTGTGTC TCTGCTGGTCCTCACTT CAAT	Repair template designed to introduce the G37R mutation in yeast <i>SOD1</i>
Amp-R	ATAATACCGCGCCACAT AGC	Amplifies a region of the AmpR gene
ChrIrev	CAGTCGTCCGTAGCAAA GC	Amplifies a region inside the pAG306 chrI plasmid
ChrIrev2	GAAGGATAGTTCGAAG CTCGC	Amplifies a region in chrI in <i>S. cerevisiae</i> upstream of pAG306 integration
Sod1KOfwd	AACAGGCAAGAAAGCA ATCGCGCAAACAATAA AACATAATTAATTATA CAGCTGAAGCTTCGTAC GC	Fwd primer for <i>SOD1</i> deletion cassette using pUG plasmids

Sod1KOrev	CTTACTACTTACTTACAT ACGGTTTTTATTCAAGT ATATTATCATTAACAGC ATAGGCCACTAGTGGAT CTG	Rev primer for <i>SOD1</i> deletion cassette using pUG plasmids
Sod1KOcheck	CGGTGTGTCGGAATTA GTAAGCGG	Upstream check primer for <i>SOD1</i> deletion
VMA2KOfwd	TTGTAAGAGTAGACAGT ACATCAAGCGAAAATAA ATATTGCAGGACAGCTG AAGCTTCGTACGC	Fwd primer for <i>VMA2</i> deletion cassette using pUG plasmids
VMA2KOrev	AAACGGACAAAATAAAA AAAGCCTTTTTCTTCAG CAACCGTCCTC GCATAGGCCACTAGTG GATCTG	Rev primer for <i>VMA2</i> deletion cassette using pUG plasmids
VMA2 WT CHK F	CTGGTAGACCCATTGAC AAC	Fwd primer to check for presence of <i>VMA2</i>
VMA2 3'UTR CHK R	GTGCTGATGTTCTTCGA GAC	Rev primer to check for presence of <i>VMA2</i>
VMA4KOfwd	ACTGTTTACAAAAGAG GCACAGAACAGGCCAC GCACCATCCGATACAGC CAGCTGAAGCTTCGTAC GC	Fwd primer for <i>VMA4</i> deletion cassette using pUG plasmids
VMA4KOrev	TCTGTTAGGAGTGTATA TGTAAGTATGTAGGTAT ACAAGCTGCTGGTCGA GCATAGGCCACTAGTG GATCTG	Rev primer for <i>VMA4</i> deletion cassette using pUG plasmids

VMA4Kocheck	GGCCATTTTCGATAAGAA CTC	Upstream check primer for <i>VMA4</i> deletion
Kdforwardstv1del	CAACAGACGCATTTCTTA TTCTCTAAAATTCCTCGA GTTATATGAATAATTCA GCTGAAGCTTCGTACGC	Fwd primer for <i>STV1</i> deletion cassette using pUG plasmids
Kdrevstv1del	AACGAAAAAAGCAGTG GGTAGATGAGAAAATT TACAGTAATTTAAGGTT AGCATAGGCCACTAGTG GATCTG	Rev primer for <i>STV1</i> deletion cassette using pUG plasmids
Kdctrlfwdstv1	CGAGAGGCCGGGAGCTG GCTC	Upstream check primer for <i>STV1</i> deletion
Kdfwdvph1del	TTTTAATTTGAATCAAA AAAAAACATTTAAAGG TTACACAAGGAAAATAC AGCTGAAGCTTCGTACG C	Fwd primer for <i>VPH1</i> deletion cassette using pUG plasmids
KdrevVph1del	TATTTAATGAAGTACTT AAATGTTTCGCTTTT AAAAGTCCTCAAAATGC ATAGGCCACTAGTGGAT CTG	Rev primer for <i>VPH1</i> deletion cassette using pUG plasmids
Kdctrlfwdvph1	CGGTATCTTCCCTCAAA GAC	Upstream check primer for <i>VPH1</i> deletion
sod1upstreamfwd2	AAACAGGCAAGAAAGC AATCG	Upstream primer for sanger sequencing of <i>SOD1</i> in 5' to 3' direction

sod1downstreamrev2	GCGCTTACTACTTACTT ACATACG	Downstream primer for sanger sequencing of <i>SOD1</i> in 3' to 5' direction
Sod1fwdTagpFA6	CGGTCCAAGACCAGCCT GTGGTGTTCATTGGTCTA ACCAACCGGATCCCCGG GTTAATTAA	Fwd primer for C-terminal tagging of <i>SOD1</i> using the pFA6a plasmid
Sod1revtagpFA6	ACTTACATACGGTTTTT ATTCAAGTATATTATCA TTAACAGAATTCGAGCT CGTTTAAAC	Rev primer for C-terminal tagging of <i>SOD1</i> using the pFA6a plasmid
sod1fwdchecktag	GTGTCTCTGCTGGTCCT CAC	Fwd check primer for <i>SOD1</i> pFA6a tagging
vma2pFa6Hafwdtag	CGGTAAGAAGAAGGAC GCCAGCCAAGAAGAATC TCTAATCCGGATCCCCG GGTTAATTAA	Fwd primer for C-terminal tagging of <i>VM42</i> using the pFA6a plasmid
vma2pFa6Harevtag	GACAAAATAAAAAAAGC CTTTTCTTCAGCAACC GTCCTCGAATTCGAGCT CGTTTAAAC	Rev primer for C-terminal tagging of <i>VM42</i> using the pFA6a plasmid
cnb13hafwdcheck	GACGATGAACAGCTGC AACA	Fwd check primer for <i>CNB1</i> pFA6a tagging
cnb13Hafwd	CACAGAAGTGGCCAAG AGTCTGACATTGCAATA CGATGTGCGGATCCCCG GGTTAATTAA	Fwd primer for C-terminal tagging of <i>CNB1</i> using the pFA6a plasmid
cnb1koctermrev	AATATTGGCATAACATA AATGAATGAAGTGTCCC	Rev primer for C-terminal tagging of <i>CNB1</i> using the pFA6a plasmid

	CTAGTCGAATTCGAGCT CGTTTAAAC	
3hactermcheckrev	GATCTGCCGGTAGAGG TGTG	Rev primer for check PCR for pFA6a plasmid tagging
vma83hafwdtag	TGAAACATTGGTTGCTG ATCAAGAAGACGATGTT ATATTCCGGATCCCCGG GTTAATTAA	Fwd primer for C-terminal tagging of <i>VM48</i> using the pFA6a plasmid
vma83harevtag	CTTACATATTTTGGAAA AGGGTCTTGTTCTGCCT GAAACTGAATTCGAGCT CGTTTAAAC	Rev primer for C-terminal tagging of <i>VM48</i> using the pFA6a plasmid
vma83hafwdcheck	AGTGAGTTGGATGAGT TGGACA	Fwd check primer for <i>VM48</i> pFA6a tagging
vma43harevtag	GTGTATATGTAAGTATG TAGGTATAACAAGCTGCT GGTCGAGAATTCGAGC TCGTTTAAAC	Rev primer for C-terminal tagging of <i>VM44</i> using the pFA6a plasmid
vma43hafwd	GGAATTGTATGGTCCTT CCAAGACAAGAAAGTTC TTTGATCGGATCCCCGG GTTAATTAA	Fwd primer for C-terminal tagging of <i>VM44</i> using the pFA6a plasmid
vma43hafwdcheck	CAACAACCGGGACGAG TACA	Fwd check primer for <i>VM44</i> pFA6a tagging
KDSOD1PCRamplifyFprime r	GAAGATGGTTTGGGC AAATG	Fwd primer for amplifying <i>SOD1</i> in <i>S. cerevisiae</i>
KDSOD1PCRamplifyRprime r	GGACATAAATCTAAGCG AGGG	Rev primer for amplifying <i>SOD1</i> in <i>S. cerevisiae</i>

2.3.3 Preparation of chemically competent *E. coli* cells

10 ml of LB media was inoculated with a colony of DH5- α grown on solid LB media. This culture was grown overnight at 37 °C with aeration and 200 rpm shaking. The next morning, 28 ml of LB media was inoculated with 8 μ l of the overnight culture, and grown at 37 °C, 180 rpm until an OD₆₀₀ of 0.5–0.7 was reached (4.5 h). 3.75 ml of 100% glycerol (pre-warmed to 37 °C) was then added to the 28 ml culture (final glycerol concentration of 11.81%). Culture was then chilled on ice for 10 min. Cells were then pelleted (4000 rpm, 4 °C). Cells were then resuspended in 30 ml of ice-cold 0.1 M MgCl₂, 15% glycerol solution. Cells were then pelleted (3800 rpm, 4 °C), resuspended in 6.25 ml of ice-cold T-salts buffer (75 mM CaCl₂, 6 mM MgCl₂, 15% glycerol) and incubated on ice for 20 min with occasional mixing. Cells were then pelleted (3600 rpm, 4 °C) and resuspended in 1.25 ml of ice-cold T-salts buffer. Resuspended cells were then aliquoted (50 μ l) into pre-cooled sterile Eppendorfs and immediately stored at -80 °C.

2.3.4 Bacterial transformation of *E. coli* cells

The bacterial transformation protocol from Addgene was used for transformation of foreign DNA into *E. coli* cells (<https://www.addgene.org/protocols/bacterial-transformation/>). Chemically competent DH5 α cells (prepared with this method (2.3.3)), were thawed on ice for 20–30 min. 10 pg–100 μ g of DNA were then added to 25–50 μ l of competent cells and gently mixed (no vortexing). The competent cell / DNA mixture was then incubated on ice for 20 min. The competent cells / DNA mixture was then heat shocked in a water bath set to 42 °C for 45 seconds. The tubes were then chilled on ice for 2 min. 1 ml of LB media was then added to the competent cells / DNA mixture and the tubes were incubated at 37 °C for 45 min. 200 μ l – 1000 μ l (depending on expected transformation efficiency. Intact plasmids have higher efficiencies than ligation reactions) of the mixture was then plated onto an LB agar plate containing the appropriate antibiotic for plasmid selection. Plates were then incubated at 37 °C overnight.

2.3.5 High efficiency yeast transformation using the LiAc/SS carrier DNA/PEG method

The high efficiency yeast transformation protocol [151], was used for transforming integration vectors, gene deletion cassettes and C-terminal tagging cassettes into *S. cerevisiae*. 5 ml of YPD media was inoculated with the *S. cerevisiae* cells required for transformation and grown overnight at 30 °C, 180 rpm with aeration. The next day, 20 ml of 2 \times YPD was inoculated to 0.1 OD₆₀₀ with the cells from the overnight and grown to an OD₆₀₀ of 0.7–1. Cells were then pelleted

(10,000 × *g* for 30 seconds) and resuspended in LiAc/SSDNA/PEG transformation mix (Table 2.11). Cells were then heat shocked at 42 °C for 40 min in a water bath. Cells were then pelleted (10,000 × *g* for 30 seconds), resuspended in 200 µl sterile H₂O and plated onto the appropriate medium for auxotrophic or antibiotic selection. Plates were incubated at 30 °C for 3–4 d and the colonies were then re-streaked onto the same selective media and grown for 2–3 d before further use.

Table 2.11 LiAc/SSDNA/PEG transformation mix.

Volume (µl)	Component
240	50% (w/v) PEG 3350
36	1 M LiAc
10	10 mg/ml Single stranded carrier DNA
variable	Plasmid DNA
To 360 µl final volume	Sterile H ₂ O

2.3.6 Quick & easy LiAc/SS carrier DNA/PEG yeast transformation

The quick & easy yeast transformation method [151], was used for transformation of *S. cerevisiae* with intact plasmids that do not require a high transformation efficiency. The method is the same as that of the high efficiency protocol (2.3.5), except that instead of using cells grown to mid-log phase (OD₆₀₀ 0.7–1), 750 µl of cells from a fresh overnight were used.

2.3.7 One-step yeast transformation protocol

The one-step yeast transformation protocol [152] was used for the CRISPR/Cas9 gene editing transformations in order to follow the exact protocol [146]. 2.5 × 10⁸ cells /ml (or 125–250 µl) from a yeast overnight in YPD were pelleted (10,000 × *g* for 30 seconds) and resuspended in 100 µl of one-step transformation mix (Table 2.12). Cells were then heat shocked at 45 °C for 30 min in a water bath. Cells were then plated directly onto the appropriate selective media.

Table 2.12 One-step transformation mix.

Volume (µl)	Component	Final Concentration
5	4 M LiAc	0.2 M
60	50% PEG 3350	30%

10	1 M DTT	100 μ M
5	10 mg/ml Single stranded carrier DNA	0.5 mg/ml
Variable	Plasmid DNA	
To 100 μ l final volume	Sterile H ₂ O	

2.3.8 Colony PCR from *E. coli* cells.

Colony PCR was performed in this study to verify that resulting colonies from a bacterial transformation contained the desired plasmid. 5–10 colonies were streaked out onto a fresh LB-amp plate and grown overnight at 37 °C. The next day, the 5–10 colonies that were streaked out were picked and resuspended in 10 μ l sterile mqH₂O. 1–2 μ l of the water with bacterial cells resuspended in it were used as a template for a PCR reaction (2.3.16) with appropriate primers to check for presence of the desired plasmid.

2.3.9 Quick genomic DNA extraction from *S. cerevisiae*

A freshly grown colony of *S. cerevisiae* was picked using a sterile pipette tip and resuspended in 20 μ l 0.02 M sodium hydroxide (NaOH). The mixture was then placed on a heat block pre-heated to 95 °C for 10 min . The mixture was then placed on ice for 10 min . Cells were then pelleted (2,000 $\times g$ for 5 min) and 1 μ L of supernatant was used as a template for PCR analysis.

2.3.10 LiAc/SDS based genomic DNA extraction from *S. cerevisiae*

A freshly grown colony was picked and resuspended in 100 μ l of 200 mM LiAc, 1% SDS solution and incubated at 70 °C for 5 min on a pre-heated heat block [153].300 μ l of 96–100% ethanol was added and then the mixture was vortexed and centrifuged to precipitate DNA (15,000 $\times g$ for 3 min). The DNA pellet was washed with 70% ethanol. The pellet was then dissolved in 100 μ l TE buffer and then the cell debris was pelleted (15,000 $\times g$ for 15 seconds). 1 μ l of supernatant was used as a template for PCR analysis.

2.3.11 Purification of plasmids from *E. coli*

Plasmids were purified from *E. coli* cells using the QIAprep Spin Miniprep Kit (Cat. No. / ID: 27106X4). 5 ml of LB media containing the appropriate antibiotic was inoculated with a colony of *E. coli* harbouring the desired plasmid (grown on solid LB agar containing the appropriate antibiotic) and grown at 37°C overnight at 200 rpm with aeration. Plasmids were extracted from *E. coli* cells following the manufacturer's instructions.

2.3.12 Quantification and purity analysis of DNA

In order to quantify the concentration of DNA samples, the absorbance at 260 nm (A_{260}) was measured. This is due to the relationship that for DNA, A_{260} of 1 = 50 $\mu\text{g}/\text{ml}$. In order to determine the purity of DNA samples the ratio between A_{260}/A_{280} was calculated to check for contamination with reagents from the extraction such as guanidine or residual phenol, with a good ratio being between 1.7–2. The ratio between A_{260}/A_{230} was calculated to check for organic compound or chaotropic salt contamination with a good value being > 1.5 .

To measure absorbance values of DNA, BMG LABTECH LVis Plates were used. 2 μl of DNA samples (obtained in 2.3.11: Purification of plasmids from *E. coli*), and 2 μl of elution buffer (as a control) were pipetted onto the wells of the LVis plate. The plate was placed in the SpectroStar Omega (BMG Labtech, UK) plate reader and an absorbance spectrum from 230–320 nm was measured.

Equation to calculate DNA concentration from A_{260} :

$$\text{Concentration } (\mu\text{g}/\text{ml}) = (A_{260}) \times \text{dilution factor} \times 50 \mu\text{g}/\text{ml}$$

2.3.13 DNA gel electrophoresis

For all DNA gel electrophoresis carried out in this study, an agarose concentration of 0.8–1% was used. Agarose powder was weighed out in a glass conical flask and 1 \times TAE buffer (40 mM Tris-base, 20 mM Acetic acid, 1 mM EDTA) was added. The agarose in 1 \times TAE was heated in a microwave on full power for 1–2 min until the agarose was fully dissolved. The mixture was allowed to cool at 25 $^{\circ}\text{C}$ for five min before adding Ethidium Bromide to a final concentration of 0.5 $\mu\text{g}/\text{ml}$ in order to visualise the DNA. The mixture was poured into a gel forming cassette, and a comb was inserted. A volume of 25 ml being used for a small agarose gel and 50 ml for a large gel. The gel was left to set for 30–45 min. Once set, the gel was placed in an electrophoresis tank, and the tank was filled with 1 \times TAE buffer until the gel was completely submerged. DNA Ladder 1 Kb Plus (Invitrogen, CAT no: 11578636) was used as a size marker following the manufacturer's instructions. 10 \times BlueJuice Gel Loading Buffer (Invitrogen, CAT no: 11578636) was used as the sample loading dye. Electrophoresis was carried out at 110 V for 25 min (or until the DNA ladder was sufficiently separated). The agarose gel was visualised using the SYNGENE G:BOX gel doc system. The GeneSys software (V 1.6.5.0) along with a synoptics 6 MP camera were used to capture images of DNA agarose gels.

2.3.14 DNA sequencing

In order to confirm the construction of various plasmids and strains in this study, plasmid and genomic DNA were sent to Eurofins Genomics (<https://eurofinsgenomics.eu/>) using the Lightrun tube barcode service for sanger sequencing. Samples were prepared as per the manufacturer's instructions (Table 2.13). For plasmids, samples extracted using the method in (2.3.11) were used. For sequencing of pcr products, samples obtained from PCR were first purified using the QIAquick PCR Purification Kit (Cat. No. / ID: 28104) before sending for sanger sequencing.

Table 2.13 Mix for sanger sequencing of plasmid DNA.

Concentration	Component
50-100 ng/ μ l (plasmid)	Purified DNA
1 ng/ μ l (150–300 bp pcr product)	
5 ng/ μ l (300–1000 bp pcr product)	
10 ng/ μ l (1000–3000 bp pcr product)	
5 μ M	Sequencing primer
To 10 μ l final volume	Sterile mqH ₂ O

2.3.15 Frozen Glycerol stock preparation of yeast and bacterial strains

To make glycerol stocks for *S. cerevisiae* cells, cells were grown overnight in 3 ml of either YPD or appropriate selective media (for plasmid selection) at 30 °C, 180 rpm with aeration. The next day, 750 μ l of overnight was mixed with 750 μ l of 40% (w/v) sterile glycerol in a cryotube. The samples were then frozen at -80 °C.

To make glycerol stocks for *E. coli* cells, cells were grown overnight in 3 ml of LB media containing the appropriate antibiotic at 37 °C, 180 rpm with aeration. The next day, 750 μ l of overnight was mixed with 750 μ l of 40% (w/v) sterile glycerol in a cryotube. The samples were then frozen at -80 °C.

2.3.16 Polymerase chain reaction using recombinant *Taq* DNA polymerase

All polymerase chain reactions (PCR) in this study were carried out using Invitrogen recombinant *Taq* DNA polymerase (Cat no: 10342053). PCR was carried out for various uses, including confirmation of the presence of plasmids in cells, confirmation of gene deletion or

tagging, confirmation of correct integration of plasmids and amplification of DNA cassettes for gene tagging or deletion. Mixtures for PCR reaction (Table 2.14) and thermocycler conditions (Table 2.15) were carried out according to the manufacturer's instructions. Annealing temperatures of primers were calculated using the online tool provided by Promega (<https://www.promega.com/resources/tools/biomath/tm-calculator/>). The extension time calculate as 90 s/kb for complex templates (genomic DNA) and 60 s/kb for simple templates such as plasmids.

Table 2.14 PCR reaction mix.

Component	Final Concentration	Volume (μ l) for 50 μ l reaction
10X PCR Buffer, -Mg	1X	5
50 mM MgCl ₂	1.5 mM	1.5
10 mM dNTP Mix	0.2 mM	1
10 μ M Forward primer	0.5 μ M	2.5
10 μ M Reverse primer	0.5 μ M	2.5
Template DNA	1-500 ng	Variable
Sterile mqH ₂ O	Up to desired final volume	To 50 μ l
<i>Taq</i> DNA Polymerase (5 U/ μ l)	1 U / 50 μ l reaction	0.2

Table 2.15 *Taq* Polymerase thermocycler steps.

Step	Temperature ($^{\circ}$ C)	Time
Initial Denaturation	94	3 min
35 PCR Cycles	Denature	94
	Anneal	\sim 55 (depending on primer T_m)
	Extend	72
		45 seconds
		30 seconds
		90 s/kb (genomic)

			60 s/kb (plasmid)
Final Extension	72		10 min
Hold	12		Indefinitely

2.3.17 Cloning of pAG306-GPD-ccdB chrI integration vectors using Gateway Technology

Advanced gateway cloning technology was employed to transfer ALS-linked mutant yeast *SOD1* inserts from entry vectors into the pAG306-GPD-ccdB chrI destination vector in order to generate expression vectors that could integrate into the *S. cerevisiae* genome at an empty region of chromosome I (199456–199457) [144]. Entry vectors were harboured in DH5- α cells and contain the ALS-linked mutant yeast *SOD1* inserts along with recombinant attL sites that flank the insert. The pAG306-GPD-ccdB chrI destination vector was harboured in DB3.1 cells which are resistant to the toxic DNA gyrase activity of CcdB, the protein encoded by ccdB. The ccdB insert was flanked by recombinant attR sites. In gateway cloning, the LR reaction, the insert is cut out of the entry vector, at the attL sites, generating sticky ends that are complimentary to the attR sites on the destination vector. In the LR reaction, the enzyme LR Clonase recombines the insert into the destination vector, generating an expression vector with attB recombinant sites flanking the desired insert and a by-product with attP recombinant sites flanking the toxic ccdB gene. Transformation of the products of the LR reaction into DH5- α cells and plating onto LB-amp agar results in the simultaneous negative selection of the by-product (due to the toxicity of the ccdB gene to DH5- α cells) and positive selection of the expression vector (due to its resistance to ampicillin from the *AmpR* gene or chloramphenicol from the *CmR* gene).

For the LR reaction, the Gateway™ LR Clonase™ II Enzyme mix (Cat no: 11791020) from Invitrogen was used. The LR reaction mix (Table 2.16) was incubated at 25 °C for 1 h. 0.5 μ l of 2 μ g/ μ l Proteinase K was then added and the mix was incubated at 37 °C for 10 min to halt the reaction. The mix was then transformed into chemically competent DH5- α cells (2.3.3) using the heat shock method (2.3.4). Plasmids were purified from the resulting colonies (2.3.11) and restriction enzyme digest analysis using NotI (which cuts in only one place for the expression vector, but in two places for unsuccessful destination vectors), followed by Sanger sequencing with the GPDPro-F primer were carried out to confirm the presence of the desired insert in the expression vector.

Table 2.16 LR reaction mix.

Chapter 2. Materials and Methods

Volume	Component
75 ng	Entry vector
50 ng	Destination vector
2.75 μ l	TE (10 mM Tris-HCL, 0.1 mM EDTA) buffer pH 8
2 μ l	LR reaction buffer
0.5 μ l	LR Clonase II

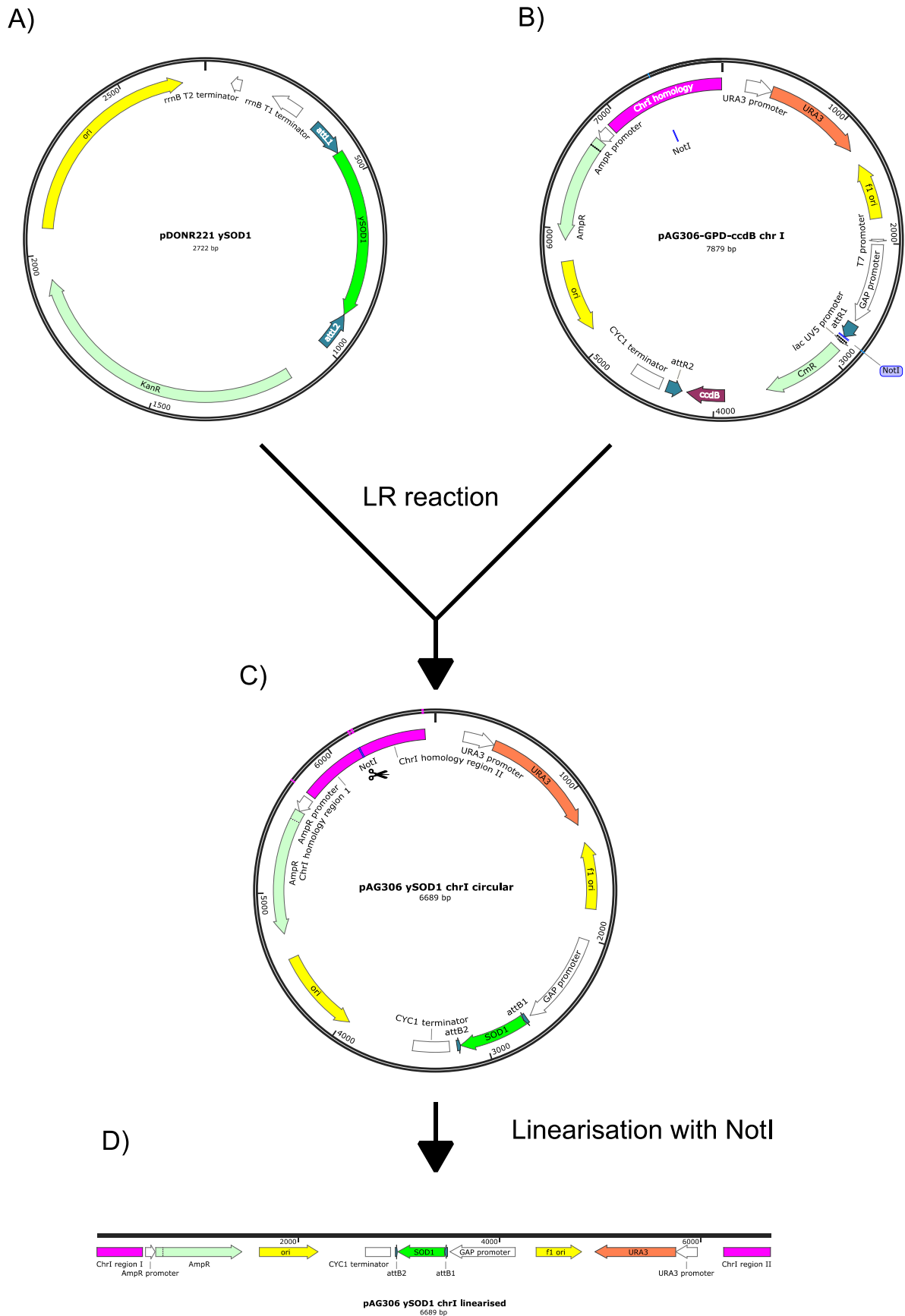


Figure 2.1 pAG306 ySOD1 chrI vector construction with gateway cloning

A) Plasmid map of the pDONR201 entry vector containing the ySOD1 insert. Contains the *KanR* gene for kanamycin resistance selection and contains attL1 and attL2 recombinant sites for gateway cloning. B) Plasmid map of the pAG306-GPD-ccdb-chrI destination vector. Contains *AmpR* for ampicillin resistance and *CmR* for chloramphenicol resistance. Also contains *URA3* for yeast growth in uracil drop-out media. Contains a region of homology to an empty region of chromosome I in yeast (199456-199457) with a NotI restriction digest site for linearisation. Contains a GPD promoter for constitutive expression of an insert. Contains attR1 and attR2 recombinant sites for gateway cloning. LR reaction between pDONR201 ySOD1 entry vector and the pAG306-GPD-ccdb-chrI destination vector produces a pAG306-GPD-ySOD1-chrI expression vector that can be integrated into chromosome I (199456-199457) of *S. cerevisiae*.

2.3.18 Cloning of the Cas9-sgRNA expression vector pML104 containing gRNA to target the yeast *SOD1* gene

The pML104 Cas9-gRNA expression vector was used to target the yeast *SOD1* gene in three different loci in order to introduce ALS-linked mutations. pML104 contains unique *SwaI* and *BclI* restriction digest sites that facilitate rapid directional cloning of the gRNA sequence using hybridized oligos that contain the gRNA sequence and the 5' structural region of the gRNA [146]. An online tool was developed by the John J. Wyrick group to aid in design of oligos for hybridization and sgRNA cloning (<http://wyrickbioinfo2.smb.wsu.edu/crispr.html>). The gRNA was selected based on proximity to the desired cut site in the gene and also based on quality information from Benchling (<https://www.benchling.com/>). Additionally, the *URA3* selection marker allows for simple removal of the plasmid from *S. cerevisiae* cells after successful gene edits are obtained by counter selecting with 5-Fluoroorotic Acid (5-FOA) (which is toxic to cells which express *URA3*).

Firstly, the pML104 vector was digested with *SwaI* (New England Biolabs, Cat no: R0604S) at 25 °C for 1 h and heat inactivated at 65 °C for 20 min. Then the *SwaI* digested pML104 vector was digested with *BclI* (New England Biolabs, Cat no: R0160S) at 50 °C for 1 h. Both restriction digests were carried out according to manufacturer's instructions. The *SwaI* and *BclI* digested pML104 plasmid was then PCR purified (QIAquick PCR Purification Kit (Cat. No. / ID: 28104).

Annealing of oligos for gRNA cloning was carried out as shown below. Oligonucleotides were hybridized at a concentration of 2 μM in 1× T4 DNA ligase Buffer (New England Biolabs, Cat no: B0202S). The mixture was placed on a heat block pre-heated to >90 °C for 5 min. After that the tube was removed from the heat and allowed to cool to room temperature. Hybridized oligos were then diluted to 0.8 μM in sterile mqH₂O. Hybridized oligos and the purified digested pML104 plasmid were then ligated overnight at 18 °C. The ligation reaction was then

transformed into DH5- α cells and colonies were confirmed by colony pcr and sanger sequencing.

Table 2.17 Hybridized oligonucleotide and *SwaI*, *BclI* digested pML104 vector ligation reaction.

Volume (μ l)	Component
7	<i>SwaI</i> , <i>BclI</i> digested pML104 plasmid
1	Hybridized oligos (0.8 μ M)
1	10 \times T4 DNA ligase Buffer
1	T4 DNA Ligase

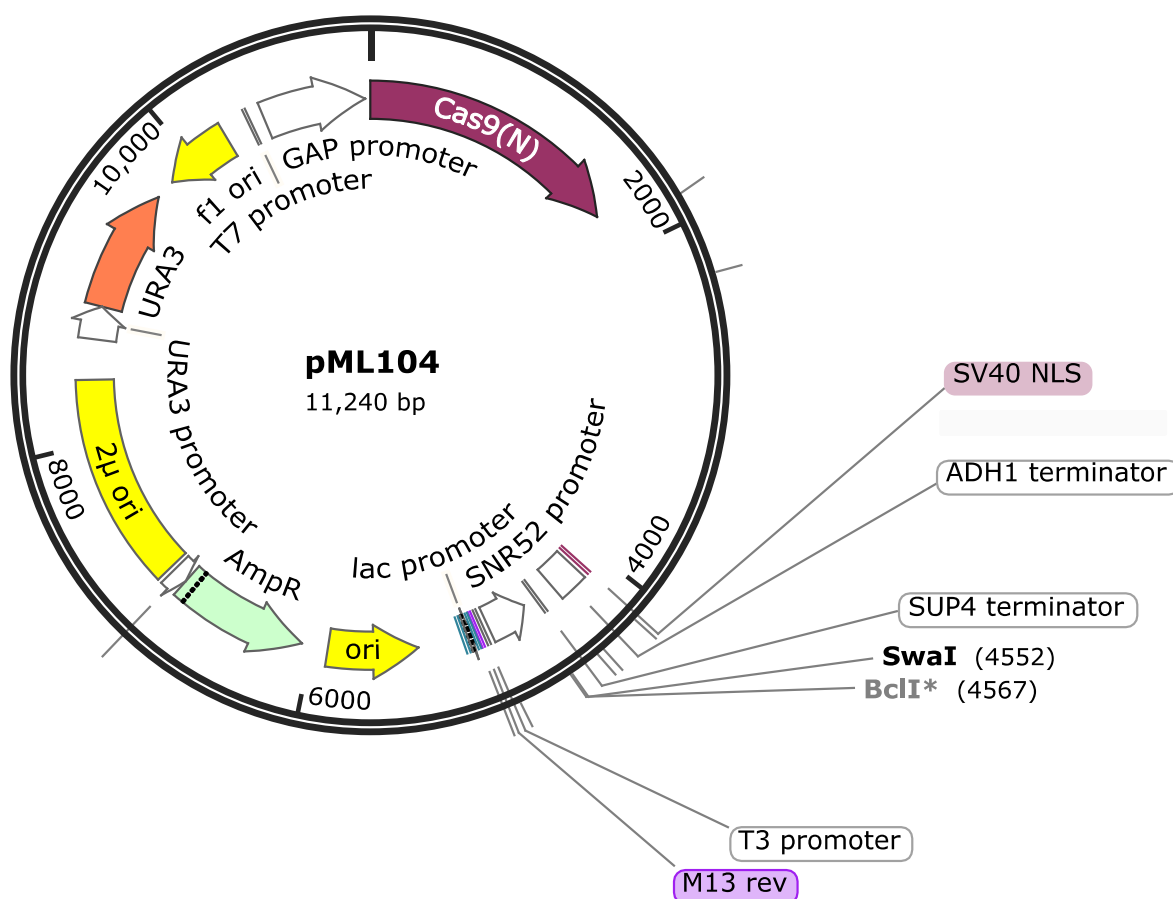


Figure 2.2 Plasmid map for pML104 Cas9 gRNA expression vector
 pML104 is a Cas9 and sgRNA expression vector that expresses Cas9 from a GPD promoter and expresses gRNA cassettes from a T3 promoter with a SUP4 terminator. Unique cutting restriction digest sites *SwaI* and *BclI* allow for fast directional cloning of the

gRNA sequence using hybridized oligos. Sanger sequencing with the M13 rev primer can be carried out to confirm successful cloning of gRNA sequence.

2.4 Yeast Strain construction

2.4.1 Integration of pAG306-GPD-ySOD1-chrI vector expressing Sod1^{WT} and Sod1^{A4V} into BY4741 and BY4741 Δ sod1 cells

The pAG306-GPD-chrI vector containing yeast *SOD1*, yeast *SOD1*^{A4V} and an empty vector control were integrated into the genome of *S. cerevisiae* in the following way. The circular pAG306 vector was linearised using the NotI restriction enzyme (Promega Express, CAT no: R6431) at 37 °C for 4 h. Confirmation of restriction digest was carried out using agarose-gel electrophoresis. The linearised pAG306 chrI vector was then transformed into BY4741 and BY4741 Δ sod1 using the high efficiency transformation protocol (2.3.5). 5 colonies were then streaked out onto SD-URA media. Correct integration of the pAG306 vector was checked by extracting gDNA from each colony (2.3.9) and carrying out confirmation PCR using the forward primer ChrIrev2, 5'-GAAGGATAGTTCGAAGCTCGC-3' and the reverse primer, AmpR, 5'-ATAATACCGCGCCACATAGC-3' (Table 2.10)

2.4.2 Generation of Sod1^{A4V}, Sod1^{H48Q} and Sod1^{G37R} mutants using CRISPR/Cas9 gene editing with pML104 plasmids.

In order to generate the A4V, H48Q and G93A mutations into the yeast *SOD1* gene, pML104 Cas9 expression vectors containing appropriate gRNA sequences were transformed into the BY4741 strain along with varying concentrations of repair template. The one-step yeast transformation protocol was used (2.3.7). A4V colonies were analysed using sanger sequencing with the oligonucleotide sod1upstreamfwd2, 5'-AAACAGGCAAGAAAGCAATCG-3' primer. The G37R and H48Q candidate colonies were analysed using the oligonucleotide Colonies containing the desired mutation were then plated onto media containing 5-FOA in order to select against the pML104-Cas9-sgRNA expression plasmid.

2.4.3 Gene knockout using HR mediated marker replacement

In order to knockout *VPH1*, *STV1*, *VMA2*, *VMA4* and *SOD1* from *S. cerevisiae*, the pUG plasmid system was used. Primers were designed as specified in the original study [149]. Deletion cassettes were amplified by PCR from the pUG plasmid (2.3.16), using primers specific to the gene being targeted. Amplification of deletion cassettes was confirmed by running agarose gel electrophoresis. Deletion cassettes (45 μ l PCR reaction) were then transformed into the desired yeast strain using the high-efficiency method (2.3.5), colonies were streaked out onto appropriate

selective media and PCR was used to check for replacement of the gene with the desired auxotrophic marker.

2.4.4 Gene C-terminal tagging

In order to C-terminally tag *SOD1*, *VMA2*, *VMA4* and *CNB1* with the 3-HA epitope, the pFA6a plasmid was used. Primers were designed as specified in the original study [148]. C-terminal tagging cassettes were amplified from the pFA6a-3HA-His3MX6 plasmid and correct amplification was confirmed by agarose gel-electrophoresis. Tagging cassettes (45 µl PCR reaction) were then transformed into the desired yeast strain using the high efficiency method (2.3.5). Colonies were streaked onto the appropriate selective media and PCR was used to check for correct tagging of the gene.

2.5 Protein methods

2.5.1 Yeast whole cell protein extraction

Whole cell protein extracts were prepared from *S. cerevisiae* cells using the following method [154]. 1×10^8 of yeast cells, either in stationary phase or exponential phase (depending on the experiment) were harvested and resuspended in 200 µl of lysis buffer (0.1 M NaOH, 0.05 M EDTA, 2% SDS, 2% β mercaptoethanol). This mixture was placed on a heat block pre-heated to 90 °C for 10 min. 5 µl of 4 M acetic acid was then added to neutralise the reaction and the tube was vortexed for 30 s. 50 µl of loading buffer (0.25 M Tris-HCL pH 6.8, 50% Glycerol, 2% SDS, 0.05% bromophenol blue) was then added to the 200 µl sample. The lysate was then cleared by centrifugation ($10,000 \times g$, 30 seconds).

2.5.2 Native yeast whole cell extracts

10 OD₆₀₀ units of cells either in stationary phase or exponential phase were harvested ($10,000 \times g$, 30 seconds) and washed in 1 ml sterile mqH₂O in a 1.5 ml Eppendorf. The pellet was then resuspended in 250 µl of lysis buffer (10 mM NaPO₄ pH 7.8, 5 mM EDTA, 0.1% (w/v) Triton X-100, 50 mM NaCl, 500 µM PMSF, protease inhibitor cocktail tablet (Roche, CAT no: . 11697498001). A volume of acid-washed glass beads (Sigma, Cat no: G8772) equal to the volume of the cell pellet was added to the tube. This mixture was then vortexed at 4 °C for 1 min, before resting 1 min on ice. This step was carried out five times. Tubes were then centrifuged (13,000 rpm, 5 min, 4 °C) and then supernatant was then transferred to a fresh pre-chilled tube. This tube was then centrifuged (13,000 rpm, 10 min, 4 °C) and the supernatant was then transferred

to a fresh pre-chilled tube. The protein concentration was determined using the Bradford assay (Sigma, CAT no: B6916).

2.5.3 SDS-polyacrylamide gel electrophoresis (SDS-PAGE)

12% SDS-PAGE gels were prepared using Bio-Rad 0.75 mm glass cassettes for use in the Bio-Rad Mini-Protean III cell. The SDS-PAGE gels consisted of a 12% stacking gel and a 4.3% resolving gel (Table 2.18). The resolving gel was poured into the 0.75 mm cassettes and 100% isopropanol was poured immediately over the resolving gel to ensure even solidification of the gel. The isopropanol was then poured away before adding the stacking gel solution and the comb to produce the sample loading wells. SDS-PAGE gels were run at 180 V for 45–60 min in SDS running buffer.

Table 2.18 SDS-PAGE reagent components.

Resolving gel	Stacking gel	SDS running buffer
126 mM Tris pH 8.8	240 mM Tris pH 6.8	0.3% Tris-HCL
0.1% SDS	0.1% SDS	1.44% Glycine
12% acrylamide (29:1)	4.3% acrylamide (29:1)	0.15% SDS
0.15% ammonium persulphate	0.23% ammonium persulphate	
0.07% TEMED	0.07% TEMED	

2.5.4 Semi-dry transfer

After completion of SDS-PAGE (2.5.3), the polyacrylamide gel was removed from the cassette and the stacking gel was discarded. The resolving gel was then placed in transfer buffer (0.0058% (w/v) Tris base, 0.0029% (w/v) Glycine, 0.00004% (w/v) SDS and 20% (w/v) methanol) for 15 min to wash off any residual chemicals from the SDS-PAGE step. Four pieces of Whatman blotting paper (Thermo Fisher), were cut into 8 × 9 cm pieces, and soaked in transfer buffer for 10 min. An 8 × 9 cm piece of Polyvinylidene difluoride (PVDF) membrane (Thermo Fisher) was wet in methanol for 30 s and then placed in transfer buffer for 10 min. Two pieces of blotting paper were placed on the anode plate of a trans-blot semi-dry transfer cell machine (Bio-Rad), followed by the PVDF membrane, the PAGE gel and then two more pieces of blotting paper. Air bubbles were rolled out using a roller. The cathode plate was placed on top of the sandwich. Semi-dry transfer was carried out at 25 V for 30 min. Upon completion of semi-dry transfer, the

PVDF membrane containing the proteins of interest was used for downstream analysis such as immunoblotting or Coomassie staining.

2.5.5 Immunoblotting

After completion of semi-dry transfer, the PVDF membrane was incubated in 5 ml of blocking solution (5% dried skimmed milk (Oxoid, CAT no: LP0033B), 1× PBS/T (Phosphate buffered saline, 0.2% Tween 20) and incubated for 1 h with shaking at room temperature. After the blocking step, the PVDF membrane was then incubated in 5–10 ml of blocking solution containing an appropriate concentration of the primary antibody, depending on which protein is being examined. Primary antibody incubation was carried out either for 1 h at room temperature, or overnight at 4 °C with shaking. After the primary antibody incubation, the PVDF membrane was washed in PBS/T for 3 × 10 min. After washing, the PVDF membrane was incubated in 10 ml of blocking solution containing an appropriate concentration of horseradish peroxidase (HRP) conjugated secondary antibody. Secondary antibody incubation was carried out for 1 h at room temperature with shaking. The PVDF membrane was then washed in PBS/T for 3 × 10 min and finally stored in PBS. At this stage the PVDF membrane was ready for detection using enhanced chemiluminescence (ECL).

2.5.6 Enhanced chemiluminescence (ECL) detection

The PVDF membrane that had been incubated in primary and secondary antibody (2.5.5) was placed in a clean plastic box. ECL solution 1 and ECL solution 2 were mixed to a 1:1 ratio and pipetted over the PVDF membrane (Table 2.19). The PVDF membrane was incubated in ECL for 1 min before being placed in cling film and visualised using the SYNGENE G:BOX gel doc system. The GeneSys software (V 1.6.5.0) along with a synoptics 6 MP camera were used to capture images of western blots.

Table 2.19 ECL solution reagents.

ECL solution 1	ECL Solution 2
2.5 mM luminol (FLUKA, CAT no: 09253)	0.0192% hydrogen peroxide
0.396 mM p-coumaric acid (Sigma, CAT no: C9008)	100 mM Tris-HCL (pH 8.5)
100 mM Tris-HCL (pH 8.5)	

Table 2.20 Primary and secondary antibodies used for immunoblotting in this study.

For all primary and secondary antibodies. The dilution was made in blocking solution (5% (w/v) skimmed milk, 1× PBS, 0.2% Tween 20).

Primary antibody	Dilution	Secondary antibody	Dilution
Anti-Sod1 (<i>C. elegans</i>) (Valeria Culotta)	1:6000	Anti-rabbit-HRP-conjugate (Dako, CAT no: P0217)	1:60,000
Anti- ATP6V1B1 (V-ATPase-B1) (Mouse) (ThermoFisher, CAT no: PA5-70208)	1:1000	Anti-rabbit-HRP-conjugate (Dako, CAT no: P0217)	1:60,000
Anti-Pgk1 (Professor Mick Tuite)	1:10,000	Anti-rabbit-HRP-conjugate (Dako, CAT no: P0217)	1:60,000
Anti-Porin (Professor Mick-Tuite)	1:2000	Anti-mouse-HRP-conjugate (Sigma, CAT no: A4416)	1:5000

2.5.7 Stripping of PVDF membrane

After ECL detection of PVDF membranes, previously bound antibodies were chemically stripped off the PVDF membrane to allow for immunoblotting of other proteins using different antibodies. The Restore Western Blot Stripping Buffer (Thermo Scientific, CAT no: 21059) was used. The PVDF membrane was briefly washed in PBS/T and the incubated in PBST/T for 2 × 15-minute washes. Then the PVDF membrane was completely immersed in 10 ml of stripping buffer and incubate at room temperature for 30 min with gentle shaking. The PVDF membrane was then washed in PBS/T for 2 × 15 min. After this step the PVDF membrane was ready to be blocked and bound to fresh antibodies for further immunoblotting.

2.5.8 Native polyacrylamide gel electrophoresis (Native-PAGE)

12 % Native-PAGE gels were prepared using Bio-Rad 0.75 mm glass cassettes for use in the Bio-Rad Mini-Protean III cell. The Native-PAGE gels consisted of a 12 % stacking gel and a 4.3 % resolving gel (Table 2.21). The resolving gel was poured into the 0.75 mm cassettes and 100 % isopropanol was poured immediately over the resolving gel to ensure even solidification of the

gel. The isopropanol was then poured away before adding the stacking gel solution and the comb to produce the sample loading wells. Native-PAGE gels were run at 144 V for 2 h and 30 min in Native-PAGE running buffer. The gel could then be used to detect sod activity via an *in-gel* colorimetric assay.

Table 2.21 Native-PAGE reagent components.

Resolving gel	Stacking gel	SDS running buffer
126 mM Tris-HCL pH 6.8	240 mM Tris-HCL pH 6.8	0.3% Tris-HCL pH 8.3
12% acrylamide(29:1)	4.3% acrylamide (29:1)	1.44% Glycine
0.15% ammonium persulphate	0.23% ammonium persulphate	
0.07% TEMED	0.07% TEMED	

2.5.9 In gel Sod activity assay using nitrotetrazolium blue (NBT) chloride.

To measure the Sod1 activity from native protein extracts from *S. cerevisiae* cells, lysates with equal amounts of protein (5 µg) were loaded on a native-PAGE gel and native-PAGE electrophoresis was carried out (2.5.8). After completion of native-PAGE electrophoresis, the gel was stained in the dark in NBT staining solution (0.05 M KPO₄ pH 7.8, 265.675 µM riboflavin (Sigma, CAT no: R4500), 0.1% (w/v) TEMED (Sigma, CAT no: T8133), 16.305 µM nitrotetrazolium blue chloride (Sigma, CAT no: N6876) for 45 min. The gel was then left under a lamp (or light) overnight to allow for colour development. Developed gels were then imaged on SYNGENE G:BOX gel doc system. The GeneSys software (V 1.6.5.0) along with a synoptics 6 MP camera were used to capture images of the gels.

2.5.10 Purification of yeast vacuoles.

Purification of yeast vacuoles was carried out using the method published by the Ungermann lab[155]. The method was modified slightly using the protocol from the Tabke lab [156] to allow for conversion of intact vacuoles into vacuole membrane vesicles that can be frozen prior to measurement of V-ATPase activity. A 1000 L flask of YPD was inoculated with 1 OD₆₀₀ unit of log phase BY4741 (or whichever strain was required) cells. Cells were grown for 16 h at 30 °C with 180 rpm shaking. The next morning, once on OD of 0.7–0.8 had been reached, cells were harvested (4400 × g, 2 min) in a Beckman Avanti JLA-10.500 rotor. Pellets were resuspended in 50 ml of DTT solution (0.1 M Tris pH 9.4, 10 mM DTT), transferred to a 50 ml falcon tube and

incubated in a water bath at 30 °C for 10 min. Cells were then centrifuged ($4000 \times g$ for 2 min), resuspended in 15 ml of spheroblasting buffer (0.16× YPD, 0.6 M sorbitol, 10 mM PIPES pH 6.5, 150 U of Zymolase 100T (MP Biomedicals CAT no: 320931) and then incubated in a water bath at 30 °C for 45 min with occasional mixing. Spheroplasts were then centrifuged (3500 rpm, 4°C) and kept on ice for all subsequent steps. Pelleted spheroplasts were gently resuspended in 2.5 ml of ice-cold 15% Ficoll-PS buffer solution (15% (w/v) Ficoll (GE Healthcare), 10 mM PIPES/KOH pH 6.8, 200 mM sorbitol). 200 µl of 0.4 mg/ml DEAE Dextran hydrochloride (Sigma, CAT no: D9885) solution was then added to the tube and spheroplasts were incubated on ice for 5 min. Spheroplasts were then transferred to a 30 °C water bath and incubated for 1.5 min to gently lyse the spheroplasts. Lysates were then transferred to a SW41 centrifuge tube (Beckman, Product No: 344059) and made up to a final volume of 5 ml with 15% Ficoll-PS buffer solution. 3 ml of 8% Ficoll-PS buffer solution was then gently poured on top of the lysate, followed by 3 ml of 4% Ficoll-PS buffer solution. Finally, PS buffer solution (10 mM PIPES/KOH pH 6.8, 200 mM) containing no Ficoll was layered on top of the 4% solution until the centrifuge tube was completely filled. SW41 tubes were placed in the SW41 Ti Swinging-Bucket Rotor (Beckman, Product No: 331362) and centrifuged ($110,000 \times g$, 4 °C for 90 min) in a Beckman Optima ultracentrifuge. 600 µl of vacuoles were collected from the 0–4% interface with a 1 ml pipette tip cut at the end. Protease inhibitor cocktail was added to a final concentration of 1× and protein concentration was calculated using the Bradford assay. To freeze the vacuoles, an equal volume of 2× buffer C (20 mM Mes/Tris pH 6.9, 10 mM MgCl₂, 50 mM KCL) was added to the vacuole sample. Samples were aliquoted into Eppendorf's and frozen at -80 °C.

2.5.11 Measurement of V-ATPase ATP-hydrolysis activity using malachite green

To measure V-ATPase-ATP hydrolysis activity, a method detecting inorganic phosphate using BIOMOL Green (Enzo Life Sciences, CAT no: AK111) was used. Vacuole extracts were thawed on ice. For experiments with recombinant Sod1, vacuole extracts were pre-incubated with recombinant bovine Sod1 (antibodies-online.com, CAT no: ABIN5571499) at 30 °C for 30 min. For experiments measuring the V-ATPase activity between two different strains, the pre-incubation step was skipped. Vacuoles were then pre-incubated in the ATP hydrolysis mixture (50 mM Tris/Mes pH 6.9, 0.1 mM Sodium orthovanadate, 0.5 mM Sodium azide, 3.75 mM MgCl₂, 20 mM KCL, Bafilomycin A1 (HelloBio, CAT no: HB1125)/DMSO control) for 10 min at 30 °C (Table 2.22). ATP was then added to the mix to a final concentration of 2 mM (in 5 mM

Tris-base) and samples were mixed and incubated at 30 °C for 20 min (or as desired). 5 µl from the ATP hydrolysis reaction was added to 245 µl of 5× HNG buffer (100 mM HEPES pH 8.8, 65 mM NaCl, 5% glycerol) at the start of the reaction and after 20 min (or other time-points as required). Samples were frozen in liquid nitrogen and stored at -20°C until phosphate detection was carried out.

Table 2.22 ATP hydrolysis assay reagent mix.

Solution	Volume (µl)	Concentration
160 mM Tris/Mes, pH 6.9	50	50 mM
0.8 mM Sodium orthovanadate, 30 mM MgCl ₂	20	0.1 mM Sodium orthovanadate, 3.75 mM MgCl ₂
4 mM Sodium Azide, 160 mM KCL	20	0.5 mM Sodium azide, 20 mM KCL
Bafilomycin A1 (10 nm) / DMSO	1	1 nM
3 µg Vacuole extract in buffer C(10 mM Tris/Mes pH 6.9, 5 mM MgCl ₂ , 25 mM KCL)	40	NA
Sterile H ₂ O	9	NA
Incubate for 10 min at 30 °C		
16 mM ATP, 40 mM Tris-base	20	2 mM ATP, 5 mM Tris-base
Total volume	160	

Phosphate detection was carried out using the malachite green detection method with BIOMOL Green [157]. ATP hydrolysis samples were thawed on ice. Inorganic phosphate (P_i) standards were created from an 800 µM stock diluted in 1× HNG buffer (20 mM HEPES pH 8.5, 13 mM NaCl, 1% glycerol), to create standards ranging from 40 µM, 20 µM, 10 µM, 5 µM, 2.5 µM, 1.25 µM , 0.625 µM and 0 µM. These were added to a 96-well plate to a volume of 50 µl. 50 µl of each

ATP hydrolysis sample was added to the 96-well plate. 100 µl of the malachite green detection reagent was added to each well and mixed by pipetting up and down using a multichannel pipet. The reaction was incubated for 25 min at room temperature. The absorbance at OD₆₅₀ was measured using a SpectroStar Omega (BMG Labtech, UK) plate reader. A P_i standard curve was created in Microsoft Excel using the OD₆₅₀ values from the P_i standards. Using the slope and Y intercept from the standard curve, the amount of bafilomycin-dependant phosphate release from the vacuoles was calculated using the following equation:

$$\frac{(\text{OD}_{650} - \text{Y intercept})}{\text{Slope}}$$

The average amount of P_i released from the technical repeats of each sample was calculated and the buffer-only control P_i released was subtracted from this number. The value obtained was then multiplied by the dilution factor (50) to obtain the total V-ATPase specific P_i produced by the vacuole extracts after addition of ATP.

2.5.12 Sample preparation and analysis of amino acids via double-derivatisation and liquid-liquid extraction

This protocol was carried out by Dr John Townsend and Dr Sreejith Jayasree Varma in Charité – Universitätsmedizin Berlin with vacuole extracts from BY4741 and BY4741 Δ *sod1* cells expressing pAG306-GPD-empty-*chrI* and pAG306-GPD-Sod1^{A4V}-*chrI*. The protocol that they used for analysis of amino acids is as follows.

Approximately 75 mg of 425–600 µm glass beads (Sigma) were added to each sample. Vacuoles were lysed in a bead beater (Spex Geno/Grinder) for 5 min at 1500 rpm. Samples were spun for 5 min at 13300 rpm in a benchtop centrifuge and 10 µL of supernatant was taken for further analysis. To a vial containing 10 µL of probe, were added sequentially 2 µL pyridine (1 M in acetonitrile), 10 µL of 100 mM aqueous Na₂CO₃ and 20 µL of 2% benzoyl chloride in acetonitrile (freshly prepared). Following a brief mixing (5 s) and incubation (1 min, 25 °C), 10 µL of diisopropylethylamine (DIPEA, 8 mM in acetonitrile), 50 µL of 1-ethyl-3-(3-dimethylaminopropyl)carbodiimide (EDC, 100 mM in acetonitrile, freshly prepared) and 20 µL of 4-bromo-N-methyl benzylamine (BNMBA, 250 mM in acetonitrile) were added. The resulting mixture was incubated at 60 °C, 900 rpm, 50 min. Following the incubation, 100 µL of chloroform was added to the mixture and was agitated for 1 min. The vial was then centrifuged (3000 rpm) to separate the top aqueous layer which was then carefully removed using a pipette and discarded. 100 µL of 0.1% aqueous formic acid was then dispensed on to the chloroform layer, agitated and centrifuged. The lower organic layer was carefully transferred to a clean vial,

evaporated to dryness, and reconstituted in HPLC grade 50% acetonitrile-water containing 0.1% formic acid. An external calibration standard mixture containing commercially available amino acids (1 mM each), were prepared in MQ water in the dilution 1:5:5:5:5 and derivatised as above. LCMS measurement was carried out on Agilent Infinity 1290 HPLC coupled to Agilent 6460 triple quadrupole mass spectrometer. The LC parameters are as follows: Solvent A and B were respectively 0.1% formic acid in water and 0.1% formic acid in acetonitrile. The chromatography was carried out using Agilent Eclipse Plus C18 column (3.0 × 50 mm) maintained at 30 °C and a flow rate of 0.3 mL/min. The applied solvent composition consisted of 50% B from 0–3.9 min followed by 100% B from 4–6 min. The column was then re-equilibrated at 50% B from 6.1–7.5 min. The MS parameters are as follows: gas flow at 8 L/min and 300 °C, sheath gas flow at 11 L/min and 300 °C, nebuliser pressure at 50 psi, capillary voltage at 3000 V (negative) and 3500 V (positive), and nozzle voltage at 500 V. Cell acceleration voltage was set at 7 V. A volume of 2 µL was injected and the analysis was carried out as dMRM in the positive mode for the transitions listed in Table XX. The generated data was processed using Quantitative Analysis for QQQ software. Each sample was injected in triplicate. Measurements below the limit of detection were excluded from further analyses. Amino acid concentrations were normalized to total protein concentration.

2.5.13 Co-immunoprecipitation

Desired strains were grown overnight in 5 ml of YPD media, 30 °C at 180 rpm shaking. The next morning, 50 ml of YPD was inoculate to OD₆₀₀ of 0.1 and grown until cells were in mid-log phase (~0.7 OD₆₀₀). Cells were centrifuged (10,000 × *g* for 30 s) and resuspended in lysis buffer (50 mM HEPES pH 7.4, 140 mM NaCl, 1 mM EDTA, 10% Glycerol, 0.5% NP40, 1 mM PMSF, 1× PIC). Glass beads were added to cells in lysis buffer and the mixture was vortexed 3 × 2 min, with 2 min intervals on ice. Mixture was then centrifuged (10,000 × *g* for 5 min, 4 °C). Supernatant was transferred to a fresh tube and centrifuged (10,000 × *g* for 15 min, 4 °C). Supernatant was transferred to a fresh tube and used for CO-IP analysis.

CO-IP was performed using the Pierce Anti-HA Magnetic Beads (ThermoScientific, CAT no: 88836). 25 µL of Anti-HA Magnetic Beads were placed in a 1.5 mL microcentrifuge tube and 175 µL of 0.05% TBS-T (Tris-Buffered Saline, 0.05% Tween 20) was added to the beads and mixed gently by vortexing. The tube was placed on a magnetic stand to pull the beads to the side and the supernatant was discarded. Beads were washed with 1 mL of 0.05% TBS-T and the supernatant discarded. The protein extract from the desired strains was added to the beads and incubated for 2 h at 4° C with gentle mixing. After 2 h beads were collected, and the unbound

sample was removed and saved for analysis. Beads were washed two times with 300 μ L 0.05% TBS-T. On both occasions, the supernatant was saved for later analysis. Beads were washed with 300 μ L sterile mqH₂O. The protein of interest was eluted from the beads by adding 100 μ L of 50 mM NaOH to the tube. Sample was gently mixed and incubated at 25 °C for 5 min. Supernatant was removed and neutralized by adding 50 μ L neutralization buffer (1 M Tris, pH 8.5). The protein from the sample was then concentrated by TCA precipitation (100 % TCA, 0.2% deoxycholate), resuspended in 1 \times Laemmli sample buffer (2% (w/v) SDS, 5% (v/v) β -mercaptoethanol, 10% (v/v) Glycerol, 62.5 mM Tris-HCL pH 6.8, 0.0025% (w/v) bromophenol blue) and boiled for 5 min at >90 °C on a pre-heated heat block. Samples were then analysed by SDS-PAGE and immunoblotting to determine the results of the CO-IP.

2.6 Whole Cell Experimental procedures

2.6.1 Measurement of yeast growth in liquid by absorbance

5 ml of appropriate media was inoculated with a colony of the required yeast strain and grown overnight at 30 °C with shaking at 180 rpm. The next morning, either 24 well (1 ml), 48 well (500 μ l) or 96 well (100 μ l) plates (Greiner) were set up with the appropriate media and inoculated to an OD₆₀₀ of 0.1 with the required *S. cerevisiae* strain. Growth was measured as the absorbance at OD₆₀₀ over time using the BMG LABTECH SPECTROstar Nano plate reader. For the analysis and processing of the absorbance at OD₆₀₀ data, the BMG LABTECH MARS data analysis software was used. The data processed in this software was then exported to Microsoft Excel and then imported into R for data analysis using the Growthcurver package. The Growthcurver package fits growth curve data to a logistic equation in order to calculate parameters such as the growth rate, initial population size, area under the curve and carrying capacity.

The logistic equation:

$$N_t = \frac{k}{1 + \left(\frac{k - N_0}{N_0}\right) e^{-rt}}$$

N_0 is the initial population size, K is the maximum size the population can get to in a particular environment, r is the growth rate if there were no restrictions imposed on the total population size. For this study the area under the curve (AUC) was used to represent overall growth.

2.6.2 BIOLOG screen

BY4741 expressing pAG306-GPD-empty-*chrI*, and pAG306-GPD-*SOD1*-A4V-*chrI* were grown overnight in 5 mL of SC media at 30 °C with 180 rpm shaking. The next morning, cells were

washed two times in sterile mqH₂O and 4.8 OD₆₀₀ units of cells were resuspended in 250 μ L of 48 \times NS (Table 2.23). Inoculating fluid was prepared with the mixtures shown in Table 2.25. For example, to inoculate the PM1 plate, which tests for carbon source utilisation, the mixture shown in Table 2.25 omits D-glucose (32 \times) from the inoculation fluid. The PM additive solutions were prepared as specified in Table 2.24. Inoculation fluid was poured into a sterile multichannel dish and pipetted into the biolog plate using a multichannel pipette. Growth of *S. cerevisiae* was monitored as specified previously (2.6.1).

Table 2.23 Recipe for 48 \times Yeast Nutrient Supplement (NS) for BIOLOG

Solution	Concentration (mM)	Concentration factor
L-histidine HCL monohydrate	0.48	48 \times
L-leucine	4.8	48 \times
L-methionine	1.2	48 \times
Uracil	1.44	48 \times

Table 2.24 Recipe for PM additive (12 \times) solutions for BIOLOG

Solution	PM1, 2, 5,9	PM3, 6, 7, 8	PM4
D-Glucose	3200 mM	3200 mM	3200 mM
L-glutamic acid monosodium	60 mM	-	60 mM
Potassium phosphate monobasic anhydrous (pH 6)	60 mM	60 mM	-
Sodium Sulphate	24 mM	24 mM	-

Table 2.25 Recipe for inoculating PM plates for BIOLOG

PM Stock Solution	PM1, 2 (mL)	PM3, 6, 7, 8 (mL)	PM4 (mL)	PM5, 9 (mL)	PM10 (mL)
IFY-0 (1.2 \times)	10	10	10	10	-
SC media	-	-	-	-	11.75

D-glucose (32×)	-	0.375	0.375	0.375	-
PM additive (12×)	1	1	1	1	-
Cells in 48× NS	0.25	0.25	0.25	0.25	0.25
Sterile mqH ₂ O	0.75	0.375	0.375	0.375	-
Total	12	12	12	12	12

2.6.3 Vacuole knockout library screen

The vacuole knockout library was constructed by transforming the pAG306-GPD-*SOD1*-A4V-*chrI* integration vector into a library of MATa gene deletion mutants encoding proteins with functions related to the vacuole and metabolism in *S. cerevisiae*. The high efficiency transformation was used (2.3.5). Correct integration of pAG306-GPD-*SOD1*-A4V-*chrI* into each mutant was confirmed by PCR and agarose gel electrophoresis analysis of the gDNA using the primers: *chrIrev2*, 5'- GAAGGATAGTTCGAAGCTCGC-3' and Amp-R, 5'- ATAATACCGCGCCACATAGC-3'.

The control and A4V 96-well plate were stamped out onto YPD agar using a sterile replicator and grown at 30 °C for 2–3 d. Once grown, cells from these plates were used to inoculate a 96-well plate with liquid YPD media, by stamping using the sterile replicator. Cells were grown overnight at 30 °C, 180 rpm shaking with parafilm around the edges of the 96-well plate to prevent evaporation. The following day, yeast cultures were diluted 1:100 in sterile mqH₂O and stamped onto different agar plates containing different conditions (SC media, SC media pH 7.5 50 mM CaCl₂ 37 °C, aa media, aa media + 40 μM menadione). Drops of yeast cells stamped onto plates were allowed to dry and then the plates were incubated at 30 °C (unless stated otherwise) for 2–3 d.

2.6.4 Measurement of yeast growth by spotting onto agar

5 ml of appropriate media was inoculated with a colony of the required yeast strain and grown overnight at 30 °C with shaking at 180 rpm. In the morning, 10 ml of appropriate media was inoculated to an OD₆₀₀ of 0.1 with cells from the overnight, and the culture was grown at 30°C, 180 rpm shaking until an OD₆₀₀ value of 0.5–0.7 was reached. Cells were then diluted down to an

OD₆₀₀ of 1 and diluted 10-fold over six serial dilutions. Using a replicator, 5 µl drops of cells from all six 10-fold dilutions were stamped onto the agar plate containing the appropriate media. Once the 5 µl drops were all dry on the agar plates, the plates were then incubated at 30 °C and left for 2–3 d. Plates were then imaged using the SYNGENE G:BOX gel doc system. The GeneSys software (V 1.6.5.0) along with a synoptics 6 MP camera were used to capture images of the agar plates.

2.6.5 Quantification of calcineurin activity by flow cytometry

Desired strains were transformed with the pAMs366 4×-CDRE-GFP-URA3 reporter plasmid using the quick & easy yeast transformation protocol (2.3.6). Colonies were then streaked out onto SC media lacking uracil to maintain the reporter plasmid. For the flow cytometry experiment, a 5 ml overnight of SC-URA media was inoculated with a colony of the desired yeast strain expressing pAMs366 4×-CDRE-GFP-URA3 and grown overnight at 30 °C with 180 rpm shaking. The next morning, this overnight was used to inoculate two 10 ml cultures of SC-URA to an OD₆₀₀ of 0.1 per strain. This culture was grown at 30 °C with 180 rpm shaking for 7 h until an OD₆₀₀ of 0.5–1 had been reached. A negative control was inoculated including BY4741 cells at an OD₆₀₀ of 0.1 with 0.5 µM FK506, a calcineurin inhibitor. Once the cultures had reached an OD₆₀₀ of 0.5–1, CaCl₂ was added to one of the 10 ml cultures to a final concentration of 50 mM. Cultures were placed back in the incubator at 30 °C for 1 h with 180 rpm shaking. After 1 h, all cultures were washed twice in sterile mqH₂O and diluted to an OD₆₀₀ of 0.1 and then resuspended in sterile 1× PBS. Cells resuspended in PBS were transferred to a 48 well plate (Greiner) with 500 µl per well.

Fluorescence intensity of cells expressing pAMs366 4×-CDRE-GFP-URA3 was analysed using the BD Accuri™ C6 Plus Personal Flow Cytometer (BD Biosciences). Measurement events were gated on the flow cytometer to ensure that singlet yeast cells were being recorded. The flow cytometer was equipped with a blue laser (488 nm) and a red laser (640 nm). The FL1 (533/30 nm) filter was used to detect the GFP fluorophore from cells expressing the 4×-CDRE-GFP reporter. Approximately 10,000 events were collected per sample and the data was acquired and analysed using the BD Accuri C6 Plus software.

2.6.6 Fluorescence microscopy

Live yeast cell samples for visualisation by fluorescence microscopy were prepared by pipetting 3 µl of a sample containing cells onto a clean glass slide (76 × 26 mm, Fisher Scientific, CAT no: BGNPL10). A cover slip that was 0.16–0.19 mm was placed onto the slide over the drop of cells,

carefully to avoid any air bubbles. A drop of immersion oil was put on the coverslip prior to placing the slide on the microscope stage.

The Wide-field fluorescence microscope was set up as follows. The microscope was an Olympus IX81 series, and the software used was Micro-Manager v1.4.22. The excitation light was emitted using the CoolLED pE4000 (CoolLED, UK) light emitting diode. The excitation light was then filtered through different filter cubes. For blue light excitation of the GFP fluorophore, Olympus U-MWB (excitation filter 450–480 nm and bandwidth 35) was used. For green light excitation of the mCherry or RFP fluorophore, Olympus U-MNG (excitation filter 530–550 nm and bandwidth of 40) was used. The Olympus UPLSAP0 100XO NA 1.4 Oil Immersion objective lens was used to focus on the sample. The metal oxide semiconductor camera, Zyla 5.5 sCMOS (ANDOR, Oxford Instruments, UK) was used to detect fluorescence. Exposure time was kept the same for each experiment when visualising the same fluorophore.

2.6.7 Analysis of images using ImageJ

Fluorescence microscopy images were captured using the ImageJ program. In order to set the scale bar on the images, the size of the camera sensor chip and the magnification was required. The size of the camera sensor chip was 6.5 μm and the magnification used was 100 \times . The scale bar in all fluorescence microscopy images shown in this study represents a distance of 5 μm .

2.6.8 Quinocrine staining

S. cerevisiae cells were stained with quinocrine to monitor vacuole acidification. 2×10^7 cells were harvested either from an overnight or a culture grown to exponential phase. The cells were washed three times in SC media with 2% glucose, buffered to a pH of 7.5 with 50 mM Na_2PO_4 . Cells were then resuspended in 100 μl of SC media with 2% glucose and pH 7.5 and quinocrine was added to a final concentration of 200 μM . Cells were incubated at 30 $^\circ\text{C}$ for 10 min and then placed on ice. Cells were then washed three times in 500 μl of ice-cold wash buffer (50 mM Na_2PO_4 , 2% glucose, pH 7.5) and then quinocrine was visualised by fluorescence microscopy using the blue light excitation filter (450–480 nm). Cells were visualised and imaged within 30 min of staining as described previously.(2.6.6).

3 Developing a stable *S. cerevisiae* model for SOD1-ALS using integration vectors.

3.1 Introduction

3.1.1 Comparison between different models of fALS

Since the discovery that mutations in *SOD1* can cause fALS back in 1993 [10], models have been developed in organisms including yeast, nematodes, flies, zebrafish, mice and iPSCs derived from patient cells to facilitate the study of *SOD1*-fALS. Each organism possesses their own advantages and disadvantages as a model for fALS [158]. The advantages of ALS models in *S. cerevisiae* are that they have a fast life cycle, they are cheap to maintain, and they are amenable to high-throughput experiments, facilitating genetic or pharmacological screens. They have a lower percent of genes with a human homologue compared to other models such as zebrafish, rodents, or iPSC-derived neurons, however many key signalling pathways are conserved. For this reason, *S. cerevisiae*-based models are excellent for generating hypotheses that can then be tested in models that are closer in homology to humans, such as zebrafish, rodents, or iPSC-derived neurons. The advantage of this method is that these models such as zebrafish, rodents and iPSC-derived neurons all have a slow life cycle and long lifespan compared to *S. cerevisiae* and they have a much higher cost, so by forming hypotheses in *S. cerevisiae* initially, a more efficient targeted approach in these models can be adopted [158].

3.1.2 Overexpression models versus stable single-copy expression models of *SOD1* associated fALS

In the past, the majority of *SOD1*-ALS models have relied upon the overexpression of mutant isoforms into different organisms in order to study their effects on different cellular processes. These models have successfully reconstituted several ALS-related pathologies in yeast, worms, flies and mice and they have contributed towards understanding how mutations in *SOD1* cause cellular dysfunction which results in the selective death of MNs. Despite this, there has been a low rate of success for ALS clinical trials suggesting that difficulties remain in translating the findings into successful therapies [159]. The finding that even overexpression of Sod1^{WT} causes ALS in mice, emphasised the need for other types of models that involve the expression of mutant Sod1 isoforms at more physiologically-relevant levels [160].

Recently, single-copy ALS models have been developed in the nematode *C. elegans* [86], in *Drosophila* [90], in Zebrafish [93] and in mice [161]. Even at lower levels of expression, these models of SOD1-ALS all recapitulated various aspects of the disease. Phenotypes observed in these single-copy models were often found to be less severe than those of overexpression models. Using both overexpression models and single-copy models in combination should allow for a more complete understanding of any toxic gain-of or loss-of functions caused by ALS-linked mutations in SOD1 [86].

3.1.3 Aim of this study

The aim of this study was to develop a single-copy SOD1-ALS model in *S. cerevisiae*. This model would enable us to study the effects of mutant Sod1 isoforms on the cell when they are expressed at lower more physiologically relevant levels. To do this, we adapted the model previously developed in *S. cerevisiae* [115] based on the overexpression of ALS-linked Sod1 isoforms using a high copy 2 μ plasmid with a constitutive GPD promoter. Using gateway cloning technology, WT yeast Sod1 and Sod1^{A4V} inserts were cloned into an integration vector that integrates into an empty region of chromosome I in *S. cerevisiae* [144], allowing for stable expression of Sod1 from the genome in either a WT or a Δ sod1 background. The strains were then characterised and tested for phenotypes that were previously observed in the overexpression model, such as growth defects and vacuole dysfunction [115]. This stable model was then used to perform a phenotypic screen using the BIOLOG system, and a genetic screen based on a library of knockouts related to vacuole and metabolic function. The BIOLOG system is a phenotypic microarray that involves high throughput testing of the growth of microbial cells on different metabolites, in order to investigate metabolic pathways such as carbon, nitrogen, phosphate, and sulphate utilisation. Additionally, osmotic, pH and ionic conditions are tested as well. This allowed us to compare the effects of the expression of more physiologically relevant levels of ALS-linked mutant Sod1 in *S. cerevisiae* and to potentially identify new or existing processes that are affected in SOD1-ALS.

3.2 Results

3.2.1 Testing the effect of Sod1^{A4V} expression on activity and abundance of Sod1 in WT and Δ sod1 cells

To study the effects of expression of both Sod1^{WT} and Sod1^{A4V} from the pAG306 chrI integration vector, immunoblotting and native *in-gel* sod activity assays were carried out. The pAG306 Sod1^{WT} and pAG306 Sod1^{A4V} plasmids were transformed into both WT and Δ sod1

backgrounds. Immunoblotting and sod activity assays were carried out on protein extracts from both cells grown to mid-log phase and cells grown to stationary phase. Densitometry analysis was carried out using ImageJ to measure the Sod1 levels relative to the total protein loaded, and the Sod1 activity level relative to the amount of Sod1 present.

For *in gel* sod activity assays, native protein extracts were ran on a native PAGE gel. The gel was then stained with a solution containing nitroblue tetrazolium (NBT), riboflavin and temed. Upon exposure to light, free radicals were generated and were used by NBT to change the colour of the gel from yellow to dark blue. Wherever there is sod activity either by Sod1 or Sod2 in *S. cerevisiae*, a band will appear on the gel due to competition between O_2^- preventing the colour change caused by NBT.

As seen in Figure 3.1 A) and B), expression of Sod1^{A4V} in a $\Delta sod1$ background did not result in a reduced amount of protein in cells grown to mid-log phase. However, expression of Sod1^{A4V} in a $\Delta sod1$ background did result in a significant loss in Sod1 activity in cells grown to mid-log phase compared to the WT empty vector control (Figure 3.1 C)). Additionally, Sod1^{A4V} could be seen to migrate further down the gel than Sod1^{WT}, suggesting a change in the folding or charge of the protein (Figure 3.1 A) and D)).

In stationary phase cells, a significant reduction in Sod1 levels in cells expressing Sod1^{A4V} in a $\Delta sod1$ background compared to the WT empty vector control was observed (Figure 3.1 D), E), and F)). On the other hand, the Sod1 activity relative to the amount of Sod1 present was not significantly different to that of the WT empty vector control. The pattern in which Sod1^{A4V} migrates faster in the gel than Sod1^{WT} could still be observed in stationary phase cells.

In summary, Sod1^{A4V} when expressed in $\Delta sod1$ cells grown to log phase, resulted in normal protein levels of Sod1 but a reduced Sod1 activity. When grown to stationary phase, Sod1 levels were reduced, but the Sod1 activity of the enzyme increased.

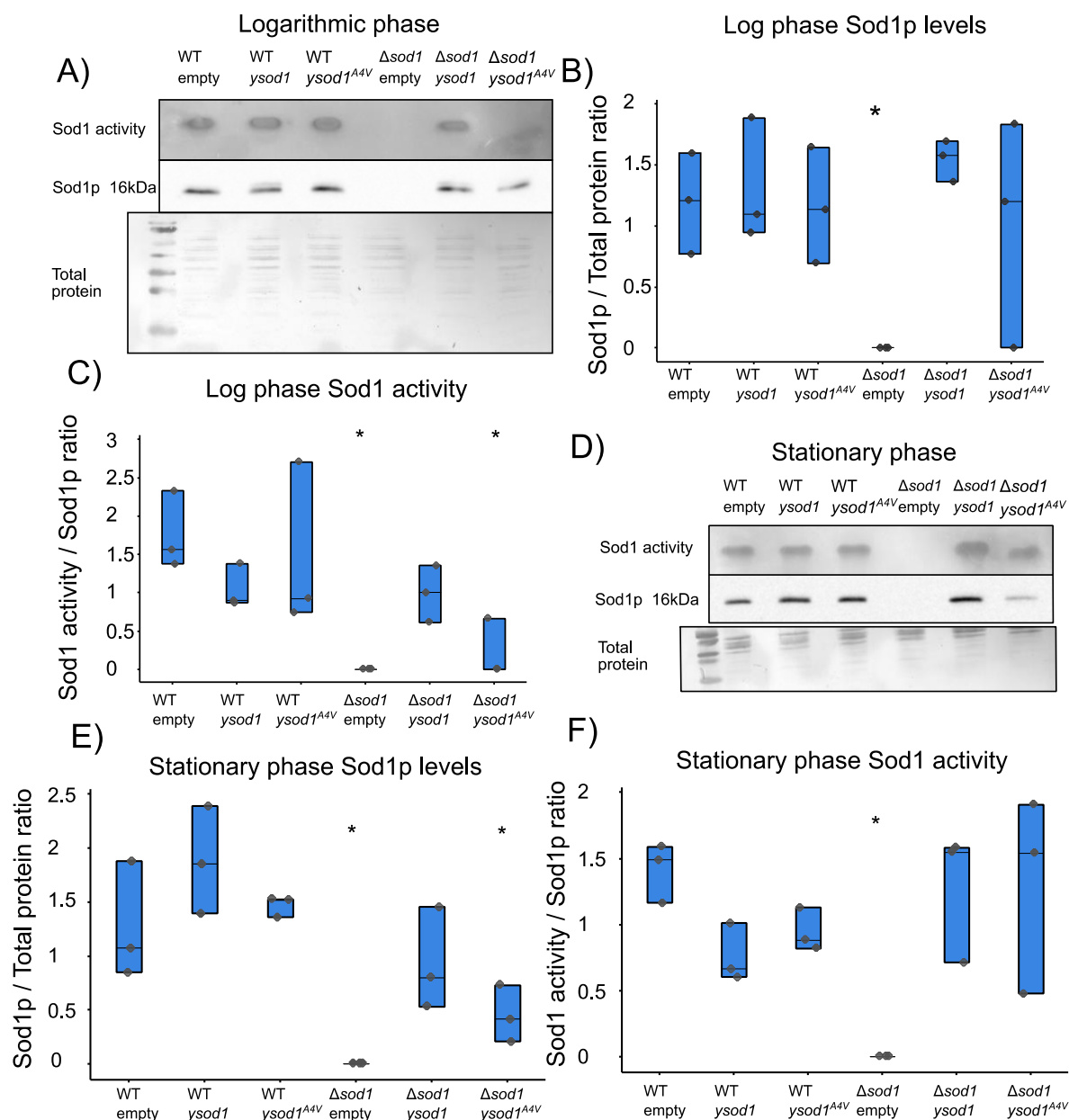


Figure 3.1 Testing the effect of the Sod1^{A4V} mutation on Sod1 activity and abundance in both WT and Δ sod1 backgrounds.

A) Native Sod activity assay of WT and Δ sod1 cells transformed with pAG306 empty chrI, pAG306 Sod1^{WT} ChrI and pAG306 Sod1^{A4V} ChrI grown to mid-log phase. Immunoblot against Sod1 and a Coomassie stain of the corresponding polyvinylidene fluoride (PVDF) membrane were included to calculate relative Sod1 levels and activities compared to the total protein. B) Quantification of Sod1 levels based on the immunoblots showed in A). C) Quantification of the sod activity normalised to the Sod1 protein level. Quantification is also based on densitometry analysis using ImageJ. N = 3. D) Native Sod activity assay of WT and Δ sod1 cells transformed with pAG306 empty chrI, pAG306 Sod1^{WT} ChrI and pAG306 Sod1^{A4V} ChrI grown to stationary phase. E) Quantification of Sod1 levels based on the immunoblots shown in D). F) Quantification of the sod activity from the Sod1 activity assay shown in D). Quantification is based on densitometry analysis using ImageJ. N = 3. The value represents the density of Sod1 bands divided by the density of the total protein from the PVDF membrane. A One-Way ANOVA comparison was used to test for statistical significance. * $p < 0.05$.

3.2.2 Testing the effect of expression of Sod1^{A4V} on growth of *S. cerevisiae* in a WT or $\Delta sod1$ background

Previously, it was observed that overexpression of ALS-linked mutant isoforms of Sod1^{WT} in *S. cerevisiae* from a high copy 2 μ plasmid led to a significant overexpression of Sod1 [115]. It was hypothesised that the overexpression of mutant Sod1 isoforms was leading to an increase in misfolded toxic fragments of Sod1. Overexpression of mutant isoforms of yeast Sod1 caused strong growth defects in a $\Delta sod1$ background. Expression of the mutant isoform of Sod1, Sod1^{A4V} from the pAG306 chrI integration vector with a GPD promoter resulted in similar levels of expression to that of Sod1^{WT} (Figure 3.1). By comparing the results from the integration vector model to the high copy plasmid model, it may be possible to distinguish between effects of elevated levels and reduced levels of mutant Sod1 in the cell. Expression of Sod1^{A4V} using a GPD promoter from the pAG306 chrI integration vector did not have any effects on the growth of cells in SC media (Figure 3.2).

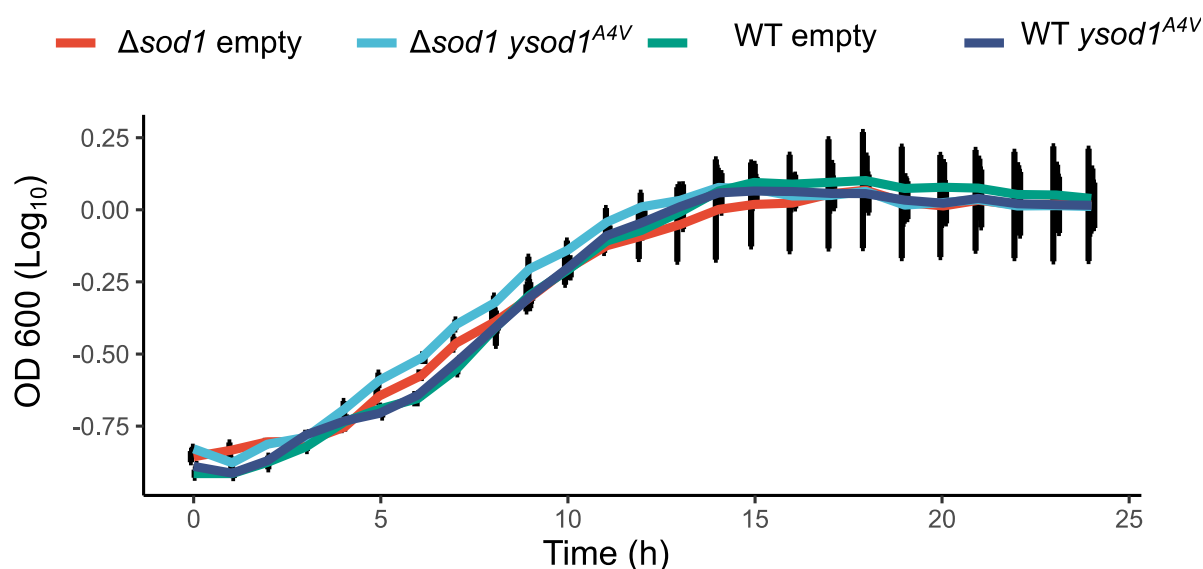


Figure 3.2 Effect of expression of Sod1^{A4V} in both WT and $\Delta sod1$ background on growth in SC media.

Growth curve displaying the growth of WT and $\Delta sod1$ cells expressing Sod1^{A4V} and an empty vector control in SC media. This experiment was carried out 3 times (N = 3) and this is a representative result. Error bars display the standard deviation between three technical replicates. The OD 600 values on the y axis is in the log₁₀ scale.

3.2.3 Assessment of the effect of expression of Sod1^{A4V} on vacuole function in *S. cerevisiae*

Previous data suggested that overexpression of mutant Sod1 isoforms in a $\Delta sod1$ background from 2 μ plasmids resulted in growth defects that were underpinned by

vacuolar and metabolic defects. $\Delta sod1$ cells that expressed mutant isoforms of Sod1 were defective in the uptake of quinocrine, indicating a loss of vacuolar acidification [115].

To test whether the comparatively lower expression of Sod1^{A4V} from an integration vector also led to vacuolar and metabolic defects, the growth of the strains in the presence of different stresses designed to challenge the function of the vacuole were tested. Cells expressing Sod1^{A4V} either in a WT or $\Delta sod1$ background did not show any sensitivity to elevated ZnCl₂ stress (Figure 3.3 B)), pH stress (Figure 3.3 C)) or salt stress (Figure 3.3 D)). As expected, $\Delta sod1$ cells expressing an empty vector showed high sensitivity to all three stresses.

To further investigate whether the vacuole lumens were normally acidified, WT and $\Delta sod1$ cells expressing, Sod1^{WT}, Sod1^{A4V} or an empty vector control were stained with the weak base quinocrine and visualised by wide-field fluorescence microscopy. Weak bases have been shown to accumulate in highly acidic intracellular organelles. Quinacrine labelling is a well-established assay to detect whether the vacuoles in yeast cells are properly acidified [162]. Expression of Sod1^{A4V} from an integration vector did not lead to any defects in quinocrine uptake, indicating that the vacuoles were properly acidified (Figure 3.4).

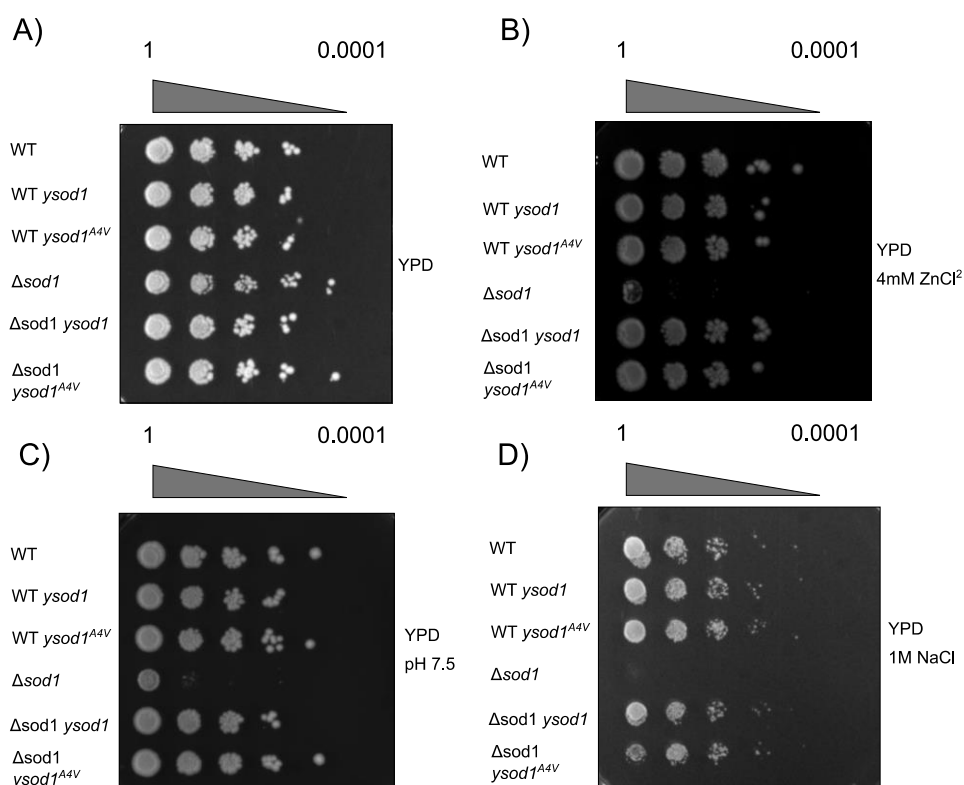
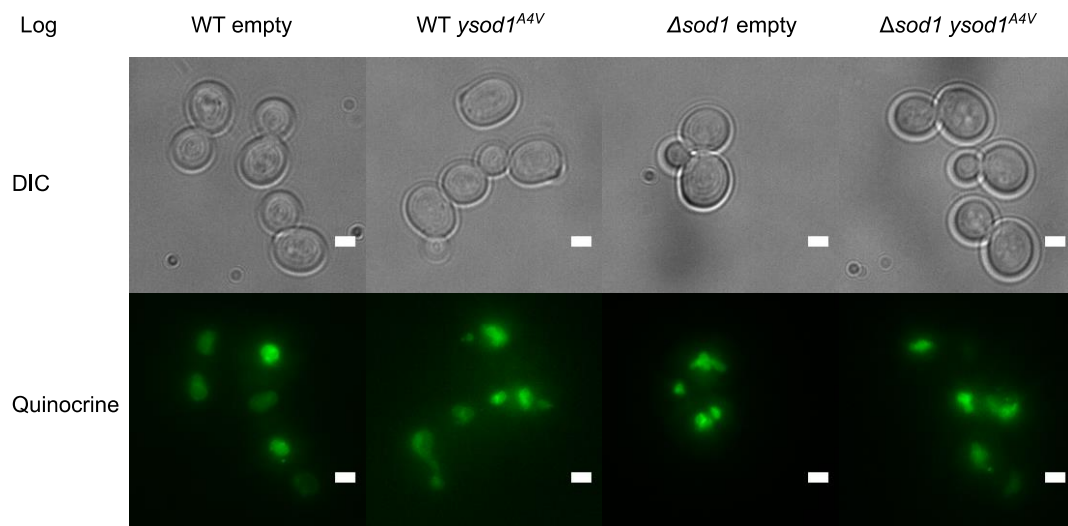


Figure 3.3 Spotting assay testing zinc sensitivity, sensitivity to alkaline pH and sensitivity to high salt levels.

Representative images of stress sensitivity spotting assays carried out on WT and $\Delta sod1$ cells expressing Sod1^{WT}, Sod1^{A4V} or an empty vector control. A) Shows growth from

integration strains spotted onto YPD agar. B) Shows growth from integration strains spotted onto YPD agar supplemented with 4 mM ZnCl₂. C) Shows growth from integration strains spotted onto YPD adjusted to pH 7.5. D) Shows growth from integrations strains spotted onto YPD media supplemented with 1 M NaCl. For all spotting assays cells were spotted in a 10-fold dilution series starting from OD 1 and ending at OD 0.0001.

A)



B)

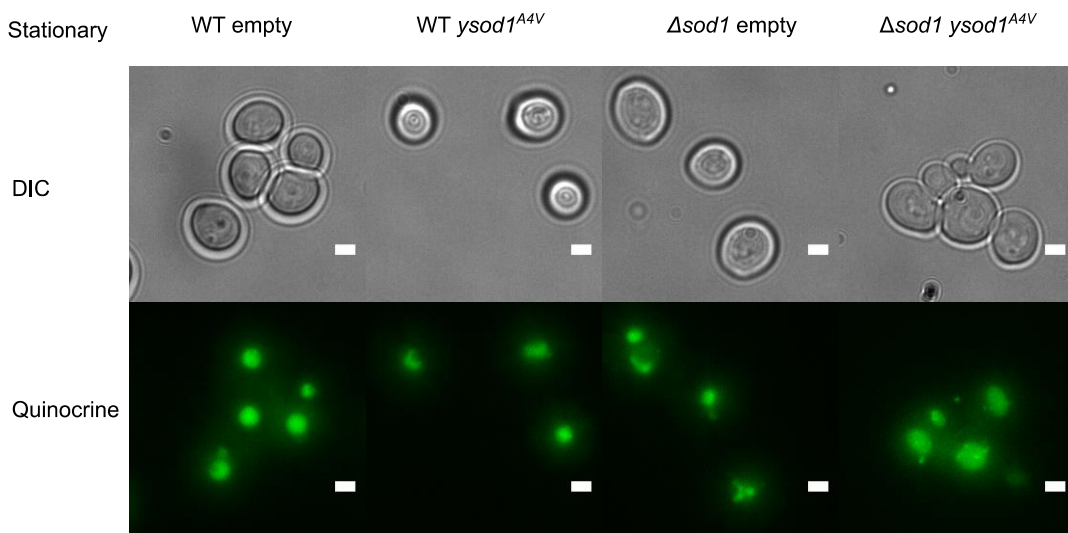


Figure 3.4 Quinocrine staining of WT and Δ *sod1* cells expressing Sod1^{A4V} or an empty vector control.

A) Display representative images of WT and Δ *sod1* cells expressing Sod1^{A4V} or an empty vector control grown to mid-log phase stained with 200 μ g/ml quinocrine captured by wide-field fluorescence microscopy. Quinocrine accumulates in the vacuole lumen if it is acidified relative to the cytosol and can be detected using a GFP filter. B) Representative images of WT and Δ *sod1* cells expressing Sod1^{A4V} or an empty vector control grown to stationary phase stained with 200 μ g/ml quinocrine as captured by wide-field fluorescence microscopy. For all images, the scale bar represents a distance of 5 μ m.

3.2.4 Testing the effect of Sod1^{A4V} expression in $\Delta sod1$ cells on the regulation of Sod1 by Torc1 signalling

Sod1 can be reversibly phosphorylated by Torc1 at Ser39 in response to nutrients, resulting in a change in conformation that inhibits its activity [69]. This allows for the Torc1 to regulate Sod1 activity in response to different nutrient signals. Initially, this interaction was discovered due to the fact that $\Delta sod1$ cells display a rapamycin resistant phenotype, in which they can grow in media supplemented with the Torc1 inhibitor rapamycin, whereas WT cells are unable able to grow. This study established Sod1 as an important component of the activation of the starvation response upon Torc1 inhibition by rapamycin.

To test whether Sod1^{A4V} interacts with the Torc1 in the same manner as Sod1^{WT}, cells expressing Sod1^{A4V} or an empty vector control were grown in SC media supplemented with 100 nm rapamycin in both WT and $\Delta sod1$ backgrounds. Cells expressing Sod1^{A4V} in a $\Delta sod1$ background displayed the same rapamycin resistant phenotype as that of $\Delta sod1$ cells (Figure 3.5 A)). Expression of Sod1^{A4V} in a WT background showed the same rapamycin sensitive phenotype as that of WT cells.

The rapamycin resistant phenotype of cells expressing Sod1^{A4V} could be due to the reduced activity and/or stability of the protein caused by the A4V mutation which displayed reduced activity, stability, and a different migration pattern in a native PAGE gel (Figure 3.1). It could also be that Sod1^{A4V} is no longer able to be phosphorylated at Ser39 by Torc1 rendering it unable to regulate its activity. To test whether the activity of Sod1^{A4V} can still be influenced by Torc1 phosphorylation, native *in-gel* Sod activity assays were carried out on cells that had been exposed to 100 nm rapamycin for 1 h or grown in media with 3% glycerol as the carbon source rather than 2% D-Glucose. Both of these conditions were previously shown to lead to an increase in Sod1 activity by blocking Torc1 inhibition [69] Switching the carbon source from 2% D-glucose to a non-fermentable carbon source such as 3% glycerol switches on mitochondrial oxidative phosphorylation and inhibits Torc1 signalling. Rapamycin inhibits Torc1 signalling by forming a complex with FK-binding protein 12 (FKB12).

In Figure 3.5 B) Sod1 activity assay gels are shown with WT cells and $\Delta sod1$ Sod1^{A4V} cells grown normally or exposed to rapamycin or glycerol for 1 h. In both WT and $\Delta sod1$ cells expressing Sod1^{A4V} there was an increase in Sod1 activity after exposure to rapamycin or glycerol. This suggests that upon inactivation of Torc1 by rapamycin or glycerol, levels of phosphorylation of both Sod1^{WT} and Sod1^{A4V} by Torc1 is decreased, resulting in an increase in Sod1 activity for both isoforms. It must be noted that the appropriate loading control has not been carried out for the

sod1 activity assays shown in Figure 3.5 B). The correct loading control would involve running denatured samples of the same samples used in the sod activity assay in Figure 3.5 B) on an SDS-PAGE gel and probing for Sod1 by immunoblotting so as to determine the level of Sod1 protein in the samples. Additionally, coomassie staining of the SDS-PAGE gels should be carried out in order to determine the total protein level in the samples. This would allow for quantification of the Sod activity in response to treatment of WT cells and $\Delta sod1$ Sod1^{A4V} cells with DMSO, rapamycin, or glycerol.

Additionally, it must be noted that more repeats of this experiment are required in order to determine whether the differences that have been observed are significant.

In summary, expression of Sod1^{A4V} in a $\Delta sod1$ background resulted in a rapamycin resistant phenotype, identical to that seen in $\Delta sod1$ cells. Expression of Sod1^{A4V} in a WT background did not lead to a rapamycin resistant phenotype. Sod activity assays of cells exposed to treatments that inhibit Torc1 signalling such as rapamycin or switching to a non-fermentable carbon source such as glycerol suggest that Sod1 activity of both WT and Sod1^{A4V} isoforms increases after Torc1 signalling is inhibited. This suggests that Sod1^{A4V} is still under regulation by Torc1 through phosphorylation as its activity increases following Torc1 inhibition. However, due to the reduced Sod1 activity and/or stability of the Sod1^{A4V} isoform, the cells display the same rapamycin resistant phenotype as the $\Delta sod1$ strain.

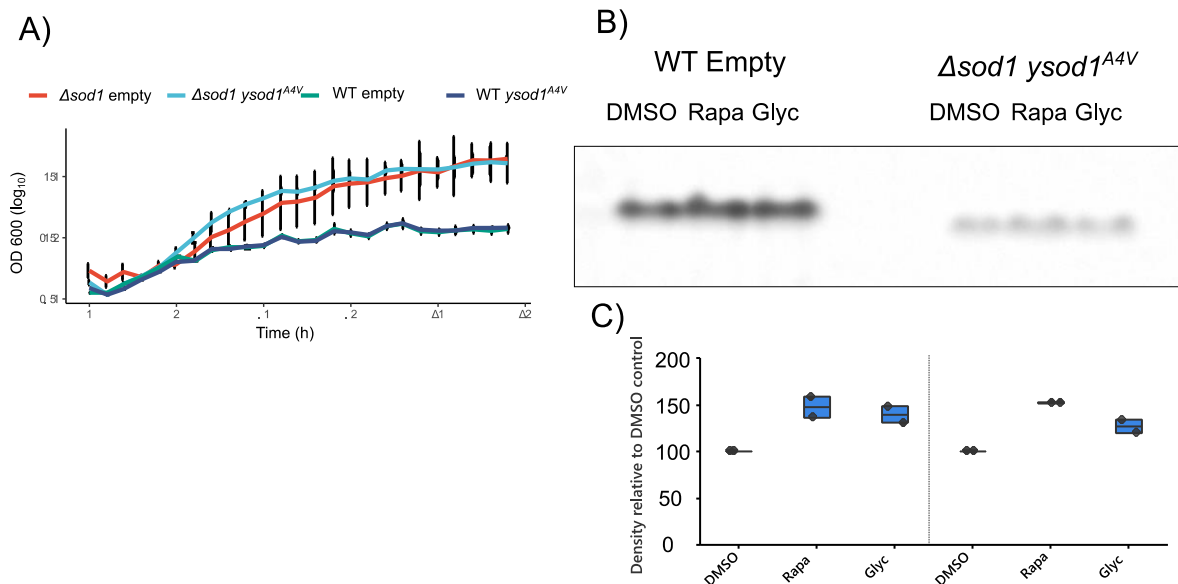


Figure 3.5 Effect of the Sod1^{A4V} mutation on the interaction between Sod1 and the Torc1 signalling.

A) Displays a growth curve of WT and $\Delta sod1$ cells expressing Sod1^{A4V} or an empty vector control grown in SC media supplemented with 100 nm rapamycin. The OD 600 values on the y axis are in the log₁₀ scale. Error bars represent the standard deviation from three technical replicates. N = 3 and this is a representative result. B) Displays a native Sod activity gel of WT cells expressing the empty vector and $\Delta sod1$ cells expressing Sod1^{A4V} in

log-phase treated with 100 nm rapamycin, or with the carbon source switched from 2% glucose to 3% glycerol for 1 h prior to native protein extraction. 5 µg of native protein extract was loaded into each well. C) Displays quantification of the Sod activity assay shown in B). Densitometry was performed using ImageJ and the density of the band was compared to the DMSO control. Each dot represents the value from one experiment. The experiment was repeated twice. N = 2

3.2.5 Screening for metabolic defects upon expression of Sod1^{A4V} using the BIOLOG phenotypic microarray.

So far the results suggested that low levels of expression of Sod1^{A4V} did not reveal the same gross vacuolar and metabolic defects observed when expressed from a 2µ plasmid [115]. We sought to determine whether subtle metabolic defects caused by expression of Sod1^{A4V} may appear when the cells were grown in nutritionally limited media. We decided to carry out a phenotypic microarray using the BIOLOG system to investigate whether expression of Sod1^{A4V} in cells under a range of nutritional limitations would reveal any novel synthetic interactions. The BIOLOG phenotypic microarray consists of ten different 96-well plates that test various processes in the cell, from utilisation of carbon sources to resistance to pH stress by measuring the growth of *S. cerevisiae* cells. A summary of the nine BIOLOG plates used in this study can be found in Table 3.1 . The composition of the media and the protocol can be found in the materials and methods section and the full results can be found in the appendix (Figure 8.1, Figure 8.2, Figure 8.3).

Table 3.1 Summary of Biolog plates.

Plate	Description
PM1	Carbon source utilisation
PM3	Nitrogen source utilisation
PM4	Phosphate & sulphate source utilisation
PM5	Nutrient supplementation
PM6	Utilisation of dipeptides as a nitrogen source
PM7	Utilisation of dipeptides as a nitrogen source
PM8	Utilisation of di-and tri peptides as a nitrogen source
PM9	Osmotic stress
PM10	pH stress

Initially two strains were chosen for the BIOLOG screen. These were BY4741 containing the pAG306 empty vector and BY4741 containing the pAG306 *SOD1^{A4V}* vector. In the results below, these strains are referred to as WT and A4V respectively. We decided to screen Sod1^{A4V}

expression in the WT background rather than the $\Delta sod1$ background, as it would more closely resemble the heterozygotic nature of human ALS disease in which the mutant *SOD1* allele is present alongside the native *SOD1* allele. The nine BIOLOG plates outlined in Table 3.1 were tested only once, and the strategy was to repeat any plates or conditions that revealed any differences between the two strains in additional replicates.

The process for analysis of the biolog results is shown in Figure 3.6. In A) the raw growth curves were plotted with blue representing the WT and red representing the A4V. The area under the curve (AUC) for each well and strain was calculated and used for comparison of growth between WT and A4V in different conditions.

Comparison of results from the plates between different strains was carried out by generating heatmaps that group similar conditions together by hierarchical clustering. This method of analysis was chosen so as to quickly identify groups of compounds that promote strong or poor growth and to observe whether expression of Sod1^{A4V} resulted in any differences between the phenotypic profile of the BY4741 strain.

For example, the results from the PM1 plate that tests for utilisation of different compounds as carbon sources in yeast showed different clusters of compounds that either promoted strong yeast growth, or very poor growth. D-glucose, D-galactose, D-mannose, and D-fructose all formed a cluster of the carbon sources that promoted the strongest growth, whereas D-Serine, L-lyxose, α -keto-butyric acid and D-threonine formed the worst growing cluster (Figure 3.7).

The WT strain appeared to grow better than WT A4V strain in conditions testing for L-arabinose, myo-inositol, m-hydroxy phenyl acetic acid, D-aspartic acid, adenosine, 2-deoxyadenosine, L-serine, D-galactose, α -D-glucose, tween 80, D-L-malic acid, acetic acid, maltose, bromo succinic acid, D-L- α -glycerol phosphate, citric acid, D-trehalose, pyruvic acid, α -keto glutaric acid, fumaric acid, glyoxylic acid, and methyl pyruvate.

Citrate, fumarate, α -keto glutaric acid and glyoxylate are all part of the TCA cycle, so the poorer growth of the A4V strain in conditions that require these compounds to be assimilated for use as carbon sources could indicate a metabolic defect.

The A4V strain appeared to grow better than the WT in certain conditions such as D-fructose-5-phosphate, inosine, glycyl-L-proline, D-ribose, sucrose and D-gluconic acid.

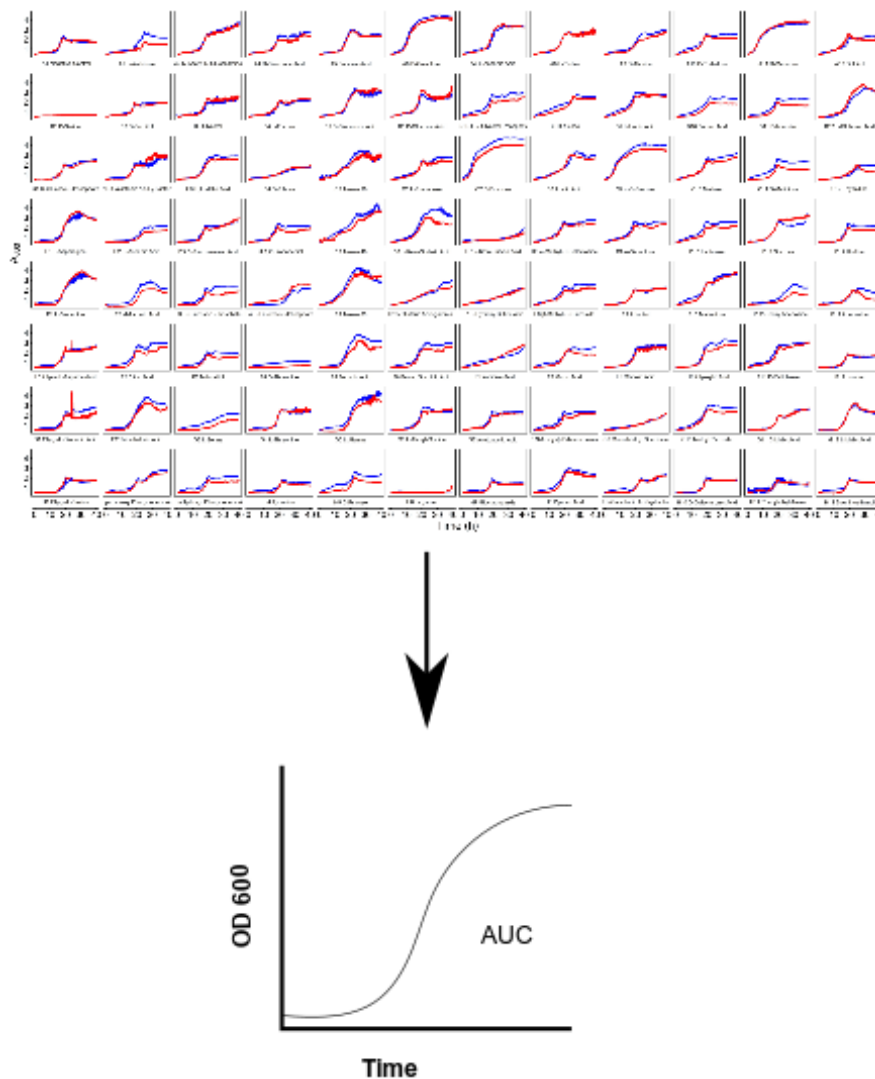


Figure 3.6 Biolog Screen Workflow.

A) Displays a panel plot of the growth curves in each well of the 96 well PM1 carbon sources plate. Blue lines represent the growth of WT and red lines represent the growth of A4V. B) Schematic describing what the AUC measurement that is used for the downstream analysis.

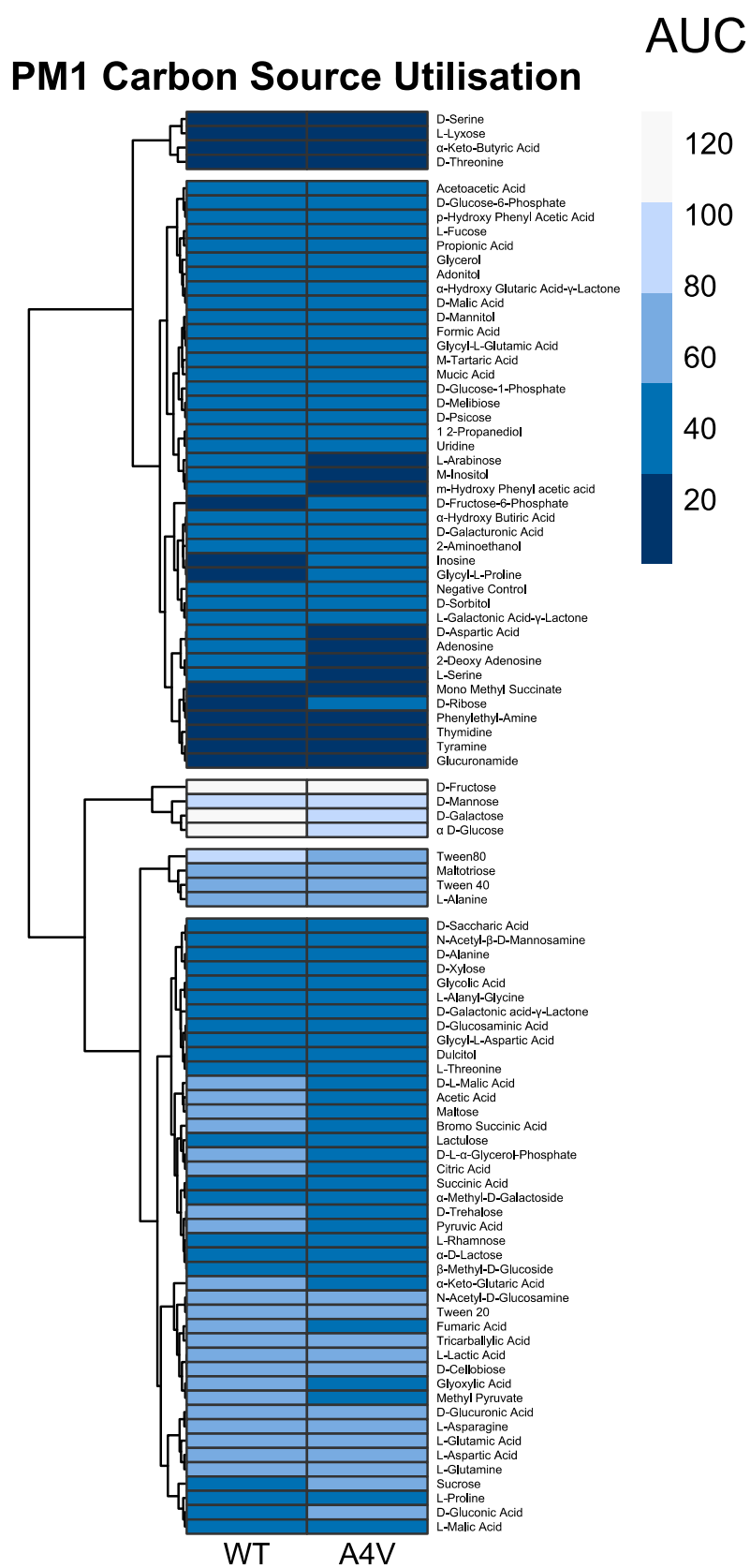


Figure 3.7 PM1 Carbon source utilisation test between WT and A4V.

AUC values from growth curves of WT and A4V from the PM1 carbon source utilisation plate. Dendrograms represent hierarchical clustering of results with more similar AUC values clustered together. Higher and lower AUC values are represented by lighter and darker colours of blue respectively. N = 1.

3.2.6 PM6, 7 and 8 testing for dipeptide utilisation as a nitrogen source were repeated

To test for utilisation of dipeptides as the nitrogen sources, cells were grown in media lacking L-glutamic acid (the preferred nitrogen source for *S. cerevisiae*). Each well of the PM6, 7 and 8 plates contained a different di or tripeptide. The ability of cells to utilise these di/tripeptides as the nitrogen source for growth was assessed by measuring absorbance at OD₆₀₀ over time. A large number of differences between WT and A4V were observed in the first round of screening of the plates PM6,7 and 8 which tested for utilisation of dipeptides as the sole nitrogen source (Figure 3.8). For this reason, we decided to repeat plates PM6, 7 and 8.

A number of clusters were identified in which the WT strain appeared to grow better than the A4V strain across all three plates. However, upon repetition of these plates, there appeared to be far less differences between the WT and A4V growth patterns in the second and third repeat. After combining the results of all three repeats together of PM7, hierarchical clustering revealed that the first A4V repeat growth pattern was the furthest away from all of the others in terms of similarity. The second and third A4V repeats formed a cluster. The second and third WT repeats also formed a cluster. A further cluster was identified with all three WT repeats. This suggests that across the three repeats, the WT results were closest together. This also suggests that the second and third A4V repeat were most similar and that the first A4V repeat was the result that differed the most (Figure 3.9).

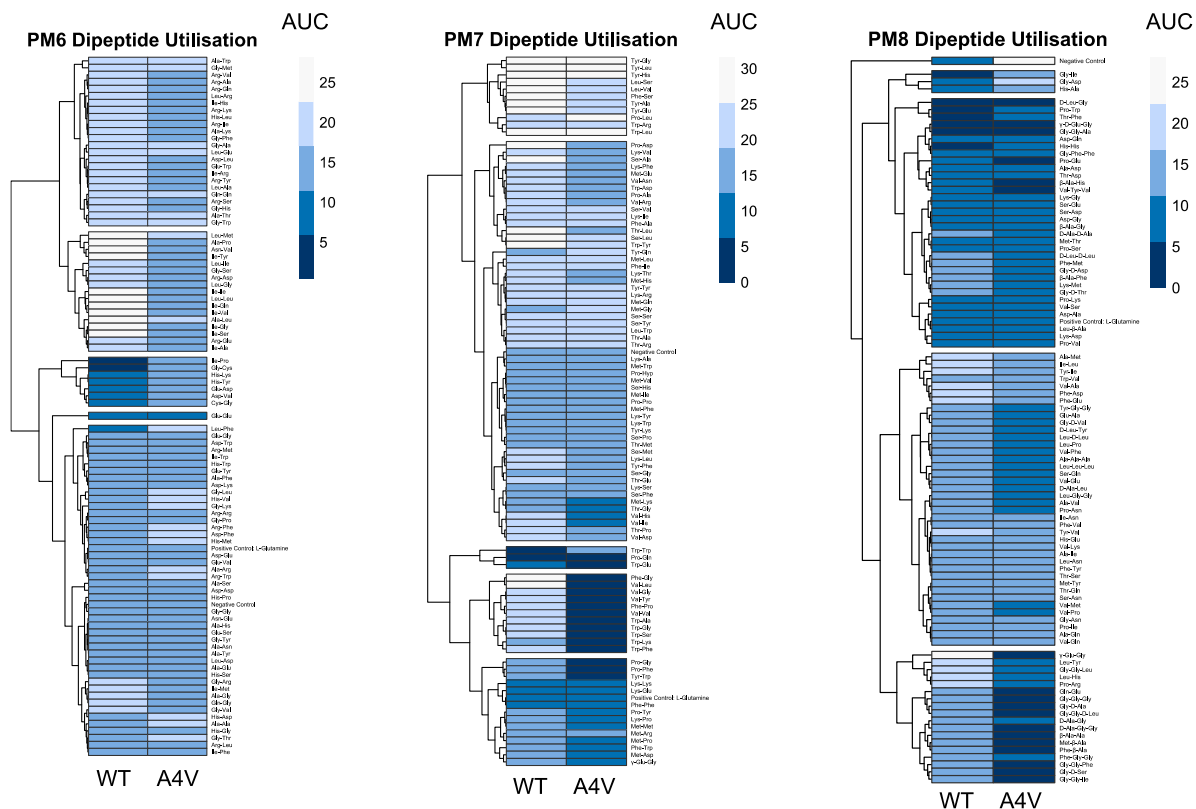


Figure 3.8 PM6, 7 and 8 screen results of WT and A4V testing for utilisation of dipeptides as a nitrogen source.

AUC values of growth of WT and A4V strains in the biolog plates PM6, 7 and 8. Dendrograms represent hierarchical clustering of different conditions to group the most similar results together. Higher and lower AUC values are represented by lighter and darker colours of blue respectively as shown by the legend. N = 1.

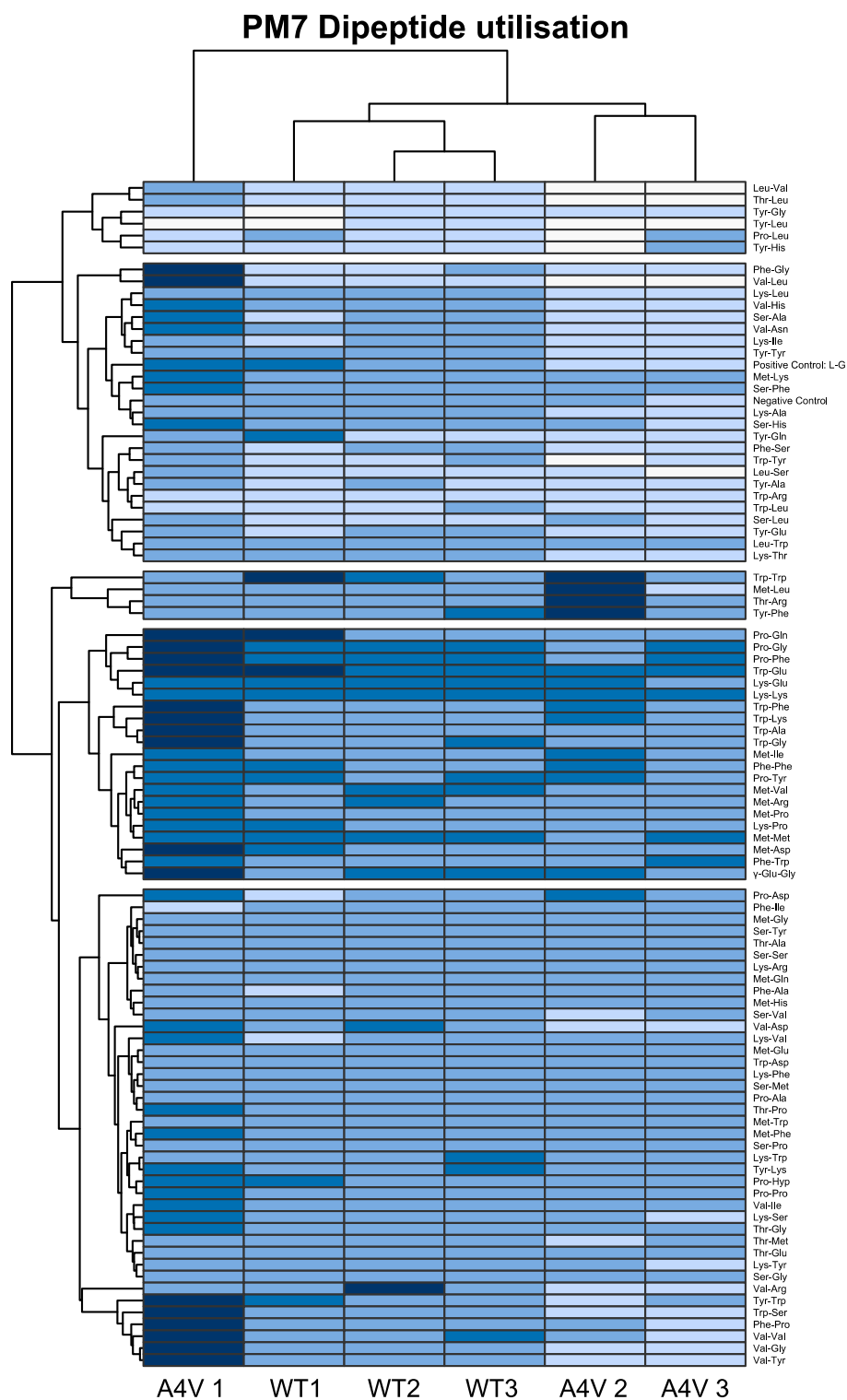


Figure 3.9 PM7 Dipeptide utilisation as a nitrogen source screen.

Heatmap of AUC values from growth curves of WT and A4V in the PM7 plate testing for utilisation of dipeptides as a nitrogen source. Columns and rows are clustered using the hierarchical clustering method. Lighter colour represents a higher AUC value and darker colour represents a lower AUC value. N = 3.

3.2.7 Further investigation of dipeptide utilisation as a nitrogen source in cells expressing mutant Sod1 isoforms

Due to the high variability encountered in the biolog screen of plates PM6, 7 and 8, we decided to further investigate the utilisation of dipeptides as a nitrogen source for growth on agar plates with a minimal media lacking a nitrogen source and supplemented with varying concentrations of different dipeptides. Spotting assays were carried out on a minimal media containing just yeast nitrogen base, only the amino acids required to satisfy the auxotrophies of the strains (leucine, uracil, histidine, lysine, and methionine) and either no nitrogen source, 2% ammonium sulphate (as the preferred nitrogen source normally found in YNB) or differing concentrations of the Ala-Leu and Leu-Leu dipeptides. 2% D-glucose was used as the carbon source. As seen in Figure 3.10 B), expression of Sod1^{A4V} in a $\Delta sod1$ or a WT background does not have any effect on the ability of *S. cerevisiae* to grow in media either lacking a nitrogen source, or with only a dipeptide provided as the nitrogen source. The $\Delta sod1$ cells expressing an empty vector displayed poorer growth compared to all the other strains in all of the different conditions tested with growth only observable in the first three spots. $\Delta sod1$ cells grown in media with the Leu-Leu dipeptide supplemented as a nitrogen source were barely able to grow at all with only growth observed at the OD₆₀₀ 1 dilution. This suggests an additional toxicity of the Leu-Leu dipeptide to cells lacking *SOD1* (Figure 3.11). In summary, expression of Sod1^{A4V} in a WT background does not impact the ability of cells to grow in media supplemented with dipeptides or lacking a nitrogen source, however cells lacking *SOD1* appear to be sensitive to the Leu-Leu dipeptide.

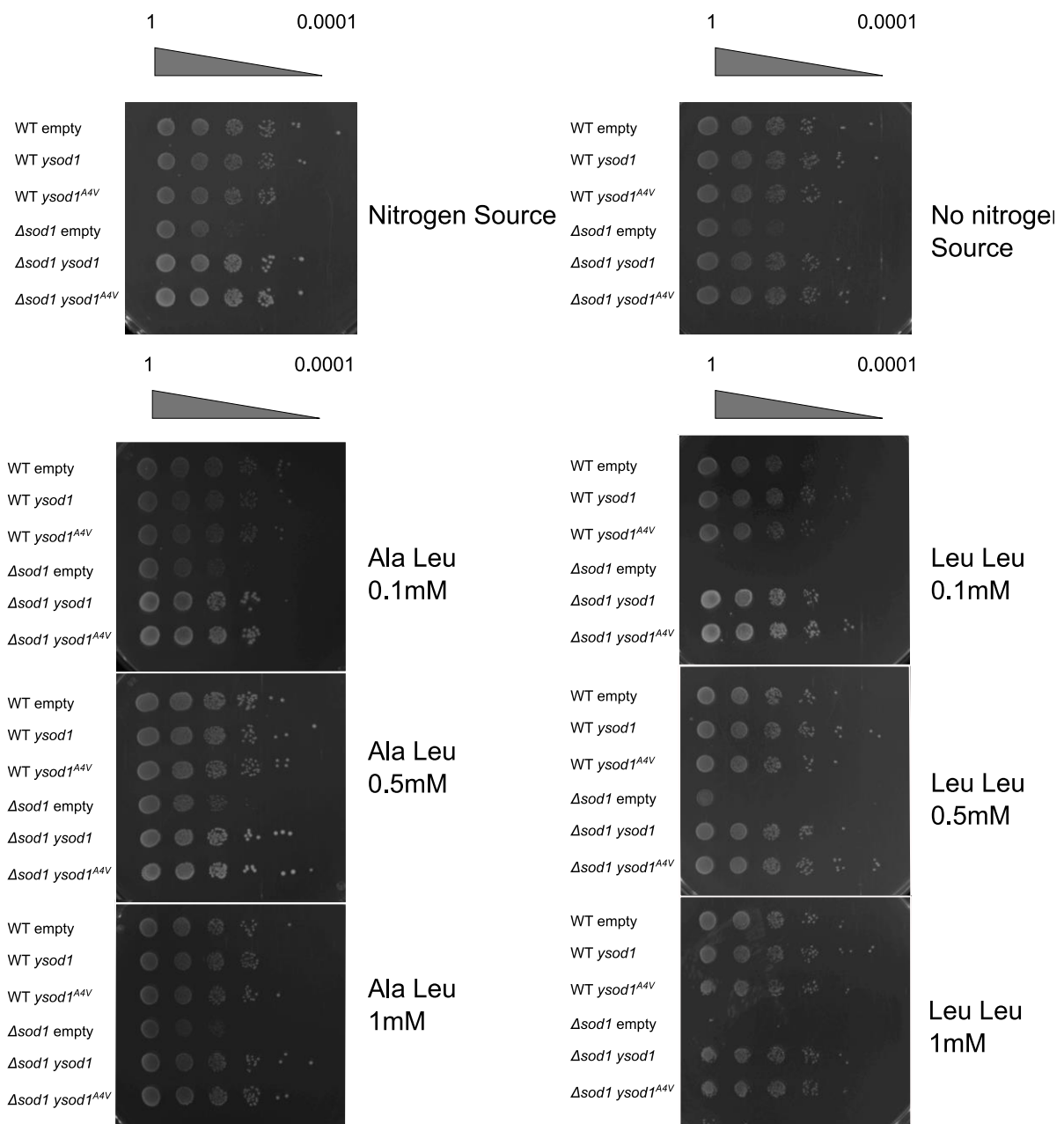


Figure 3.10 Cells expressing Sod1^{A4V} do not have any defects in dipeptide uptake or utilisation.

A) Representative image of cells stained with fluorescein isothiocyanate (FITC) conjugated to a Leu-Leu dipeptide captured by wide-field fluorescence microscopy. B) Spotting assays of integration strains grown in media lacking the normal nitrogen source (2% ammonium sulphate) supplemented with varying concentrations (0.1 mM, 0.5 mM, and 1 mM) of Ala-Leu and Leu-Leu dipeptides. N = 3.

3.2.8 Testing the growth of WT and $\Delta sod1$ cells expressing Sod1^{A4V} in combination with menadione induced oxidative stress

As no growth defects were observed in WT or $\Delta sod1$ cells expressing Sod1^{A4V} when grown in media supplemented with varying concentrations of the Ala-Leu and Leu-Leu dipeptides, it was decided to add in a stress that should challenge the function of the Sod1 enzyme. Addition of

oxidative stress through the O_2^- generating agent menadione should challenge the sod activity of the Sod1 enzyme by generating high levels of O_2^- . As shown earlier (Figure 3.1), the Sod1^{A4V} isoform had reduced activity and stability, so it should have a reduced capability in converting O_2^- into H_2O_2 and H_2O . The aim was to investigate whether addition of oxidative stress in combination with different nitrogen sources could reveal underlying defects in WT or $\Delta sod1$ cells expressing Sod1^{A4V}.

Addition of 40 μ M menadione caused defects in $\Delta sod1$ cells expressing Sod1^{A4V} regardless of whether there was a nitrogen source (2% ammonium sulphate) or not, or whether the nitrogen source was the Leu-Leu dipeptide (Figure 3.11). No growth defects were observed in any conditions upon expression of Sod1^{A4V} in a WT background. The $\Delta sod1$ cells expressing an empty vector could not grow at all in plates supplemented with 40 μ M menadione. This suggested that the Sod1^{A4V} isoform is less capable at converting O_2^- into H_2O_2 and H_2O most likely due to the decreased sod activity and decreased stability of the enzyme.

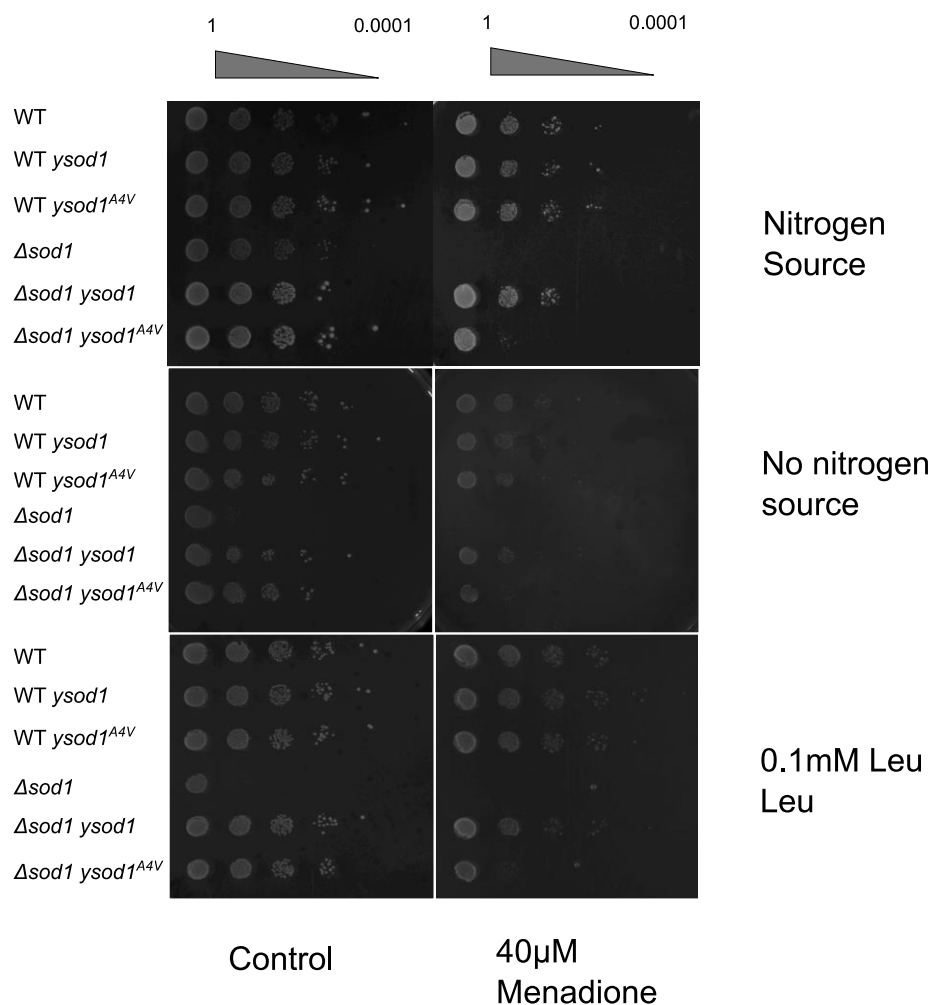


Figure 3.11 Spotting assays investigate growth using different nitrogen sources in combination with menadione induced oxidative stress.

Spotting assays of integration strains spotted onto YNB (without amino acids) agar supplemented with the minimum amino acids required to satisfy the auxotrophies of the

strains (uracil, leucine, lysine, methionine, and histidine). Plates were then supplemented with either 2% ammonium sulphate (preferred nitrogen source), 0.1 mM Leu-Leu, or nothing as a control. Plates either contained 40 μ M menadione or an ethanol control. Cells were spotted from OD₆₀₀ 1 and then downwards in a tenfold dilution series. N = 3.

3.2.9 Expression of Sod1^{A4V} into a library of knockouts related to the function of the vacuole in yeast.

Previous results obtained from overexpressing mutant Sod1 isoforms on a 2 μ plasmid in yeast cells demonstrated that expression of mutant isoforms in a Δ *sod1* background led to metabolic defects and a vacuolar acidification defect [115]. For this reason, we decided to screen for synthetic interactions between expression of mutant Sod1^{A4V} and different deletions in genes linked to a number of vacuolar and metabolic functions in the *S. cerevisiae*. The vacuole knockout library layout can be seen in Figure 3.12 A). The control plate contains 72 knockouts from the MATa deletion library. The A4V plate contains the same 72 knockouts that have had the pAG306 chrI vector expressing Sod1^{A4V} integrated into the genome. For both the control and A4V plate, the first six strains in wells A1–A6 contained the strains, WT (BY4741 pAG306 empty vector), WT SOD1 (BY4741 pAG306 Sod1^{WT}), WT SOD1^{A4V} (BY4741 pAG306 Sod1^{A4V}, Δ *sod1* (Δ *sod1* pAG306 empty vector), Δ *sod1* Sod1 (pAG306 Sod1^{WT}), Δ *sod1* Sod1^{A4V} (pAG306 Sod1^{A4V}). A range of mutants lacking genes encoding amino acid, metal ion and other transporters found on the vacuole membrane were tested. The pAG306 *SOD1*^{A4V} vector was integrated into each knockout and confirmed by PCR.

The strategy was to express Sod1^{A4V} into a library of knockouts and then screen for any synthetic interactions, initially by spotting onto agar with media supplemented with various stresses (Figure 3.12 B)). Potential synthetic interactions were then identified by comparing the growth between WT and A4V by eye and also by measuring growth as the pixel density of each spot using ImageJ. The fold change in growth of each strain compared to the WT was then calculated to normalise for variance between each plate. Then the fold change of the strains expressing Sod1^{A4V} was divided by the fold change of the equivalent strains that were not transformed (Figure 3.12 C)).

The conditions used for the screen were SC media, SC media buffered to pH 7.5 with 50 mM CaCl₂, YNB with 2% ammonium sulphate and the minimum number of amino acids required to permit growth in the strain background (uracil, leucine, histidine, methionine, and lysine) and the same minimal media supplemented with 40 μ M menadione to induce oxidative stress.

Once any possible synthetic interactions were identified from the initial spotting assay experiments, these would be tested further using liquid growth assays. Representative images of the spotting assay are shown in Figure 3.12.

From this screen, 10 knockouts were identified that reproducibly showed synthetic interactions upon expression of Sod1^{A4V}. After further validation in liquid media by performing growth assays in SC media only two knockouts $\Delta ego3$ and $\Delta pmc1$ showed reproducible reductions in growth upon expression of Sod1^{A4V}. These growth curves are shown in Figure 3.14. *EGO3* encodes a homodimeric subunit of the Ego complex in *S. cerevisiae* that plays a role in recruiting the TOR complex to the vacuole membrane in response to nutrient levels [163]. *PMC1* encodes a vacuolar Ca²⁺ ATPase that imports calcium into the vacuole from the cytoplasm and participates in calcium homeostasis [164]. These results suggest that expression of Sod1^{A4V} could cause growth defects in cells that are lacking *EGO3* or cells that are lacking *PMC1* and have perturbed calcium homeostasis.

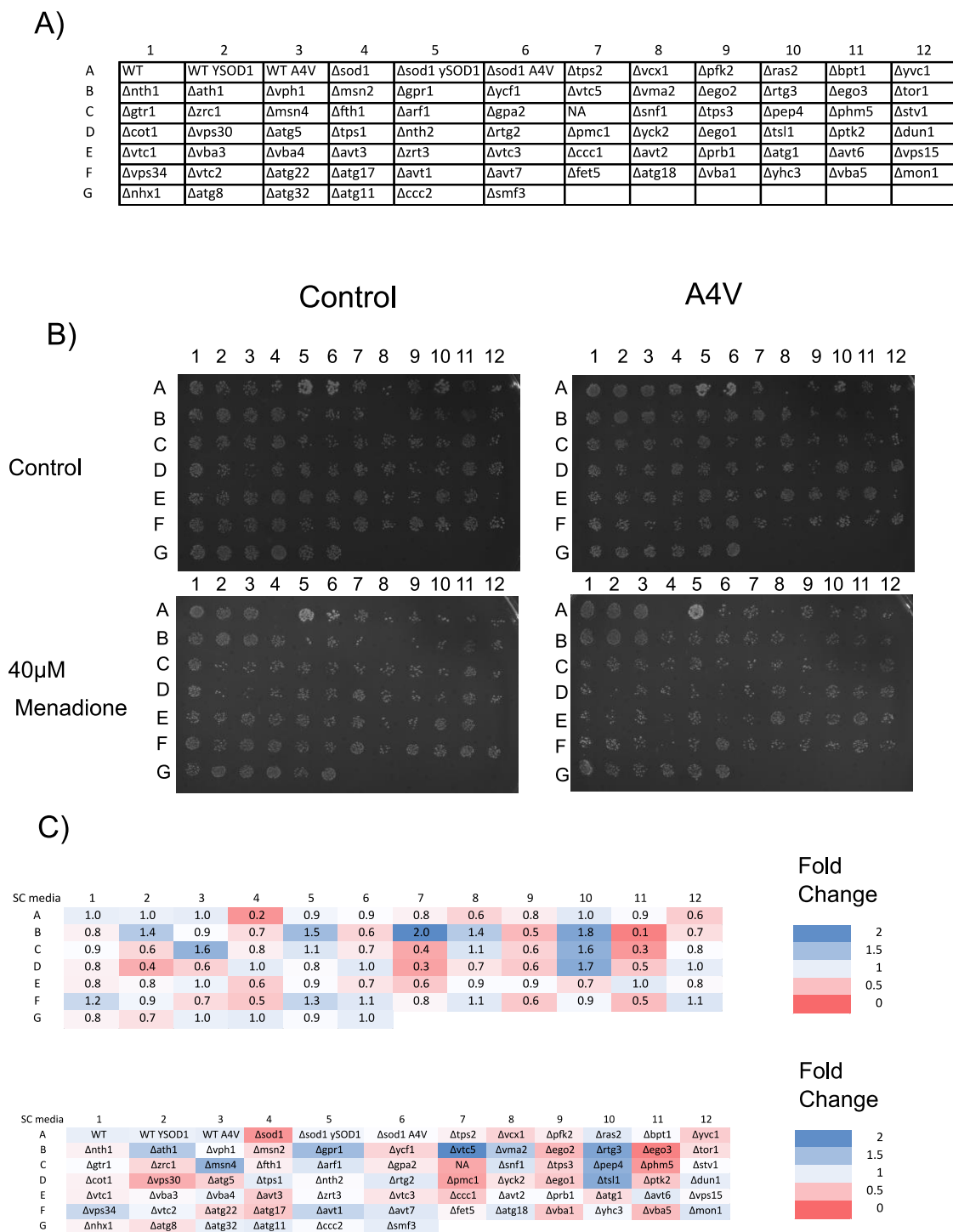


Figure 3.12 Spotting assays in different media conditions were carried out to screen for synthetic effects upon expression of Sod1^{A4V}.

A) Displays spotting assays in control media and in the same media supplemented with 40 μ M menadione. This experiment was carried out four times and potential synthetic interactions were investigated further using liquid growth assays. B) Displays a heatmap showing the fold change in growth (as measured by colony size) compared to the WT control. Colony size was calculated by measuring the intensity on ImageJ. These heatmaps display the average fold change values over all the experiments. N = 3.

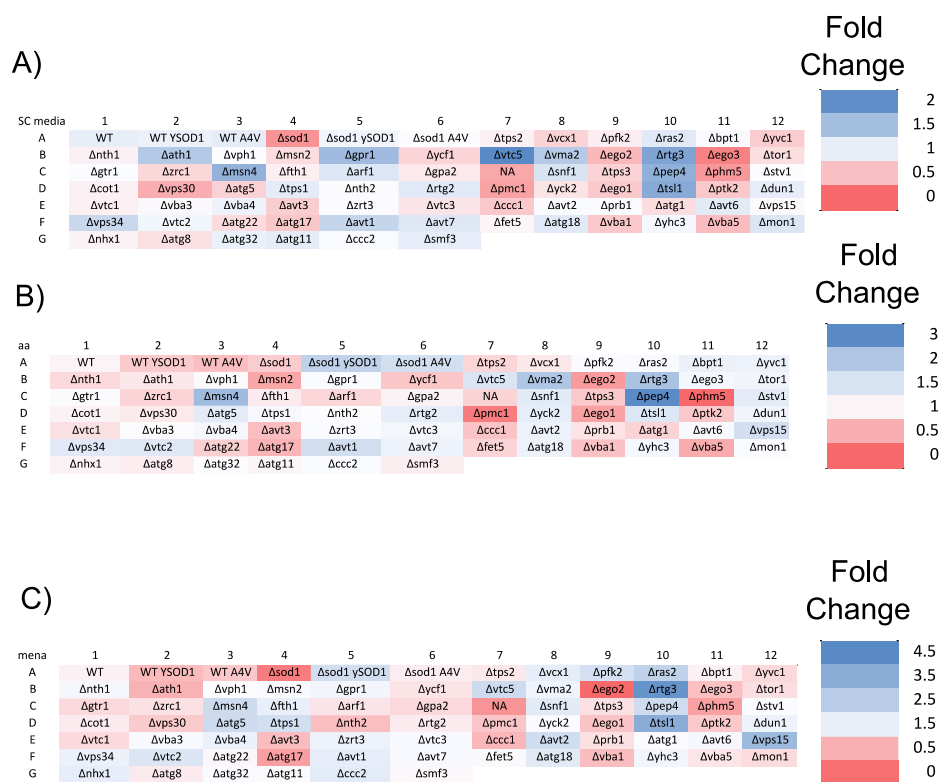


Figure 3.13 Fold change between WT and A4V from vacuole knockout library screen in different conditions.

A) Fold change between WT and A4V in colony size (as measured by pixel density) in SC media after 48 h. B) Fold change between WT and A4V in colony size in the same minimal media used in Figure 3.10 labelled aa. C) Fold change between WT and A4V in colony size in minimal aa media supplemented with 40 μ M menadione. For all of A), B) and C) the strains in wells A1 to A6, WT, WT YSOD1, WT A4V, Δ sod1, Δ sod1 ySOD1 and Δ sod1 A4V represent the strains: BY4741 pAG306 empty vector, BY4741 pAG306 Sod1^{WT}, BY4741 pAG306 Sod1^{A4V}, Δ sod1 pAG306 empty vector, Δ sod1 pAG306 Sod1^{WT}, Δ sod1 pAG306 Sod1^{A4V}. For these strains, the fold change shown is the fold change to the WT in A1. For all experiments above, N = 3.

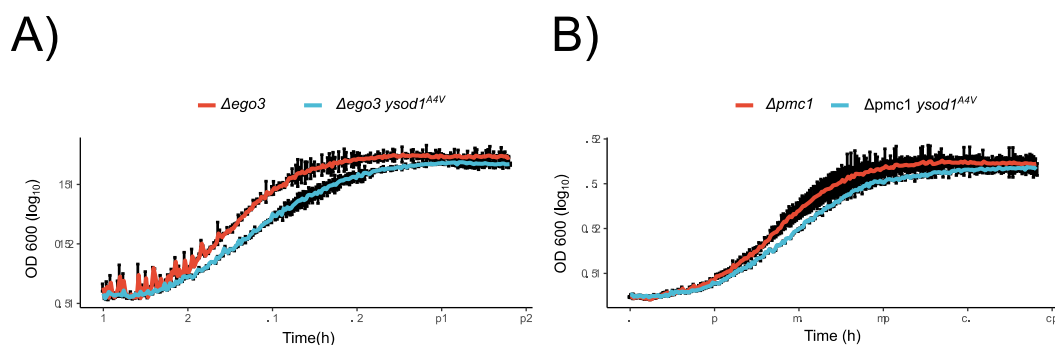


Figure 3.14 Synthetic interactions identified in the knockout screen.

A) Displays a growth curve of $\Delta ego3$ cells and $\Delta ego3$ cells expressing pAG306 Sod1^{A4V} in SC media. B) Displays a growth curve of $\Delta pmc1$ cells and $\Delta pmc1$ cells expressing pAG306 Sod1^{A4V} in SC media. Error bars display standard deviation of three technical repeats. N = 3. For both A) and B), the OD 600 value on the y axis is shown in the log₁₀ scale.

3.3 Discussion

3.3.1 Comparison between the integration vector model and the overexpression model of SOD1-ALS

The aim of this study was to develop a stable model of SOD1-ALS, by constitutively expressing Sod1^{A4V} under the GPD promoter from a vector integrated in an empty region of chromosome I in *S. cerevisiae*. As discussed previously, numerous single-copy stable models of SOD1-ALS have been developed in a range of organisms in order to study the effects if ALS linked Sod1 mutants on the cell when expressed at lower, more physiologically relevant levels. The aim was to then characterise the integrated SOD1-ALS model and compare it to the overexpression model that had previously been developed in *S. cerevisiae* [115].

The results from this study demonstrated that the integration model of SOD1-ALS that was constructed in this study produced similar expression levels of Sod1^{WT} and Sod1^{A4V} to that of native Sod1 in log-phase *S. cerevisiae* cells. In stationary phase cells, the protein levels of Sod1^{A4V} were much lower compared to that of Sod1^{WT}. Furthermore, the integration model was stable, no maintenance in selective media was required. Sod activity assay results indicated that Sod1^{A4V} when expressed from the integrated vector possessed reduced sod activity compared to Sod1^{WT} in log phase. In comparison, Sod1^{A4V} when overexpressed possessed no sod activity at all in log-phase [115]. In stationary phase cells, the sod activity of Sod1^{A4V} increased when expressed from both the integrated vector and the overexpression vector relative to its activity in log-phase [115].

The similar expression levels of Sod1^{WT} and Sod1^{A4V} compared to native Sod1 suggest that the integration model is suitable for studying the effects of lower, physiologically relevant levels of Sod1 expression on *S. cerevisiae*. In comparison, immunoblots from cells overexpressing Sod1^{WT}

showed much higher levels of protein compared to that of native Sod1. The reduction in Sod1^{A4V} protein levels observed in stationary phase cells when expressed from the integrated vector suggest that Sod1^{A4V} is being degraded or is inherently unstable. This is supported by an *in silico* study of the thermodynamics of 75 ALS-linked mutant isoforms of Sod1, that 70 of them had decreased stability and an increased propensity to aggregate [165]. Another study investigating the free energy landscape of 10 different ALS-linked mutant Sod1 isoforms discovered that they are linked with perturbations in the stability of Sod1 across different levels of maturation of the enzyme. [166].

In the *in-gel* sod activity assays, Sod1^{A4V} was observed to migrate faster than Sod1^{WT} or native Sod1. Protein migration in native PAGE is determined by their net charge, size, and structure. A protein will migrate faster through a native PAGE gel when it has a higher negative charge density. This suggests that Sod1^{A4V} has a higher net negative charge density compared to Sod1^{WT} or native Sod1. So far, studies have found Sod1^{A4V} to have a similar net negative charge to WT native Sod1 [167]. In the future, it will be important to explore why the Sod1^{A4V} isoform migrates faster than the Sod1^{WT} isoform in *S. cerevisiae*.

In conclusion, the activity and abundance of Sod1^{A4V} from the integration model follows a similar pattern to that of the overexpression model [115]. Sod activity is low in log-phase and increased in stationary phase. Additionally, proteins levels of Sod1^{A4V} were found to decrease in stationary phase for both the integration model and overexpression model. They key differences between the two models were that protein levels in the integration were more similar to that of native Sod1, whereas in the overexpression model protein levels were much higher. A limitation to this comparison is that the results from the overexpression model are from a previous study. In the future it would be useful to compare the sod activity and expression levels in one experiment for a true comparison. We concluded from this that the integration vector model of SOD1-ALS was a suitable model for studying the effects of physiologically relevant levels of Sod1^{A4V} on the cell.

3.3.2 Lack of cytotoxicity or vacuole dysfunction in the SOD1-ALS integration model

Once the integration model of SOD1-ALS was developed, we aimed to test the effect of physiologically relevant levels of Sod1^{A4V} on *S. cerevisiae*. This was achieved by testing for phenotypes previously observed in the overexpression model of SOD1-ALS, namely growth defects, sensitivity to stresses and vacuole dysfunction.

The results from this study indicated that expression of Sod1^{A4V} from a genomically integrated vector did not lead to growth defects of *S. cerevisiae* cells in YPD, or in any stressful conditions such as 4mM ZnCl₂, 1M NaCl, or media buffered to pH 7.5. Expression of Sod1^{A4V} actually rescued the phenotypes of $\Delta sod1$ cells in all of the above-mentioned stresses. Additionally, $\Delta sod1$ cells expressing Sod1^{A4V} from the integrated vector did not display any defect in vacuole acidification.

These results suggest that the Sod1^{A4V} isoform retains enough sod activity to rescue all of the phenotypes from $\Delta sod1$ cells. This is supported by the study in which it was demonstrated that just the expression of 1% of the total Sod1 pool in the cell was enough to rescue all of the oxygen-dependant phenotypes of $\Delta sod1$ cells [56]. As the growth assays in YPD media, media containing 4mM ZnCl₂, media containing 1M NaCl and media buffered to pH 7.5 were carried out on cells in stationary phase, it could be that the increased sod activity that was observed previously in stationary phase of the Sod1^{A4V} isoform could explain its ability to rescue the $\Delta sod1$ phenotypes. The results also demonstrate that the integrated *SOD1*-ALS model differs significantly from the overexpression *SOD1*-ALS model in the lack of growth defects, cytotoxicity, stress sensitivity and vacuole dysfunction observed [115]. In the future, it would be useful to repeat the same growth assays in cells grown to mid log-phase, where the sod activity of Sod1^{A4V} was observed to be at its lowest. Additionally in the future it could be useful to create a *SOD1*-ALS model where the expression of Sod1^{A4V} is placed under a titratable promoter such as the *GAL1* promoter [56] whereby expression of Sod1 can be controlled by different concentrations of galactose in the growth media. This would allow for us to test at what level the expression of Sod1^{A4V} becomes cytotoxic to *S. cerevisiae* cells.

3.3.3 Sod1^{A4V} loss of function with the rapamycin resistance phenotype

As the stable expression of Sod1^{A4V} was not observed to cause any cytotoxicity when expressed in WT or $\Delta sod1$ cells, we aimed to investigate specific conserved interactions between Sod1 and other proteins that have been previously demonstrated in *S. cerevisiae*. We decided to investigate whether the A4V mutation in *SOD1* has any effect on the interaction between Sod1 and Torc1 (described previously whereby Torc1 regulates the activity of Sod1 in response to nutrient levels. Mutations in the Torc1 pathway lead to either sensitivity to rapamycin (in the case of positive factors such as Torc1) or resistance to rapamycin (in the case of negative factors such as Sod1, and Ccs1). In nutrient rich conditions, rapamycin activates the starvation response, resulting in growth arrest. $\Delta sod1$ cells treated with 100 nm rapamycin fail to enter growth arrest even in

nutrient conditions. The aim of this experiment was to test whether cells expressing the Sod1^{A4V} isoform would show sensitivity or resistance to rapamycin.

The result from this study suggest that expression of Sod1^{A4V} caused rapamycin resistance in the $\Delta sod1$ background but not in the WT background. Additionally, results suggest the sod activity of Sod1^{WT} and Sod1^{A4V} increase upon inhibition of Torc1 (via rapamycin or switching of the carbon source to glycerol), suggesting that the sod1 activity of both isoforms is being negatively regulated by Torc1.

The rapamycin resistance phenotype appears to be a novel loss of function phenotype of the Sod1^{A4V} isoform. As Sod1^{A4V} in the integration model was observed to rescue the phenotypes of $\Delta sod1$ with regards, to stress sensitivity and vacuole defects, it was expected that it would also rescue the rapamycin resistant phenotype. This suggests that the Sod1^{A4V} isoform is unable to carry out its role in regard to the starvation response upon Torc1 inhibition in the same way that Sod1^{WT} is. The interaction between Sod1 and Torc1 has been suggested to be important for the modulation of cellular ROS levels to enable cells to proliferate in nutrient rich conditions while at the same time reducing oxidative damage during nutrient limited environments [62]. A recent study demonstrated that in *S. cerevisiae*, Sod1 may regulate the function of many proteins in the cell through cysteine oxidation. There was a specific enrichment in proteins that function in amino acid biogenesis [50]. In the future, other ALS-linked isoforms of Sod1 could be tested for the rapamycin resistant phenotype, to investigate whether this loss of function could be a universal factor between all mutant isoforms. The screen that was previously described [50] could be repeated with $\Delta sod1$ cells expressing Sod1^{WT} or Sod1^{A4V} to investigate whether the cysteine oxidation state of all of the proteins identified differs in cells expressing Sod1^{A4V}.

3.3.4 Phenotypic screening with the BIOLOG system

One of the primary reasons for developing the stable *SOD1*-ALS model that expresses Sod1^{A4V} from a genomically integrated vector was to perform genetic or chemical screens to enable the identification of potential novel pathways in *S. cerevisiae* that are affected by the expression of Sod1^{A4V}.

The BIOLOG phenotypic microarray was chosen as a chemical screen as it is allowed for testing different aspects of *S. cerevisiae* metabolism such as carbon & nitrogen source utilisation, phosphate and sulphate source utilisation, salt and osmotic stress tolerance and pH stress tolerance. We adopted the approach of performing the whole BIOLOG screen once, followed

by repeating plates that displayed the largest (if any) differences between the WT strain and the A4V strain. The original BIOLOG protocol involved measuring growth in each plate using a proprietary dye based on tetrazolium redox chemistry that is a readout for metabolic activity [168]. For this screen we decided to measure growth directly by measuring the absorbance at OD₆₀₀ over 48 h.

The plates pm 6, 7, and 8 that measured the utilisation of di/tripeptides as nitrogen sources in *S. cerevisiae* displayed the largest number of differences between the WT and A4V strain after the first round of screening. For this reason, they were selected to be repeated. However, after repeating the plates three times, no reproducible differences were observed. Hierarchical clustering analysis of the different repeats suggested that the first repeat of A4V differed the most from all of the profiles of repeat two and three. It is not clear what could be the cause of the large variability that was in the results from the biolog screen.

In conclusion, we could not identify novel pathways that were affected by the expression of Sod1^{A4V} in the WT background from the BIOLOG screen. In the future it could be worth repeating the BIOLOG screen using the proprietary redox dye and plate reader equipment as it would allow for all of the BIOLOG plates to be assayed at the same time thereby reducing variation from any technical errors. In the future it would also be useful to compare $\Delta sod1$ cells expressing Sod1^{WT} or Sod1^{A4V} as results from this study and the previous overexpression model study suggest that in *S. cerevisiae* Sod1^{A4V} is more cytotoxic in the $\Delta sod1$ background. Furthermore, for the plates pm 3, 6, 7 and 8 measuring the utilisation of amino acids and di/tri peptides as nitrogen sources, the use of a prototrophic *S. cerevisiae* background in the future would allow for more accurate results, as it would allow for the growth of experimental strains in media lacking any amino acid supplements. Even low concentrations of amino acids in the media can affect the expression of amino acid and di/tri peptide uptake machinery, thereby affecting the results [169].

It would be worth further investigating the other results observed in the BIOLOG screen between the WT and A4V strains. For example, in the PM1 plate testing for carbon source utilisation, the A4V strain appears to grow worse when required to utilise some compounds involved in the TCA cycle, such as citrate, fumarate, α -keto glutaric acid and glyoxylate as a carbon source. This could be suggestive of a potential defect in the TCA cycle for cells expressing Sod1^{A4V}.

In order to test whether the stable expression of Sod1^{A4V} in the WT or $\Delta sod1$ background gave rise to defects in the ability to use dipeptides as a nitrogen source. We grew WT and $\Delta sod1$ cells

in a minimal media containing yeast nitrogen base with no amino acids, supplemented with just the amino acids required to satisfy the auxotrophies of the strains. This media was supplemented with different concentrations of the Ala-Leu, and Leu-Leu dipeptides. No differences in growth were observed in the ability of WT or $\Delta sod1$ expressing Sod1^{A4V} cells. This suggests that in this stable model of SOD1-ALS, the expression of Sod1^{A4V} does not impact the ability of cells to grow on different nitrogen sources. Cells lacking SOD1 appeared to be sensitive to the Leu-Leu dipeptide as they couldn't grow at all in plates containing it.

3.3.5 Potential synthetic interactions between Sod1^{A4V} and EGO3/ PMC1

Another aim of creating the stable SOD1-ALS integration vector model system was to use it for genetic screening to identify any potential novel genetic interactions. A library of knockouts of genes with functions relating to the vacuole and metabolism in *S. cerevisiae* was created as the previous results observed in the overexpression model of SOD1-ALS, suggested that vacuole dysfunction was a key part of the toxicity that was observed in cells overexpressing mutant isoforms of Sod1. The pAG306 vector expressing Sod1^{A4V} was integrated each strain from the knockout library and correct integration was confirmed by PCR. The knockout screen was carried out in SC media, aa media (minimal media with only the amino acids required to satisfy the auxotrophies of the strains (uracil, leucine, histidine, methionine, and lysine) and aa media containing 40 μ M menadione. From this screen, synthetic growth defects were identified in cells lacking EGO3 and cells lacking PMC1.

EGO3 encodes Ego3, a homodimeric subunit of the ego complex in *S. cerevisiae*. The ego complex is made up of Ego1, Ego2, and Ego3 [163]. From the screen, neither $\Delta ego1$ nor $\Delta ego2$ were found to display synthetic defects in combination with the expression of Sod1^{A4V}. The ego complex mediates the activation of Torc1 in response to amino acid levels by acting as a scaffold for the RAG GTPases Gtr1 and Gtr2. The Ego3 homodimer is structurally analogous to that of the heterodimer of LAMTOR2 and LAMTOR3 in mammalian cells [170]. It has also been suggested that along with its function as a scaffold of the EGO complex, EGO3 and EGO1 could be performing a direct regulatory role in Torc1 activation. This is because the mammalian equivalent of the ego complex, the regulator complex was found to exhibit guanine nucleotide exchange factor (GEF) activity towards the RAG GTPases RaGA and RaGB in response to amino acids in a manner dependent on V-ATPase activity [171]. Cells that lack EGO3 display reduced Torc1 activity and a failure to recover from rapamycin induced growth arrest. However, this cannot explain the synthetic growth defect observed with the expression of Sod1^{A4V} as if that were the

case then similar synthetic interactions would have been observed with the other members of the ego complex, Ego1 and Ego2 [172].

The other synthetic interaction that was identified is in cells lacking *PMC1* a gene that encodes Pmc1, a Ca^{2+} transporter that imports calcium ions from the cytosol into the vacuole. Pmc1 plays a crucial role in calcium homeostasis, ensuring that high levels of Ca^{2+} in the cytosol are restored to normal levels by importing it into the vacuole whereupon it can be stored [164]. Pmc1 works alongside another transporter Vcx1 which also imports Ca^{2+} in exchange for exporting a H^+ ion. Expression of Pmc1 is upregulated by calcineurin in response to high calcium levels via the Crz1 transcription factor. This synthetic interaction between the loss of *PMC1* and expression of Sod1^{A4V} suggests that the impaired calcium homeostasis of the $\Delta pmc1$ strain could be bringing out an underlying toxic function of the Sod1^{A4V} isoform.

In the future, it will be important to test both of these synthetic interactions by re-expressing the deleted gene back into the cells so as to test whether the effect is reversed. Additionally, re-making the strains independently from the construction of the screen and testing them for the same phenotypes.

4 Developing CRISPR/Cas9 strategies for generating ALS linked SOD1 mutants in *S. cerevisiae*.

4.1 Introduction

4.1.1 Development of genome editing in *S. cerevisiae*

Genome editing is one of the most powerful techniques available in cell biology. The ability to edit the genome of many different organisms is fundamental for studying the functions that genes have in the cell. As mentioned previously, *S. cerevisiae* is one of the most powerful model organisms available for genome editing due to its extremely well-characterised genome, the ease with which it can be transformed and its preference towards homologous recombination (HR) over non-homologous end joining (NHEJ).

A major breakthrough in genome editing in *S. cerevisiae* came when it was discovered that DNA cassettes can be integrated into the genome during *S. cerevisiae* transformation by HR and by using restriction enzymes to digest circular plasmids in regions of homology to the *S. cerevisiae* genome integration efficiency could be greatly enhanced [173]. This paved the way for the development of gene disruption techniques using PCR, in which either an antibiotic or auxotrophic selection marker flanked by regions of DNA homologous to the gene of interest are amplified by PCR and then transformed into *S. cerevisiae*, resulting in the replacement of the gene with the selection marker. An example of this is the kanMX cassette giving resistance for kanamycin in bacteria and gentamicin (G418) in *S. cerevisiae* [174]. From this, gene deletion libraries [122], GFP reporter libraries [175] and other collections have been developed.

In *S. cerevisiae*, antibiotic resistance selection markers and auxotrophic selection markers are used. It has been reported that in some cases, the use of auxotrophic selection markers can affect the phenotypes observed which can cause some problems when trying to analyse the phenotypes that arise from gene editing [176]. Furthermore, the limited number of selection markers available can be problematic if a number of gene edits are required to be made. To counter this, marker removal and recycling strategies have been developed such as the Cre-LoxP recombinase system [177].

Genome editing involving the incorporation of DNA cassettes using HR is greatly enhanced by the introduction of a double-stranded break (DSB) in the DNA, specifically at the locus where the edit is required. Technologies have been developed using various enzymes that can introduce

Chapter 4. Developing CRISPR/Cas9 strategies for generating ALS linked SOD1 mutants in *S. cerevisiae*.

DSBs into the DNA. Initially zinc-finger nucleases (ZFNs)[178] and transcription activator-like effector nucleases (TALENs) [179] were harnessed for more efficient genome editing. More recently, CRISPR/Cas RNA-guided nucleases (CRISPRs) have emerged as the most powerful tool for precise efficient genome editing.

4.1.2 CRISPR/Cas9 system discovery and function

CRISPR stands for clustered regularly interspaced short palindromic repeats. In recent years, CRISPR/Cas9 has emerged as one of the most powerful tools in genome editing due to the precision, high efficiency, and relative simplicity that it offers. CRISPRs were initially discovered in 1987 in a study that sequenced the *iap* gene in *E. coli* [180]. The study identified five highly homologous sequences, 29 nucleotides long that repeated after each other. At the time the function of this structure was unknown, however in 2007 it was shown that these palindromic repeats (CRISPRs) and their associated Cas (CRISPR-associated) endonucleases are part of a defence mechanism that bacteria and archaea possess to protect against viruses [181].

CRISPR/Cas associated immunity occurs in three main steps. Firstly, after viral challenge, the bacteria incorporate small fragments of the viral sequence (protospacers) into its chromosome in what is known as a CRISPR array. Secondly, these repeats are transcribed into precursor CRISPR RNA molecules (pre-crRNA) and then cleaved into short crRNA sequences that can base pair with the complementary sequences of the invading virus. Finally, the Cas endonuclease recognises these ~20 bp crRNA molecules that have base paired with the viral DNA directly upstream of the protospacer adjustment motif (PAM). The Cas endonuclease then cuts the DNA and creates a DSB [182].

4.1.3 Utilisation of CRISPR/Cas9 system for genome editing

The CRISPR/Cas system has been engineered so that it can be used in a wide range of different organisms to facilitate gene editing. The *Streptococcus pyogenes* CRISPR/Cas system is the most well studied and it involved the Cas9 endonuclease which recognises the nucleotides 5'-NGG-3' as its PAM site. It was shown that by expressing Cas9 alongside a guide RNA (gRNA) cassette, Cas9 can be directed to any genomic locus with an appropriate PAM site whereupon it will cleave the DNA. By including an appropriate repair template, precise genome editing can be achieved ([183]).

In *S. cerevisiae*, CRISPR/Cas9 tools have been developed usually consisting of a plasmid that expresses Cas9 under a constitutive promoter and gRNA under an RNA polymerase III promoter to ensure that the gRNA is expressed in an unmodified state [184]. The repair template

that is required to incorporate the desired edits can either be expressed from a plasmid, generated by PCR, and co-transformed into the cell along with the Cas9 and gRNA expressing plasmid, or synthesised as a single-stranded oligo (ssOligo). Usually, the repair template is ~95 bp long. The repair template sequence should consist of the gene edits that are desired, silent mutations to the PAM site or gRNA sequence directly upstream of it (to prevent further binding of Cas9 once successful edits have occurred) and 40 bp homology arms flanking these edits (to ensure incorporation of the repair template into the genome by HR).

4.1.4 Using CRISPR/Cas9 editing to generate a single-copy *S. cerevisiae* model for SOD1-associated ALS

Most ALS models that have been studied have relied upon the overexpression of mutant isoforms of Sod1 into various organisms. As discussed in the introduction, these models have been able to reconstitute several ALS related pathologies, in yeast, worms, flies and mice and they have contributed enormously to the understanding in how mutations in *SOD1* cause cellular dysfunction. However, it has become clear that overexpression models should not be relied upon alone. It has been shown that even the overexpression of Sod1^{WT} can cause deleterious effects in different organisms [160]. This suggests a role for Sod1^{WT} protein in ALS, however it also emphasises the need for ALS models that study the effect of mutant Sod1 isoforms, when expressed at more physiologically relevant levels. Recently, single-copy ‘knock-in’ models of ALS have been developed in a number of different organisms including nematodes [86], flies [90], zebrafish [93] and mice [161] with all of them presenting various aspects of the disease. The phenotypes observed in these single-copy models are often less severe than those seen in overexpression models.

4.1.5 Aim of this study

The aim of this study is to generate ALS-linked mutations in the *SOD1* gene using CRISPR/Cas9 editing in *S. cerevisiae* and to characterise the effect (if any) these mutations have on the Sod1 enzyme. The mutations that we have chosen to engineer are Sod1^{A4V}, Sod1^{G57R} and Sod1^{H48Q} as they have been previously studied in an overexpression based yeast *SOD1*-ALS model [115]. The pML104 plasmid created by the Wyrick group was used for CRISPR/Cas9 editing. In this vector, Cas9 is expressed under the constitutive TDH3 promoter, and it is followed by an ADH1 terminator sequence. The gRNA is expressed under the RNA polymerase III promoter SNR52 (to allow for expression of unmodified gRNA) and is followed by a SUP4 terminator sequence. The gRNA expression cassette is flanked by BclI and SmaI restriction enzyme cut sites allowing for easy cloning of the ~20 bp gRNA sequence. The pML104 plasmid

Chapter 4. Developing CRISPR/Cas9 strategies for generating ALS linked SOD1 mutants in *S. cerevisiae*.

uses a *URA3* selection marker allowing for counter-selection using 5-FOA after successful genome editing has been achieved to remove the CRISPR/Cas9 machinery from the cell [146]. The ability to generate point mutations in the endogenous *SOD1* gene should provide a simple way to study the effect of ALS-linked mutations on the function of *SOD1* under its own promoter.

4.2 Results

4.2.1 Guide RNA and repair template designs

The aim of this project was to construct a single-copy stable *S. cerevisiae* model of ALS by introducing the A4V, G37R and H48Q mutations to the *SOD1* gene. To achieve this, different gRNA sequences and repair templates were designed. The gRNA sequences were designed using the tool developed by Wyrick et al (<http://wyrickbioinfo2.smb.wsu.edu/crispr.html>). Inputting the gene name into the tool mentioned above generated a list of all the PAM sites that could be targeted, their corresponding gRNA sequences, and the two oligos required for cloning the gRNA sequences into the empty pML104 vector.

Three different PAM sites were chosen to generate the Sod1^{A4V}, Sod1^{G37R}, and Sod1^{H48Q} mutations, respectively. To generate the Sod1^{A4V} mutation, the gRNA sequence at position 6 in *SOD1* was used. Its sequence was 5'-TCAAGCAGTCGCAGTGTAAAGG-3'. To generate the Sod1^{G37R} mutation, the gRNA sequence at position 113 in *SOD1* was used. Its sequence was 5'-ACAGTCCTAACGCAGAACGTGGG-3'. To generate the Sod1^{H48Q} mutation, the gRNA sequence at position 148 was used. Its sequence was 5'-GAGTTTGGAGATGCCACCAATGG-3'. The different gRNA sites were all chosen to target PAM sites that were as close as possible to where the edits were intended to be made (Figure 4.1, Table 4.1).

ssOligo repair templates were designed to be ~95 bp long, with homology arms of at least 45 bp on each side of the PAM site. Repair templates included the edits so as to introduce the intended ALS-linked mutations. They were also designed to include silent mutations either to the PAM site, or to the gRNA sequence directly upstream of the PAM site. Introduction of these silent mutations was crucial as cells that had successfully repaired the DSB in the DNA caused by the CRISPR/Cas9 machinery by HR using the repair template would no longer be susceptible to cutting at the PAM site. This allowed for positive selection, as the cells that had incorporated the desired mutations would be able to grow despite expressing CRISPR/Cas9 machinery. Cells that have not got the desired mutations in the PAM site would most likely suffer from toxicity due to Cas9 DNA cleavage.[146]. Two repair templates were designed to generate the Sod1^{A4V} mutation.

The first repair oligo included silent mutations in the PAM site changing ‘AGG’ to ‘AAG’ and the second repair oligo included silent mutations in the gRNA sequence directly upstream of the PAM site changing the C at position 15 to an A and the A at position 24 to a G. The repair template designed for the G37R mutation contained a silent mutation changing the PAM site from ‘GGG’ to ‘GGC’. The repair template for the H48Q mutation contained silent mutations in the gRNA sequence directly upstream of the PAM site with the A at position 156 changed to a C and the C at position 162 changed to an A. These repair templates can be seen in (Figure 4.1). From now on the pML104 vectors used in this study will be referred to as the empty gRNA vector, *SOD1*-A4V gRNA vector, *SOD1*-G37R gRNA vector and *SOD1*-H48Q gRNA vector respectively. The ssOligo repair templates will be referred to as in (Table 4.1).

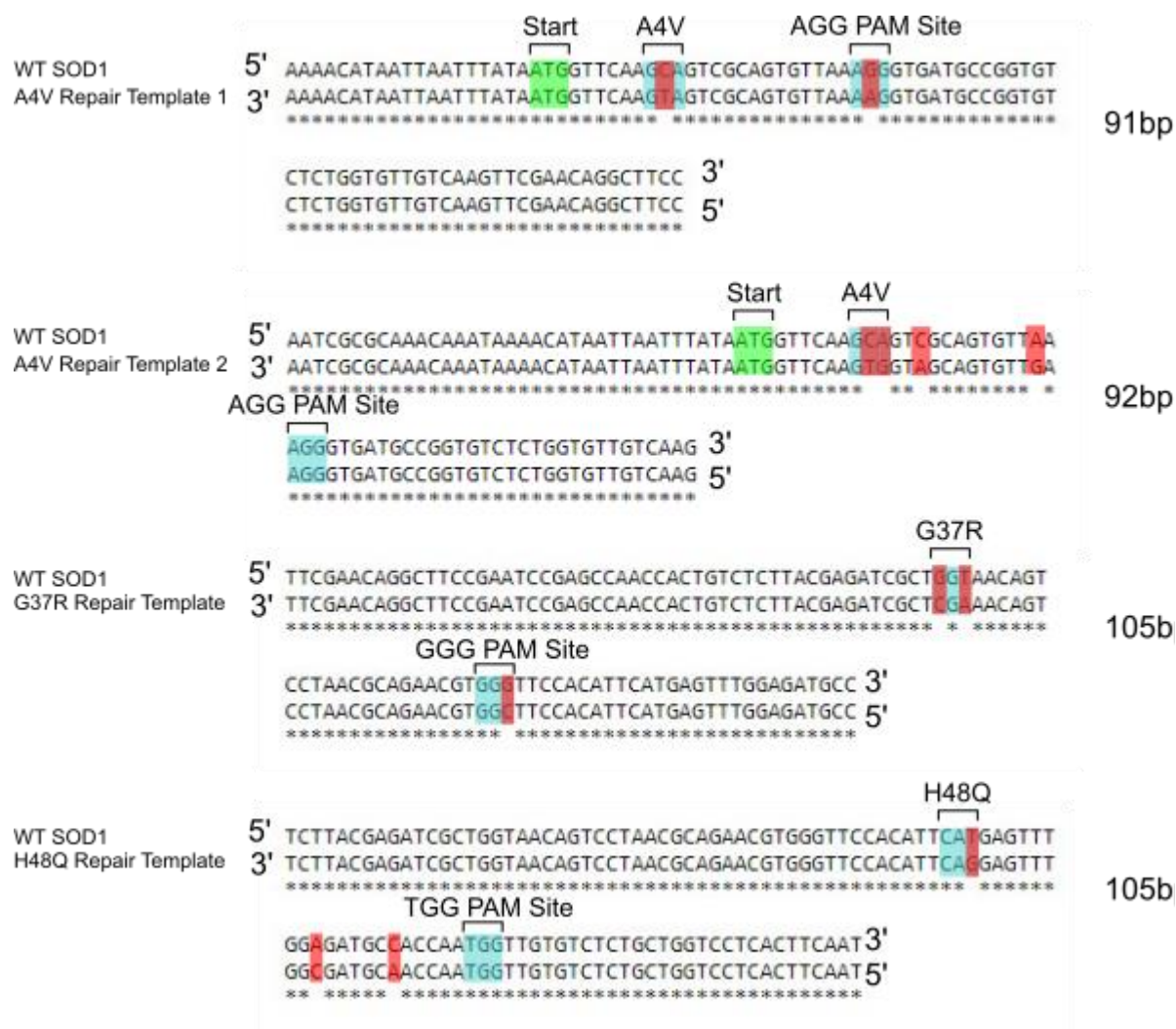


Figure 4.1 Nucleotide sequences of the different repair template designs utilised to generate the A4V, G37R and H48Q mutations in *SOD1*.

Designs are shown as the repair template sequence aligned to the *S. cerevisiae SOD1*^{WT} nucleotide sequence. Alignments were generated using the clustal omega multiple sequence alignment software (<https://www.ebi.ac.uk/Tools/msa/clustalo/>). Start codons were

highlighted in green, sites of interest were highlighted in blue, and mutations in the repair templates were highlighted in red.

Table 4.1 Summary of characteristics of different ssOligo repair templates used.

Name	Length (bp)	Mutation	Strategy
<i>SOD1</i> -A4V repair template 1	91	GCA to GTA. Alanine to Valine at position 4.	Silent mutation in the PAM site. 5'-AGG-3' to 5'-AAG-3'
<i>SOD1</i> -A4V repair template 2	92	GCA to GTG. Alanine to Valine at position 4.	Silent mutations in the sgRNA sequence upstream of PAM site.
<i>SOD1</i> -G37R repair template	105	GGT to CGA. Glycine to Arginine at position 37.	Silent mutation in PAM site. GGG to GGC.
<i>SOD1</i> -H48Q repair template	105	CAT to CAG. Histidine to Glutamine at position 48.	Silent mutations in the sgRNA sequence upstream of PAM site.

4.2.2 Screening colonies for phenotypes previously observed upon overexpression of mutant isoforms of Sod1 in *S. cerevisiae* failed to identify correct mutants.

The initial strategy adopted for identifying potentially successful mutations in the *SOD1* gene generated by CRISPR/Cas9 editing was to screen for phenotypes that had been previously observed in cells that overexpressed Sod1 mutant isoforms from a 2 μ plasmid. These phenotypes included, growth defects, menadione sensitivity and a quinocrine uptake defect [115]. The BY4741 strain was transformed with the *SOD1*-A4V gRNA vector, *SOD1*-G37R gRNA vector and *SOD1*-H48Q gRNA vector in separate transformations along with their respective ssOligo repair templates. The resulting colonies from this transformation were picked and screened as mentioned above. It was found that the presence of the above-mentioned phenotypes did not appear to correlate with the presence of the desired mutation.

4.2.3 Increasing concentrations of repair template resulted in improved transformation efficiency

Using the previous approach described above screening for colonies based on phenotypes expected from ALS-linked *SOD1* mutations, the Sod1^{A4V}, Sod1^{G37R} and Sod1^{H48Q} mutants were not identified. In this approach, 150 ng of the gRNA vector and 100 pmoles of the ssOligo repair template were used in the transformation. To optimise the transformation protocol, increasing the concentration of repair template were tested and the associated transformation efficiency was measured. Transformations were carried out using the empty pML104 plasmid with no gRNA sequence cloned in as a positive control and the pML104 plasmid with the gRNA sequence cloned in as a negative control. pML104 with gRNA was transformed into the cells with increasing amounts of ssOligos repair template from 100, 200, to 500 pmol.

Transformations with the empty gRNA vector produced 90 colonies, indicating a higher transformation efficiency. Transformations with the *SOD1*-A4V, *SOD1*-G37R and *SOD1*-H48Q gRNA vectors alone with no ssOligo repair template resulted in extremely poor transformation efficiency with less than 10 colonies being formed. For the Sod1^{G37R} mutation, the initial concentration of 100 pmol resulted in only one colony, however higher concentrations of 200 pmol and 500 pmol of repair template resulted in 30 colonies each.

For the Sod1^{H48Q} mutation, a similar result was observed. The *SOD1*-H48Q gRNA vector transformation produced ten colonies. Upon addition of the ssOligo repair template, the transformation efficiency increased to 20 colonies with 200 pmol of repair template and 45 colonies with 500 pmol of repair template.

For the Sod1^{A4V} mutation, the transformation efficiency remained exceptionally low despite the addition of high concentrations of repair template. The first repair template strategy that included a silent mutation in the PAM site failed to increase transformation at all. However, the second repair template strategy including silent mutations in the gRNA sequence upstream of the PAM site increased transformation efficiency modestly to 15 colonies

In summary, an increase in concentration of the ssDNA Oligo repair template led to an increase in transformation efficiency (Figure 4.2).

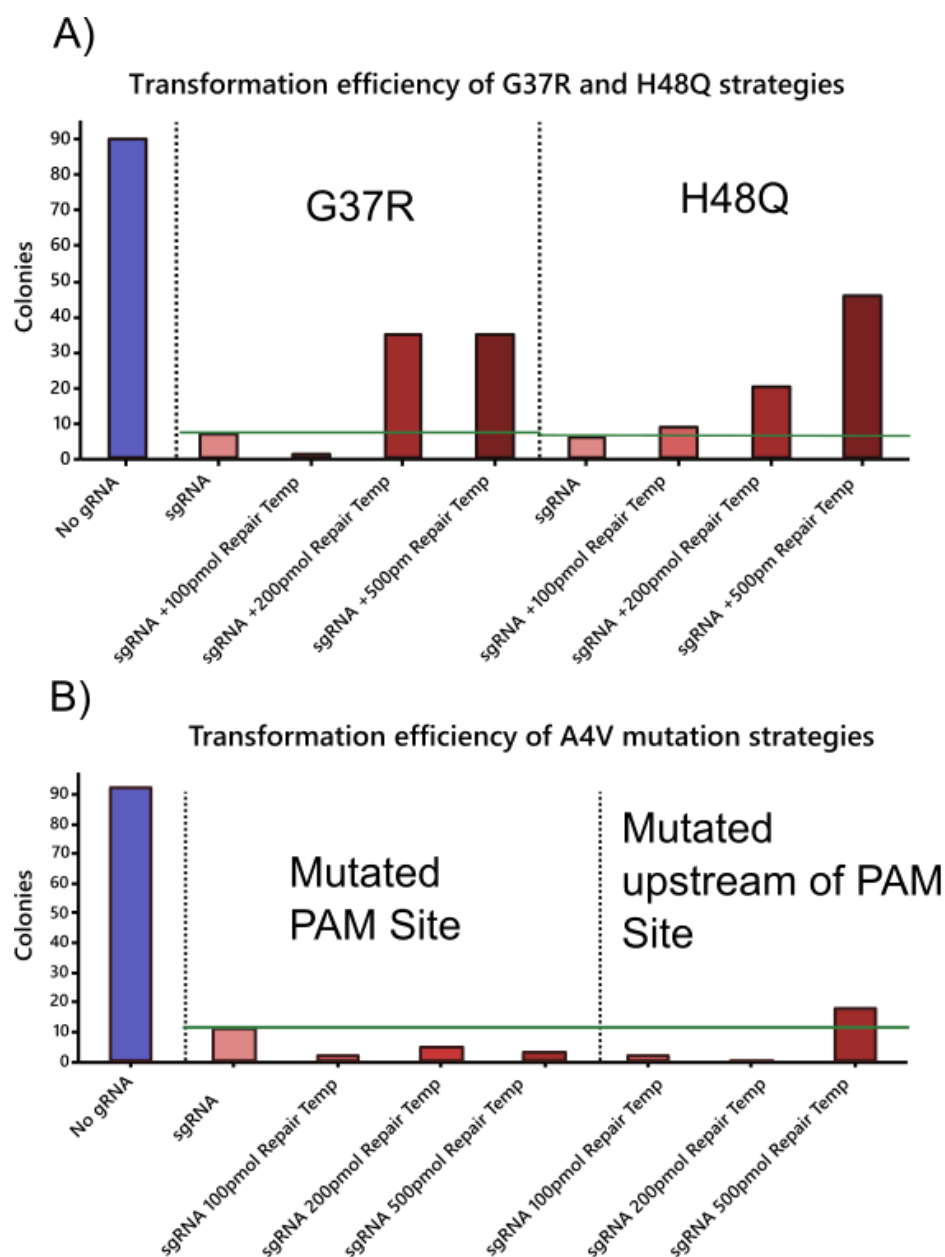


Figure 4.2 Transformation efficiency of CRISPR/Cas9 transformations with varying concentrations of repair template.

A) Displays the transformation efficiencies from BY4741 cells transformed with the pML104 vector containing gRNA sequences targeting PAM sites next to the G37R locus or the H48Q locus respectively. Cells were transformed with pML104 containing no gRNA as a positive control as there should be no targeted CRISPR/Cas9 DNA DSB resulting in a high transformation efficiency. Increasing concentrations of the repair template were used.

B) Displays the same as in A) except for the A4V mutation strategy. Two different repair templates were compared, one with mutations in the PAM site and the other with mutations upstream of the PAM site. Transformation efficiency was measured as the number of colonies counted. The plasmid amount was kept constant at 150 μ g, and the number of cells was also constant at 4 OD₆₀₀ units ($\sim 3.6 \times 10^7$ cells). N = 1 for both A) and B).

4.2.4 Generation of Sod1^{A4V}, Sod1^{G37R} and Sod1^{H48Q} mutations using CRISPR-Cas9 genome editing

To check for presence of the desired mutations, the *SOD1* gene was subsequently analysed by Sanger sequencing within colonies isolated from transformants obtained using 500 pmoles of the ssOligos repair template as they had the highest transformation efficiencies. Normal sized colonies were picked instead of small colonies as it was suggested by that the first colonies to grow from the transformation were most likely to contain the correct edits [146].

All three desired mutations were successfully identified within transformants as shown in Figure 4.3. For the A4V mutation, two out of 18 sent (11.1%) were correct. For the G37R mutation eight out of 16 (50%) were correct. For the H48Q mutation three out of 17 (17.6%) were correct. The effects of these mutations on the amino acid sequence of the Sod1 protein is shown in Figure 4.4. For both the G37R and H48Q clones, a second change of V14F was observed. This could be an artifact of the Sanger sequencing as it is at the start of the sequencing reaction and the quality of the reads is poor.

A4V

A4V	101	5'	ATGGTTCAAGTGGTAGCAGTGTGAAGGGTGATGCCGGTGTCTCTGGTGTGTC AAGTTC	160
WT	1	3'	ATGGTTCAAGCAGTAGCAGTGTGAAGGGTGATGCCGGTGTCTCTGGTGTGTC AAGTTC	60
A4V	161		GAACAGGCTTCCGAATCCGAGCCAACCACTGTCTCTTACGAGATCGCTGGTAACAGTCCCT	220
WT	61		GAACAGGCTTCCGAATCCGAGCCAACCACTGTCTCTTACGAGATCGCTGGTAACAGTCCCT	120
A4V	221		AACGCAGAACGTGGGTTCACATTATGAGTTTGGAGATGCCACCAATGGTTGTGTCTCT	280
WT	121		AACGCAGAACGTGGGTTCACATTATGAGTTTGGAGATGCCACCAATGGTTGTGTCTCT	180
A4V	281		GCTGGTCTCACTTCAATCCTTCAAGAAGACACATGGTGTCCAACCTGACGAAGTCAGA	340
WT	181		GCTGGTCTCACTTCAATCCTTCAAGAAGACACATGGTGTCCAACCTGACGAAGTCAGA	240
A4V	341		CATGTCGGTGACATGGGTAACGTAAGACGGACGAAAAATGGTGTGGCCAAGGGCTCCTTC	400
WT	241		CATGTCGGTGACATGGGTAACGTAAGACGGACGAAAAATGGTGTGGCCAAGGGCTCCTTC	300
A4V	401		AAGGACTCTTTGATCAAGCTTATCGGTCTACCTCCGTTGTAGGCAGAAAGCGTCTGTATC	460
WT	301		AAGGACTCTTTGATCAAGCTTATCGGTCTACCTCCGTTGTAGGCAGAAAGCGTCTGTATC	360
A4V	461		CACGCCGGCCAAGATGACTTAGGTAAGGGTGACACTGAAGAATCTTTGAAGACTGGTAAT	520
WT	361		CACGCCGGCCAAGATGACTTAGGTAAGGGTGACACTGAAGAATCTTTGAAGACTGGTAAT	420
A4V	521		GCCGGTCCAAGACCAGCCTGTGGTGTATTGGTCTAACCAACTAA	565
WT	421		GCCGGTCCAAGACCAGCCTGTGGTGTATTGGTCTAACCAACTAA	465

G37R

G37R	18	5'	GGTGTGTCAAGTTCGAACAGGCTTCCGAATCCGAGCCAACCACTGTCTCTTACGAGATC	77
WT	46	3'	GGTGTGTCAAGTTCGAACAGGCTTCCGAATCCGAGCCAACCACTGTCTCTTACGAGATC	105
G37R	78		GCTCGAACAGTCTAACGCAGAACGTGGTTCCACATTATGAGTTTGGAGATGCCACC	137
WT	106		GCTCGTAACAGTCTAACGCAGAACGTGGTTCCACATTATGAGTTTGGAGATGCCACC	165
G37R	138		AATGGTTGTGTCTGTCTGGTCTCACTTCAATCCTTCAAGAAGACACATGGTGTCTCA	197
WT	166		AATGGTTGTGTCTGTCTGGTCTCACTTCAATCCTTCAAGAAGACACATGGTGTCTCA	225
G37R	198		ACTGACGAAGTCAGACATGTCTGGTGACATGGGTAACGTAAGACGGACGAAAAATGGTGTG	257
WT	226		ACTGACGAAGTCAGACATGTCTGGTGACATGGGTAACGTAAGACGGACGAAAAATGGTGTG	285
G37R	258		GCCAAGGGCTCCTTCAAGGACTCTTTGATCAAGCTTATCGGTCTACCTCCGTTGTAGGC	317
WT	286		GCCAAGGGCTCCTTCAAGGACTCTTTGATCAAGCTTATCGGTCTACCTCCGTTGTAGGC	345
G37R	318		AGAAGCGTCTTTATCCACGCCGGCCAAGATGACTTAGGTAAGGGTGACACTGAAGAATCT	377
WT	346		AGAAGCGTCTTTATCCACGCCGGCCAAGATGACTTAGGTAAGGGTGACACTGAAGAATCT	405
G37R	378		TTGAAGACTGGTAATGCCGGTCCAAGACCAGCCTGTGGTGTATTGGTCTAACCAACTAA	437
WT	406		TTGAAGACTGGTAATGCCGGTCCAAGACCAGCCTGTGGTGTATTGGTCTAACCAACTAA	465

H48Q

H48Q	10	5'	GGT-TCTCTGGTGTGTC AAGTTCGAACAGGCTTCCGAATCCGAGCCAACCACTGTCTCT	68
WT	37	3'	GGTGTCTCTGGTGTGTC AAGTTCGAACAGGCTTCCGAATCCGAGCCAACCACTGTCTCT	96
H48Q	69		TACGAGATCGCTGGTAACAGTCTAACGCAGAACGTGGGTTCACATTCAAGAGTTTGGG	128
WT	97		TACGAGATCGCTGGTAACAGTCTAACGCAGAACGTGGGTTCACATTCAAGAGTTTGGG	156
H48Q	129		GATGCCAACCAATGGTTGTGTCTGTCTGGTCTCACTTCAATCCTTCAAGAAGACACAT	188
WT	157		GATGCCAACCAATGGTTGTGTCTGTCTGGTCTCACTTCAATCCTTCAAGAAGACACAT	216
H48Q	189		GGTGTCTCAACTGACGAAGTCAGACATGTCTGGTGACATGGGTAACGTAAGACGGACGAA	248
WT	217		GGTGTCTCAACTGACGAAGTCAGACATGTCTGGTGACATGGGTAACGTAAGACGGACGAA	276
H48Q	249		AATGGTGTGGCCAAGGGCTCCTTCAAGGACTCTTTGATCAAGCTTATCGGTCTACCTCC	308
WT	277		AATGGTGTGGCCAAGGGCTCCTTCAAGGACTCTTTGATCAAGCTTATCGGTCTACCTCC	336
H48Q	309		GTTGTAGGCAGAAAGCGTCTTATCCACGCCGGCCAAGATGACTTAGGTAAGGGTGACACT	368
WT	337		GTTGTAGGCAGAAAGCGTCTTATCCACGCCGGCCAAGATGACTTAGGTAAGGGTGACACT	396
H48Q	369		GAAGAATCTTTGAAGACTGGTAATGCCGGTCCAAGACCAGCCTGTGGTGTATTGGTCTA	428
WT	397		GAAGAATCTTTGAAGACTGGTAATGCCGGTCCAAGACCAGCCTGTGGTGTATTGGTCTA	456
H48Q	429		ACCAACTAA	437
WT	457		ACCAACTAA	465

Figure 4.3 GATC Sanger sequencing results of the *SOD1* gene amplified from colonies.

SOD1 was amplified from the genomic DNA (gDNA) of colonies obtained by transformation with pML104 gRNA plasmids and repair template. Sequencing results were compared to *SOD1* in the reference genome of *S. cerevisiae* S288C using NCBI BLAST (<https://blast.ncbi.nlm.nih.gov/Blast.cgi>). ALS linked mutations were highlighted in red, whereas silent mutations to the PAM site, or upstream of the PAM site were highlighted in blue.

A4V			
A4V	1	MVQVAVLKGDAGVSGVVKFEQASESEPTTVSYE	180
WT	1	MVQVAVLKGDAGVSGVVKFEQASESEPTTVSYE	180
A4V	181	AGPHFNPFKKTGHGAPTDEVRHVGDMGNVKTDE	360
WT	181	AGPHFNPFKKTGHGAPTDEVRHVGDMGNVKTDE	360
A4V	361	HAGQDDLKGKGT EESLKTGNAGPRPACGVIGL	465
WT	361	HAGQDDLKGKGT EESLKTGNAGPRPACGVIGL	465
G37R			
G37R	9	GFSGVVKFEQASESEPTTVSYEIA	188
WT	37	GSVVKFEQASESEPTTVSYEIA	216
G37R	189	GAPTDEVRHVGDMGNVKTDE	368
WT	217	GAPTDEVRHVGDMGNVKTDE	396
G37R	369	EESLKTGNAGPRPACGVIGL	437
WT	397	EESLKTGNAGPRPACGVIGL	465
H48Q			
H48Q	9	GFSGVVKFEQASESEPTTVSYEIA	188
WT	37	GSVVKFEQASESEPTTVSYEIA	216
H48Q	189	GAPTDEVRHVGDMGNVKTDE	368
WT	217	GAPTDEVRHVGDMGNVKTDE	396
H48Q	369	EESLKTGNAGPRPACGVIGL	437
WT	397	EESLKTGNAGPRPACGVIGL	465

Figure 4.4 Amino acid alignment of translated sequences from successful CRISPR/Cas9 clones

Displays the nucleotide translation BLAST results of sequences obtained from sequencing colonies from CRISPR/Cas9 editing transformations. Sequences were analysed against the *S. cerevisiae* S288C genome. WT describes the S288C reference genome. Highlighted in green are the desired amino acid changes. Highlighted in red are undesired amino acid changes.

4.2.5 Effect of ALS-linked mutations generated by CRISPR/Cas9 on activity and expression of Sod1

To test whether the various ALS-linked mutations Sod1^{A4V}, Sod1^{G37R}, and Sod1^{H48Q} had any effect on the activity and expression of Sod1, *in-gel* SOD activity assays and western blots were carried out. Native protein extracts from BY4741, the two successful Sod1^{A4V} that were identified (clone 1 and clone 2) and a $\Delta sod1$ mutant were run on a native PAGE protein gel.

The Sod1^{A4V} mutation had a strong effect on sod activity of Sod1 (Figure 4.5). However, as a western blot analysis has not yet been carried out on these samples, it is unknown whether the Sod1^{A4V} affects abundance of Sod1 and/or activity. Furthermore, the Sod1^{A4V} mutation led to a faster migration in the native NBT gel, similarly to the results observed in the integration strain model of *SOD1*-ALS.

The Sod1^{H48Q} mutation showed an increased abundance in Sod1 from a western blot compared to the WT. (Figure 4.6 A) and B)). The Sod1^{H48Q} mutation also led to a decrease in Sod1 activity compared to the WT (Figure 4.6 A) and C)).

The Sod1^{G37R} mutation led to a decrease in Sod1 protein abundance and activity (Figure 4.6 D), E) and F)).

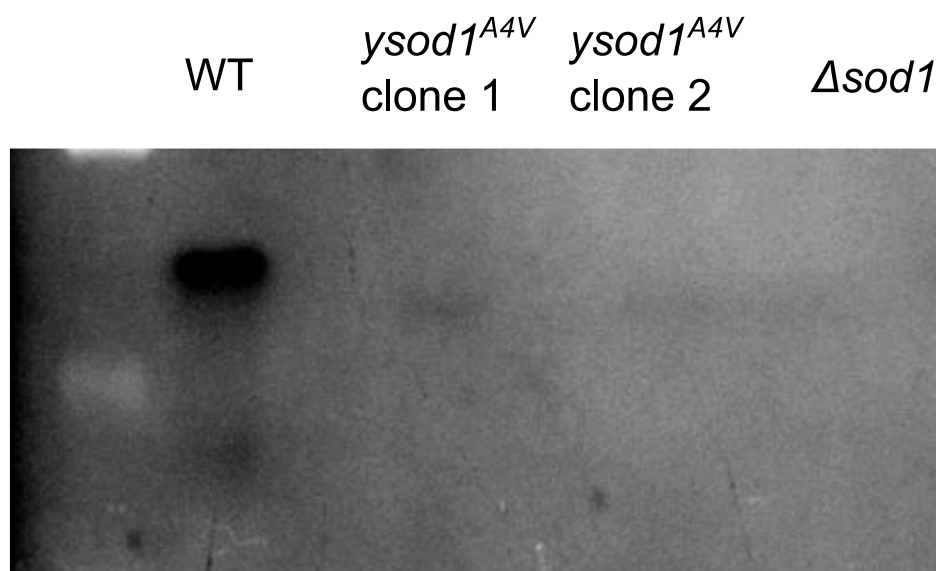


Figure 4.5 Effect of Sod1^{A4V} mutation on activity of Sod1.

NBT native gel Sod activity assay showing the sod activity of Sod1 enzymes in *S. cerevisiae*. BY4741 and $\Delta sod1$ are included as positive and negative controls, respectively. Two different clones containing the Sod1^{A4V} mutation generated by CRISPR/Cas9 editing are included. Protein levels were normalised to 3 μ g using a Bradford assay prior to loading the gel.

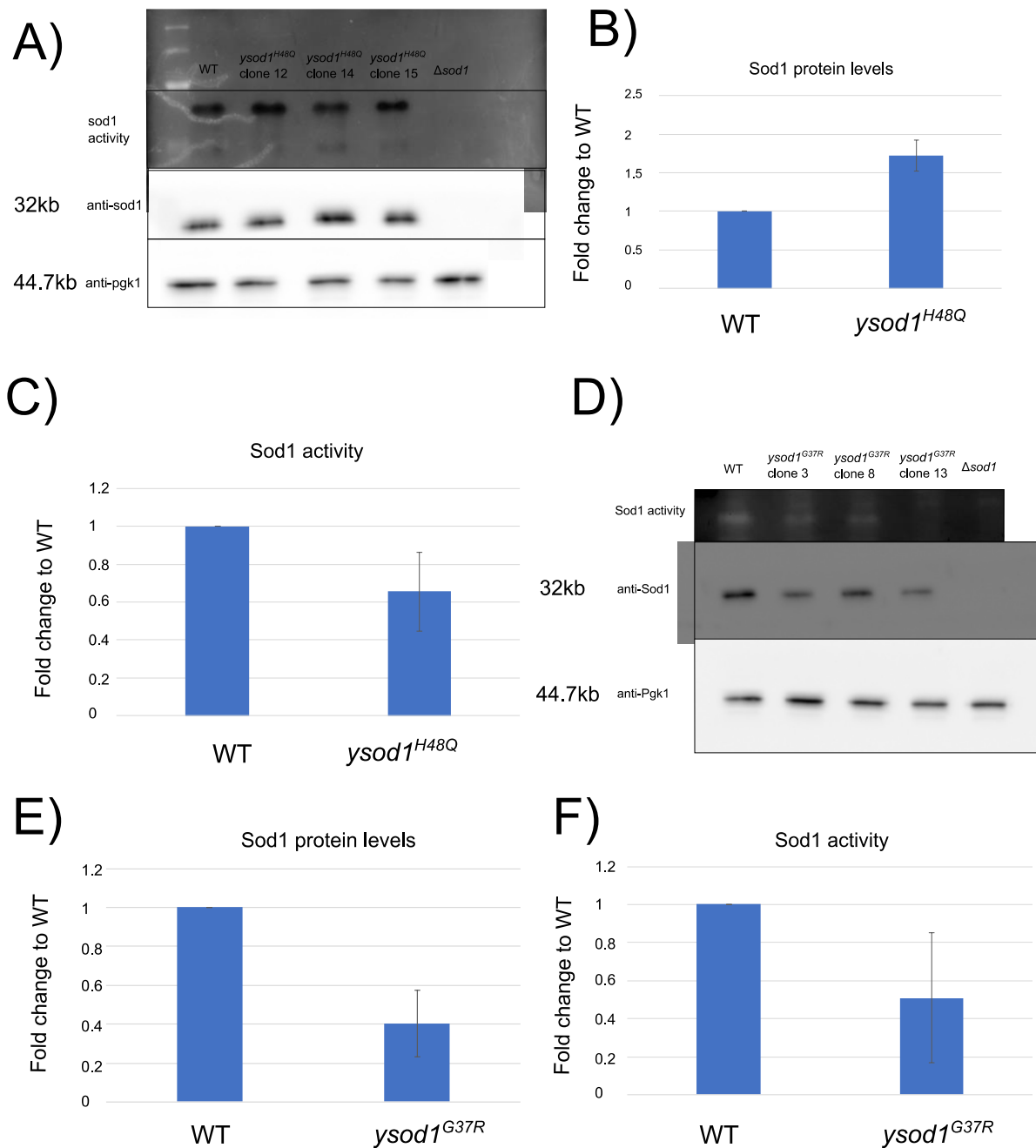


Figure 4.6 Effect of *Sod1*^{H48Q} and *Sod1*^{G37R} mutations on Sod1 activity and expression.

A) Displays the results of a Sod activity assay using a native gel stained with NBT. Three different clones containing the *Sod1*^{H48Q} mutation were studied to test similarity between different CRISPR clones. Levels of Pgk1 were probed as a loading control. B) Displays average Sod1 protein levels from the three *Sod1*^{H48Q} clones normalised to the Pgk1 loading control. Sod1 protein level is displayed as the fold change compared to the WT control. C) Displays the quantification of the Sod1 activity level. This is the ratio of Sod1 activity to Sod1 protein levels. The Sod1 activity is displayed as fold change compared to the wild-type control. D) Shows the results of a Sod1 activity assay and a western blot comparing the activity and abundance of three *Sod1*^{G37R} clones to the WT. Pgk1 is used as a loading control. E) Shows the quantification of the average Sod1 protein levels of the three *Sod1*^{G37R} mutants compared to the loading control from the western blot shown in D). The Sod1 protein levels are shown as fold change compared to the WT control. F) Displays the

Chapter 4. Developing CRISPR/Cas9 strategies for generating ALS linked SOD1 mutants in *S. cerevisiae*.

quantification of the average Sod1 activity level of the three Sod1^{G37R} mutants compared to the WT control. Sod1 activity is shown as fold change compared to the WT. N = 3.

4.3 Discussion

In this study, the aim was to develop a stable single-copy model of *SOD1*-ALS. CRISPR/Cas9 genome editing was used to generate the Sod1^{A4V}, Sod1^{G37R} and Sod1^{H48Q} mutants in *S. cerevisiae*. The A4V mutation was achieved by the 5'-GCA-3' to 5'-GTA-3' point mutation. The G37R mutation was created by the 5'-GGT-3' to 5'-CGA-3' point mutations. The H48Q mutation was achieved by the 5'-CAT-3' to 5'-CAG-3' point mutation (Table 4.1).

4.3.1 Strategy for identifying correct mutants

Three different gRNA vectors were cloned containing different 20 bp gRNA sequences designed to target different PAM motifs in the *SOD1* gene. Appropriate PAM motifs were selected using the tool created by the Wyrick lab. Another tool available on the Benchling website helped with PAM site selection as it provided on and off target accuracy scores (<https://www.benchling.com/>).

The initial strategy that was adopted was to pick colonies from transformations of WT with the three different gRNA vectors and to pre-screen them for phenotypes that had been previously observed in a *S. cerevisiae* model for *SOD1*-ALS that overexpressed Sod1^{A4V}, Sod1^{G37R} and Sod1^{H48Q} in a $\Delta sod1$ background. These phenotypes included growth defects, sensitivity to the menadione and a vacuole acidification defect [115]. Despite identifying colonies with defects in growth and sensitivity to menadione, these phenotypes did not seem to correlate with the colonies possessing the desired mutation.

The second strategy for identifying the correct mutants was to simply sequence the *SOD1* gene from the gDNA from all the normal sized colonies from each transformation without pre-screening for any phenotypes. Using this strategy, correct mutants were identified for Sod1^{A4V}, Sod1^{G37R} and Sod1^{H48Q}. Frequency of successful mutants found from the colonies tested varied largely between mutants with 11.1% correct for Sod1^{A4V}, 50% for Sod1^{G37R} and 17.6% for Sod1^{H48Q}. For both Sod1^{G37R} and Sod1^{H48Q} a second edit of V14F has been observed in the sequencing data. However, this is right at the start of the sequencing reaction and the quality of the read is quite low, suggesting that this is an artifact of the sequencing. Further sequencing of the whole gene should be carried out to confirm this.

The results suggest that strains with ALS-linked mutations in the endogenous *SOD1* gene generated by CRISPR/Cas9 editing may not have the same phenotypes as *S. cerevisiae* cells

overexpressing ALS-linked mutant Sod1 isoforms. In this study, the initial strategy of pre-screening for smaller colonies with growth defects, and sensitivity to menadione actually reduced the chances of selecting for colonies with the desired mutations. The second strategy of selecting normal sized colonies and screening by amplifying the *SOD1* gene and analysing the sequence by sanger sequencing resulted in the identification of correct mutants for all three desired mutations.

4.3.2 Comparison of gene editing efficiency with other studies

The initial transformation conditions used 150 ng of the gRNA vector and 100 pmoles of the ssOligo repair template [146]. It was decided to test whether increasing amounts of ssOligo repair template could increase the transformation efficiency. Increasing concentrations of the ssOligo repair template increased the transformation efficiency of all the transformations except with the Sod1^{A4V} transformation with the *SOD1*-A4V repair template 1. Using 500 pmoles of repair template gave the highest transformation efficiency in this study (Figure 4.2). This suggested that increasing the amount of repair template in the transformation reaction was increasing transformation efficiency, possibly by increasing the chances of the repair template being used to repair the DSB by HR.

In the study that initially created the pML104 CRISPR/Cas9 expression vectors, a range of 50–250 ng of gRNA vector was used and 12.5–125 pmoles of ssOligo repair template was used. Using those conditions, targeting the *TRP1* gene in *S. cerevisiae* 86 colonies were obtained among which 97% (from the 36 normal sized colonies tested) contained the correct *trp*- edit [146]. In comparison, for the Sod1^{G37R} mutation, using 500 pmoles of repair template and 150 ng of the gRNA vector, there were 35 colonies, and 50% (from the 18 normal sized colonies tested) contained the correct edit. A few factors can account for the difference in efficiencies observed. Firstly, a double-stranded Oligo (dsOligo) repair template was used in the *TRP1* study whereas in this study a ssOligo repair template was used. Secondly, there could be different efficiencies for different PAM sites and edits depending on their location in the genome. Even in this study, the number of transformants and the frequency of succesful edits from those transformants was highly variable between each mutation.

The results from this study suggest that increasing the concentration of the ssOligo repair template can increase the transformation efficiency of the pML104 vector that expresses Cas9 and the gRNA cassette. The results also suggest that different gene locuses and edits can have differences in the frequency of succesful mutations observed.

Effect of Sod1^{A4V}, Sod1^{G37R} and Sod1^{H48Q} mutations on Sod1 activity and abundance

Chapter 4. Developing CRISPR/Cas9 strategies for generating ALS linked SOD1 mutants in *S. cerevisiae*.

We aimed to test whether the ALS linked mutations A4V, G37R and H48Q in the endogenous *SOD1* gene would cause difference in the activity and/or abundance of the enzyme. In-*gel* sod activity assays were carried out alongside western blot analysis to study the effects of the three ALS-linked mutation on the activity and abundance of Sod1 in *S. cerevisiae*.

Native protein extracts from Sod1^{A4V} cells grown to mid-log phase showed a marked decrease in Sod1 activity compared to the WT control, consistent with previous results in *S. cerevisiae* [115]. Due to time-constraints, western blot analysis could not be carried out, so it is yet to be understood whether Sod1^{A4V} affects the abundance and/or activity of Sod1. It was also observed that the band representing Sod1 from the Sod1^{A4V} lysate migrated faster in the native gel than that of the Sod1^{WT} band (Figure 4.5). The reduced activity compared to Sod1^{WT} and the shift in migration through native PAGE observed are similar to the results from the model in which Sod1^{A4V} is expressed from a genomically integrated vector.

Native protein extracts from Sod1^{H48Q} cells grown to mid-log phase showed an increase in abundance compared to the Sod1^{WT} lysates, and a slightly decreased Sod1 activity when calculated by ImageJ densitometry (Figure 4.6 A)). The Sod1 activity observed between Sod1^{H48Q} and Sod1^{WT} was similar, however when corrected for the increase abundance of Sod1^{H48Q} the activity appeared to be lower than that of Sod1^{WT} extracts. These results differ significantly from those observed upon overexpression of Sod1^{H48Q} in $\Delta sod1$ cells where Sod1^{H48Q} showed a decrease in abundance to the WT and had no Sod1 activity at all [115].

Native protein extracts of Sod1^{G37R} cells grown to mid-log phase showed a decrease in abundance and activity compared to the Sod1^{WT} lysates according to ImageJ densitometry analysis (Figure 4.6 B)). These results differ from the overexpression model where Sod1^{G37R} showed a similar abundance to Sod1^{WT} and no Sod1 activity at all. Overall, these results are consistent with previous studies in which it is thought that the Sod1^{G37R} mutation confers decreased stability and proper folding of the Sod1 enzyme possibly explaining the reduction in abundance and activity that was observed.

Further analysis of these mutants is required to confirm the activity and abundance results observed. Preliminary growth analysis and spotting assays to test sensitivity to menadione and the Vma⁻ phenotype suggested that similar to the *SOD1*-ALS integration model, the Sod1 mutants, Sod1^{A4V}, Sod1^{G37R}, and Sod1^{H48Q} generated by CRISPR/Cas9 editing in this chapter did not show on cytotoxicity (appendix: Figure 8.5). No Vma⁻ phenotype or sensitivity to menadione was observed either (appendix: Figure 8.6 and Figure 8.7).

4.3.3 Conclusion and future directions

In conclusion, the CRISPR/Cas9 genome editing system was successfully used to create the Sod1^{A4V}, Sod1^{G37R} and Sod1^{H48Q} mutations in the endogenous *S. cerevisiae SOD1* gene without any selection marker. Differences in mutation efficiency were observed across all three desired edits. It was found that increasing the amount of repair template improved the transformation efficiency. In the future this CRISPR/Cas9 editing can be used to generate more *SOD1*-ALS-linked mutants in *S. cerevisiae* and potentially other ALS-linked gene mutations as well. These will hopefully aid in our ability to model the disease in *S. cerevisiae* and further understand how mutations in *SOD1* give rise to MND in humans.

ALS-linked mutations in the *SOD1* gene led to differences in activity and abundance of Sod1 in cells grown to mid-log phase. It will be important to test the activity and abundance in stationary phase *S. cerevisiae* cells as it has been suggested that the conditions in stationary phase cells are more representative of the post-mitotic environment of neurons. Differences were observed between the same Sod1 mutations in the overexpression model and the single-copy model highlighting the effect that expression level can have on the phenotypes observed with ALS-linked mutant isoforms. Preliminary characterisation suggests that the Sod1^{A4V}, Sod1^{G37R}, and Sod1^{H48Q} mutants generated by CRISPR do not show any cytotoxicity.

5 Investigating the interaction between Sod1 and the V-ATPase

5.1 Introduction

5.1.1 Function of the Vacuole in *S. cerevisiae*

The vacuole is the most acidic compartment in the cell with a pH of <5–6.5 depending on growth conditions [185]. In *S. cerevisiae*, the vacuole is structurally and functionally akin to the lysosomes in mammalian cells and the plant vacuole. Originally thought to simply be an endpoint organelle where endocytic and degradative pathways end, the vacuole is now understood to be a central hub for coordinating cellular homeostasis. In *S. cerevisiae*, the vacuole regulates pH homeostasis, metal ion homeostasis, polyphosphate stores, autophagy, amino acid signalling and several other central processes to the working of the cell. Around 27% of proteins that localise to the vacuole have transporter activity [186]. These include the many amino acid and metal ion transporters found on the vacuole membrane. With regards to the makeup of the lipid content, the membrane of the vacuole is distinct from that of the plasma membrane [187], allowing it to be a highly dynamic structure, a characteristic which is key for the vacuole to respond to different signals and stresses appropriately. For example, in cells that are growing exponentially, there are a few small vacuoles, whereas in stationary phase cells, there is usually one large vacuole. This ability of the vacuole to undergo fusion and fission appropriately in different situations is crucial in maintaining homeostasis in the cell. Vacuole acidification is critical for the many functions mentioned above. The main enzyme that controls vacuolar acidification is the multi-subunit vacuolar ATPase pump (V-ATPase), uses the energy from ATP hydrolysis to pump H⁺ ions across the vacuole membrane.

5.1.2 Consequences of loss of vacuole acidification

The loss of vacuole or lysosome acidification has severe consequences to the cell. Nearly all of the functions of the vacuole in maintaining cellular homeostasis rely on the acidification of its lumen. Loss of vacuole/lysosome acidification is lethal in all organisms except fungi. In fungi, loss of vacuole acidification leads to a conditional lethality called the *Vma*⁻ phenotype. In yeast cells with unacidified vacuoles, cells cannot grow in media buffered to an alkaline pH >7.5, they are sensitive to exposure to high levels of calcium ions, high temperature (37 °C)[188], oxidative stress [189] and more. *S. cerevisiae* has emerged as the leading model in studying the vacuole and the V-ATPase since fungi are the only organisms in which loss of vacuole acidification is not

lethal. Screening for mutants that displayed the Vma^- phenotype led to the discovery of the many subunits of the V-ATPase [190].

5.1.3 The V-ATPase

The V-ATPase is an enzyme with 14 subunits, that possesses a V_1 domain that is exposed to the cytoplasm and a V_0 domain that is bound to a membrane. These domains are analogous to the F_1 and F_0 domains of the mitochondrial F-ATP synthase enzyme. ATP hydrolysis is facilitated by a conformational change involving rotation of the central stalk that then facilitates proton transport through the proton pore [191]. The V-ATPase is highly evolutionarily conserved from yeast to mammals with some subunits sharing up to 80% homology in the genes that they are encoded by. The V_1 domain of the V-ATPase possesses three copies of the catalytic A subunit encoded by *VMA1* and three copies of the regulatory B subunit encoded by *VMA2*. The C, D, E, F, G and H subunits encoded by *VMA5*, *VMA8*, *VMA4*, *VMA7*, *VMA10* and *VMA13* respectively make up the rotor and stator regions of the enzyme.

In the V_0 domain, the 'a' subunit is the only V-ATPase subunit in *S. cerevisiae* to have two isoforms. It can be encoded by *VPH1* or *STV1*. This subunit makes up part of the proton pore but is also thought to contain sorting information as V-ATPases with 'a' subunits that are encoded by *VPH1* localise to the vacuole membrane and have been shown to be more active and to respond more to glucose signalling control [192]. V-ATPases with 'a' subunits that are encoded by *STV1* are localised to the golgi and endosomal compartments and are less responsive to glucose signalling [192]. Deletion of either one of *VPH1* or *STV1* alone doesn't cause a Vma^- phenotype in *S. cerevisiae*, they must both be deleted for the cells to have the Vma^- phenotype. In mammalian cells, the 'a' subunit has four isoforms encoded by *ATP6V0A1*, *ATP6V0A2*, *TCIRG1* and *ATP6V0A4* [193]. Similar to *S. cerevisiae*, each isoform is thought to contain targeting information. In mammalian cells the subunits 'a1', 'a2', and 'a3' are all thought to target V-ATPases to intracellular organelles such as lysosomes, phagosomes, and secretory granules in a wide range of tissues. V-ATPases containing the 'a1' subunit are expressed in all tissues but mainly in the brain and liver in mice, [194] and are localised to the plasma membranes of presynaptic vesicles at nerve cell terminals [195]. V-ATPases containing the 'a2' subunit are expressed in the heart, brain, liver, and kidney in mice, [194] and are targeted to early endosomes [196]. V-ATPases containing the 'a3' isoform are induced during osteoclast differentiation and are localised to the plasma membrane of osteoclasts [194] The 'a4' subunit encodes V-ATPases are expressed only in the kidney, epididymis and inner ear and target V-ATPases to the plasma membrane of intercalated cells [197].

A key component of the proton pore in the V_0 domain is the c ring made up of the subunits c, c' and c'' encoded by *VMA3*, *VMA11* and *VMA16* in *S. cerevisiae* respectively. Subunits d and e encoded by *VMA6* and *VMA9* also make up part of the V_0 domain.

5.1.4 Regulation of V-ATPase activity by reversible disassembly

The proton pumping activity of the V-ATPase is regulated through a process called reversible disassembly, in which the V_1 domain disassembles from the V_0 domain and becomes diffuse in the cytosol. In this disassembled state, ATP hydrolysis cannot occur, and the proton pore is closed. The most characterised regulator of reversible disassembly is glucose signalling, for example, when D-glucose is exhausted from the growth media. Therefore, when nutrient levels are low, cells can conserve energy (in the form of cytosolic ATP) by increasing the level of disassembled V-ATPase complexes until more nutrients have been obtained. Reversible disassembly is promoted by the regulator of ATPase of vacuoles and endosomes (RAVE) complex made up of Skp1, Rav1 and Rav2. Without the RAVE complex, V-ATPases cannot reassemble properly upon re-addition of glucose to the media [198]. The RAVE complex is also important for the initial assembly of the V-ATPase independent of glucose signalling [199]. Reversible disassembly is not an all or nothing response. In cells grown in media containing 2% glucose, assembly levels of all V-ATPase complexes have been shown to be at around 55–70%. Upon removal of glucose from the media, only 15–20% of V-ATPase complexes were assembled. Upon re-addition of glucose to the media, assembly levels returned to 55–70% after just five min. It was also observed that after overnight growth in raffinose, a carbon source that *S. cerevisiae* prefers less than glucose, the assembly levels were 45% [200]. In summary, V-ATPases assembly levels can be dynamically regulated depending on the carbon source available most likely to conserve ATP.

5.1.5 Regulation V-ATPase activity by redox signalling

Reduction–oxidation (redox) signalling has also been implicated in the regulation of V-ATPase activity in bovine clathrin-coated vesicles. A disulphide bond was found to form between Cys254 of the catalytic subunit A and another proximal cysteine residue upon exposure to oxidation from sulphhydryl reagents. The formation of this disulphide bond due to exposure to sulphhydryl reagents was found to inhibit proton transport. This effect could be reversed by the reducing agent dithiothreitol (DTT) [201], [202]. Furthermore, *S. cerevisiae* cells lacking *CYS4* (a gene that encodes cystathionine beta-synthase, an enzyme involved in the first step of cysteine biosynthesis), display a Vma^- phenotype due to reduced cellular glutathione levels. This Vma^- phenotype can be partially suppressed by mutation of the conserved cysteine at 261 [203].

In summary, some evidence exists that suggests that the V-ATPase is also capable of being regulated by redox signalling.

5.1.6 Sod1 and the vacuole

Cells lacking *SOD1* in *S. cerevisiae* have a fragmented vacuole phenotype [204]. This phenotype is only present in aerobically grown cells and can be rescued by removal of iron or supplementation with manganese [205]. Cells lacking *SOD1* display phenotypes indicative of metabolic dysfunction which cannot simply be explained by oxidative stress. These include a sensitivity to alkaline pH, a sporulation defect and sensitivity to certain metals.

Overexpression of mutant isoforms of Sod1, Sod1^{A4V}, Sod1^{G37R}, Sod1^{H48Q}, Sod1^{G93A} and Sod1^{S134N} in a $\Delta sod1$ background in *S. cerevisiae* caused toxic effects due to metabolic dysfunction. $\Delta sod1$ cells expressing ALS-linked mutant isoforms had growth defects, a quinocrine uptake defect, significant alterations in metabolite levels, and a defect in autophagy [115]. Furthermore, deletion of *SOD1* produces a synthetic lethality with deletion of *VMA2* the gene that encodes subunit B of the V-ATPase [189].

5.1.7 Aim of this study

The aim of this study is to test whether Sod1 interacts with the V-ATPase in *S. cerevisiae* using a protein complementation assay (PCA) based on dihydrofolate reductase (DHFR). Initially we determined whether deletion of *SOD1* in our strain background leads to sensitivity to alkaline pH, zinc, and a fragmented vacuole phenotype. We then tested for protein-protein interaction (PPI) between Sod1 and the V-ATPase and investigated the nature of this interaction with respect to cell function in *S. cerevisiae*.

5.2 Results

5.2.1 Loss of *SOD1* leads to phenotypes indicative of vacuole dysfunction

Loss of *SOD1* has been shown to cause phenotypes that may be associated with dysfunction of the vacuole in *S. cerevisiae* such as sensitivity to alkaline pH, sensitivity to transition metals and fragmented vacuoles [188]. At the start of this study, it was important to check whether deletion of *SOD1* also caused these phenotypes in the background used in this study, BY4741[115]. Cells lacking *SOD1* were unable to grow in media that had been buffered to pH 7.5 (Figure 5.1). In minimal media, both WT and $\Delta sod1$ grew at a similar rate and reached a similar final cell density. When grown in media buffered to pH 7.5 however, WT cells grew at a

reduced rate and reached stationary phase at a lower cell density, whereas $\Delta sod1$ cells were unable to grow at all. This suggests an inability in $\Delta sod1$ cells to regulate pH homeostasis.

To test whether *SOD1* was important for the ability to cope with elevated metal levels, WT and $\Delta sod1$ cells were grown in minimal media supplemented with 4 mM $ZnCl_2$. As shown in Figure 5.1 B), WT cells were able to grow in media supplemented with 4 mM $ZnCl_2$ whereas $\Delta sod1$ cells were unable to grow. This suggests that $\Delta sod1$ cells are unable to manage high levels of Zinc. Vacuole fragmentation is a well-documented phenotype that has been shown in $\Delta sod1$ cells [204]. To test whether $\Delta sod1$ cells in the background used in this study had fragmented vacuoles, fluorescence microscopy of WT and $\Delta sod1$ cells with an endogenous Vph1-GFP tag was carried out. *VPH1* encodes the 'a' subunit of the V-ATPase and is a stable marker for the vacuole membrane. As seen in Figure 5.1 C), cells lacking *SOD1* displayed fragmented vacuoles. These results showed that in the BY4741 background, loss of *SOD1* results in the inability to grow at a high pH, sensitivity to high levels of zinc ions and fragmented vacuoles, suggesting that the function of the vacuole may be compromised upon deletion of *SOD1*.

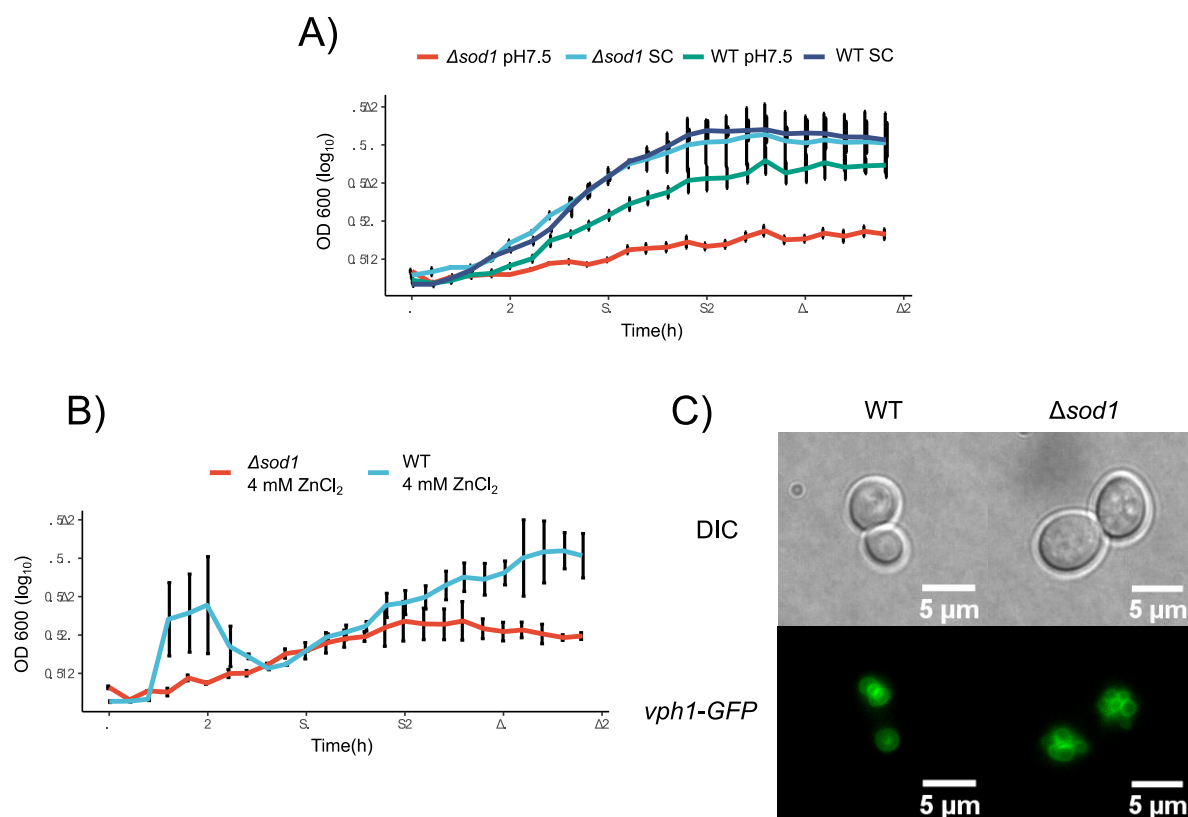


Figure 5.1 Deletion of *SOD1* causes phenotypes linked to vacuole dysfunction in the BY4741 background.

A) Growth curve of WT and $\Delta sod1$ cells grown in SC media unbuffered or buffered to pH 7.5. Growth curve shows one representative biological replicate. Error bars represent standard deviation between technical replicates. This is a representative result from two biological replicates. N = 2. Error bars represent the standard deviation between three

technical replicates. B) Growth curve shows one representative biological replicate. Error bars represent standard deviation between technical replicates. This is a representative result from three biological replicates ($N = 3$). Error bars represent the standard deviation between three technical replicates. D) Fluorescence microscopy of WT and $\Delta sod1$ cells expressing *VPH1* c-terminally tagged with GFP as a vacuole membrane reporter. Cells were grown in SC media and 100 \times magnification was used.

5.2.2 $\Delta sod1$ mutants contain increased levels of basic amino acids

The vacuole plays a crucial role in the storage and transport of amino acids. The vacuole is also a central hub for amino acid sensing and Torc1 signalling. To test whether loss of *SOD1* resulted in perturbed amino acid metabolism, the free amino acid signature of $\Delta sod1$ from the dataset produced by the Ralser group [206] was analysed. In the dataset, the amino acid concentrations of 4686 strains were collected. The Mahalanobis distance was calculated to measure the distance between the $\Delta sod1$ amino acid signature and that of the overall average. The Mahalanobis distance is defined as a measure of the distance between a point P and a distribution D. In the study, a mahalanobis distance of >30 indicated a p value of < 0.05 and therefore a significantly different amino acid signature from the overall average. In Figure 5.2 A), the Mahalanobis distance of $\Delta sod1$ and several vacuole membrane amino acid transporter mutants were compared. Of the 13 strains, only $\Delta avt1$, $\Delta avt3$, $\Delta avt7$, $\Delta vba5$ and $\Delta sod1$ strains possessed significantly different amino acid signatures from the overall average. In Figure 5.2 B), the percent of change in each amino acid concentration between $\Delta sod1$ and the average is shown. Tyrosine has the largest decrease in concentration in $\Delta sod1$ cells with a 63% decrease. Alanine (21%), arginine (34%), glycine (38%), histidine (38%) and lysine (51%) showed the largest increases in concentration relative to the average. By sorting amino acids into their different types: acidic, aliphatic, aromatic, basic, polar neutral and unique it was observed that the basic amino acid group consisting of arginine, histidine and lysine showed the largest increase in $\Delta sod1$ cells (41%) compared to the average. Basic amino acid levels were significantly higher than all of the other amino acid types except for unique amino acids. Overall, the amino acid profiles of $\Delta sod1$ cells show that there is a significant difference in the amino acid signature and that there is an increase in basic amino acids in the cells.

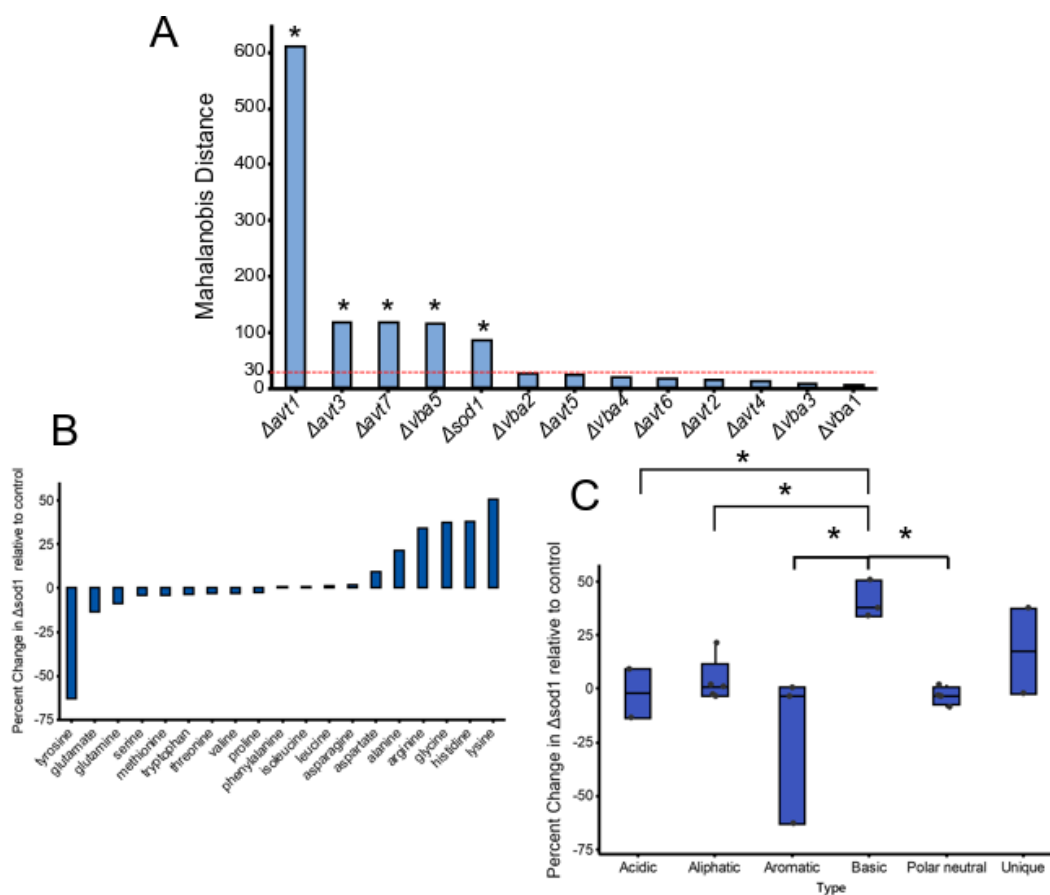


Figure 5.2 Analysis of the Ralser free amino acid measurement dataset.

A) This shows the Mahalanobis distance of multivariate outlyingness. This shows how different the amino acid profile is from the overall average in the dataset (4686 strains). A value of over 30 is significant. B) The percent change in amino acid concentrations between $\Delta sod1$ and the overall dataset average. C) Box plot displaying the percent change in amino acid concentrations of different amino acid types between $\Delta sod1$ and the overall dataset average. One-way ANOVA was used to measure difference between the means. Turkey post-hoc test was used to identify statistically different types of amino acids. * $p < 0.05$.

5.2.3 Sod1 interacts with the V₁ domain of the V-ATPase in a dihydrofolate reductase protein complementation assay

As it was observed that loss of *SOD1* led to an inability to grow at elevated pH, sensitivity to metal stress and a perturbed amino acid profile, it was hypothesised that Sod1 could be interacting with the V-ATPase. *S. cerevisiae* cells lacking any of the subunits of the V-ATPase display a partial Vma⁻ phenotype. The Vma⁻ phenotype includes an inability to grow at elevated pH, sensitivity to metals and in most cases a loss of vacuole acidification. As $\Delta sod1$ cells display phenotypes that seemingly overlap with the Vma⁻ phenotype it was hypothesised that Sod1 could be interacting with the V-ATPase in some way.

To test for protein-protein interactions (PPI) between Sod1 and all of the V-ATPase subunits, an *in vivo* protein complementation assay (PCA) involving fragments of the murine dihydrofolate reductase (DHFR) enzyme was used. *S. cerevisiae* cells are sensitive to methotrexate (MTX), a compound which binds to DHFR and inhibits its function. DHFR reduces dihydrofolic acid to tetrahydrofolic acid. Tetrahydrofolic acid is an essential substrate used to produce purines, pyrimidines and other important compounds required for cell growth and proliferation [125]. Inhibition of DHFR in *S. cerevisiae* by MTX is lethal. This assay takes advantage of this by utilising a mutant isoform of DHFR (L22F and F31S) that is resistant to MTX inhibition. By C-terminally linking bait and prey proteins to fragments of the mutant DHFR isoform, resistance to MTX can be used as a reporter for protein complementation as interaction between the bait and prey proteins will reconstitute the mutant DHFR fragments resulting in an active MTX resistant DHFR isoform (Figure 5.3 A)).

In this experiment, Sod1 was used as the bait and various subunits of the V-ATPase that are outlined in Table 5.1 were used as the prey. Haploid bait and prey strains were mated together and diploids that possessed both bait and prey DHFR linked proteins were selected for. Growth assays of all diploid bait and prey combinations in SC media and in SC media supplemented with 200 µg/ml of MTX were carried out to screen for any PPIs.

As seen in Figure 5.3 C) for the V₀ subunits and F) for the V₁ subunits, all diploid strains grew normally in SC media and at the same rate as the BY4743 WT control. Quinocrine staining of diploids was carried out to check if linking of the DHFR fragment to the various V-ATPase subunits impaired the function of the V-ATPase thereby causing a loss of vacuole acidification (data not shown). All the interaction diploids took up the quinocrine dye indicating that they possessed acidified vacuoles and functional V-ATPases. As seen in Figure 5.3 D), none of the diploid bait-prey combinations were able to grow in media supplemented with 200 µg/ml MTX, suggesting that the DHFR fragments were not reconstituted in any of the diploid bait-prey combinations for subunits of the V₀ domain of the V-ATPase. The relative growth of each bait-prey diploid was calculated as described and none of the bait-prey diploids had a relative growth that was significantly different from the negative control BY4743 (Figure 5.3 E)). Growth curve analysis of bait-prey diploids from the V₁ domain of the V-ATPase showed four diploids that were able to grow in SC media supplemented with 200 µg/ml MTX (Figure 5.3 G)). The relative growth showed that the diploids strains Sod1^{bait} Vma2^{prey}, Sod1^{bait} Vma4^{prey} and Sod1^{bait} Vma8^{prey} showed a significantly higher relative growth value compared to the negative control, indicating that the bait and prey proteins were in close enough proximity to reconstitute the linked mutant DHFR fragments. Sod1^{bait} Vma2^{prey} had a relative growth of 7.5, Sod1^{bait} Vma8

Chapter 5. Investigating the interaction between Sod1 and the V-ATPase

$\text{Vma4}^{\text{prey}}$ had a relative growth of 5.5 and $\text{Sod1}^{\text{bait}} \text{Vma4}^{\text{prey}}$ had a relative growth value of 3.8. Therefore, the $\text{Sod1}^{\text{bait}} \text{Vma2}^{\text{prey}}$ diploid had the strongest resistance to MTX and the $\text{Sod1}^{\text{bait}} \text{Vma4}^{\text{prey}}$ diploid had the weakest resistance to MTX. In Figure 5.3 B), the subunits that are encoded for by the diploids that showed resistance to MTX are mapped onto the known structure of the V-ATPase. *VMA2* encodes the B subunit, *VMA4* encodes the E subunit and *VMA8* encodes the D subunit (Table 5.1). All three subunits that were identified are found in the V_1 domain that is exposed to the cytosol.

Table 5.1 Summary of subunits of the V-ATPase in *S. cerevisiae*.

Gene	Subunit	Function
<i>VMA1</i>	A	Contains the catalytic domain whereupon nucleotides can bind
<i>VMA2</i>	B	Contains nucleotide binding sites but no catalytic domain
<i>VMA4</i>	E	Part of the peripheral stalk subcomplex with G
<i>VMA5</i>	C	Soluble subunit that detaches from the rest of the V_1 domain upon reversible disassembly
<i>VMA6</i>	d	Part of the membrane pore domain and is required for assembly of the V_1 domain
<i>VMA7</i>	F	Part of the central rotor axle. Required for assembly of the V_1 domain
<i>VMA8</i>	D	Part of the central rotor axle
<i>VMA9</i>	e	Integral part of the V_0 domain
<i>VMA10</i>	G	Part of the peripheral stalk subcomplex with E
<i>VMA11</i>	c'	Subunit of the C ring that rotates past the 'a' subunit in response to ATP hydrolysis
<i>VMA13</i>	H	Prevents ATP hydrolysis when V_1 and V_0 are not assembled
<i>VMA16</i>	c''	Subunit of the C ring that rotates past the 'a' subunit in response to ATP hydrolysis
<i>STV1</i>	a	Isoform of the 'a' subunit that encodes V-ATPase complexes found on the golgi and endosomal membranes
<i>VPH1</i>	a	Isoform of the 'a' subunit that encodes V-ATPase complexes found on the vacuole membranes

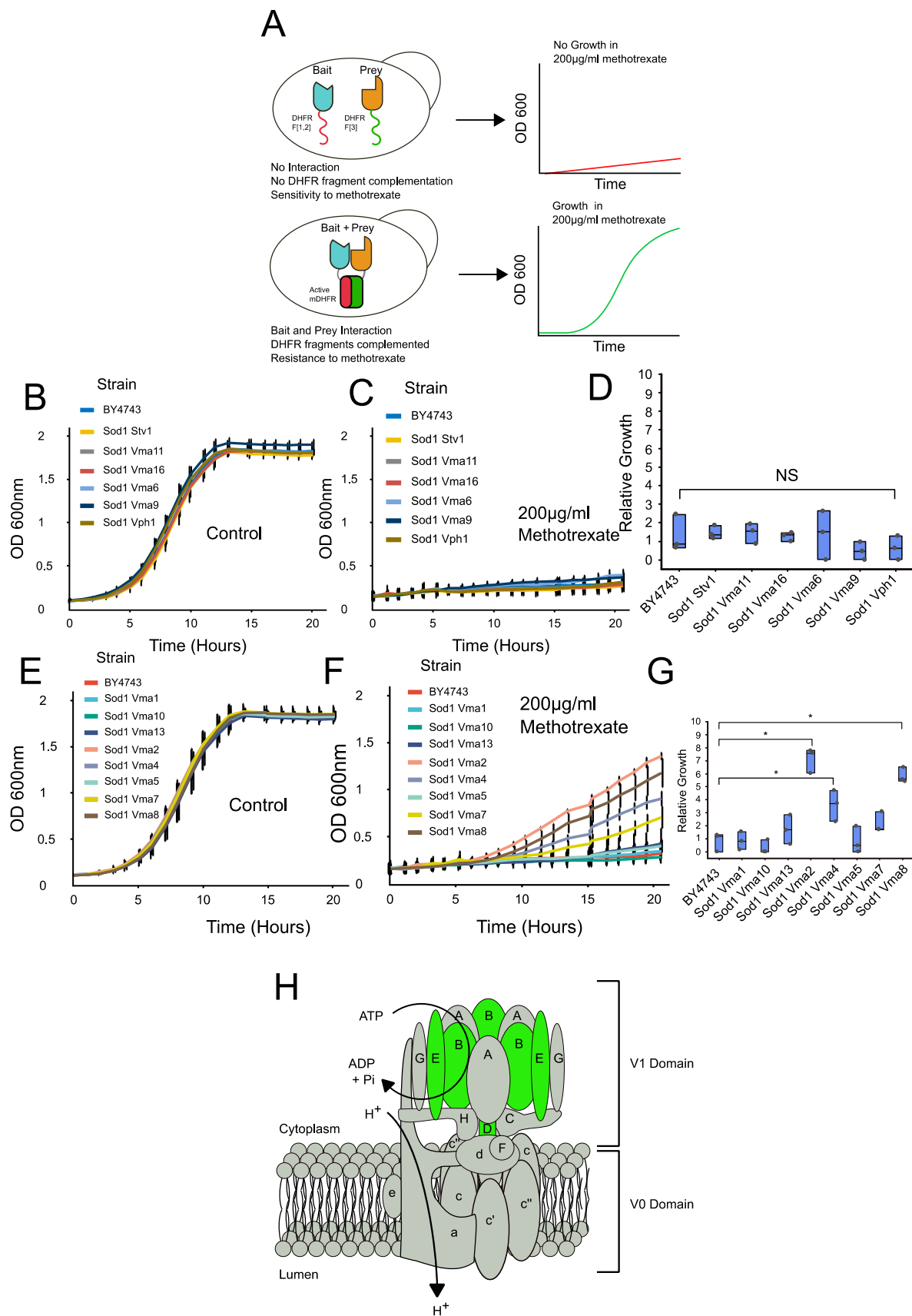


Figure 5.3 DHFR-PCA assay between Sod1 and the V-ATPase.

A) Schematic demonstrating the theory behind the DHFR-PCA assay. Interaction between bait and prey proteins results in complementation of two DHFR fragments of a murine

DHFR isoform that is resistance to MTX inhibition. Interaction between bait and prey results in resistance to MTX inhibition. B) Diagram of the V-ATPase in *S. cerevisiae*. The subunits of the V-ATPase that showed resistance to methotrexate in the DHFR PCA assay have been coloured in green. C) Growth curves of Sod1^{bait} and V-ATPase V₀ domain subunit in SC media. D) Growth curves of Sod1^{bait} and V-ATPase V₀ domain subunits in SC media supplemented with 200 µg/ml MTX. E) Relative growth quantification of growth curves of Sod1^{bait} and V₀ domain of the V-ATPase subunits shown in C) and D). F) Growth curves of Sod1^{bait} and V₁ domain of V-ATPase subunits grown in SC media. G) Growth curves of Sod1^{bait} and V₁ domain of V-ATPase subunits grown in SC media supplemented with 200 µg/ml MTX. H) Relative growth calculations of growth curves of Sod1^{bait} and V₁ domain of the V-ATPase subunits shown in F) and G). For all growth curves, a representative result is shown from three biological replicates. N = 3. Error bars represent the standard deviation from three technical repeats. For relative growth boxplots in E) and H), diploids that grew significantly compared to the BY4743 negative control were tested by a One-Way ANOVA (* $p < 0.05$).

5.2.4 Extrachromosomal overexpression of *SOD1* reduced the relative growth of the Sod1^{bait} Vma4^{prey} diploid.

Results from the DHFR-PCA screen using Sod1 as the bait and various subunits of the V-ATPase as the prey suggested that Sod1 is in close enough proximity in the cell to the V₁ domain of the V-ATPase to be able to reconstitute two fragments of the mutant DHFR isoform, thereby conferring resistance to MTX. To investigate whether native Sod1, not linked to a DHFR fragment could interact with Vma2, Vma4 and Vma8 on the V₁ domain of the V-ATPase, Sod1 was overexpressed extrachromosomally under a GPD promoter in the diploid bait-prey strains. It was hypothesised that expression of Sod1^{WT} could reduce the relative growth of the diploids by competing with Sod1^{bait} for interaction with Vma2^{prey}, Vma4^{prey} and Vma8^{prey} (Figure 5.4 A)).

Growth curves from the PCA assay for Sod1^{bait} Vma2^{prey}, Sod1^{bait} Vma4^{prey} and Sod1^{bait} Vma8^{prey}, are shown in Figure 5.4 B), C) and D) respectively. For the Sod1^{bait} Vma2^{prey} diploid, there was no significant difference from the relative growth calculation (Figure 5.4 E). For the Sod1^{bait} Vma4^{prey} diploid, the Sod1^{bait} Vma4^{prey} diploid overexpressing Sod1 from a 2µ plasmid showed a significant decrease in relative growth compared to the empty control. For the Sod1^{bait} Vma8^{prey} diploid, there was no significant difference in relative growth in cells overexpressing Sod1 compared to the empty vector control.

In summary, expression of Sod1 significantly reduced the resistance to MTX in the Sod1^{bait} Vma4^{prey} diploid but not in the Sod1^{bait} Vma2^{prey} diploid, or the Sod1^{bait} Vma8^{prey} diploid. This suggests that overexpression of Sod1 into the Sod1^{bait} Vma4^{prey} reduces the interaction between Sod1^{bait} and Vma4^{prey} whereas it does not reduce the interaction between Sod1^{bait} and Vma2^{prey}. This indicated that Sod1 could be interacting with Vma4

as the protein complementation can be disrupted by addition of extra Sod1 which may be competing with the DHFR bound Sod1^{bait} (Figure 5.4 A)).

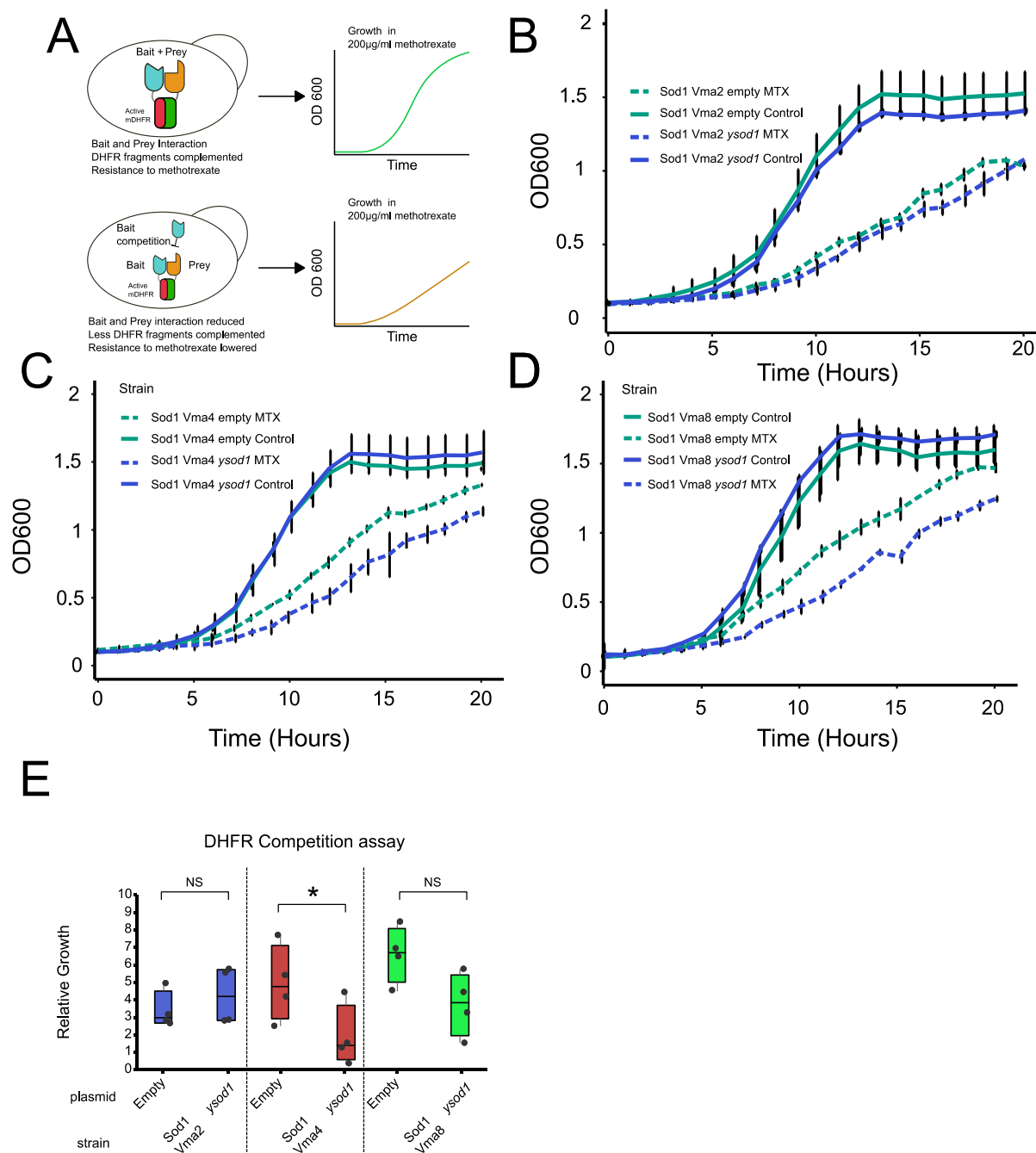


Figure 5.4 DHFR-PCA competition assay.

A) Graphic demonstrating the theory behind the DHFR-PCA competition assay. In theory, competition for the bait-prey interaction should reduce the number of DHFR complexes that are reconstituted resulting to a decrease in resistance to MTX. B) Growth curves of Sod1^{bait} Vma2^{prey} diploid. C) Growth curves of Sod1^{bait} Vma4^{prey} diploids. D) Growth curves of Sod1^{bait} Vma8^{prey} diploids. For all growth curves shown in B)–D), one representative result of three biological repeats is shown. Error bars display the standard deviation between three technical replicates. Normal lines represent the growth in SC media, whereas broken lines represent growth in SC media supplemented with 200 µg/ml MTX. Lines of the empty vector control are coloured green whereas lines of the Sod1

expressing strain are blue. E) Relative growth of Sod1^{bait} Vma2^{prey}, Sod1^{bait} Vma4^{prey} and Sod1^{bait} Vma8^{prey} diploids expressing either an empty vector (pAG425) or Sod1 (pAG425 ySod1) Relative growth was calculated as in Figure 5.3. N = 3. Significance (* $p < 0.05$) was calculated by One-Way ANOVA comparison. Individual data points correspond to one biological repeat.

5.2.5 Overexpression of *PDE2* decreases the interaction between Sod1 and Vma2 DHFR fragments.

The V-ATPase is highly regulated by a dynamic process known as reversible disassembly. Reversible disassembly describes when the V₁ domain of the V-ATPase detaches from the V₀ membrane-embedded domain and becomes soluble in the cytosol. (Figure 5.5 A). The C subunit detaches from the V₁ domain as well [200]. In this state the V-ATPase is unable to pump H⁺ protons across the membrane. Reversible disassembly is controlled by several signals in the cell. Protein kinase A (PKA) signalling is a well characterised regulator of reversible disassembly. High PKA signalling acts as a signal for V-ATPase assembly whereas low PKA signalling results in increase disassembly of V-ATPases [207]

To investigate whether decreasing PKA signalling could affect the interaction between Sod1 and the V-ATPase subunits that was observed in the DHFR-PCA, a plasmid expressing the high affinity phosphodiesterase Pde2 was transformed into the diploid strains Sod1^{bait} Vma2^{prey}, Sod1^{bait} Vma4^{prey}, Sod1^{bait} Vma8^{prey}. Overexpression of Pde2 increases hydrolysis of adenosine monophosphate (AMP), which is a secondary messenger required for activation of the PKA subunits Tpk1, Tpk2 and Tpk3 in *S. cerevisiae*. Therefore, overexpression of Pde2 indirectly inhibits PKA signalling [208].

As shown in Figure 5.5 B) and E), the Sod1^{bait} Vma2^{prey} diploid that overexpressed Pde2 grew significantly slower in SC media supplemented with 200 µg/ml MTX compared to the empty vector control. No significant difference in growth was observed when grown in normal SC media. No differences in growth in media supplemented with 200 µg/ml MTX were observed in the Sod1^{bait} Vma4^{prey} and Sod1^{bait} Vma8^{prey} diploids when overexpressing Pde2 or an empty vector control (Figure 5.5 C), D) and E)). In summary, reduction of PKA signalling by overexpression of the phosphodiesterase Pde2, resulted in a significant decrease in relative growth of the Sod1^{bait} Vma2^{prey} diploid indicating less DHFR complexes are being formed when PKA signalling is reduced. As PKA signalling has been shown to be a positive regulator of V-ATPase assembly, this result suggests that when PKA signalling is decreased, and less V-ATPase structures are assembled, the interaction between Sod1 and Vma2 decreases.

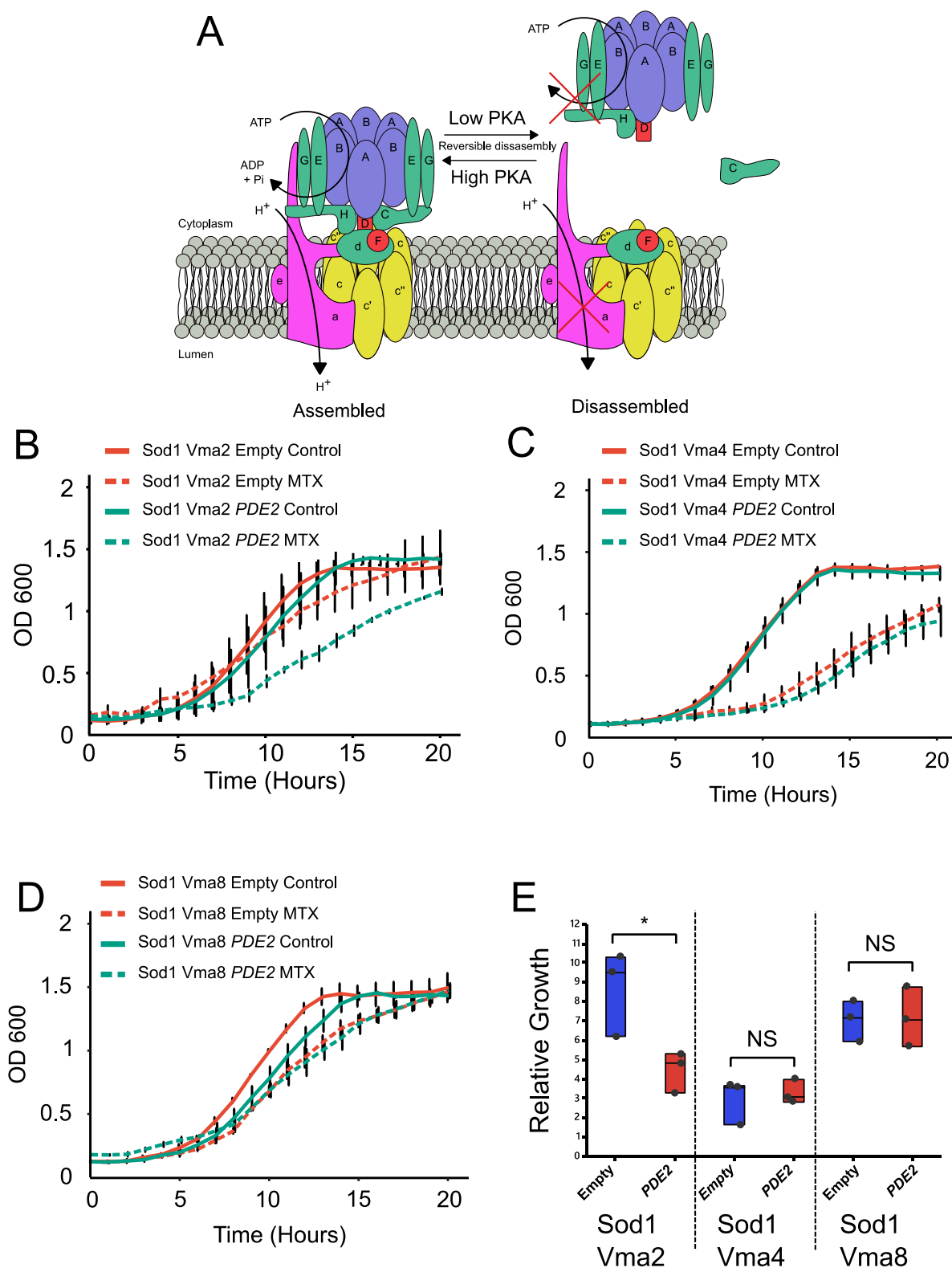


Figure 5.5 Effect of overexpression of *PDE2* on Sod1/V-ATPase interaction by DHFR-PCA.

A) Graphic illustrating the process of reversible disassembly of the V-ATPase in *S. cerevisiae* and how PKA signalling plays a role as an assembly factor. B) Growth curve illustrating the growth of Sod1^{bait} Vma2^{prey} diploids overexpressing Pde2 or an empty vector control with and without 200 µg/ml MTX. C) Growth curve of Sod1^{bait} Vma4^{prey} diploids overexpressing Pde2 or an empty vector control with and without 200 µg/ml

MTX. D) Growth curve of Sod1^{bait} Vma8^{prey} diploids overexpressing Pde2 or an empty vector control with and without 200 µg/ml MTX. For all growth curves B)–D), one representative result of three biological repeats is shown. Error bars represent standard deviation between three technical replicates. E) Box plot of the relative growth value calculated from three biological replicates of the DHFR protein complementation assay. N = 3. One way ANOVA comparison between the interaction diploid and BY4743 negative control were carried out to test for differences in relative growth. * $p < 0.05$.

5.2.6 Removal of glucose increases the interaction between Sod1 and the V-ATPase

Reversible disassembly of the V-ATPase is also controlled by the presence and absence of D-glucose in *S. cerevisiae*. To study the effect that varying glucose concentrations in the media has on the interaction between Sod1 and the V-ATPase, Sod1^{bait} Vma2^{prey} and Sod1^{bait} Vma4^{prey} diploids were grown in media containing different amounts of D-glucose.

In Figure 5.6 B), in normal SC media, growth of the Sod1^{bait} Vma2^{prey} diploid decrease as the glucose concentration decreases. When treated with MTX, cells grown in 2% D-glucose grew better than those in 0.2% and 0% D-glucose, however there was no difference in growth between cells in 0.2% glucose and 0% glucose (Figure 5.6 C)). Relative growth calculation (Figure 5.6 F)) showed that the relative growth of cells grown in 0% D-glucose increased significantly compared to 0.2% and 2% D-glucose for the Sod1^{bait} Vma2^{prey} diploid. This indicated that when there was no glucose available and the majority of V-ATPases were disassembled, the interaction between Sod1 and Vma2 increased significantly. With the Sod1^{bait}, Vma4^{prey} diploid, there was a significant increase in relative growth in cells grown in 0.2% D-glucose compared to 2% D-glucose, as well as cells grown in 0% D-glucose compared to cells grown in 2% D-glucose (Figure 5.6). This suggests that as glucose concentrations go down and the majority of V-ATPase complexes are disassembled, the interaction between Sod1 and Vma4 increases significantly. In summary, it was observed that with lower concentrations of glucose in the cell, the relative growth of the Sod1^{bait} Vma2^{prey} and Sod1^{bait} Vma4^{prey} diploids increased indicating an increased number of DHFR complexes being formed. This result suggests that when the V-ATPase is disassembled in conditions of low glucose, the interaction between Sod1 and the V-ATPase becomes stronger.

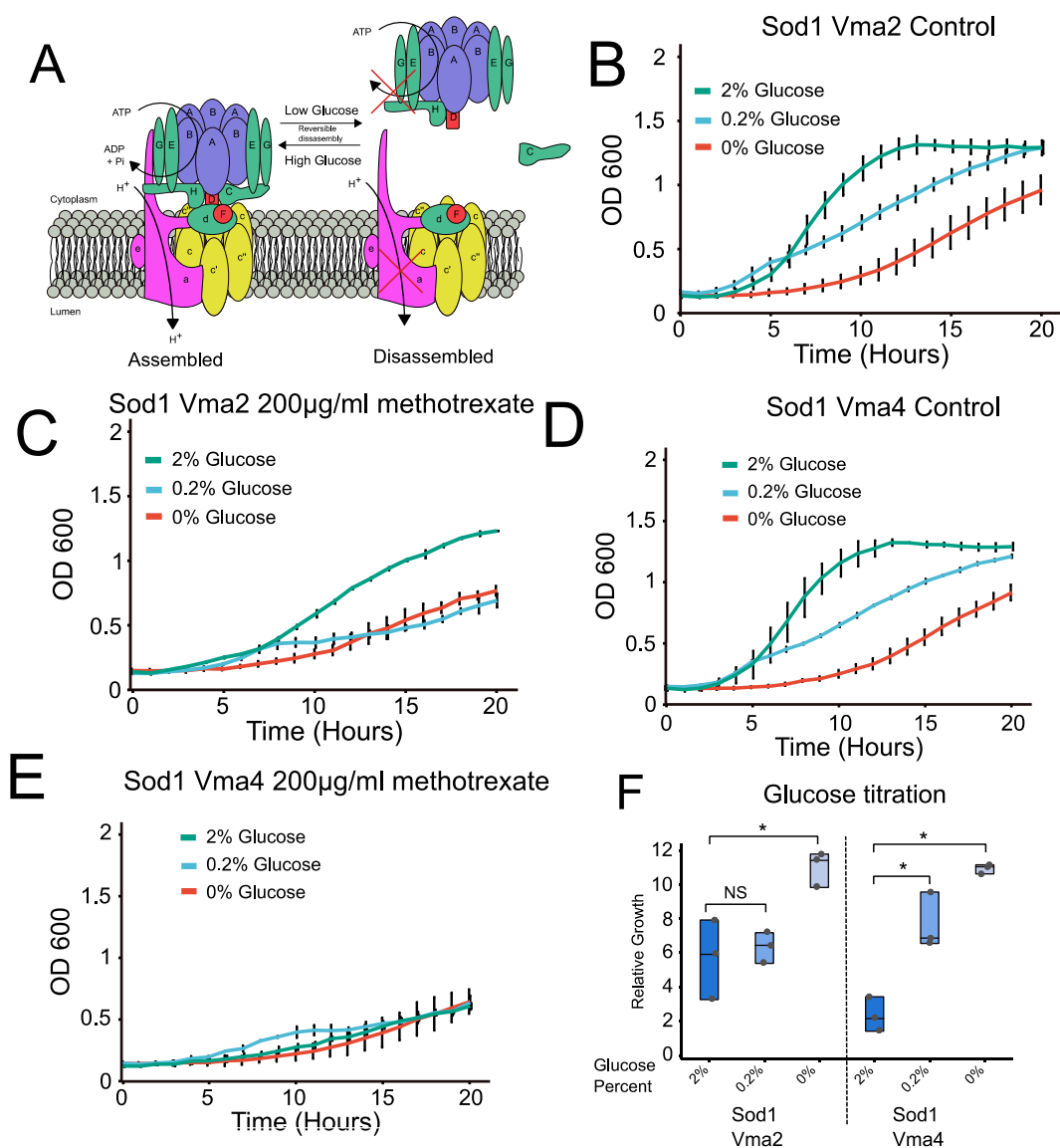


Figure 5.6 Testing the effect of glucose titration on the Sod1/V-ATPase interaction by DHFR-PCA.

A) Graphic illustrating reversible disassembly of the V-ATPase and the role that glucose signalling plays. Low glucose levels lead to disassembly of the V-ATPase whereas high glucose levels result in increased assembly. B) Growth curve of Sod1^{bait} Vma2^{prey} diploid in SC media supplemented with different concentrations of D-Glucose (% w/v). C) Growth curves of Sod1^{bait} Vma2^{prey} diploid in SC media supplemented with 200 µg/ml MTX and differing concentrations of D-glucose (% w/v). D) Growth curve of Sod1^{bait} Vma4^{prey} diploid in SC media supplemented with different concentrations of D-Glucose (% w/v). E) Growth curves of Sod1^{bait} Vma2^{prey} diploid in SC media supplemented with 200 µg/ml MTX and differing concentrations of D-glucose (% w/v). One representative result from three biological replicates is displayed. Error bars represent the standard deviation between three technical replicates. F) Relative growth value calculated from three biological replicates of the DHFR-PCA assay. N = 3. One-Way ANOVA was used to test for significance. * $p < 0.05$

5.2.7 Effect of deletion of *VPH1*, *STV1* on the interaction of Sod1 and the V-ATPase by DHFR-PCA.

In *S. cerevisiae*, the V-ATPase can be found on the membranes of vacuoles, endosomes and the golgi apparatus. V-ATPases found on the vacuoles possess an 'a' subunit that is encoded by the gene *VPH1* whereas V-ATPases on the golgi apparatus and endosomes have an 'a' subunit that is encoded by the gene *STV1*. To test whether Sod1 interacts specifically with V-ATPases on the vacuole membrane or with endosomal/golgi V-ATPases, *VPH1* and *STV1* were deleted from the Sod1^{bait} Vma2^{prey} and Vma4^{prey} haploids. The haploids were then mated together and selected for diploids lacking both copies of the *VPH1* or *STV1* gene.

In the DHFR-PCA assay of Sod1^{bait} Vma2^{prey}, Sod1^{bait} Vma4^{prey}, and Sod1^{bait} Vma8^{prey} diploids lacking *STV1* similar results were observed. Deletion of *STV1* did not affect growth of the diploids in normal SC media or in SC media supplemented with 200 µg/ml MTX (Figure 5.7 B, C and D). In the same experiment repeated for Sod1^{bait} Vma2^{prey}, Sod1^{bait} Vma4^{prey}, and Sod1^{bait} Vma8^{prey} diploids lacking *VPH1*, similar results to that of diploids lacking *STV1* were observed. In summary, this data suggests that deletion of *STV1* or *VPH1* does not affect the interaction between Sod1 and Vma2, Vma4 and Vma8 as there is no significant difference in the relative growth values. This indicates that when *STV1* is deleted that Sod1 is still interacting with *VPH1* encoded V-ATPases and that when *VPH1* is deleted that Sod1 is still interacting with *STV1* encoded V-ATPases.

5.2.8 Effect of deletion of *VMA2* or *VMA4* on the interaction of Sod1 and the V-ATPase by DHFR-PCA.

As it has been previously observed that both Stv1 and Vph1 are capable of compensating for the other when the gene coding for them is deleted [209], we decided to carry out the same experiment but for cells lacking either *VMA2* in the case of the Sod1^{bait} Vma4^{prey}, and Sod1^{bait} and Vma8^{prey} diploids, or *VMA4* in the case of the Sod1^{bait} Vma2^{prey} diploid. Deletion of either *VMA2* or *VMA4* results in the inability of all V-ATPase complexes in the cell to assemble. Deletion of *VMA2* significantly reduced the relative growth value of the Sod1^{bait} Vma4^{prey}, and Sod1^{bait} Vma8^{prey} diploids. Deletion of *VMA4* did not significantly reduce the relative growth value of the Sod1^{bait} Vma2^{prey} diploid (Figure 5.8, Figure 5.7 D)). From the growth curves, it can be observed that the Sod1^{bait} Vma2^{prey} diploid lacking *VMA4* is able to grow in media supplemented with 200 µg/ml MTX, whereas both the Sod1^{bait} Vma4^{prey} and Sod1^{bait} Vma8^{prey} diploids lacking *VMA2* were unable to grow at all in SC media supplemented with 200 µg/ml MTX. This suggests that after deletion of *VMA2*, Sod1 no longer interacts with Vma4 or Vma8.

Chapter 5. Investigating the interaction between Sod1 and the V-ATPase

After deletion of *VMA4*, Sod1 can still interact with Vma2. In cells lacking *VMA2* or *VMA4*, the V-ATPase cannot assemble and the V₁ domain is diffuse in the cytosol. This suggests that the Sod1 interaction with the V-ATPase is stronger when it is assembled and at the vacuole membrane.

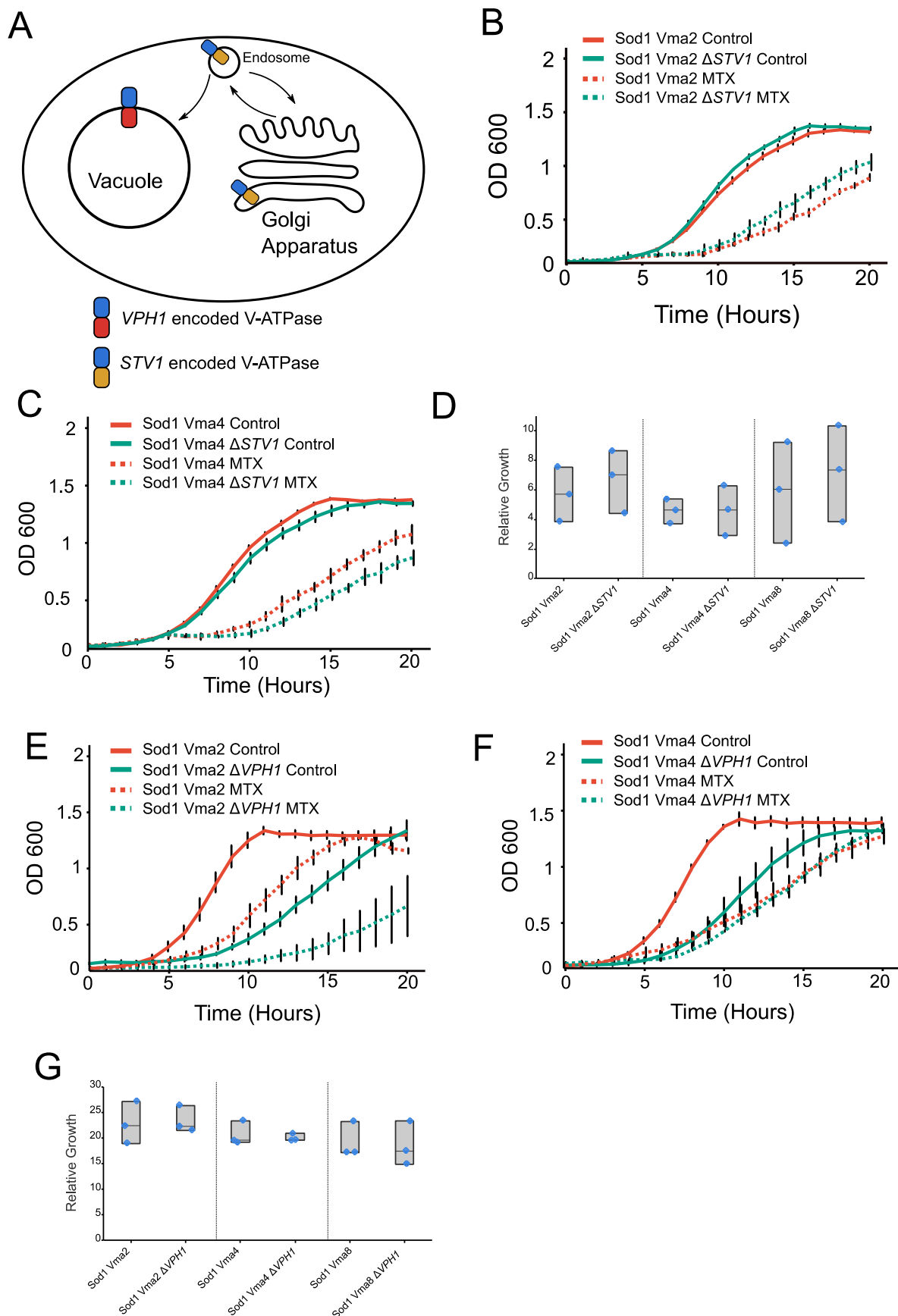


Figure 5.7 Interaction of Sod1 with different isoforms of the V-ATPase.

A) Graphic illustrating the localization of *VPH1* and *STV1* encoded V-ATPases. V-ATPases with the 'a' subunit encoded by *VPH1* are found on the vacuole membrane

whereas V-ATPases with the ‘a’ subunit encoded by *STV1* are found on endosomes and the golgi apparatus. B) PCA growth curve of the Sod1^{bait} Vma2^{prey} diploid with and without the *STV1* gene. C) PCA growth curve of the Sod1^{bait} Vma4^{prey} diploid with and without *STV1*. D) Relative growth calculation from PCA assay in the Sod1^{bait} Vma2^{prey}, Vma4^{prey} and Vma8^{prey} diploids with and without *STV1* from three biological replicates. E) PCA growth curve of the Sod1^{bait} Vma2^{prey} diploid with and without *STV1*. F) PCA growth curve of the Sod1^{bait} Vma4^{prey} diploid with and without *STV1*. G) Relative growth calculation from PCA assay in the Sod1^{bait} Vma2^{prey}, Sod1^{bait} Vma4^{prey} and Sod1^{bait} Vma8^{prey} with and without *VPH1*. from three biological replicates. For all growth curves a representative result of three biological replicates is shown. Error bars represent standard deviation between three technical replicates. For all boxplots, each datapoint represents a biological replicate.

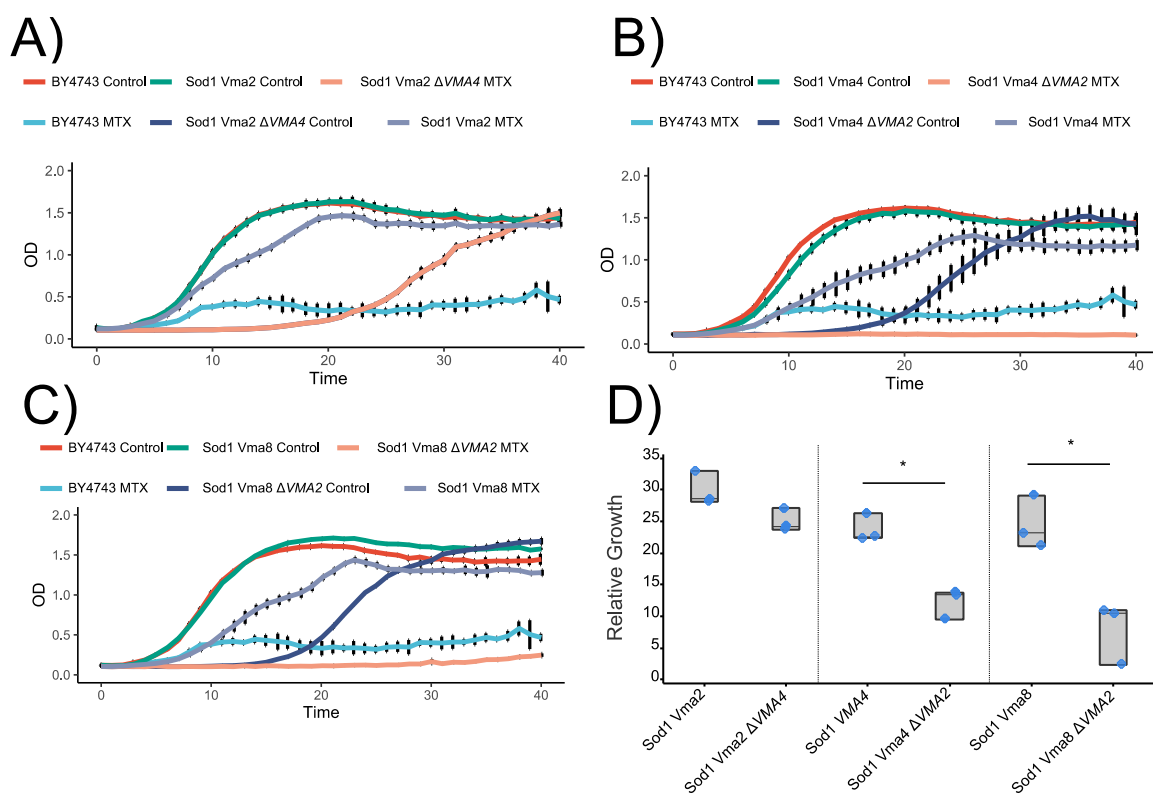


Figure 5.8 PCA assay between Sod1 and V-ATPase in *VMA2* and *VMA4* deletions.

A) PCA growth curve of Sod1^{bait} Vma2^{prey} diploid with and without *VMA4*. B) PCA growth curve of Sod1^{bait} Vma4^{prey} diploid with and without *VMA2*. C) PCA growth curve of Sod1^{bait} Vma8^{prey} with and without *VMA2*. D) Relative growth calculation from Sod1^{bait} Vma2^{prey}, Vma4^{prey} and Vma8^{prey} PCA assay from three biological repeats. N = 3. Statistically significant differences (* $p < 0.05$) are calculated from a One-Way ANOVA comparison.

5.2.9 DHFR-PCA screening revealed interactions between Sod1/Ego3 and Sod1/Rav1.

As it had been observed that Sod1 interacts with four subunits of the V₁ domain of V-ATPase in *S. cerevisiae* via a DHFR-PCA assay, we decided to check for interaction between Sod1 and the F-ATP synthase pump located in the mitochondria. This is due to the high degree of conservation

Chapter 5. Investigating the interaction between Sod1 and the V-ATPase

between V-ATPases and F-ATPsynthases and due to the fact that a small pool of Sod1 localises to the IMS. [210][211]. The F-ATPase subunits Atp2, Atp7, Atp14, Atp15 and Atp16 were selected to test for interaction with Sod1 as they are all part of the F₁ domain of the F-ATPsynthase, the equivalent of the V₁ domain in the V-ATPase where Vma2, Vma4 and Vma8 are found. The following diploids were generated: Sod1^{bait} Atp2^{prey}, Sod1^{bait} Atp7^{prey}, Sod1^{bait} Atp14^{prey}, Sod1^{bait} Atp15^{prey}, Sod1^{bait} Atp16^{prey}. As seen in Figure 5.9, none of the diploids were able to grow in SC media supplemented with 200 µg/ml MTX, suggesting that Sod1 does not interact with the F₁ domain of the F-ATPsynthase in *S. cerevisiae*.

Ego3, one of the subunits of the EGO complex, responsible for acting as a scaffold for the GEFs Gtr1 and Gtr2 to recruit the TOR complex to the vacuole membrane [163] was found in Chapter 3 to produce a synthetic slow growth phenotype alongside the expression of the ALS-linked mutant isoforms of Sod1, Sod1^{A4V}. Furthermore, the mammalian equivalent of the EGO complex called the RAGULATOR has been shown to be in a complex with the V-ATPase in mammalian cells [212]. To test whether Sod1 is also interacting with Ego3, the diploid Sod1^{bait} Ego3^{prey} was generated. It was observed that the diploid was able to grow in SC media supplemented with 200 µg/ml MTX suggesting that Sod1 is interacting with Ego3 (Figure 5.9). The RAVE complex was screened as it is considered an accessory to the V-ATPase and plays a crucial role in regulating assembly and disassembly of the pump.

The Sod1^{bait} Rav1^{prey} diploid was able to grow in media supplemented with 200 µg/ml MTX whereas the Sod1^{bait} Rav2^{prey} and Sod1^{bait} Skp1^{prey} diploids were not (Figure 5.9). This indicates that Sod1 can interact with Rav1, but not Rav2 or Skp1.

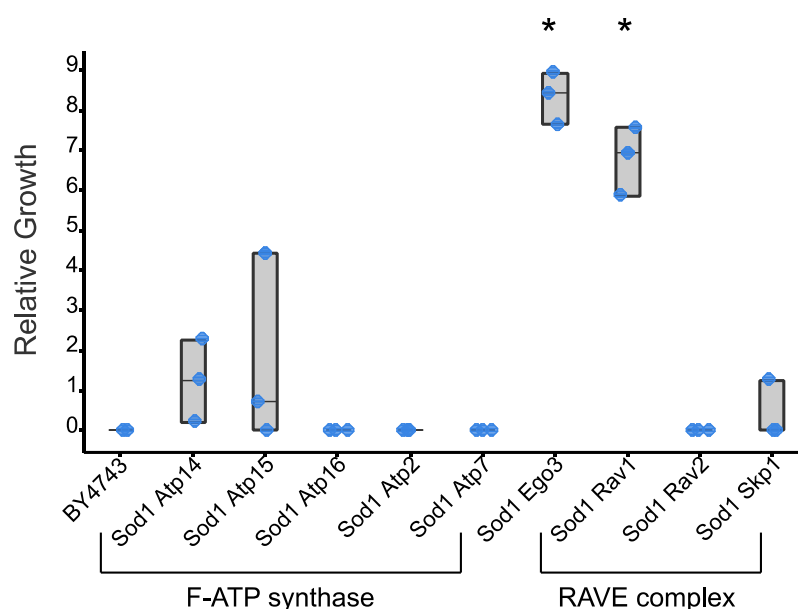


Figure 5.9 Further DHFR-PCA screening of F-ATP synthase subunits, Ego3 and subunits of the RAVE complex.

Relative growth quantification of DHFR-PCA screening of the F-ATP synthase subunits that correspond to same subunits of the V_1 domain of the V-ATPase that were previously identified, Ego3 and the RAVE complex. Relative growth is quantified as before from three biological replicate growth assays in media supplemented with 200 $\mu\text{g}/\text{ml}$ MTX and a control. $N = 3$. Values of zero indicate no growth. One-Way ANOVA comparison was used to test for significant difference in relative growth between diploids and the negative control BY4743 (* $p < 0.05$).

5.2.10 Effect of *SOD1* deletion on assembly of the V-ATPase

In order to monitor the effect of *SOD1* deletion on the assembly state of the V-ATPase, a reporter for V-ATPase assembly was used [213]. This dual reporter involved the ‘a’ subunit of the V_0 domain of the V-ATPase C-terminally tagged with GFP and the C subunit of the V_1 domain of the V-ATPase C-terminally tagged with RFP. When the V-ATPase complexes are in an assembled state, both the GFP and RFP signal localise to the vacuole membrane and profile plots of the cells overlay each other. When the V-ATPase is in a disassembled state, for example when the carbon source is switched from glucose to galactose, the RFP signal representing Vma5 becomes more diffuse in the cytosol and a shift can be observed in the profile plots.

To study whether assembly of the V-ATPase complexes are functional in cells lacking *SOD1*, *SOD1* was deleted from the Vph1::GFP Vma5::RFP reporter strain and cells were visualised in both media containing glucose and galactose as the carbon source. No difference was observed between WT and Δsod1 cells in terms of the GFP and RFP signals. For both strains, GFP and RFP signals localised to the vacuole membrane in media containing glucose and RFP became diffuse in the cytosol in media containing galactose (Figure 5.10). This suggests that the deletion of *SOD1* has no effect on the assembly and disassembly of the V-ATPase.

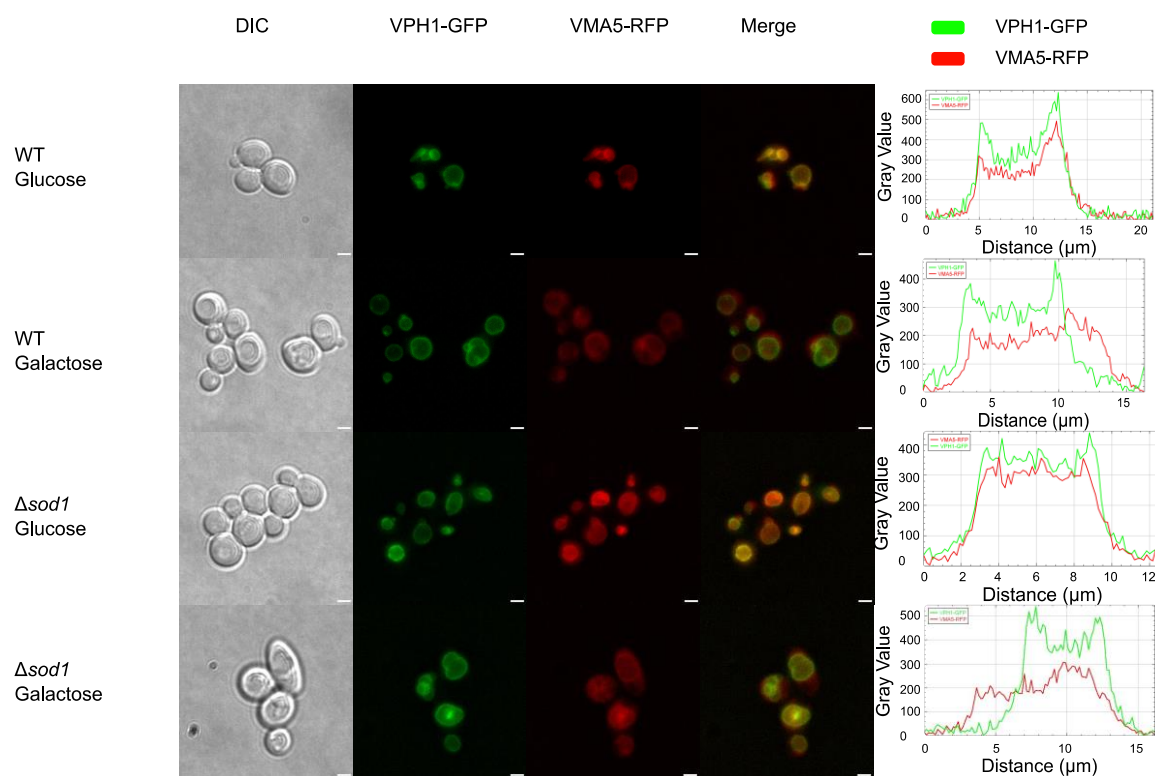


Figure 5.10 Reversible disassembly of the V-ATPase in response to glucose deprivation.

Wide-field fluorescence microscopy of WT and $\Delta sod1$ cells with Vph1::GFP and Vma5::RFP in order to test the assembly of the V-ATPase complex. Vph1::GFP is a reporter for the V_0 domain and should be localised to the vacuole membrane at all times. Vma5::RFP becomes diffuse in the cytosol upon disassembly of the V-ATPase. Representative profile plots (taken from FIJI (imagej) of both GFP and RFP signals are shown to demonstrate their distribution in the cell. In WT and $\Delta sod1$ cells grown on glucose, the distance (μm) in the profile plots of the GFP and RFP signals are identical. In WT and $\Delta sod1$ cells grown on galactose, the distance (μm) in the profile plots of the GFP and RFP signals differ from each other. Cells were grown to mid-log phase in SC media before visualisation. For the galactose media, cells were washed twice to remove any traces of glucose. Scale bar represents a distance of 5 μm .

5.2.11 Recombinant bovine Sod1 affects V-ATPase ATP hydrolysis activity *in vitro*.

The previous results in this chapter suggest that Sod1 is within close proximity to the subunits Vma2, Vma4 and Vma8 *in vivo* in *S. cerevisiae*. To test whether the Sod1 enzyme can interact with the V-ATPase *in vitro*, vacuoles were extracted from the BY4741 strain of *S. cerevisiae* and V-ATPase activity assays were carried out in the presence of varying concentrations of recombinant bovine Sod1 enzyme to test whether certain concentrations of active Sod1 present in the solution could affect V-ATPase ATP hydrolysis activity. ATP hydrolysis activity was indirectly measured using the malachite green phosphate detection system [157] to measure the

amount of inorganic phosphate produced by isolated vacuoles after the addition of 200 mM ATP. The amount of phosphate produced with and without the V-ATPase specific inhibitor bafilomycin were compared to calculate the V-ATPase specific activity (Figure 5.11 A). Isolated vacuoles were stained with the lipophilic dye FM4-64 and visualised by fluorescence microscopy (Figure 5.11 B). V-ATPase activity over time was measured from isolated vacuoles in the presence of 1, 10 and 100 ng of recombinant bovine Sod1 (Figure 5.11). From this time-point assay it was determined that an endpoint of 15 min would be used as the reaction had not saturated by that point and ATP was still being actively consumed. As shown in Figure 5.11 D), the presence of 0.1 μ g and 1 μ g of recombinant bovine Sod1 significantly decreased the ATP hydrolysis activity of the control vacuoles from 138 μ M (6.2 + = - 6.2) of inorganic phosphate produced, to 106 μ M (15 + = - 15) by 0.1 μ g and 107 μ M (26 + = - 26) by 1 μ g of Sod1 respectively. This data suggests an interaction between recombinant bovine Sod1 and the *S. cerevisiae* V-ATPase *in vitro*.

To test whether V-ATPase activity differed between WT and Δ *sod1* cells, vacuoles from 3 independent cultures of WT and Δ *sod1* were harvested and tested for V-ATPase activity as shown in Figure 5.13. There was no difference in the percent change in bafilomycin specific ATP hydrolysis in Δ *sod1* cells compared to WT cells. This suggests that there is no difference in V-ATPase activity between WT and Δ *sod1* cells.

Western blot analysis of Ficoll fractions from the vacuole extraction showed that Sod1 was present in the vacuole enriched 0–4% interface (Figure 5.12).

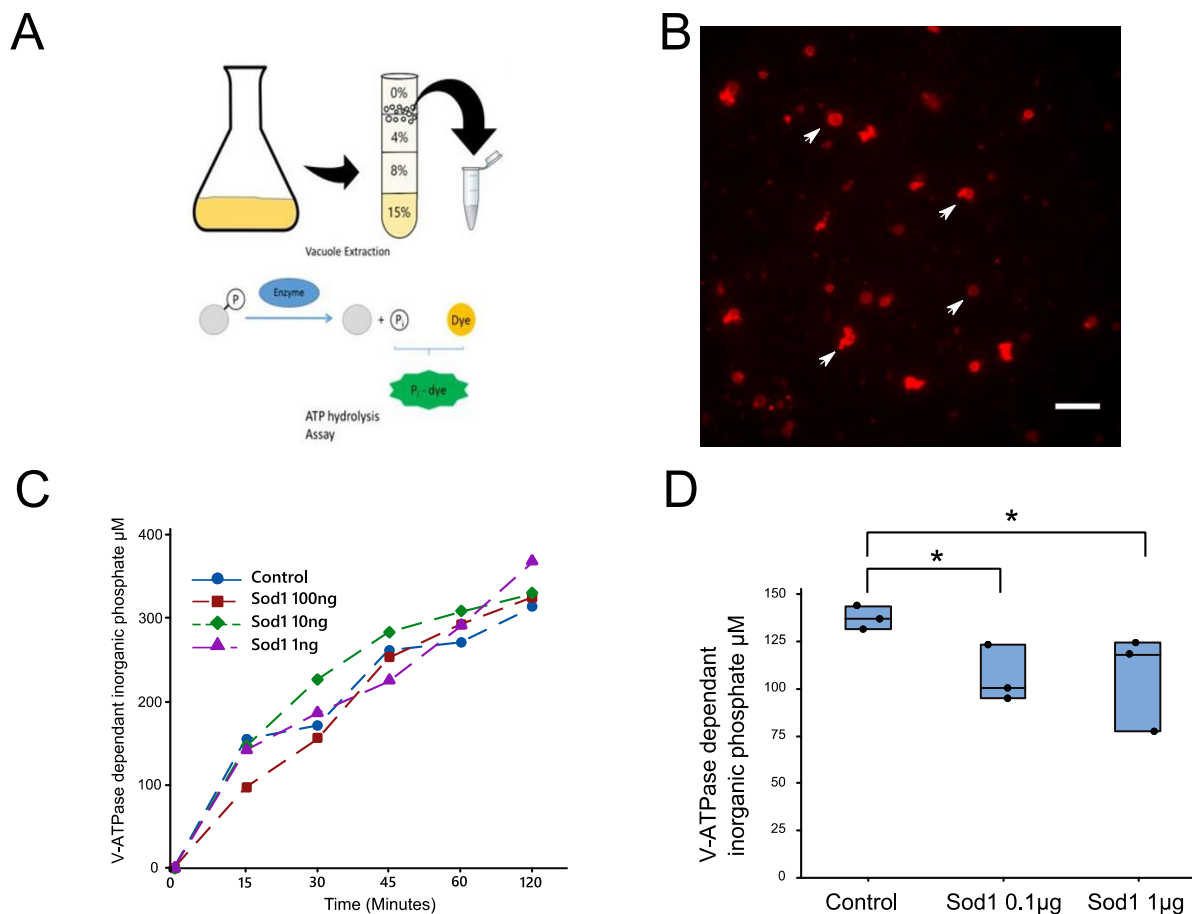


Figure 5.11 Effect of Sod1 on V-ATPase ATP hydrolysis activity.

A) Graphic illustrating the vacuole extraction protocol followed by malachite green detection of inorganic phosphate produced from ATP hydrolysis. B) Fluorescence microscopy image of isolated vacuoles stained with 3 μ M FM4-64 lipophilic dye. Scale bar in the bottom right corner indicates a length of 5 μ m. 100 \times magnification was used. C) Time course assay of V-ATPase activity assay. V-ATPase activity is determined by the difference in inorganic phosphate produced from vacuole samples with and without the V-ATPase inhibitor bafilomycin a1. This plot represents one biological replicate. D) Boxplot of V-ATPase activity of vacuoles with increasing amounts of recombinant Sod1 enzyme present. Average of three biological replicates. One-way ANOVA comparison was used to test for significance. * $p < 0.05$. N = 3.

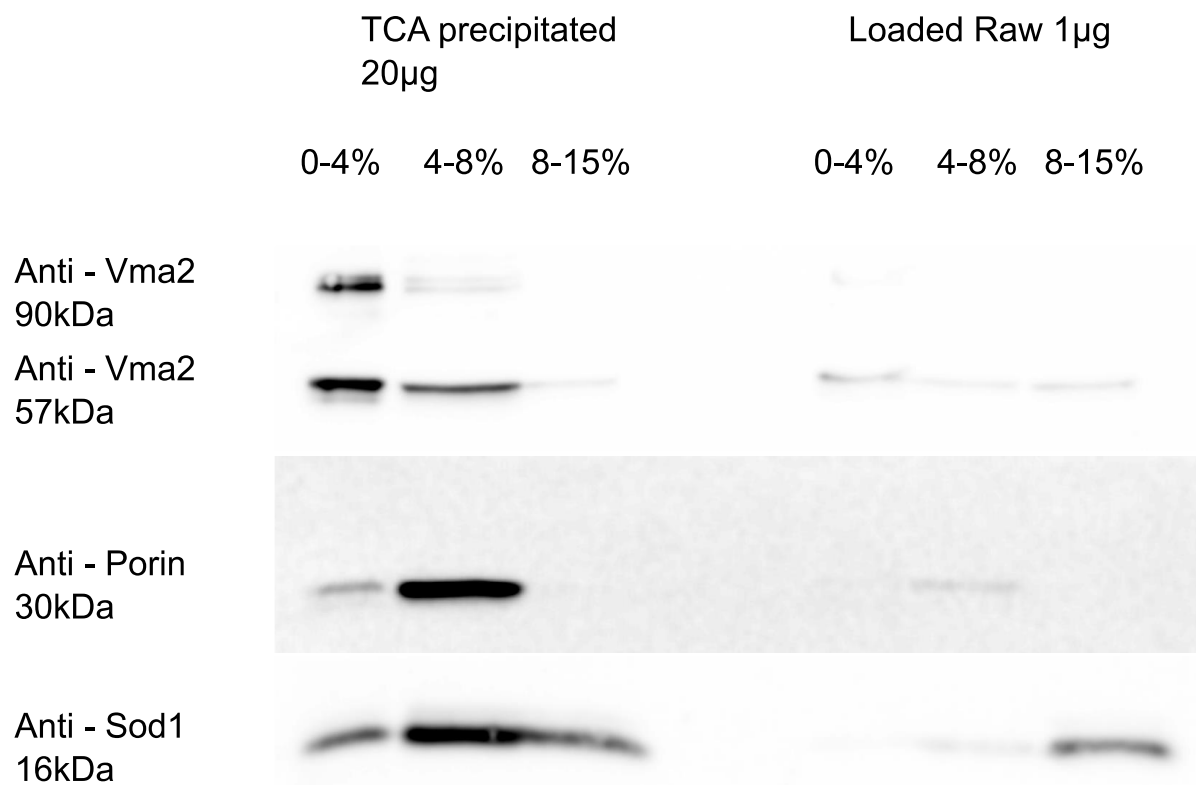


Figure 5.12 Western blot of ficoll fractions from vacuole extraction of BY4741. Western blot for Vma2, Porin and Sod1 in ficoll fractions from a vacuole extraction of BY4741 cells. 0–4%, 4–8% and 8–15% refers to the intervals between the 15%, 8%, 4% and 0% ficoll media in the vacuole extraction. Trichloroacetic acid (TCA) precipitation was performed to concentrate the protein for analysis. Vacuoles are usually enriched at the 0–4% ficoll interval.

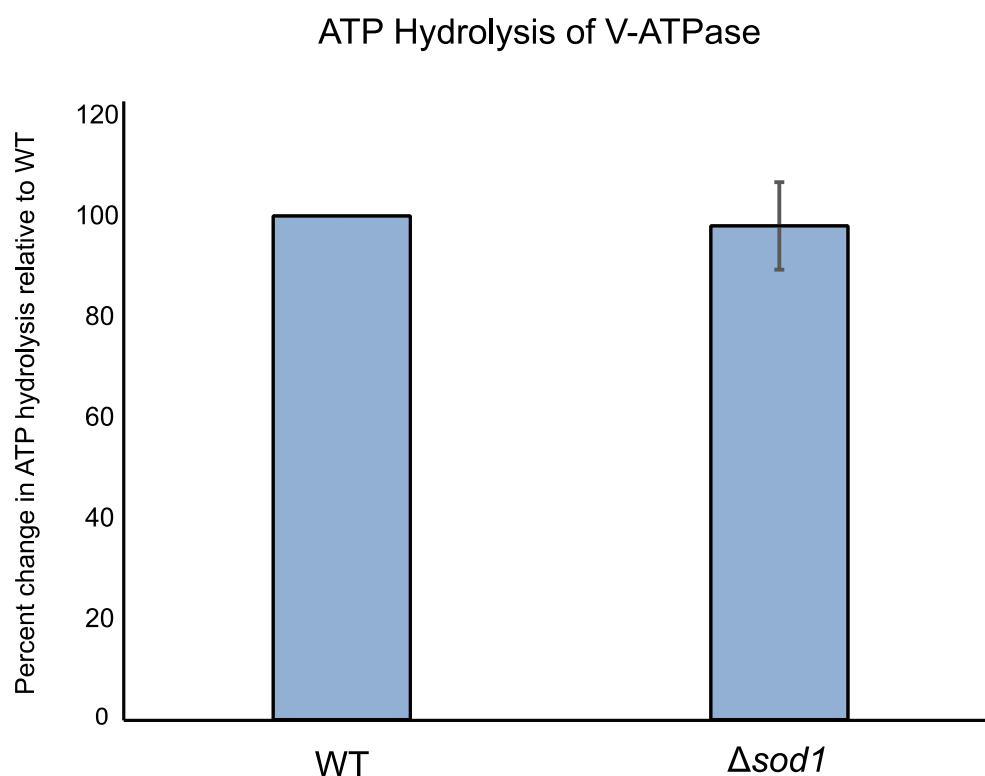


Figure 5.13 V-ATPase activity assay comparing WT and Δ sod1.

Bar chart displaying the percent change in bafilomycin sensitive ATP hydrolysis between WT and Δ sod1 cells relative to the WT control. Bar chart displays the mean of three biological repeats and error bars denote the standard deviation between these values. N = 3.

5.2.12 Sod1 was not found to be co-immunoprecipitated along with Vma2, Vma4 and Vma8

To further investigate the interaction between Sod1 and the V-ATPase, we decided to immunoprecipitate Sod1, Vma2, Vma4 and Vma8 fusions, C-terminally tagged with the 3HA tag, using anti-HA magnetic beads. The aim with this method was to confirm the results of the DHFR screen and to potentially identify other members of the complex by downstream mass spectrometry analysis.

As seen in Figure 5.14, we were unable to identify Sod1 by immunoblotting in any of the immunoprecipitants of Vma2-3HA, Vma4-3HA and Vma8-3HA. Likewise, Vma2 was not identified in the Sod1 immunoprecipitant. In the Vma4-3HA and Vma8-3HA pulldown, Vma2 was identified by western blotting as expected. This result indicates that Sod1 cannot be co-immunoprecipitated with the V-ATPase using C-terminal 3HA tags under the conditions used.

Additionally, it was observed that two different sizes of Vma2 were identified by Western blotting Figure 5.14, one size at 55 kDa, and one size at 110 kDa. The known molecular weight of Vma2 is 57.7 kDa, this suggests that the size at 55 kDa that has been observed is the correct

size. Currently, it is unclear whether the signal that has been detected at 100 kDa is non-specific or specific to Vma2. Alternatively, the band for Vma2 that has been observed at 110 kDa could be due to a post-translational modification (such as phosphorylation or glycosylation), or due to dimerization of the protein. Western blot analysis of yeast cells lacking *VMA2* compared to WT yeast cells could be carried out to determine whether the band at 110 kDa is specific to Vma2 or not.

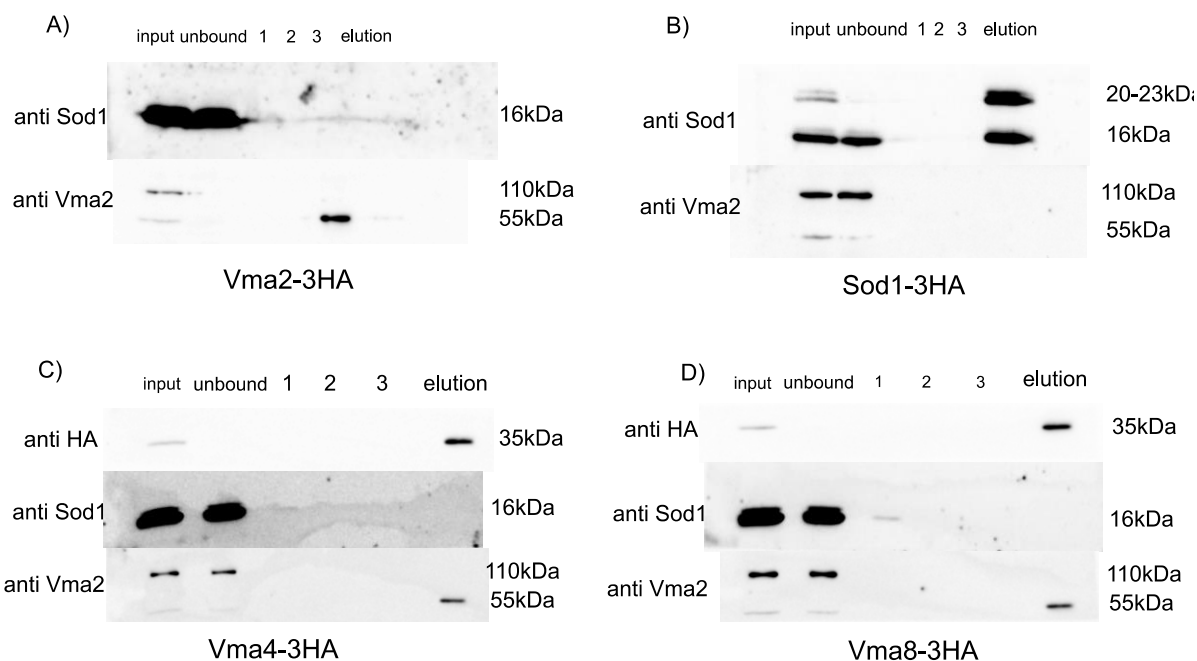


Figure 5.14 Western blots of Co-IP between Sod1 and Vma2, Vma4 and Vma8.

A) Western blot displaying immunoprecipitation (IP) of Vma2-3HA using anti HA magnetic beads. B) Western blot displaying IP of Sod1-3HA using anti HA magnetic beads. C) Western blot displaying IP of Vma4-3HA using anti HA magnetic beads. D) Western blot displaying IP of Vma8-3HA using anti HA magnetic beads. Input refers to 10% of the initial lysate. Unbound refers to 10% of the lysate after incubation with anti-HA beads for 2 h at 4 °C. 1, 2 and 3, refer to the supernatant at each wash step known as the flow through. Examination of the flow through is important to verify whether unattached proteins have been cleared from the beads through the wash steps. Elution refers to the immunoprecipitated protein eluted from the anti HA beads.

5.2.13 Measurement of the amino acid content of vacuoles from WT and $\Delta sod1$ cells

Previously it had been observed that the whole cell amino acid profile was significantly different in cells lacking *SOD1*. As a large amount of the cells amino acid pool is stored in the vacuole, we were interested in measuring the amino acid content from the vacuole extracts of WT and $\Delta sod1$ cells that had previously been prepared to test whether the loss of amino acid homeostasis observed in $\Delta sod1$ cells was due to a loss of amino acid homeostasis in the vacuole.

To do this, we collaborated with Dr St John Townsend and Dr Sreejith Jayasree Varma from the lab of Prof. Dr Markus Ralser at the Charité University in Berlin. Three independent vacuole extracts from WT and $\Delta sod1$ cells were sent. Amino acid content was measured by liquid chromatography–mass spectrometry (LCMS). Alanine, arginine, asparagine, glycine, serine, and threonine were not able to be detected at the time of writing. From the amino acids that were detected, both histidine and lysine levels were both significantly reduced in $\Delta sod1$ cells (Figure 5.15). Interestingly, in the whole cell amino acid measurements, both histidine and lysine levels were increased (Figure 5.2). The experiment was repeated after the protocol had been modified in order to detect alanine, arginine, asparagine, glycine, serine, and threonine. In the repeat that was carried out, no difference in the levels of histidine and lysine were observed. Overall, it cannot be concluded from these experiments whether there are any differences in the levels of amino acids in vacuole extracts from WT and $\Delta sod1$ cells.

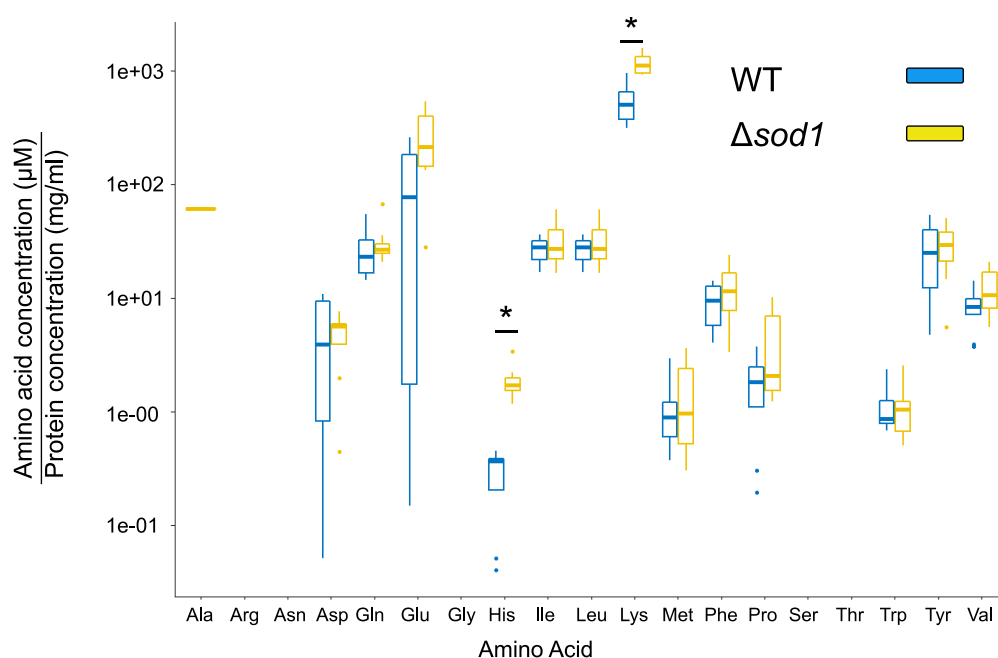


Figure 5.15 Amino acid content of vacuoles from WT and $\Delta sod1$ cells

Measurement of vacuole amino acid content in WT (yellow) and $\Delta sod1$ (red) both expressing pAG306-GPD-empty-*chrI* control vector. On the y axis, the amino acid concentration (μM) normalised to the total protein concentration of the sample (mg/mL) is shown in the log₁₀ scale. One-Way ANOVA test was used to test for statistical differences between the amino acid concentrations in WT and $\Delta sod1$. * $p < 0.05$. N = 3.

5.3 Discussion

5.3.1 Vacuole dysfunction in cells lacking SOD1

The aim of this chapter was to explore the vacuolar and metabolic defects observed in cells lacking *SOD1*. We sought to confirm whether the loss of *SOD1* in the *S. cerevisiae* background

used in this study would also cause vacuolar and metabolic defects. Results showed that the loss of *SOD1* lead to a sensitivity to all of the stresses tested as well as vacuole fragmentation. We conclude that in our strain background (BY4741), the loss of *SOD1* causes vacuole and metabolic defects.

We hypothesised that amino acid homeostasis in *S. cerevisiae* could be perturbed in cells lacking *SOD1*, as the vacuoles a central role in regulating amino acid homeostasis via its many amino acid transporters. Analysis of the Ralser dataset and measurements from vacuole extracts from WT and $\Delta sod1$ cells demonstrated that amino acid homeostasis was perturbed in cells lacking *SOD1*. This finding is supported by recent data in which the deletion of *SOD1* was shown to cause changes in protein abundance, cysteine oxidation in a number of proteins, with a specific enrichment in amino acid biogenesis [50]. Additionally, in the overexpression model of *SOD1*-ALS, metabolite analysis by NMR indicated perturbations in amino acid homeostasis as well upon deletion of *SOD1* or overexpression of *SOD1*-ALS [115]. A potential limitation of the amino acid measurements from the vacuole extracts of WT and $\Delta sod1$ cells in this study is that the strain background contains auxotrophies for uracil, leucine, methionine, and histidine. In the future, repeating the amino acid measurements of WT and $\Delta sod1$ vacuole extracts in a prototrophic strain may allow for more representative amino acid measurements. The vacuole extract amino acid measurements by LC-MS were unable to produce any data for alanine, arginine, or glycine. More recent data from the same collaborators were able to produce measurements for alanine, arginine, and glycine. In the second experiment, there were no differences in the values of all of the amino acid concentrations (including histidine or lysine) between WT and $\Delta sod1$ vacuole extracts.

5.3.2 Interaction of Sod1 with the V-ATPase

As the deletion of *SOD1* causes vacuole and metabolic defects, and the overexpression of ALS-linked mutant isoforms of Sod1 causes a vacuole acidification defects in *S. cerevisiae* [115], we sought to investigate whether Sod1 interacts with the V-ATPase. As previously discussed, the V-ATPase is a multisubunit enzyme that is acidifies the lumen of the vacuole.

Results from DHFR-PCA assays in this study suggest that Sod1 interacts with the V₁ domain of the V-ATPase. Specifically, with Vma2, Vma4, and Vma8. The effect of signalling pathways such as PKA or glucose signalling on the interaction between Sod1 and the V-ATPase from the DHFR-PCA assay do not seem to correlate. It was observed that in the DHFR-PCA diploids overexpressing *PDE2*, that the strength of the interaction between Sod1 and Vma2 decreased, whereas the interaction between Sod1 and Vma4/Vma8 was not affected. Additionally, it was

observed in conditions of glucose starvation, that the interaction between Sod1 and Vma2/Vma4 was significantly stronger. This suggests that PDE2 overexpression and glucose starvation have separate effects on the V-ATPase, and its potential interaction with Sod1. Further investigation of the effects of *PDE2* overexpression and glucose starvation using a different approach to measure the strength of the interaction between Sod1 and Vma2/Vma4/Vma8 such as CO-IP, or FLIM-FRET is required in order to confirm the observations that were made in this study. The finding that Sod1 interacts with the V-ATPase is supported by the fact that in a mass spectroscopy screen in human cells, Sod1 was found to interact with ATP6V1A and ATP6V1B, the mammalian homologues of Vma1 and Vma2 respectively [214]. Additionally, a genetic interaction between Sod1, and genes encoding any of the single copy subunits of the V-ATPase in yeast such as *VMA2* and *VMA4*. Deletion of *VMA2* or *VMA4* is synthetically lethal when combined with the deletion of *SOD1* [189]. This is because cells without active V-ATPase complexes suffer from chronic oxidative stress, and deletion of *SOD1* from these cells increases the level of endogenous stress to a lethal level. A limitation in this study is that we were unable to identify Sod1 in anti-HA immunoprecipitates from *S. cerevisiae* strains with Vma2, Vma4 and Vma8 C-terminally tagged with the 3HA epitope in the conditions tested. It could be that the possible interaction between Sod1 and the V₁ domain of the V-ATPase is transient and was not able to withstand the conditions of the CO-IP. Addition of a cross-linking step in order to preserve more transient interactions could allow for possible detection of Sod1 in V-ATPase IP samples.

When either *VMA2* or *VMA4* are deleted in *S. cerevisiae*, all V-ATPase complexes are abolished, the most severe Vma⁻ phenotype is observed and cells cannot grow in alkaline pH, are sensitive to metal ions and are defective in quinocrine uptake into the vacuoles [190]. Early interaction studies carried out using IP techniques in deletions of single subunits of the V-ATPase demonstrated that certain subcomplexes formed in the V-ATPase prior to full assembly of the enzyme. For example, when *VMA4* was deleted, a sub complex of Vma1 and Vma2, the catalytic and regulatory subunits A and B could be identified. When *VMA2* was deleted, a sub-complex of Vma4 and Vma10 and a different sub-complex of Vma8 and Vma7 were identified [215] [216]. The results from this study suggest that Sod1 can interact with the subcomplex of Vma2 and Vma1 when *VMA4* is deleted whereas Sod1 cannot interact with Vma4 in the subcomplex of Vma4 and Vma10 when *VMA2* is deleted. Additionally, Sod1 cannot interact with the subcomplex of Vma8 and Vma7 when *VMA2* is deleted. This suggests that interaction between Sod1 and Vma2 is the initial point of interaction.

From the same DHFR-PCA assay, it was observed that Sod1 interacts with members of the RAVE complex, Rav1, and Skp1, but not Rav2. The RAVE complex promotes assembly of V-ATPase complex at the vacuole membrane in response to glucose re-addition. Rav1 associates with the V-ATPase at the Vma4, Vma10 and Vma5, which make up the E, G, and C subunits [217]. Currently no previous evidence in *S. cerevisiae* or any other organisms exists that is indicative of an interaction between Sod1 and the RAVE complex. A subunit of the ego complex, EGO3 was also found to interact with Sod1 in the DHFR-PCA assay. Currently there is no other evidence for an interaction between Sod1 and Ego3 that has been published, however in mammalian cells, the homologue of Ego3 called LAMTOR2 associates with the homologue of Vma2 called ATP6V1B in an interaction that is important for recruitment of MTORC1 to the lysosome membrane in response to nutrient signals[212]. The fact that Sod1 interacts with proteins that have well characterised, evolutionarily conserved interactions with the V-ATPase is overall supportive for an interaction between Sod1 and the V-ATPase.

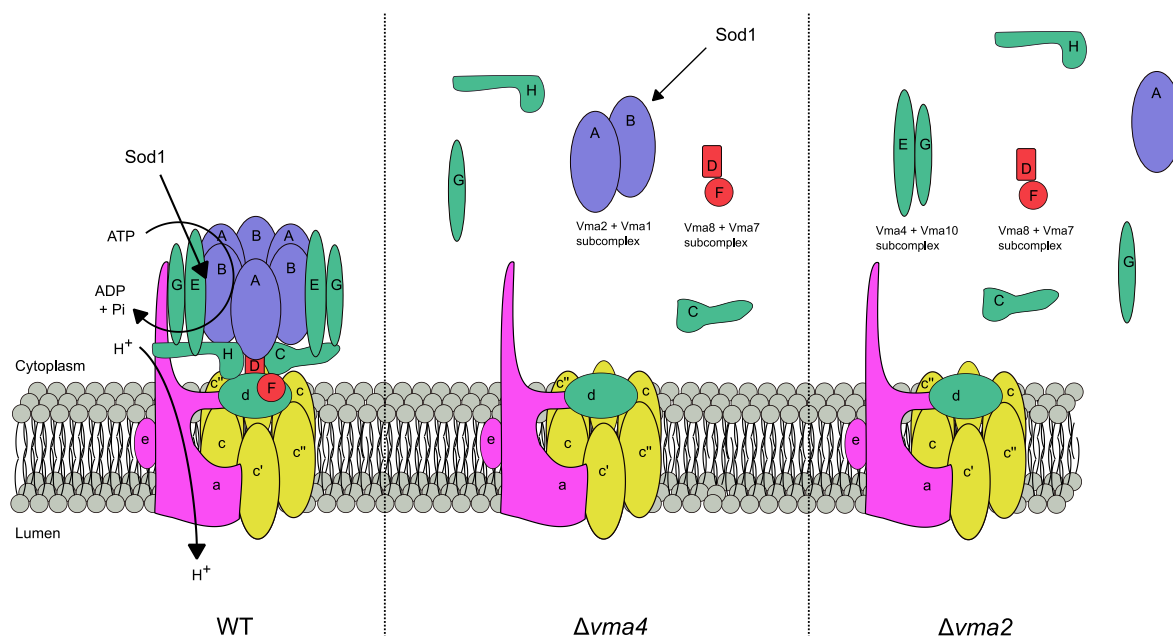


Figure 5.16 Interaction of Sod1 with different sub-complexes of the V₁ domain of the V-ATPase.

Schematic depicting the interaction of Sod1 with the V₁ domain of the V-ATPase in different deletions. In WT cells the V-ATPase is fully assembled and the V₁ domain is attached to the V₀ domain. In this scenario ATP hydrolysis can be carried out along with proton pumping and Sod1 interacts with Vma2, Vma4 and Vma8, (I.e., subunits B, E and D of the V-ATPase). In $\Delta vma4$ cells, the V₁ domain cannot fully form. A sub-complex of subunit B and A (I.e., Vma2 and Vma1) and a distinct sub-complex of subunit D and F (I.e., Vma8 and Vma7) form. Sod1 can interact with the Vma2, Vma1 sub-complex. In $\Delta vma2$ cells, the V₁ domain also cannot fully form. A sub-complex of subunit E and G (I.e.,

Vma4 and Vma10) and a distinct sub-complex of subunit D and F (I.e., Vma8 and Vma7) form. Sod1 cannot interact with either of these sub complexes.

5.3.3 Effect of Sod1 on V-ATPase activity

As the results so far from the study suggested that Sod1 may be interacting with the V-ATPase, and that a previous study observed that the overexpression of ALS-linked mutant Sod1 isoforms caused vacuole acidification defects, we sought to investigate whether Sod1 can affect V-ATPase activity in any way.

In this study, in cells lacking *SOD1*, vacuoles are fragmented, however they do not have a quinocrine uptake defect indicating that the vacuole lumen is sufficiently acidified. Cells lacking *SOD1* also do not show any defects in disassembly of the V-ATPase. Recombinant bovine Sod1 had an effect on V-ATPase activity in vacuole vesicles extracted from *S. cerevisiae* suggesting an ability for Sod1 to interact with the V-ATPase *in vitro*. It has been demonstrated in the past that the activity of V-ATPase can be impaired by exposure to N-ethylmaleimide due to oxidation of Cys254. It could be that the H₂O₂ that is being produced by the recombinant bovine Sod1 enzyme is oxidatively modifying an exposed residue on one of the subunits of the V-ATPase thereby modifying its activity. Despite this, vacuole extracts from WT and $\Delta sod1$ cells have the same level of V-ATPase ATP hydrolysis activity. These results suggest that Sod1 is not important for regulation of V-ATPase activity or assembly in *S. cerevisiae*.

In conclusion, the results suggest that Sod1 interacts with the V₁ domain of the V-ATPase enzyme in *S. cerevisiae* at the Vma2, Vma4, and Vma8 subunits. Additionally, Sod1 interacts with members of the RAVE complex, Rav1, and Skp1, as well as Ego3 from the ego complex. The results from this study do not identify a role for the interaction between Sod1 and the V-ATPase. Sod1 does not seem to be required for V-ATPase activity. As amino acid homeostasis is perturbed in $\Delta sod1$ cells and the V-ATPase has been suggested in playing a role as a vacuolar amino acid sensor, it could be that the interaction between Sod1 and the V-ATPase is important for this function somehow. In the future, confirming this interaction in yeast using CO-IP or FLIM/FRET methods as well as testing whether the interaction is conserved in mammalian cells will be important. Additionally, exploring the precise cellular function that the interaction between Sod1 and the V-ATPase mediates will be important.

6 Investigating the interaction between Sod1 and Calcineurin

6.1 Introduction

6.1.1 Calcineurin complex

Calcineurin (protein phosphatase 2B) is a highly evolutionarily conserved complex that is an important component in Ca^{2+} signalling. Calcineurin is a heterodimeric phosphatase complex made up of a catalytic A subunit around 58–64 kDa and a regulatory B subunit ~19 kDa. The protein phosphatase activity of calcineurin requires the binding of one Ca^{2+} ion to the regulatory B subunit and also the binding of one calmodulin molecule to the complex [218]. When there is no Ca^{2+} or calmodulin bound to calcineurin, the A and B subunits are bound to each other in an autoinhibitory conformation. Upon Ca^{2+} and calmodulin binding, a conformational change occurs resulting in an active calcineurin complex. Calcineurin can be inhibited pharmacologically by FK506 and cyclosporin A as they form a complex with immunophilins (cyclophilins and FKBP proteins) in the cell. This drug-immunophilin complex can then inhibit calcineurin activity [219] (Figure 6.1).

6.1.2 Calcineurin in *S. cerevisiae*

Calcineurin is highly evolutionarily conserved from yeast to humans. In *S. cerevisiae*, there are two isoforms of the A subunit, Cna1 encoded by *CNA1* and Cmp2 encoded by *CMP2*. They have redundant functions, meaning that calcineurin activity is not lost if either *CNA1* or *CMP2* are deleted from the cell. If both are deleted simultaneously then calcineurin activity is lost. The B subunit is called Cnb1 and is encoded by *CNB1*. Cnb1 is essential to calcineurin activity [220].

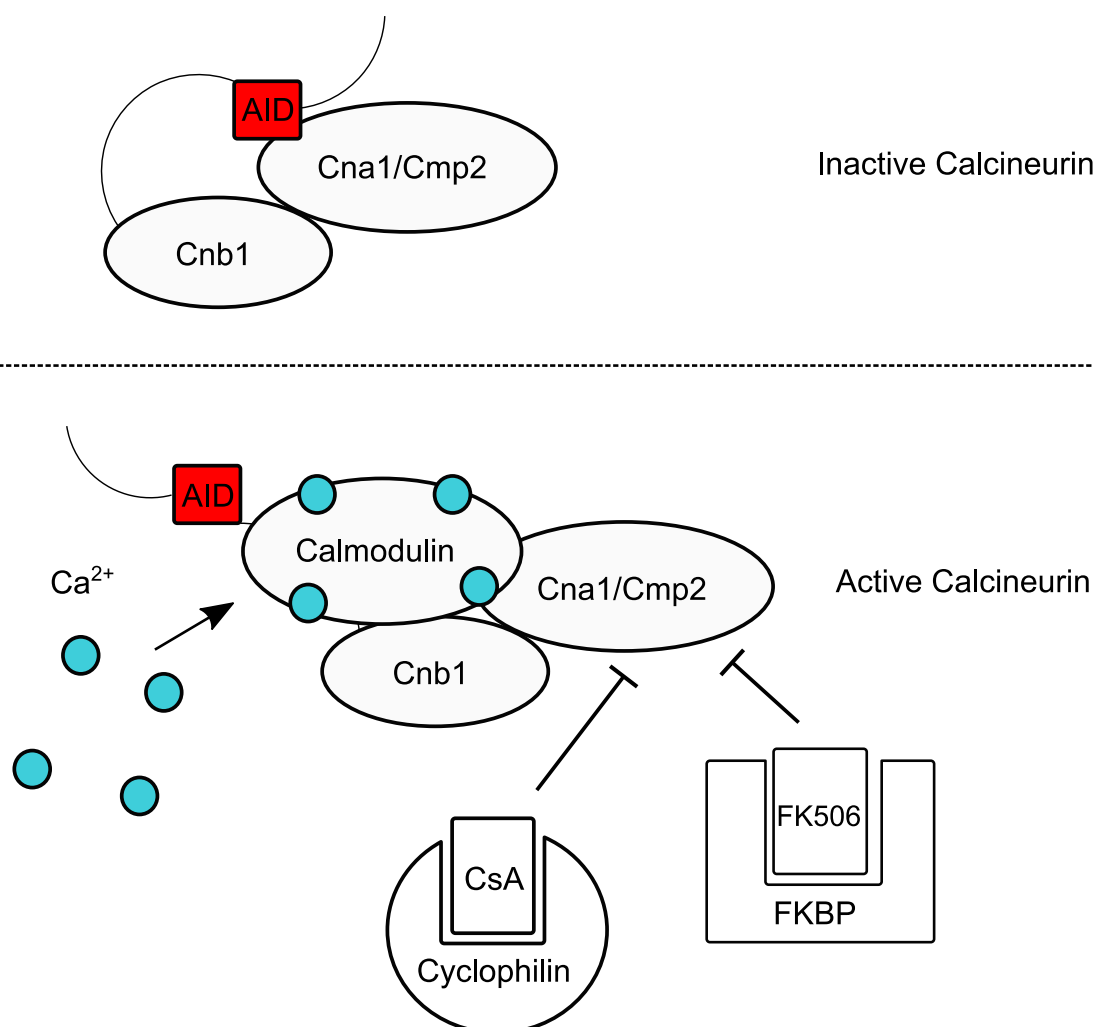


Figure 6.1 Calcineurin in *S. cerevisiae*. Structure and activation by calmodulin.

In the absence of Ca²⁺ and calmodulin, the calcineurin complex exists in an autoinhibitory state. The autoinhibitory domain (AID) at the C-terminus of Cnb1, is in a conformation which inhibits calcineurin activity. Upon binding of the Ca²⁺/Calmodulin complex, Cnb1 undergoes a conformational change resulting in the removal of the AID from the catalytic A subunit. Active calcineurin can be pharmacologically inhibited by the CsA/cyclophilin complex or the FK506/FKBP complex.

Disruption of calcineurin activity in *S. cerevisiae* leads to loss of viability under certain conditions such as high levels of certain ions (LiCl and MnCl₂) high salt levels, exposure to extracellular alkaline pH (> 7.5), or a lengthy incubation with the α -factor yeast mating pheromone [221][222]. α -factor addition to cells induced Ca²⁺ influx and subsequent intracellular Ca²⁺ accumulation [223]. Under standard laboratory conditions, cytosolic Ca²⁺ levels are low and therefore calcineurin is barely active. Upon exposure to stresses such as cell wall stress, high salt levels, and exposure to alkaline pH cytosolic Ca²⁺ levels increase and calcineurin becomes activated. Activation of calcineurin results in the expression of genes related to cell survival via the dephosphorylation of key substrates, the most well-known being the transcription factor Crz1 [224]. It is not yet fully understood why cytosolic Ca²⁺ levels increase in the cell upon

exposure to stress. This could be mediated by Ca^{2+} transporters located on the plasma membrane such as Cch1 [225] or Mid1 [226], or it could be that the vacuole membrane Ca^{2+} transporters Yvc1 and Pmc1 play a role too [227].

6.1.3 Calcineurin and ALS

Calcineurin and its role in regulating calcium homeostasis is thought to play a role in ALS pathogenesis. MNs possess features that make them selectively vulnerable compared to other cell types to loss of calcium homeostasis. Proteins called Ca^{2+} buffering proteins (CaBPs) that are important for buffering Ca^{2+} levels such as parvalbumin and calbindin are expressed at low levels in MNs [228]. Additionally, MNs highly express a specific type of calcium permeable AMPA (α -amino-3-hydroxy-5-methyl-4-isoxazole propionic acid) receptor [229]. AMPA receptors in MNs lack the GluR32 subunit which renders them highly permeable to Ca^{2+} . The low expression of calcium buffering proteins, combined with the high expression of Ca^{2+} permeable receptors is thought to render MNs highly susceptible to loss of calcium homeostasis compared to other neuronal cell types. High intracellular calcium levels have been observed in ALS mouse models [119], Overly elevated levels of intracellular Ca^{2+} in neurons leads to triggering of apoptosis via dephosphorylation of the pro-apoptotic factor called BAD (Bcl-2 associated agonist of cell death) by calcineurin [230], misfolding and aggregation of proteins [231] ER stress and induction of the unfolded protein response possibly due to ER Ca^{2+} pool depletion [232].

Calcineurin regulates Ca^{2+} homeostasis in neurons in multiple ways. In MNs, at the post-synapse, calcineurin has been observed to regulate the influx of Ca^{2+} ions through voltage-gated calcium channels (VGCCs). Upon Ca^{2+} influx through L-type VGCCs, calcineurin becomes activated and localised to the L-type VGCCs by the A-kinase anchoring protein 79/150 whereupon it inhibits their activity [233]. Calcineurin inhibits Ca^{2+} influx through N-methyl-D-aspartate receptors (NMDARs) via dephosphorylation a site on the C-terminal end of the NR2A subunit [234]. Calcineurin also inhibits activity of the AMPA receptor via dephosphorylation of serine 845 of the GluR1 subunit [235]. Calcineurin regulates neurotransmission, plasticity and connectivity of the synapses of neurons at the transcriptional level via the nuclear factor for activated T-cell (NFAT) transcription factor [236]. Furthermore, in lymphocyte samples taken from ALS patients, calcineurin activity was found to be markedly decreased, compared to samples from healthy control individuals [237].

6.1.4 Calcineurin and Sod1

Calcineurin has previously been shown to interact with Sod1 in various organisms. It has been suggested that the Fe-Zn metal centre of calcineurin is vulnerable to oxidative damage from free

radicals and that the presence of Sod1 provides a protection due to its antioxidant function. Sod1 was identified as a protective factor of calcineurin activity from eluates of rat brain homogenates tested for calcineurin activity [238]. This study also showed that in *S. cerevisiae*, $\Delta sod1$ mutants had very low calcineurin activity compared to the WT.

Furthermore, in *S. cerevisiae*, deletion of *SOD1* leads to similar phenotypes to deletion of *CNB1* the gene encoding for the regulatory subunit of calcineurin Cnb1 that is essential for calcineurin activity. These phenotypes include failure to grow in media buffered to an alkaline pH, sensitivity to high salt levels (1M NaCl), sensitivity to oxidative stress, and an inability to recover from G1 arrest after α -mating pheromone treatment. The similarity in phenotypes between the loss of *SOD1* and the loss of calcineurin activity suggest connectivity in the pathways that they are involved in in the cell.

6.1.5 Aim of this study

The aim of this study is to investigate the interaction between Sod1 and the calcineurin complex in *S. cerevisiae*. We aim to confirm whether calcineurin activity is decreased in live $\Delta sod1$ cells containing a transcriptional reporter for calcineurin activity, and also to check whether the interaction is physical as well using a DHFR-PCA. Using the simple yeast system, the effect of different ALS-linked isoforms of Sod1 on the activity of calcineurin can be studied.

6.2 Results

6.2.1 I-TASSER modelling of ALS-linked mutant isoforms of Sod1

I-TASSER is an online tool that uses an algorithmic pipeline to carry out protein structure and function predictions based on a peptide sequence. This platform can generate secondary structure predictions, 3D structure models, ligand binding site predictions and protein structure predictions. The aim of this *in silico* experiment was to investigate whether mutations in *SOD1* that are linked to ALS would lead to any differences in the I-TASSER structure and function predictions. Amino acid sequences of Sod1^{WT}, Sod1^{A4V}, Sod1^{G37R} and Sod1^{H48Q} were submitted for analysis to the I-TASSER online server. As a positive control the Sod1^{WT} sequence was resubmitted along with an additional file specifying where secondary structure such as which residues make up α -helices, β -sheets, and coils.

The I-TASSER tool works by firstly retrieving template proteins with similar folds from the PDB database using an approach called LOMETS (locally installed meta-threading approach). Secondly, the template proteins identified in the first step are reconstructed into full-length

models using replica-exchange Monte Carlo simulations. Regions that have still not been aligned to any template sequence at this stage are built using ab initio modelling. A tool called SPICKER is then used to calculate the low free-energy states of these models. In the third stage, the models generated in the second step are put through the same replica-exchange Monte Carlo simulations from the first step however using the information previously gathered in steps one and two, the process is refined. These models are then clustered, and the lowest energy structures (the best) are then selected. Finally, a tool called REMO builds full 3D atomic models from the refined structures by optimizing the hydrogen bonding network. The final result is a 3D model that can then be cross references against existing experimentally generated protein models in order to predict ligand binding sites and functions of the protein.

I-TASSER modelling of amino acid sequences corresponding to Sod1^{WT}, Sod1^{A4V}, Sod1^{G37R}, Sod1^{H48Q} resulted in slight differences in the secondary structures predicted to be present. For comparison, the Sod1^{WT} amino acid sequence was submitted with a supplementary file supplying secondary structure information for I-TASSER to use. This is called Sod1^{WTact}. The predicted secondary structures along with the protein disorder level are shown in Figure 6.2. As shown in Sod1^{WTact}, the Sod1 protein in *S. cerevisiae* has been shown experimentally to have nine β -sheet structures and two α -helices. I-TASSER modelling of the Sod1^{WT} amino acid sequence predicted the 9 β -sheets correctly, but only predicted one α -helix. For Sod1^{A4V}, Sod1^{G37R} and Sod1^{H48Q} there are nine β -sheets correctly predicted, however the I-TASSER model failed to predict any α -helices at all (Figure 6.2). The protein disorder level as shown by the normalized B-factor did not appear to differ at all between any of the different sequences analysed (Figure 6.2)

The second output of the I-TASSER analysis was to predict the solvent accessibility from the protein sequence. Exposed residues are likely to be involved in some PTM or could be important for a function of the protein. In the I-TASSER analysis, each residue was given a predicted solvent accessibility value between one and nine, with nine being the most exposed and one being the most buried. As shown in Figure 6.3, the solvent accessibility does not differ much between any of the sequences analysed by I-TASSER. Sod1^{H48Q} shows some slight differences, however the solvent accessibility value never differed by more than one point.

The 3D atomic models generated by I-TASSER all show α -helices (pink) and β -sheets (yellow) (Figure 6.4). This result is in contrast with the secondary structure prediction shown in Figure 6.2 which does not predict any α -helix structures in any of the ALS-linked Sod1 isoforms.

Reassuringly the predicted functions of the final models predicted by I-TASSER S for Sod1 were as expected based on its known activities, such as sod activity, homo-dimerization activity, chaperone activity and Fe/Zn ion binding (Table 6.1). However, the less well-defined role as an

interactor with protein phosphatase 2B (calcineurin) was also detected for Sod1 and the mutant isoforms tested. Although loss of *SOD1* has been shown to affect calcineurin activity, an interaction in yeast has not been investigated to date and may be important in understanding both cellular roles of Sod1 and the dysfunction associated with ALS linked mutants.

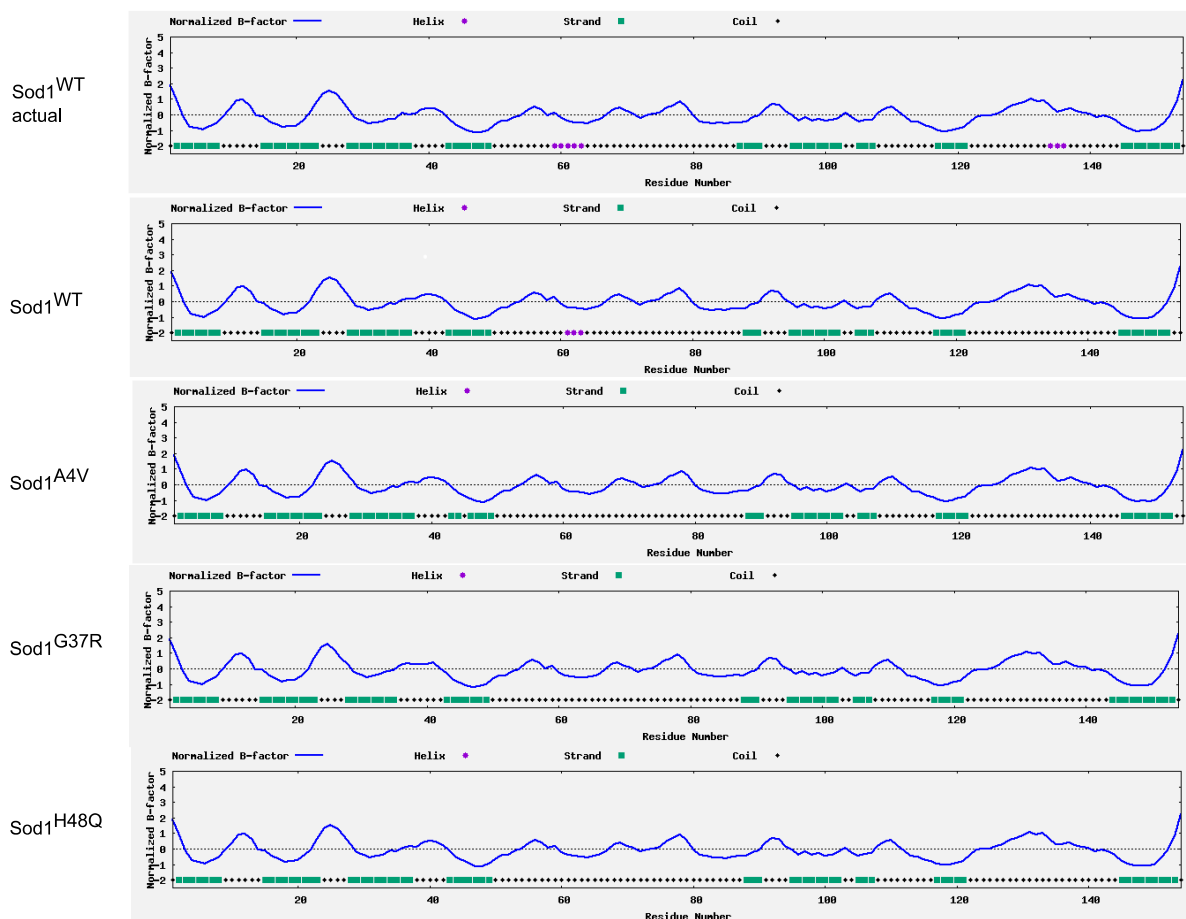


Figure 6.2 I-TASSER modelling predicted secondary structures and disorder level.

Displays the secondary structures and protein disorder level predicted by the I-TASSER modelling. β -strands are represented by turquoise squares, α -helices are represented by purple circles and coils are shown with black circles. The normalized B-factor is a prediction of the disorder level of the protein, a positive value is indicative of a higher level of disorder and a negative value means more order.

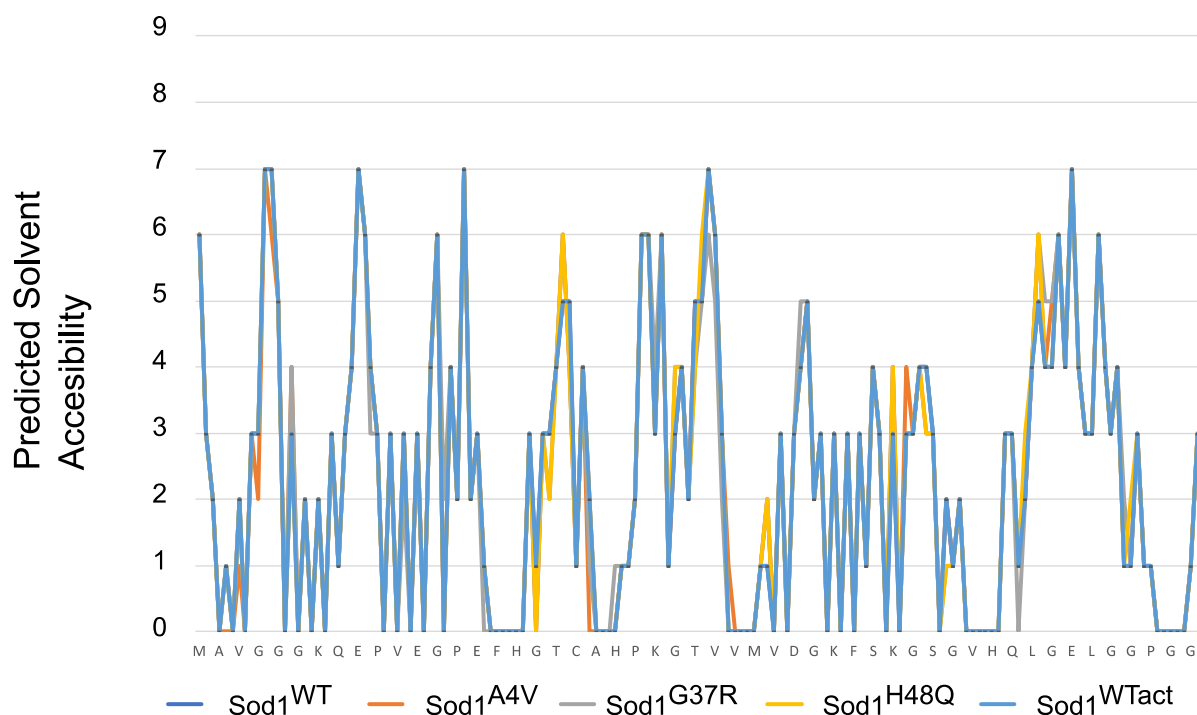


Figure 6.3 I-TASSER predicted solvent accessibility.

Predicted solvent accessibility as calculated in the I-TASSER modelling. Values closer to zero indicate a buried residue, whereas values closer to nine indicate an exposed residue.

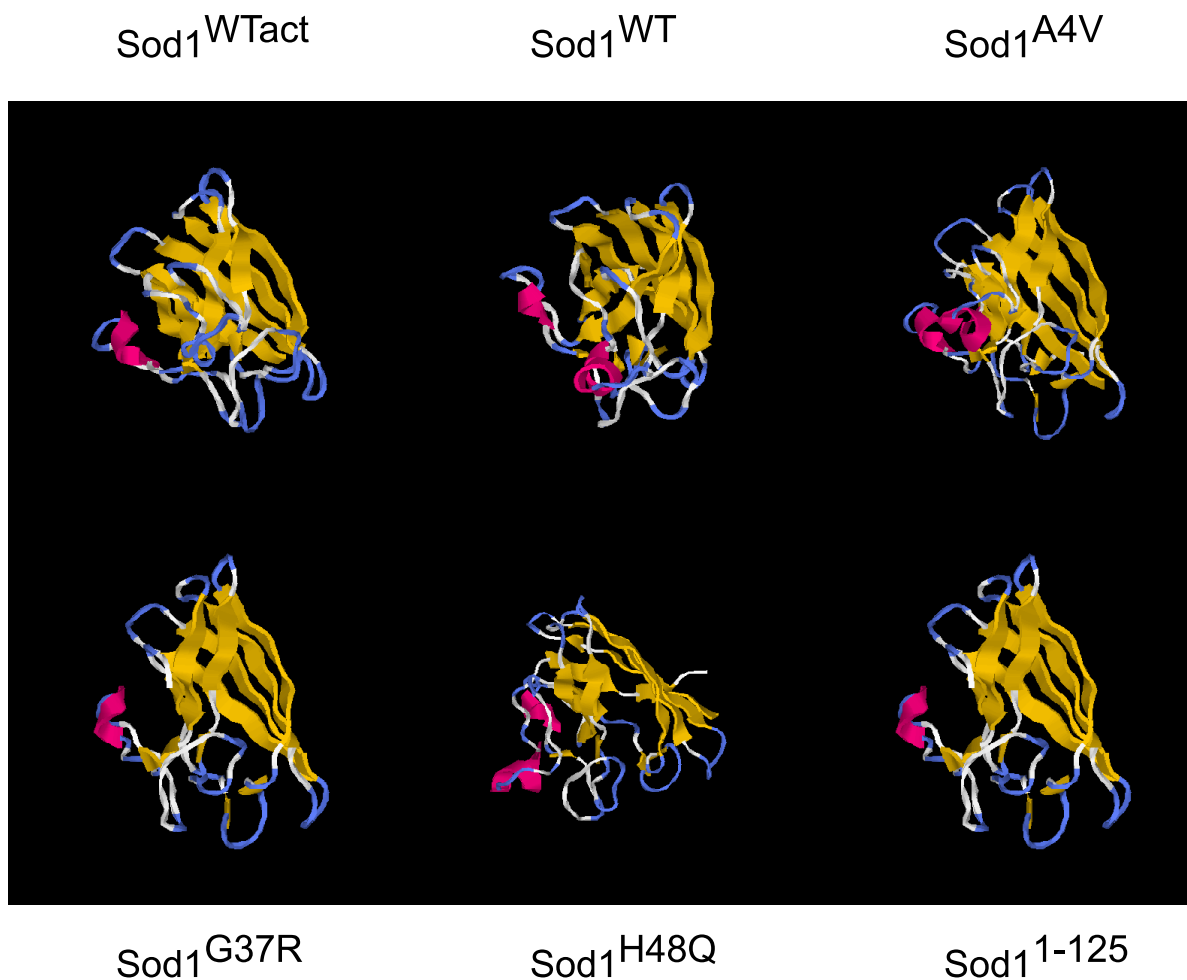


Figure 6.4 3D model predictions made by I-TASSER.

Images of the 3D models generated by I-TASSER based on the amino acid sequences submitted. B-sheets are coloured in yellow, and α -helices are coloured in pink.

Table 6.1 Consensus prediction of Go-Terms from I-TASSER modelling

Go-Terms	Process	Sod1 ^{WT} actual	Sod1 ^{WT}	Sod1 ^{A4V}	Sod1 ^{G37R}	Sod1 ^{H48Q}
GO:0004784	Superoxide dismutase activity	1	1	1	1	1
GO:0030346	Protein phosphatase 2B binding	0.95	0.99	0.99	0.95	0.99
GO:0051087	Chaperone binding	0.95	0.99	0.99	0.95	0.99
GO:0008270	Zinc ion binding	0.99	0.99	1	0.99	1
GO:0005507	Copper ion binding	0.99	0.99	1	0.99	1
GO:0042803	Protein homodimerization activity	0.95	0.95	0.99	0.99	0.99
GO:0004842	Ubiquitin-protein transferase activity	0.79	0.78	0.8	N/A	0.79

6.2.2 Investigating calcineurin / Sod1 and V-ATPase interactions in vivo

I-TASSER analysis of the Sod1 amino acid sequence suggested a putative interaction with the calcineurin complex in *S. cerevisiae*. To investigate this, we made use of a DHFR-PCA assay to screen for interaction between Sod1 and the three subunits of the calcineurin complex, Cnb1, Cna1 and Cmp2 respectively.

The following diploids were generated for the DHFR assay:

- 1) Cnb1^{bait} Cna1^{prey} and Cnb1^{bait} Cmp2^{prey} as a positive controls, as the subunits of the calcineurin complex should be in close enough proximity to reconstitute the MTX resistant DHFR fragments.
- 2) Sod1^{bait} Cnb1^{prey}, Sod1^{bait} Cna1^{prey} and Sod1^{bait} Cmp2^{prey}.

As shown in Figure 6.5 A) and B), the positive control diploids Cnb1^{bait} Cmp2^{prey} and Cnb1^{bait} Cna1^{prey} were both able to grow in SC media supplemented with 200 μ g/ml methotrexate, indicating that the DHFR fragments are within close proximity to one another. Furthermore, the Sod1^{bait} Cnb1^{prey}, Sod1^{bait} Cna1^{prey} and Sod1^{bait} Cmp2^{prey} diploids were all able to grow in SC media supplemented with 200 μ g/ml MTX as seen in Figure 6.5 C), D) and E) respectively. This indicates that Sod1 was in close enough proximity to Cnb1, Cna1 and Cmp2 to allow for reconstitution of the DHFR fragments, resulting in resistance to MTX. This suggests that Sod1

may interact with the calcineurin complex in *S. cerevisiae* cells. The relative growth of all the diploids tested were significantly higher than that of the negative control BY4743 (Figure 6.5 F)).

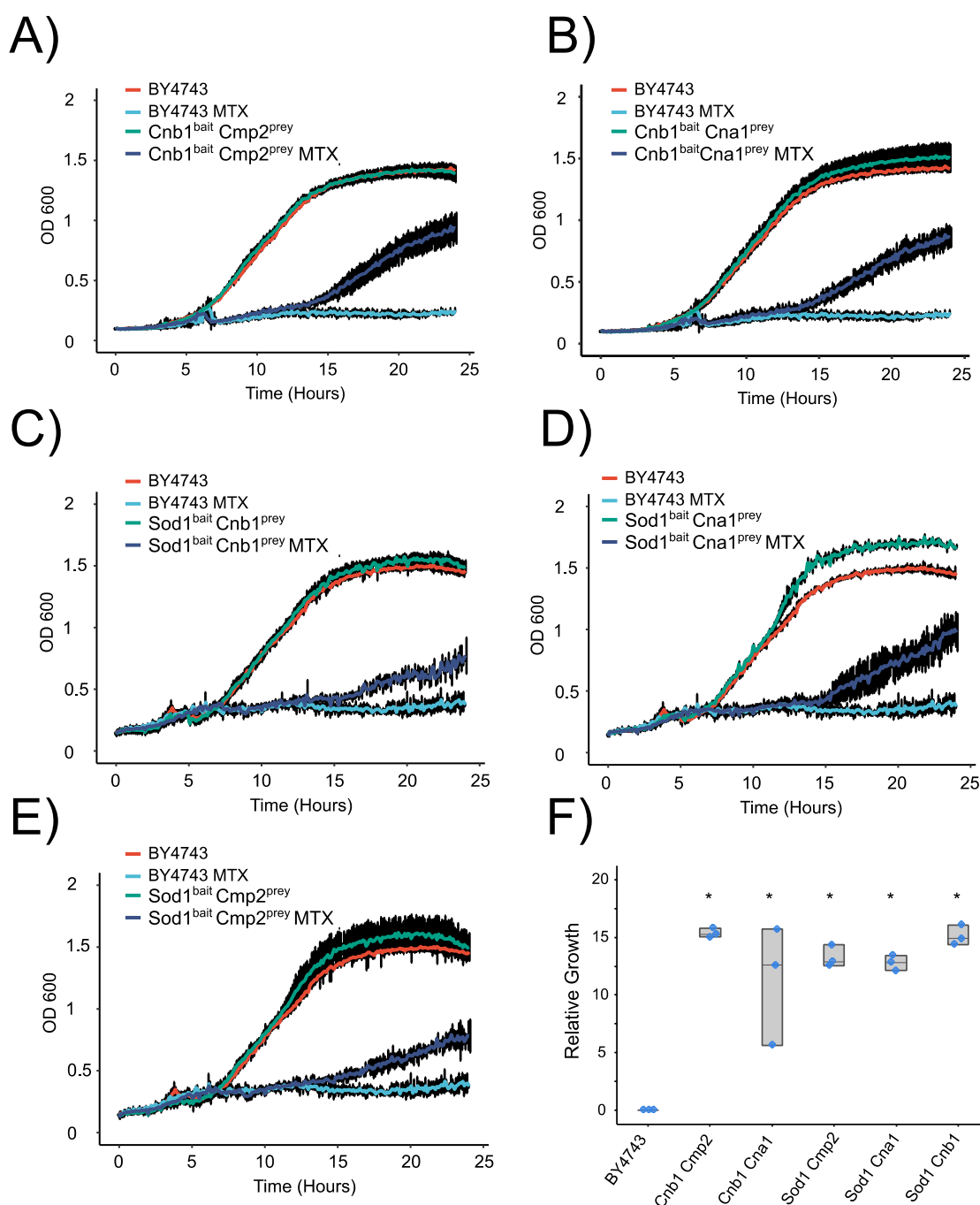


Figure 6.5 DHFR PCA assay of Sod1 and Calcineurin.

A) Line graph of DHFR assay of *Cnb1^{bait} Cmp2^{prey}* diploid in SC media and SC media with 200 μ g/ml MTX. B) Displays a line graph of the *Cnb1^{bait} Cna1^{prey}* diploid grown in SC media and SC media with 200 μ g/ml MTX. C) Displays for a line graph of the *Sod1^{bait} Cnb1^{prey}* diploid grown in SC media and SC media with 200 μ g/ml MTX. D) Displays the line graph of the *Sod1^{bait} Cna1^{prey}* diploid grown in 200 μ g/ml MTX. E) Displays the same as in A) but for the *Sod1^{bait} Cmp2^{prey}* diploid. For A) to E) error bars represent the standard deviation between three technical replicates. Line graph is a representative result of three biological repeats. MTX in the legend stands for MTX (200 μ g/ml). F) Displays

the relative growth calculation of the DHFR screen carried out between Sod1 and the various subunits of the calcineurin complex Cnb1, Cmp2 and Cna1. The boxplot represents the mean of three biological replicates. N = 3. One-Way ANOVA comparison between relative growth of the PCA diploid and the BY4743 control was used to test for statistical significance (* $p < 0.05$).

As an interaction between Sod1 and subunits Vma2, Vma4 and Vma8 of the V-ATPase had been identified (in Chapter 5) using the DHFR-PCA assay, it was decided to test whether the calcineurin complex interacts with those same subunits of the V-ATPase that were found to interact with Sod1. This was done by generating diploids with Cmp2^{bait} and Vma2^{prey}, Vma4^{prey} and Vma8^{prey}, Cnb1^{bait} Vma2^{prey}, Vma4^{prey} and Vma8^{prey}, and Cna1^{bait} and Vma2^{prey}, Vma4^{prey} and Vma8^{prey}. The relative growth calculations of the DHFR assays between these diploids can be seen in Figure 6.6. Out of all the above-mentioned diploids tested, four showed a significantly increased relative growth compared to the negative control. These were Cna1^{bait} Vma2^{prey}, Cnb1^{bait} Vma4^{prey}, Cmp2^{bait} Vma4^{prey} and Cnb1^{bait} Vma8^{prey}. This result suggests that in *S. cerevisiae*, calcineurin may interact with the V-ATPase.

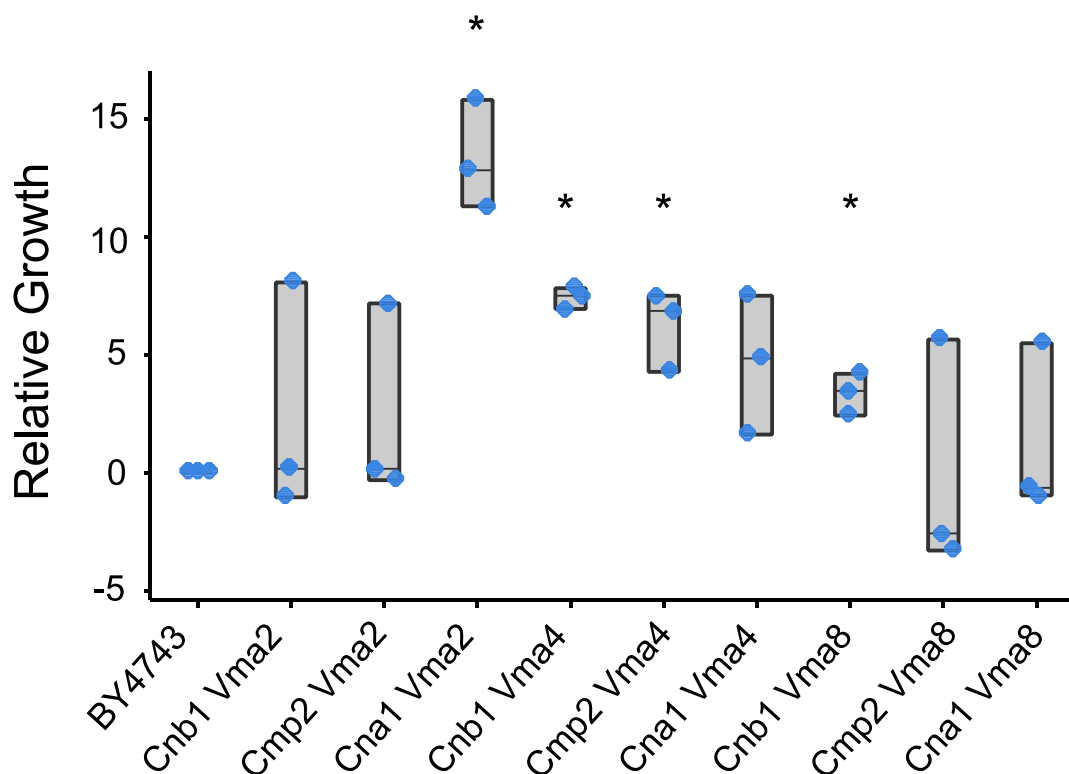


Figure 6.6 Relative growth calculation from DHFR screen between calcineurin and the V-ATPase.

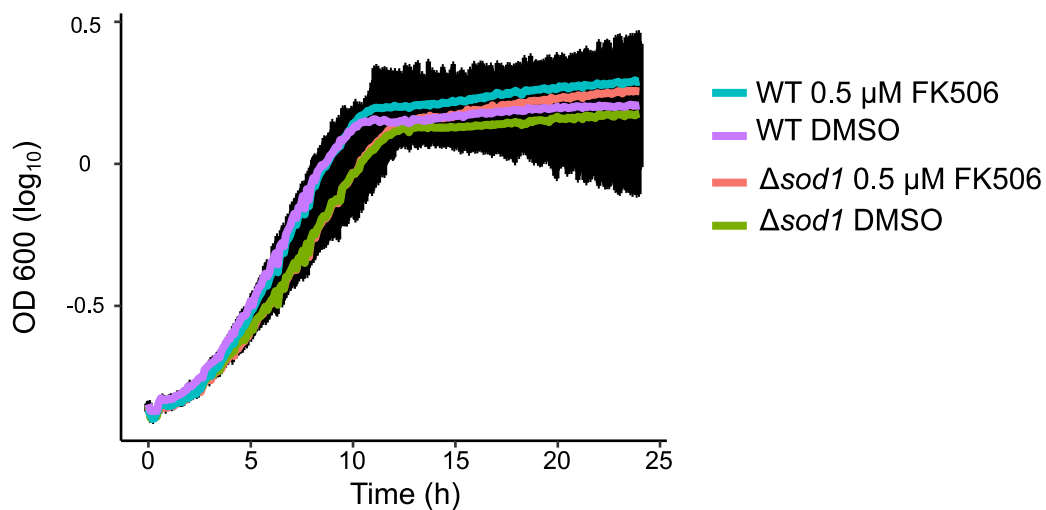
Boxplot displaying the relative growth calculations from the DHFR screen carried out between the calcineurin subunits Cnb1, Cmp2, Cna1 and the V-ATPase subunits identified in the interaction with Sod1, namely Vma2, Vma4 and Vma8. Each data point on the boxplot displays the relative growth value from one biological repeat. Significance (* $p < 0.05$ in a One-way ANOVA test) means that the relative growth of the diploid in question is significantly different compared to the BY4743 negative control. N = 3.

6.2.3 Sensitivity of WT and $\Delta sod1$ strains to calcineurin inhibition using FK506

After identifying the interaction between Sod1 and the calcineurin complex using the DHFR-PCA assay, we were interested in investigating the effect of pharmacological inhibition of calcineurin in cells that lack *SOD1*. To do this, the calcineurin inhibitor FK506 was used. Liquid growth curve assays were conducted in both WT and $\Delta sod1$ cells at 0.5 μM and 100 μM concentrations. These concentrations were chosen as 0.5 μM inhibits calcineurin activity (appendix Figure 8.4) completely as seen by flow cytometry analysis of a transcriptional calcineurin activity reporter [147], and 100 μM exhibited the strongest effect on growth on WT cells after different concentrations of FK506 were tested (0.5 μM , 10 μM , 50 μM , 100 μM). In Figure 6.7 A) and C), the effects of 0.5 μM FK506 can be observed. In WT cells, the treatment of 0.5 μM FK506 led to a significant increase in the AUC value, as cell number continued to increase gradually in stationary phase compared to the DMSO control. The same continued growth in stationary can be observed in $\Delta sod1$ cells treated with 0.5 μM FK506 although the AUC value was not significantly different to the DMSO control. WT cells treated with 0.5 μM FK506 grew significantly better than $\Delta sod1$ cells treated with the same concentration.

$\Delta sod1$ cells treated with 100 μM FK506 grew significantly worse than the DMSO control, whereas WT cells did not. Treatment with 100 μM FK506 exacerbated the mild growth defect of $\Delta sod1$ cells compared to WT (Figure 6.7 B) and D) (Figure 6.8).

A)



B)

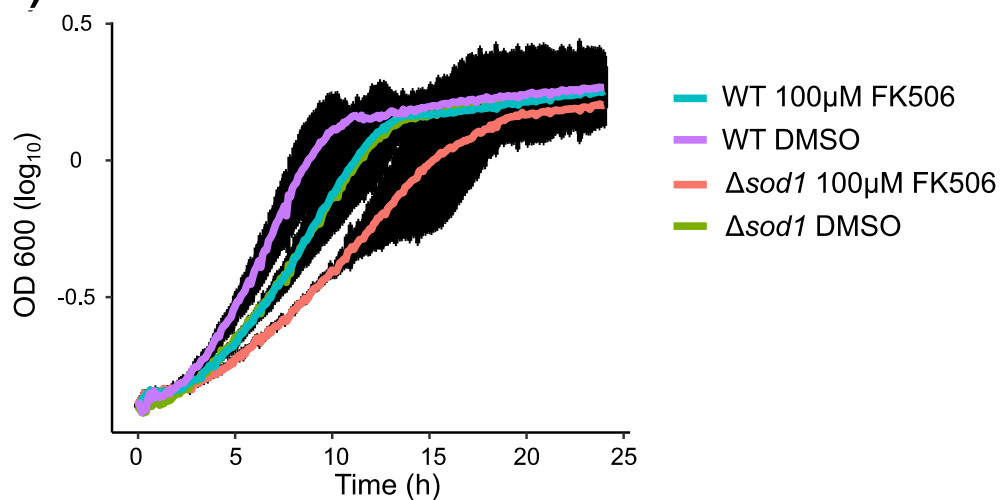


Figure 6.7 Growth curves of WT and $\Delta sod1$ cells in presence of FK506, a calcineurin inhibitor.

A) Growth curve of WT and $\Delta sod1$ cells grown in SC media containing either 0.5 μM FK506 or a DMSO control. B) Growth curve of WT and $\Delta sod1$ cells grown in SC media containing either 100 μM FK506 or a DMSO control. Error bars show the standard deviation between three biological replicates. N = 3.

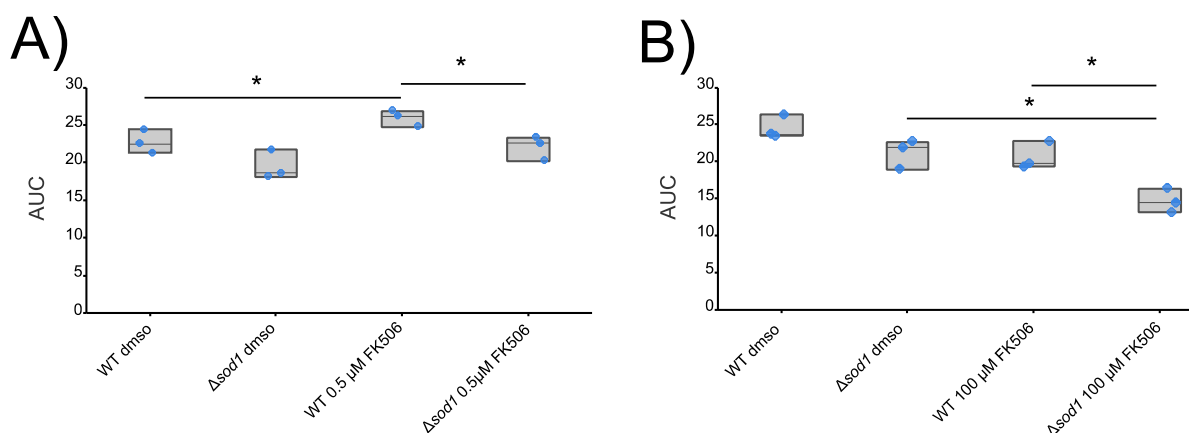


Figure 6.8 AUC calculation from the growth curve of WT and $\Delta sod1$ FK506 experiment.

A) and B) AUC calculated from the growth curves of WT and $\Delta sod1$ cells treated with 0.5 μ M FK506 Figure 6.7 A) and 100 μ M FK506 Figure 6.7 B). In all boxplots, each data point represents a biological replicate. Significant differences between two conditions (* $p < 0.05$) as calculated by a One-Way ANOVA comparison. N = 3.

6.2.4 Measurement of calcineurin activity by flow cytometry in response to $CaCl_2^{2+}$ treatment in WT and $\Delta sod1$ cells.

As a possible interaction between Sod1 and Cnb1, Cna1 and Cmp2 of the calcineurin complex had been identified by using the DHFR-PCA assay, we decided to investigate whether the deletion of *SOD1* had any effect on calcineurin activity.

To measure calcineurin activity a transcriptional GFP reporter plasmid was employed [147]. This reporter comprises of GFP, C-terminally linked to a 4-fold repeat of the calcineurin-dependant response element (CDRE). CDRE is a calcineurin-dependent DNA response element that is bound to by Crz1 after Crz1 has been dephosphorylated by calcineurin. In this calcineurin activity reporter system, activation of calcineurin, leads to the dephosphorylation of Crz1 which then binds to 4 \times -CDRE which drives expression of the GFP reporter. Using this reporter, calcineurin activity can be measured in live *S. cerevisiae* cells by flow cytometry.

The process for measuring calcineurin activity by flow cytometry using the 4 \times -CDRE-GFP reporter can be seen in Figure 6.9 A), B) and C). As discussed in depth in the introduction (6.1.1), the phosphatase activity of calcineurin is activated by calmodulin in a Ca^{2+} dependant manner. Treatment of the cells with 50 mM $CaCl_2^{2+}$ 1 h prior to measurement resulted in a 10-fold increase in calcineurin activity compared to the negative control (Figure 6.9 D)). The overlay plot shows the FITC-A value (log scale) of WT cells grown to mid-log phase, either treated with Ca^{2+} for 1 h prior to measurement or untreated. FITC-A described the GFP fluorescence detected via the FL1 detector which filters at 530/30 nm. The addition of Ca^{2+} shifted the peak of FITC-A from between 10^2 and 10^3 to 10^4 indicating a large increase in fluorescence intensity of the 4 \times -CDRE-GFP reporter in response to calcium. The population of cells to be measured

was gated as described in Figure 6.9 A), B) and C). Initially cells were gated by size, and then further gated to select the 'singlet' population and avoid any 'doublets' or clumps of cells. Using this method, the activity of calcineurin in response to Ca^{2+} treatment was measured in WT and Δsod1 cells grown to mid-log phase. Without Ca^{2+} addition both WT and Δsod1 showed similar levels of median FITC of ~ 1000 units. However, upon addition of Ca^{2+} 1 h prior to measurement, the median FITC value of WT was significantly higher at 15520 units than that of Δsod1 at 5207 units. This suggests that calcineurin activity in response to Ca^{2+} is reduced in cells lacking *SOD1*. The fold change increase in calcineurin activity in response to calcium treatment was 15 for WT and 5 for Δsod1 (Figure 6.9 F)).

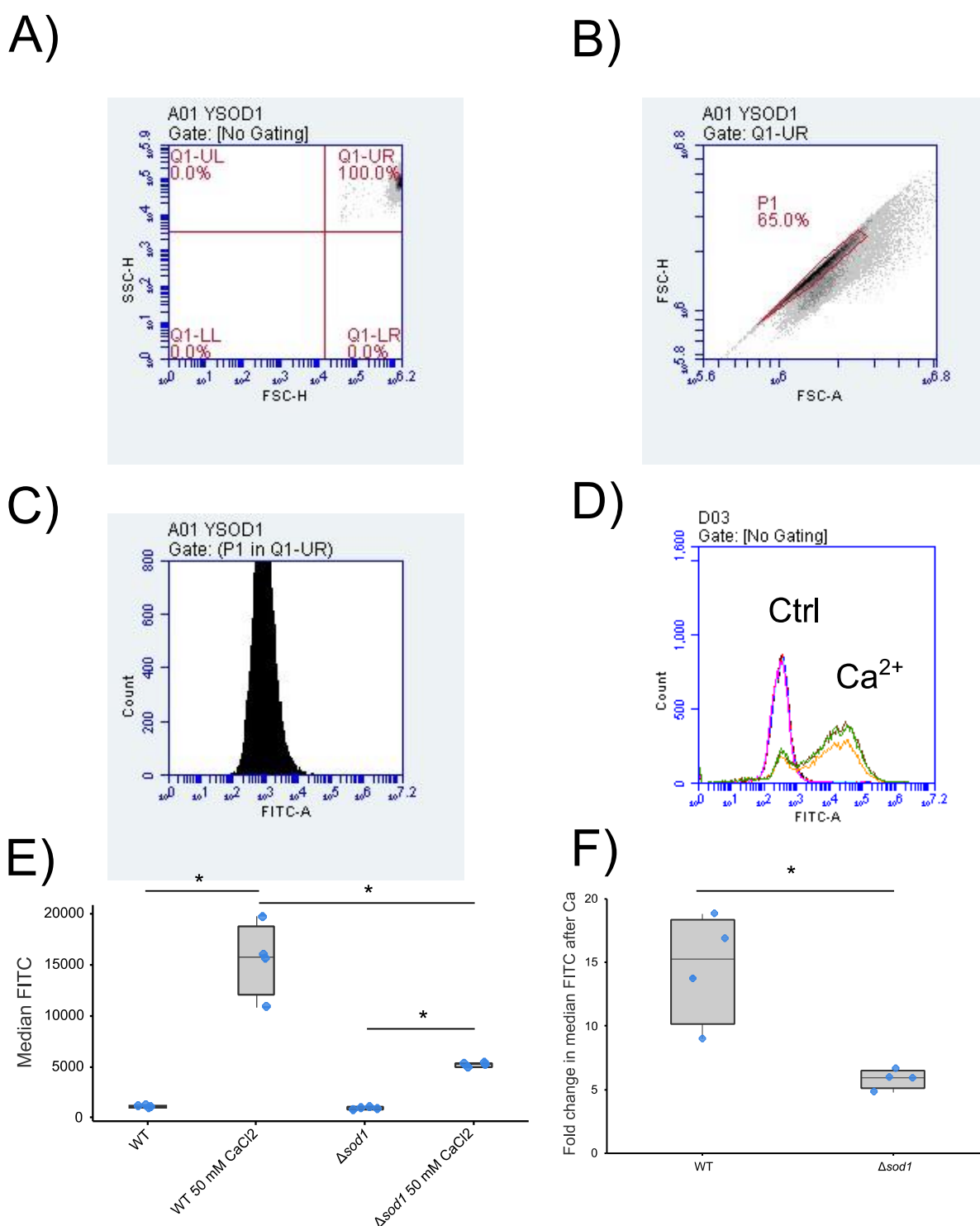


Figure 6.9 Flow cytometry of a transcriptional reporter for calcineurin activity of WT and $\Delta sod1$ cells before and after $CaCl_2^{2+}$ treatment.

A)–C) Displays the method of gating the cells for analysis of FITC fluorescence intensity by flow cytometry. A) has side-scatter height (SSC-H) on the y axis and forward-scatter height (FSC-H) on the x axis. Cells are in the upper right corner in the upper right quadrant. B) shows FSC-H on the y axis and forward-scatter area on the x axis (FSC-A). This plot allows to select ‘singlet’ cells, rather than ‘doublets’ or clumps of cells. C) shows the count of cells on the y axis and the FITC-A reading of the gated ‘singlet’ cells from the middle plot. D) Displays an overlay plot of the FITC-A value of WT cells treated with Ca^{2+} for 1 h prior to measurement or not. E) Quantification of the median FITC value from

WT and $\Delta sod1$ cells treated with Ca^{2+} prior to measurement. F) Shows the fold change in median FITC for both WT and $\Delta sod1$ cells before and after treatment with 50 mM $CaCl_2$ for 1 h. For both E) and F) Each dot represents a biological replicate. Statistically significant differences are calculated from One-way ANOVA comparison (* $p < 0.05$). N = 3.

6.2.5 Measurement of calcineurin activity by flow cytometry in response to $CaCl_2^{2+}$ treatment in WT and $\Delta ccs1$ cells.

As it was previously observed that the deletion of *SOD1* lead to a reduction in calcineurin activity upon addition of $CaCl_2^{2+}$ in *S. cerevisiae* cells, we were interested in whether the presence of inactive Sod1 would lead to the same phenotype as the $\Delta sod1$ mutant. To investigate this, the $\Delta ccs1$ mutant was used. *CCS1* encodes the copper chaperone for Sod1 in *S. cerevisiae* and is critical for the full metalation and maturation of the Sod1 enzyme [239]. $\Delta ccs1$ deletions in *S. cerevisiae* do not possess any fully mature active Sod1 protein and therefore usually share many phenotypes to the $\Delta sod1$ strain.

Measurement of calcineurin activity in WT, $\Delta sod1$ and $\Delta ccs1$ revealed that the basal calcineurin activity (without $CaCl_2^{2+}$ addition) was significantly higher in the $\Delta ccs1$ strain compared to that of the WT and $\Delta sod1$ mutant (Figure 6.10 A)). The fold change in calcineurin activity after $CaCl_2^{2+}$ treatment showed that the $\Delta ccs1$ deletion shares the same phenotype as the $\Delta sod1$ deletion. Both $\Delta ccs1$ and $\Delta sod1$ have a significantly reduced fold change in calcineurin activity in response to calcium compared to the WT (Figure 6.10 B)). Analysis of Sod1 activity showed that there was no Sod1 activity detected in the $\Delta ccs1$ strain but that there was still Sod1 protein present albeit less than the WT (Figure 6.10 C)).

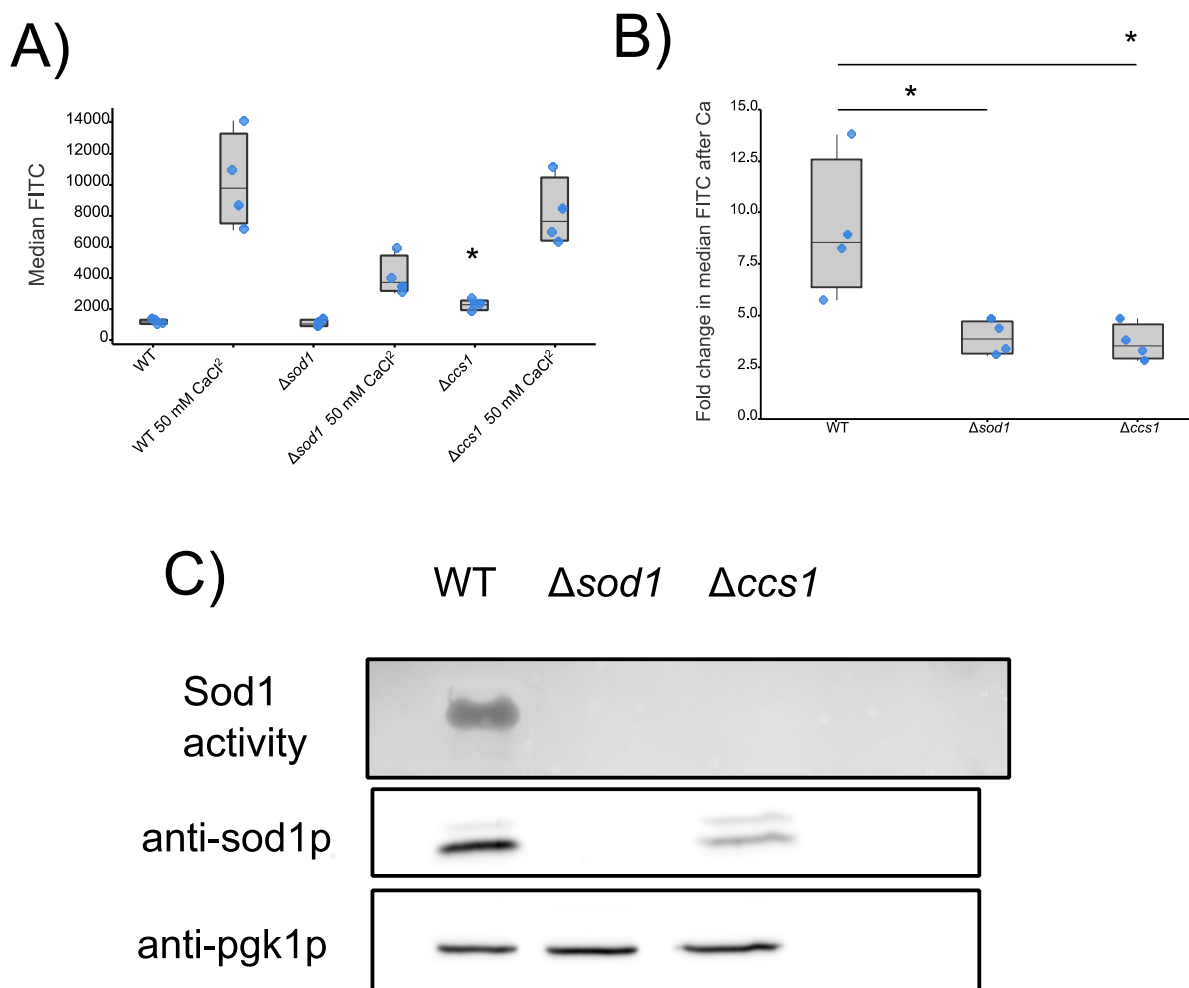


Figure 6.10 Effect of deletion of *CCS1* on calcineurin activity.

A) Median FITC quantification from flow cytometry of WT, $\Delta sod1$ and $\Delta ccs1$ with the 4 \times -CDRE-GFP reporter either with or without 1 h of 50 mM CaCl₂⁺ treatment. B) Fold change of median FITC after CaCl₂⁺ treatment. For both A) and B), statistically significant differences are calculated from a One-Way ANOVA comparison to the WT control condition (* $p < 0.05$). N = 3. C) Sod activity assay of WT, $\Delta sod1$ and $\Delta ccs1$ cells used in A). Western blotting of Sod1 and Pgk1 were included.

6.2.6 Further investigation of effects of Sod1 on calcineurin activity

As an interaction between Sod1 and Cna1, Cnb1 and Cmp2 had been identified using the DHFR-PCA assay, and the calcineurin activity in response to Ca²⁺ in $\Delta sod1$ and $\Delta ccs1$ cells had been observed to be significantly lower than in WT cells, we decided to test the calcineurin activity in other deletions of genes that encode proteins that interact with Sod1 in *S. cerevisiae* to see if any of them show the same phenotype as the $\Delta sod1$ strain.

In the previous chapter, an interaction between Sod1 and the V-ATPase had been identified also using the DHFR-PCA assay. As calcineurin plays an important role in calcium transport at the vacuole membrane (discussed in the introduction), regulating the function of the Ca²⁺-ATPase, Pmc1. Furthermore, deletion of *CNB1* along with *VMA2* or *VMA4* has been shown to result in

a synthetic lethality in *S. cerevisiae* [240]. Furthermore, we identified that the expression of Sod1^{A4V} in $\Delta pmc1$ cells showed a synthetic growth defect. It was decided to measure the calcineurin activity in $\Delta vma2$ and $\Delta vma4$ with and without Ca²⁺ exposure. No significant difference was observed between the median FITC values from flow cytometry of WT, $\Delta vma2$ and $\Delta vma4$ strains containing the 4 \times -CDRE-GFP reporter. This suggests that there is no difference in the calcineurin activity upon deletion of *VMA2* or *VMA4*.

Similarly, it was decided to measure the calcineurin activity in $\Delta yck1$, $\Delta yck2$ and $\Delta akr1$. *YCK1* and *YCK2* encode the casein kinases that are important mediators in glucose signalling and are stabilised by Sod1 in *S. cerevisiae* [61]. As they share redundant functions with each other the $\Delta akr1$ mutant was used as it encodes a palmitoyl transferase called Akr1 which prevents the palmitoylation of both Yck1 and Yck2 rendering them unable to function correctly. Using $\Delta akr1$ essentially models a double deletion of *YCK1* and *YCK2* [241]. No significant difference was observed between the median FITC values from flow cytometry of WT, $\Delta yck1$, $\Delta yck2$ and $\Delta akr1$ strains containing the 4xCDRE-GFP reporter. This suggest that there is no difference in the calcineurin activity upon deletion of *YCK1*, *YCK2* and *AKR1*.

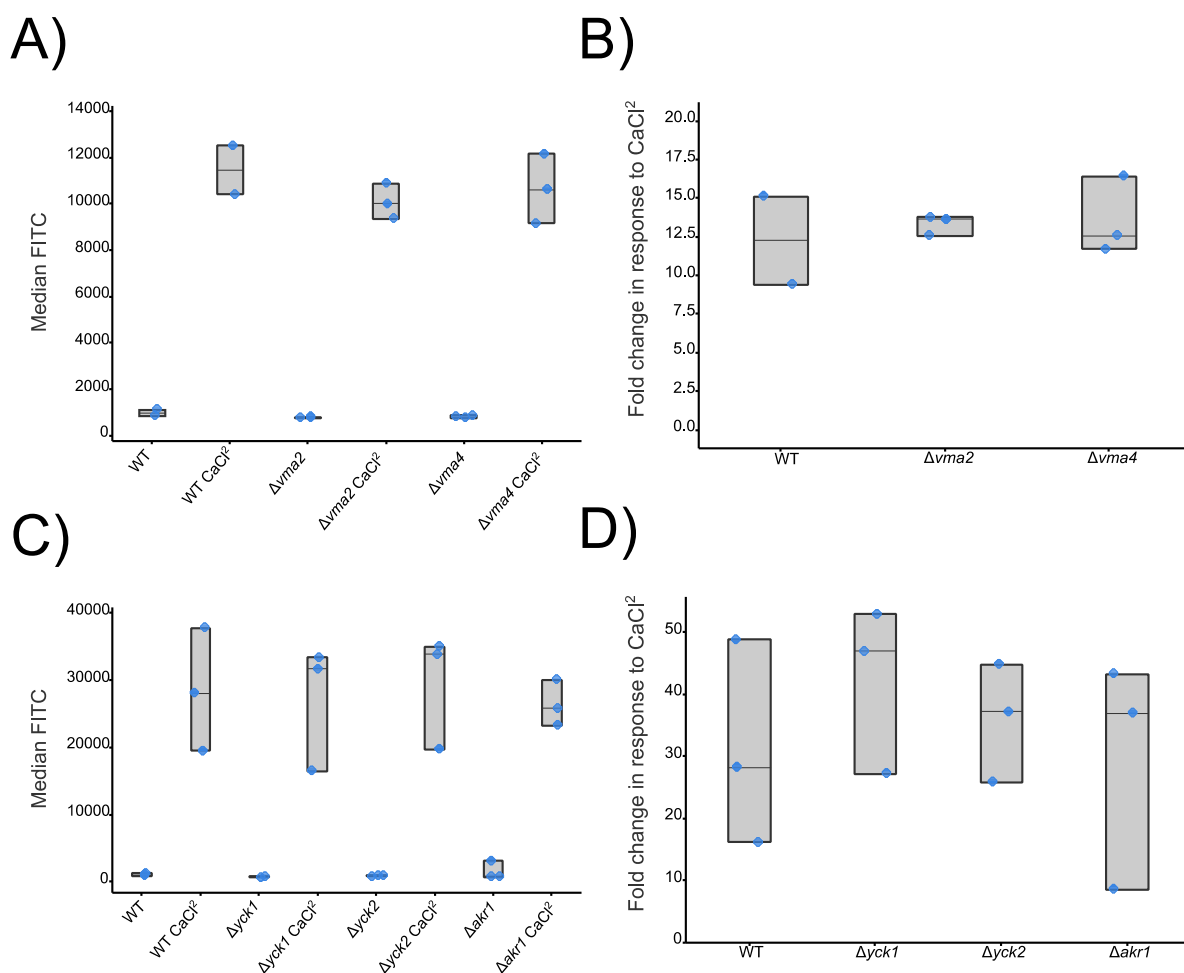


Figure 6.11 Calcineurin activity of V-ATPase deletions and casein kinase deletions

A) Quantification of the median FITC value from flow cytometry of WT, $\Delta vma2$, and $\Delta vma4$ cells containing the 4 \times -CDRE-GFP reporter treated with or without Ca²⁺ for 1 h. Each datapoint represents a biological replicate. B) Shows the fold change in calcineurin activity before and after CaCl²⁺ treatment. C) Shows the median FITC values from flow cytometry of WT, $\Delta yck1$, $\Delta yck2$ and $\Delta akr1$ cells expressing a transcriptional reporter for calcineurin activity before and after CaCl²⁺ treatment. D) Shows the fold change in calcineurin activity after CaCl²⁺ treatment in WT, $\Delta yck1$, $\Delta yck2$ and $\Delta akr1$ cells. N = 3 for all A) – D).

6.2.7 Effect of overexpression of ALS-linked mutant isoforms of SOD1 on calcineurin activity

So far, an interaction between Sod1 and calcineurin had been identified by the DHFR-PCA assay, and reduced calcineurin activity had been observed in $\Delta sod1$, and $\Delta yck1$ cells. A role of calcineurin and calcium homeostasis in the pathogenicity of ALS has been reported [242]. ALS-linked mutant isoforms of Sod1 have been shown to also interact with calcineurin, but to destabilise the complex leading to reduced calcineurin activity [237].

To investigate whether ALS-linked mutations in *SOD1* affect calcineurin activity in *S. cerevisiae*, different mutant isoforms of Sod1 were expressed in both WT and $\Delta sod1$ backgrounds and the calcineurin activity was measured by flow cytometry using the 4 \times -CDRE-GFP reporter.

Overexpression of Sod1^{A4V} and Sod1^{G37R} in the $\Delta sod1$ background from a 2 μ plasmid showed a significant decrease in the fold change in median FITC value in response to calcium treatment between $\Delta sod1$ cells that express Sod1^{A4V} and Sod1^{G37R} compared to cells that express Sod1^{WT}, indicating that calcineurin activity in response to Ca²⁺ treatment is reduced (Figure 6.12 A) and B)).

It has previously been reported that products of misfolded unstable ALS-linked Sod1 isoforms that have been broken down in the cell can cause cytotoxicity. This has been shown previously in a chick spinal cord model where expression of truncated forms of the Sod1 protein exerted cytotoxic effects [243]. Additionally, in the yeast overexpression model of *SOD1*-ALS it was observed that expression of truncated fragments of Sod1 caused cytotoxicity in the $\Delta sod1$ background, despite the fragments possessing no sod activity [115]. To investigate whether truncated fragments of yeast Sod1 caused any effect on calcineurin activity, truncated Sod1 products of 115 and 125 amino acids were expressed into WT and $\Delta sod1$ cells expressing the 4 \times -CDRE-GFP reporter. The fragment size of 115, and 125 of the truncated Sod1 protein was selected as these were the fragment sizes that were previously shown to cause cytotoxic effects when overexpressed into cells lacking *SOD1*[115].

Overexpression of fragments of Sod1, Sod1¹⁻¹¹⁵ and Sod1¹⁻¹²⁵ in the $\Delta sod1$ background also exhibited a significant decrease in fold change in median FITC in response to calcium treatment compared to the Sod1^{WT} control (Figure 6.12 C) and D).

Overexpression of Sod1^{A4V} and Sod1^{G37R}, Sod1¹⁻¹¹⁵ and Sod1¹⁻¹²⁵ in a WT background did not show a significant increase in fold change in median FITC after calcium treatment compared to WT empty vector control (Figure 6.13 B)).

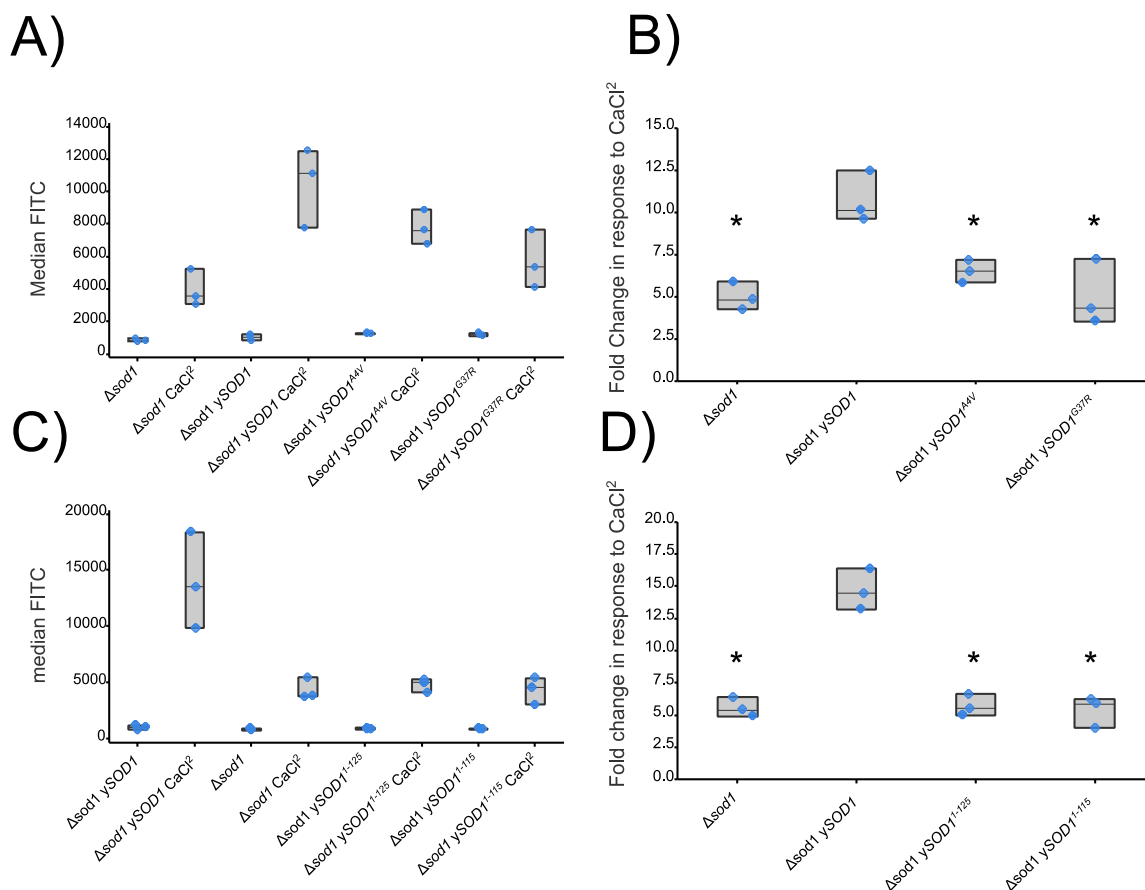
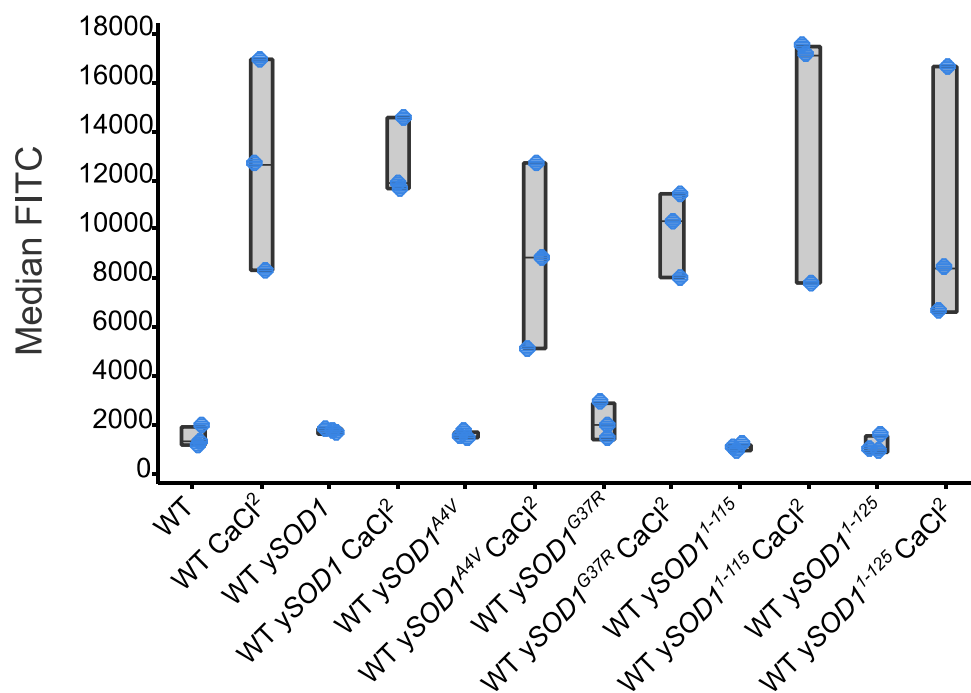


Figure 6.12 Effect of expression of ALS-linked mutant isoforms and fragments of *SOD1* into a $\Delta sod1$ background on calcineurin activity.

A) Quantification of median FITC from flow cytometry of $\Delta sod1$ cells overexpressing mutant Sod1 isoforms Sod1^{A4V} and Sod1^{G37R} from a 2 μ plasmid before and after 1 h treatment with 50 mM CaCl₂⁺. Each datapoint represents a biological repeat. B) Shows the fold change in median FITC after exposure to CaCl₂⁺. Strains that have a significantly different (* $p < 0.05$) median FITC value to the $\Delta sod1$ Sod1^{WT} strain as per a One-Way ANOVA comparison are denoted with *. C) Quantification of median FITC value from flow cytometry of $\Delta sod1$ cells overexpressing the fragments of Sod1, Sod1¹⁻¹¹⁵ and Sod1¹⁻¹²⁵ from a 2 μ plasmid before and after treatment with CaCl₂⁺. Each datapoint represents a biological repeat. D) Shows the fold change in median FITC after exposure to CaCl₂⁺. Statistically significant differences (* $p < 0.05$) were calculated as per a One-Way ANOVA comparison. N = 3 for all A) – D).

A)



B)

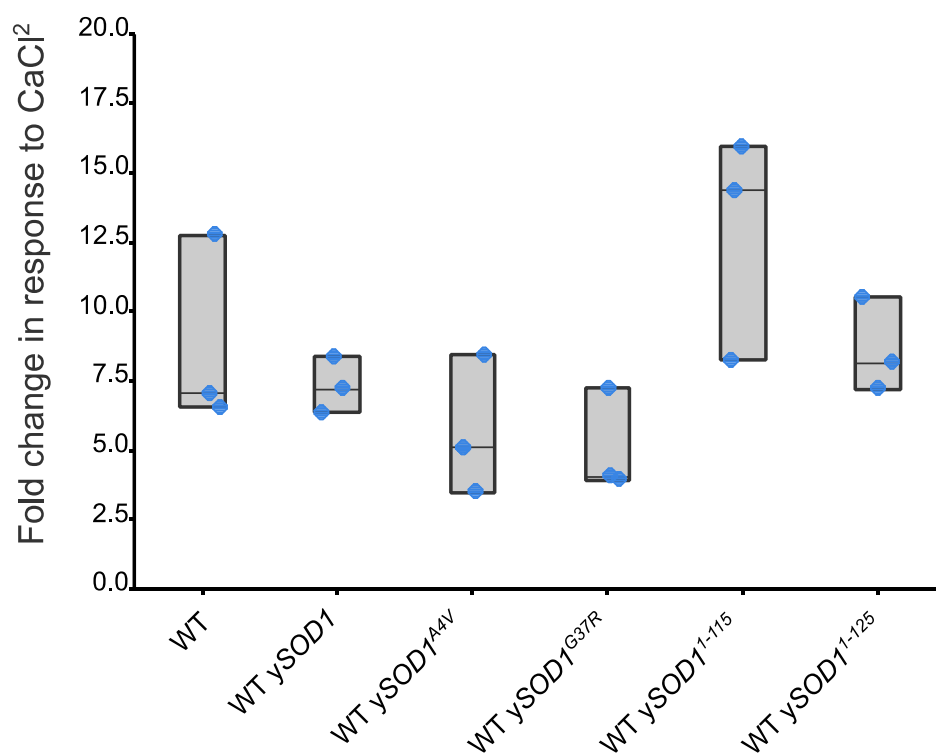


Figure 6.13 Effect of overexpression of various Sod1 isoforms in a WT background on calcineurin activity.

A) Median FITC values from flow cytometry of a transcriptional reporter for calcineurin activity. ALS linked mutant isoforms of Sod1, Sod1^{A4V} and Sod1^{G37R} along with fragments

of Sod1, Sod1¹⁻¹¹⁵ and Sod1¹⁻¹²⁵ were overexpressed in WT cells. Calcineurin activity was measured in cells treated with or without 50 mM CaCl²⁺ for 1 h. Each datapoint represents a biological replicate. B) Fold change in median FITC value after exposure to CaCl²⁺. Each datapoint represents a biological replicate. Statistically significant differences were calculated with a One-Way-ANOVA comparison (* $p < 0.05$). N = 3.

6.3 Discussion

6.3.1 SOD1 interaction with Calcineurin

The aim in this chapter was to explore the interaction between Sod1 and calcineurin in yeast. I-TASSER modelling predicted calcineurin binding in all the isoforms of Sod1 tested. Additionally, the Sod1 interaction with calcineurin has been reported in other organisms.

The results from DHFR-PCA assays in this study suggest that Sod1 interacts with all three subunits of the calcineurin complex in *S. cerevisiae*. An interaction between Sod1 and calcineurin is supported by previous literature in which Sod1 was found to co-purify with calcineurin and act as a protective factor towards its activity in rat brain homogenates [238]. Results from this study also suggest that calcineurin interacts with the V₁ domain of the V-ATPase, similarly to Sod1. No interaction between calcineurin and the V-ATPase has been reported previously, although a genetic interaction has been observed whereby deletion of one of the single copy subunits of the V-ATPase in combination with the Cnb1 subunit of calcineurin causes a synthetic lethality [244].

6.3.2 Effect of Sod1 and ALS-linked Sod1 mutants on calcineurin activity

We aimed to test whether the loss of *SOD1* had any effect on calcineurin activity in *S. cerevisiae* and whether the expression of ALS-linked Sod1 mutants had any effect on calcineurin activity. Flow cytometry results indicated that, in the absence of *SOD1*, calcineurin activation in response to intracellular Ca²⁺ increase is greatly diminished. This suggests that the presence of Sod1 is required for the full activation of calcineurin by calcium and calmodulin. This is supported by a previous study in which it was found that Sod1 co-purifies with calcineurin in rat brain homogenates, and acts as a protective factor [238].

In this study, the deletion of *CCS1* encoding Ccs1 the copper chaperone for Sod1 resulted in a similar failure for calcineurin to become activated in response to elevated levels of Ca²⁺. In $\Delta ccs1$ cells, an inactive form of Sod1 is expressed. This suggests that in *S. cerevisiae*, active Sod1 is required for calcineurin activation by calcium and calmodulin. A previous study demonstrated using a human N-terminal and rat C-terminal Sod1 chimera, which possessed very little sod activity, that its presence resulted in the activation of calcineurin. Therefore, even some Sod1 isoforms with little activity can activate calcineurin in some conditions [245]. In this study, $\Delta sod1$

cells overexpressing Sod1^{A4V}, Sod1^{G37R}, and Sod1^{H48Q}, all displayed reductions in calcineurin activation in response to increased intracellular Ca²⁺ compared to $\Delta sod1$ cells overexpressing Sod1^{WT}. In the WT background, no reduction in calcineurin activation was observed upon overexpression of ALS-linked Sod1 mutant isoforms. These results suggest that in *S. cerevisiae*, ALS-linked mutant isoforms of Sod1 have a reduced ability to enable the full activation of calcineurin by calcium and calmodulin, compared to Sod1^{WT}. Overexpression of Sod1^{A4V}, Sod1^{G37R}, and Sod1^{H48Q} in $\Delta sod1$ cells was previously demonstrated to produce unstable isoforms of Sod1 that possess no detectable sod activity in log-phase [115]. Overexpression of fragments of Sod1, Sod1¹⁻¹¹⁵ and Sod1¹⁻¹²⁵ did not rescue the low calcineurin activation in $\Delta sod1$ cells and had no effect in the WT background. It could be that the lack of sod activity of these ALS-linked Sod1 isoforms contributes to their inability to promote full calcineurin activation. In support of these findings, a study that compared ALS patients (sALS and fALS) with a healthy control group, observed that the lymphocytes of ALS patients possessed around half the calcineurin activity of that of the healthy control individuals [237]. Another study also reported a reduction in protection of calcineurin by ALS-linked Sod1 isoforms and it suggested that the reduction in protection correlated with disease severity in fALS patients with the corresponding mutation [246].

We also aimed to test whether other known, or potential interactors of Sod1, Yck1, Yck2, Vma2, Vma4, or Akr1 had any effect on calcineurin activity when deleted from *S. cerevisiae*. Deletion of the genes encoding for all of these proteins had no significant effect on calcineurin activity. This suggests that they are not downstream of Sod1 with regard to its function in relation to promoting the activity of calcineurin in response to calmodulin binding.

6.3.3 Inability of I-TASSER modelling to predict α -helix for Sod1 mutant isoforms

Predicted secondary structures (Figure 6.2) generated by I-TASSER modelling of amino acid sequences of ALS-linked mutant isoforms of Sod1 showed that the three mutant isoforms Sod1^{A4V}, Sod1^{G37R} and Sod1^{H48Q} did not have a predicted α -helix at residues 59–63 compared to the Sod1^{WT}. This could be due to differences in the overall structure of the protein caused by the three mutations tested. ALS-linked mutations in *SOD1* are associated with propensity for protein misfolding and aggregation [247]. The I-TASSER modelling was unable to predict the full secondary structure of the Sod1^{WT} sequence as it did not show the second α -helix normally located at residues 134–136. This α -helix is associated with proper zinc binding. Loss of α -helices

in the secondary structure of Sod1 is associated with an increase in destabilisation and propensity to aggregate according to molecular dynamics simulations [248].

No other differences were observed in the other outputs produced from the I-TASSER modelling. Predicted disorder level of the protein remained the same with all isoforms tested and solvent accessibility did not change either. 3D atomic models generated looked similar, and the consensus GO term functions predicted were the same with all of the isoforms. The lack of differences in the outputs can potentially be explained by the method in which I-TASSER carries out its analysis. As it compares the sequences provided to protein sequences in various databases, it will match all the isoforms to the same Sod1^{WT} structures found in the databases. Since the outputs are guided heavily by the structures that are matched to the sequences, it is normal that there won't be many differences in the final output.

In summary, I-TASSER modelling of Sod1^{WT}, Sod1^{A4V}, Sod1^{G37R} and Sod1^{H48Q} sequences revealed differences in the secondary structures predicted for each amino acid sequence which could be indicative of an increase in destabilisation of the protein. The results also suggest that Sod1 interacts with both of the A subunits and the B subunits of calcineurin in yeast using a DHFR-PCA assay. Furthermore, flow cytometry data suggests that calcineurin activity in response to Ca²⁺ is reduced in cells lacking a fully mature and active Sod1 enzyme. As discussed in the introduction, reduced calcineurin activity in yeast means that cells cannot respond to environmental stress via activation of the calcineurin dependant transcription factor Crz1 and they have a reduced ability to internalize Pma1 in response to loss of V-ATPase activity to regulate pH homeostasis (Figure 6.14). In the context of ALS, the consequence of loss of calcineurin signalling is a loss of Ca²⁺ homeostasis which leads to MN death via mitochondrial apoptotic pathways, ER stress leading to protein misfolding and aggregation and also reduced levels of the less toxic dephosphorylated form of TDP-43[249].

It could be that the accumulation of intracellular Ca²⁺ in yeast after exposure to stress could be an upstream signal for cellular death. Intracellular Ca²⁺ accumulation in mammalian cells is thought to be an important upstream signal for death receptor-independent necroptotic death involving the phosphorylation of RIPK1 (receptor-interacting Ser/Thr protein kinase 1) by Ca²⁺/Calmodulin. The homologue of RIPK1 in yeast is RIP [250]. Another way in which high cytosolic Ca²⁺ can cause cell death is by increasing the levels of Ca²⁺ in the mitochondria. Increased mitochondrial Ca²⁺ leads to production of ROS in the mitochondria and the opening of mitochondrial proton pores (from multiple enzymes including the F-ATPases and VDAC

channels). The resulting mitochondrial dysfunction causes the phosphorylation of RIPK1 and MLKL which leads to necrosome formation and necroptotic cell death [251].

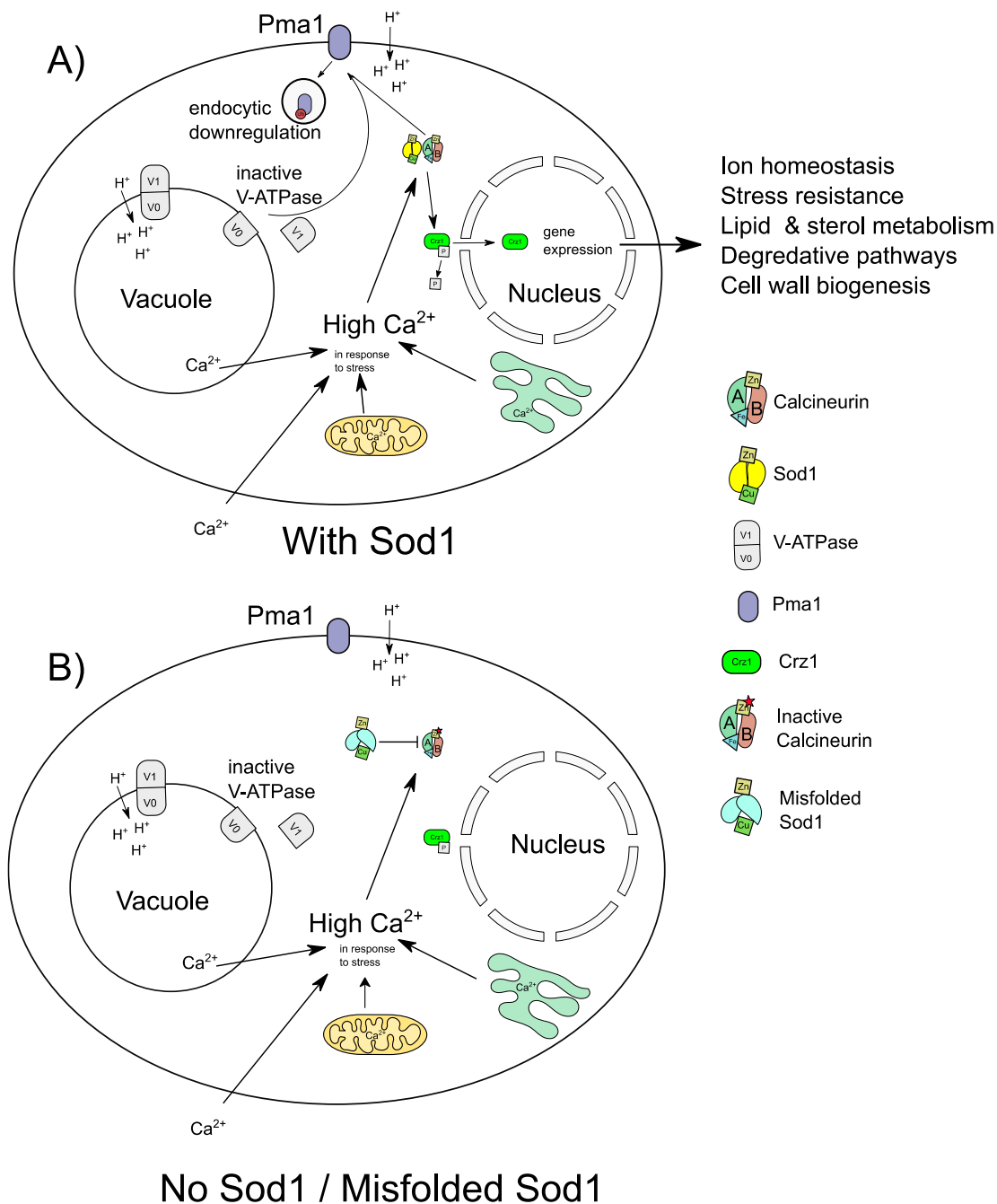


Figure 6.14 Visual model of the function of Calcineurin in *S. cerevisiae* and the effect of Sod1 on its function.

A) Calcineurin is activated by high levels of Ca^{2+} in the cell. As shown above, sources of Ca^{2+} in the cell are the vacuole, mitochondria, ER, and extra cellular environment. Through an unknown mechanism, intracellular Ca^{2+} levels rise in response to environmental stress. High intracellular Ca^{2+} along with calmodulin activates calcineurin. Activated calcineurin upregulates the expression of genes related to stress resistance through dephosphorylation of the transcription factor Crz1. In its phosphorylated form, Crz1 is localised in the cytoplasm, whereas upon dephosphorylation, Crz1 translocated to the nucleus and activated gene expression. Calcineurin also functions to maintain pH homeostasis if activity of the V-ATPase is compromised. Upon V-ATPase inhibition, the plasma membrane

bound P-ATPase Pma1 is ubiquitinated and endocytosed in order to reduce its activity. This process is dependent on active calcineurin. B) In cells that lack *SOD1*, or where Sod1 is misfolded, due to an ALS-linked mutation, calcineurin activity is much lower. This could be that the Fe/Zn centre of calcineurin is more vulnerable to redox regulation in the absence of active Sod1. Inactive calcineurin results in cells being unable to respond to the high Ca^{2+} upon onset of cell stress. Therefore, cells lacking active calcineurin cannot upregulate genes related to stress resistance via Crz1 or maintain pH homeostasis via endocytic downregulation of Pma1.

7 Final Discussion

7.1 Perspectives

The aim of this study was firstly to develop new models of *SOD1*-ALS in *S. cerevisiae* that expressed Sod1 at a lower level, similar to that of Sod1 under its endogenous promoter. This was achieved in two ways, firstly by adapting the overexpression plasmids previously used to model *SOD1*-ALS in *S. cerevisiae* [115] and secondly by using CRISPR/Cas9 gene editing to introduce ALS-linked mutations into the endogenous *SOD1* gene.

Secondly, the aim of this study was to investigate the findings previously observed in the overexpression model that indicated that overexpression of Sod1^{A4V} causes vacuole dysfunction in yeast. To do this, an interaction between Sod1 and the V-ATPase was explored. The third and final aim of the study was to investigate the interaction between Sod1 and calcineurin in *S. cerevisiae* and test whether ALS-linked Sod1 mutant isoforms affected calcineurin activity and if so how. Perspectives on the findings in this study and their overall relevance towards *S. cerevisiae* and ALS are discussed below.

7.2 Reduced expression of Sod1^{A4V} is not toxic to *S. cerevisiae* in a $\Delta sod1$ background.

7.2.1 Dose-dependent effects of mutant *SOD1*

In this study, two different stable single-copy models of *SOD1*-associated ALS were constructed and characterised. Firstly, a model involving the expression of various ALS-linked mutant *SOD1* alleles from a constitutive GPD promoter from an advanced gateway expression vector integrated into an empty region of chromosome I in the genome. This involved adapting the plasmids that had been previously used in the development of an overexpression based yeast model for *SOD1*-associated ALS [115]. The second model that was constructed involved the introduction of the Sod1^{A4V}, Sod1^{G37R}, and Sod1^{H48Q} mutations into the endogenous *SOD1* locus using CRISPR/Cas9 gene editing. Results from both models developed in this study suggest that when ALS-linked mutant isoforms of Sod1 are expressed in *S. cerevisiae* at levels similar to that of native Sod1, there is no overt cytotoxicity observed in the cells.

As previously mentioned, the level of expression of ALS-linked mutant Sod1 seems to correlate with the degree of toxicity observed in *SOD1*-ALS models across a range of different organisms. In a rat model of *SOD1*-ALS, it was observed that the copy number of SOD1^{G93A} was directly proportional to the severity of the disease [120]. Transgenic overexpression of SOD1^{A4V} into

zebrafish embryos produced induced abnormal MN axon branching and shortened axons in a dose-dependent manner [92].

It could be that the overexpression of ALS-linked mutant Sod1 isoforms, which are inherently prone to misfolding, overwhelms the protein quality control systems in the cell. There are two main protein quality control pathways in *S. cerevisiae*, the ubiquitin-proteasome system (UPS) and the autophagosome-vacuole pathways, both of which are highly evolutionarily conserved. The UPS involves the covalent attachment of the small protein ubiquitin to a misfolded protein, in a process called ubiquitylation. Ubiquitylation is a process that is understood to be comprised of three steps. Firstly, a ubiquitin protein is bound and activated by an E1 ubiquitin activating enzyme in an ATP-dependant manner. Secondly, ubiquitin is then transferred to an E2 ubiquitin conjugating enzyme. Thirdly, an E3 ubiquitin ligase specifically binds the target protein, and mediates the transfer of ubiquitin to a lysine residue on the target protein. Several round of ubiquitylation occur whereby another ubiquitin protein is covalently attached in the same way, to a lysine residue on the previous ubiquitin protein. This process produces long ubiquitin chains on the target protein (polyubiquitylation) which can target the protein for degradation at the 26S proteasome [252]. Sod1 has been demonstrated to be polyubiquitylated at Lys63 [253].

The autophagosome – vacuole degradation pathway involves the targeting of proteins to the vacuole for degradation by its hydrolytic enzymes. For example, the general amino acid permease (Gap1) is targeted to the vacuole in *S. cerevisiae* for degradation in nutrient rich conditions. Interestingly, the sorting of Gap1 to the vacuole for degradation occurs after its ubiquitylation at Lys9 and Lys16 [254]. Proteins can be sorted to the vacuole for degradation either by autophagy or the cytosol to vacuole targeting pathway (CVT).

It is possible that the overexpression of mutant isoforms of Sod1 that are inherently prone to misfolding into yeast could overwhelm the UPS pathway or the autophagosome-vacuole degradation pathways. This could explain the dose-dependent toxicity that is generally occurred when modelling *SOD1*-ALS in different organisms. A similar dose-dependent toxicity was observed in a PD model in *S. cerevisiae* where α -syn was expressed as one-copy, two copies or from a 2 μ vector. As in this study, expression of one-copy of two mutant isoforms of α -syn had no effect on growth, whereas two-copy expression completely inhibited growth. Expression from a 2 μ vector led to strong growth defects in yeast. This suggests that the expression levels of disease genes in *S. cerevisiae* can have significant effects on the phenotype observed.

In the future, to test whether protein quality control defects may cause defects in the *SOD1*-ALS integration model, Sod1^{A4V} could be expressed in *S. cerevisiae* strains lacking genes that are

essential for function of the UPS pathway or the autophagosome-vacuole degradation pathway. This would test whether genetic disruption of protein quality control pathways in *S. cerevisiae* could lead to cytotoxicity in the integrated *SOD1*-ALS model. Additionally, a model of *SOD1*-ALS could be constructed whereby the level of expression of *SOD1*^{A4V} is controlled by a titratable promoter. Thereby allowing to identify precisely at what expression level does *SOD1*^{A4V} become toxic to the cell.

7.2.2 Differences between expression of yeast *SOD1* and human *SOD1* into *S. cerevisiae*

In the human ALS condition, fALS-linked *SOD1* mutant alleles are usually present in one copy, along with one copy of native *SOD1*. It has been observed in multiple *SOD1*-ALS models that the presence of mutant Sod1 can encourage the misfolding and gain of toxic function, of native Sod1 [255][256]. In another *S. cerevisiae* model of *SOD1*-ALS, it was shown that the expression of WT human *SOD1* and human *SOD1*^{A4V} into $\Delta sod1$ cells formed toxic heterodimers of Sod1. These Sod1 heterodimers, comprising of WT human *SOD1* and *SOD1*^{A4V}, produced more deleterious effects on *S. cerevisiae* cells compared to cells designed to express *SOD1*^{A4V} homodimers. The results from that study showed that heterodimers containing WT and mutant Sod1 isoforms were more toxic to *S. cerevisiae* than homodimers of either Sod1^{WT} alone, or mutant Sod1 alone [257]. It has been proposed that Sod1^{WT} may slow down the aggregation of mutant Sod1. Aggregation of misfolded mutant Sod1 is thought to be a protective feature in the cell. Slowing down aggregation of mutant Sod1 could result in an increase in more harmful soluble misfolded species of Sod1.

In contrast, in this study, when yeast Sod1^{A4V} was expressed into *S. cerevisiae* cells that already had a copy of native Sod1, no toxic effects were observed, and the presence of native Sod1 actually rescued the sensitivity to menadione that was observed in $\Delta sod1$ cells expressing *SOD1*^{A4V}. The study mentioned above involved the expression of human *SOD1* into *S. cerevisiae*, whereas in the *SOD1*-ALS integration model developed in this study, yeast *SOD1* was expressed. We can conclude that in the *SOD1*-ALS integration model developed in this study, and the *SOD1*-ALS overexpression model previously developed, the expression of WT yeast Sod1, alongside Sod1^{A4V} has a protective effect and actually reduces the cytotoxicity observed. A similar observation was made previously with the overexpression *SOD1*-ALS model.

7.3 Sod1 and V-ATPase interaction

Currently it is understood that defects in vacuole function in $\Delta sod1$ cells stems from alterations in iron homeostasis that are caused due to elevated endogenous oxidative stress [204]. The vacuole fragmentation phenotype in $\Delta sod1$ cells can be rescued by the overexpression of Slt2 in a process that involved the induction of actin polymerisation [258]. Deletion of single-copy subunits of the V-ATPase such as Vma2, result in chronic oxidative stress and a synthetic lethality with the deletion of *SOD1* that can be rescued in the absence of atmospheric oxygen [189].

Previous findings in *S. cerevisiae* suggested a toxic gain-of function that is related to the yeast vacuole [115]. The yeast vacuole is analogous to the mammalian lysosome, and lysosomal dysfunction has been associated with a number of neurodegenerative disorders, including ALS.

The finding in this study that Sod1 interacts with Vma2, Vma4 and Vma8, all subunits of the V₁ domain of the V-ATPase in yeast suggests that not only is there a genetic interaction between the Sod1 and the V-ATPase, but there may also be a physical interaction as well.

Vacuolar acidification is not affected in cells that do not have *SOD1*, suggesting that V-ATPase activity is not affected by the absence of Sod1. Furthermore, in this study, the V-ATPase activity measured from WT and $\Delta sod1$ vacuole extracts showed no differences between the two strains. However, in cells that overexpress ALS-linked mutant isoforms of Sod1, vacuole acidification is lost, suggesting a potential toxic gain-of function caused by overexpression of ALS-linked Sod1 mutations [115]. Cells that express ALS-linked mutant isoforms of Sod1 at lower levels, more similar to that of Sod1^{WT}, do not have a vacuole acidification defect, suggesting that this toxic gain-of function is only apparent if mutant Sod1 is expressed to a high enough level.

Furthermore, V-ATPase activity in the presence of different concentrations of recombinant bovine Sod1 was slightly reduced in measurements from vacuole extracts from WT cells.

Whether there is a role for Sod1 in regulating the activity of the V-ATPase is unclear. It has been previously suggested that the activity of the V-ATPase can be regulated by redox signalling, specifically by modification of a conserved cysteine residue in Vma1 (subunit A) [203], [259]. Therefore, Sod1 could be interacting with the V-ATPase in a similar way to how it interacts with the casein kinases Yck1, and Yck2, in which it binds to them and modifies their function via the local production of H₂O₂.

There is an online database called MetOsite (<https://metosite.uma.es/>), that collects data of any methionine residues that have been experimentally shown to possibly be involved in regulatory processes. Oxidation of methionine residues have been suggested as a reversible PTM that can

regulate the function of proteins [260]. In the database, it can be observed that there are numerous methionine sites that are oxidized by H_2O_2 , in the V-ATPase subunits, Vma1, Vma2, and Vma4, [260], [261]. These could potentially be targets for Sod1. Another possibility is that Sod1 could play a protective role to the V-ATPase with regards to damage from oxidative stress in the way that it has been shown to be necessary for protection of the P-type ATPase at the plasma membrane Pma1 [262]. Further experiments will be necessary to probe the nature of the interaction between Sod1 and the V-ATPase.

Amino acids can be taken up from the extracellular environment of cells. They can also be transported into and out of the vacuole and mitochondria. Amino acids are the crucial metabolic building blocks in *S. cerevisiae* and their balance is maintained by numerous transporters on the plasma membrane, the vacuole membrane, and the inner mitochondrial membrane. The vacuole contains 25% of the cells total volume of amino acids and acts as a vital store when amino acids are needed by the cell either during nitrogen starvation or protein synthesis. The activity of proton-coupled amino acid transporters relies on the proton gradient that is produced by the coordinated action of the P-ATPase on the plasma membrane encoded by *PMA1* and the V-ATPase on the vacuole membrane. Ypq3 transports histidine from the cytoplasm to the vacuole membrane. Due to the reduced level of histidine in vacuole extracts from $\Delta sod1$ cells compared to the WT, it could be that the function of this transporter is impaired in some way. Ypq3 is thought to be the secondary histidine transporter compared to Avt1 and it is expressed at relatively low levels in nutrient rich conditions. Ypq3 expression increases in histidine depleted media [263]. As with Ypq1 and Ypq2, Ypq3 is sorted to the vacuole membrane via the alkaline phosphatase pathway (ALP) by the AP-3 complex. When the ALP pathway is inhibited, Ypq1 and Ypq2 are still sorted to the vacuole membrane via the endosomes. Ypq3 on the other hand becomes mis localised to the lumen of the vacuole [264]. To check whether Ypq3 is at the vacuole membrane in $\Delta sod1$ cells, a strain with Ypq3 tagged with GFP could be visualised by fluorescence microscopy. Ypq3 has also been reported to be positively regulated by the transcription factor Lys14, in that when cytosolic lysine levels are high, Ypq3 expression is repressed [265]. Given the defects in lysine metabolism in cells lacking *SOD1*, this could be another way in which Ypq3 is affected.

7.3.1 Perturbed amino acid homeostasis in cells lacking *SOD1*

Results from this study and others suggest that the loss of *SOD1* in *S. cerevisiae* causes perturbed amino acid levels in the cell [115], [206]. LC-MS analysis of vacuole extracts from WT and $\Delta sod1$ suggested possibly lower levels of histidine and lysine in the vacuoles of cells lacking *SOD1*

compared to the WT. Analysis of amino acid profiling data [206] demonstrated that levels of histidine, lysine, glycine, arginine and alanine were increased in $\Delta sod1$ cells compared to the overall amino acid average profile across 4678 gene deletions. Levels of tyrosine were decreased.

It has been reported that around 70% of the cellular pool of histidine, lysine and arginine are normally stored in the vacuole [266]. For that reason, it was expected that the increases in lysine, arginine, and histidine in $\Delta sod1$ cells observed from the amino acid profiles in the Ralser database, would be reflected in the LC-MS analysis of the vacuole extracts from WT and $\Delta sod1$ cells. As the levels are not increased in the vacuole upon loss of *SOD1*, it is possible that the increase in lysine, histidine, arginine, alanine, and glycine could be due to increased uptake of amino acids from the extracellular media or increased amino acid biogenesis.

A recent study measured the change in abundance of a large number of proteins between WT and $\Delta sod1$ cells [50]. In *S. cerevisiae* cells lacking *SOD1*, the abundance of a number of proteins that are involved in amino acid biogenesis increases. These are mainly proteins involved in the lysine biosynthesis pathway (Lys9, Lys12, Lys20, Lys2, Lys4, and Lys21), and proteins involved in the arginine biosynthesis pathway. Interestingly, the abundance of the general amino acid permease (Gap1) is significantly decreased. Gap1 is understood to be downregulated by being endocytosed and degraded when there is a favourable nitrogen source and nutrients are richly available [267]. Overall, it can be concluded that in cells lacking *SOD1*, amino acid biogenesis could be upregulated through a mechanism that is as of yet not fully understood.

7.3.2 The role of the V-ATPase in amino acid sensing and Torc1 activation

Relatively few differences in amino acid levels were observed in vacuole extracts from WT and $\Delta sod1$ cells, save for leucine and histidine. The results suggest that overall, amino acid storage in the vacuole is not largely affected in cells lacking *SOD1*. The V-ATPase is thought to play a role in amino acid sensing, whereby it activates Torc1 upon sensing amino acids in the vacuole lumen. As an interaction between *SOD1* and the V-ATPase was observed in this study, and the amino acid profile of cells lacking *SOD1* is significantly different to the overall average, it could be that Sod1 plays a role in the sensing of amino acids in the vacuole through the V-ATPase. The different potential mechanisms whereby V-ATPase has been suggested to act as an amino acid sensor are outlined below.

Amino acid sensing in the vacuole is thought to work by the accumulation of amino acids in the lumen, resulting in the activation of the TOR complex at the vacuole membrane by its GEFS RAGA/B and RAGC/D in mammalian cells or Gtr1 and Gtr2 in *S. cerevisiae*. These GEFS are

anchored to the vacuole/lysosome membrane by the RAGULATOR complex (mammalian cells) or EGO complex (*S. cerevisiae*). The RAGULATOR complex has been shown to be in a complex with the V-ATPase where LAMTOR1/Ego1 interacts with ATP6VOC /Vma3 at the V₀ domain and LAMTOR2/Ego3 interacts with ATP6V1B1 / Vma2 at the V₁ domain. In the absence of amino acids, the interaction between LAMTOR2 and the V₁ domain strengthens, whereas the interaction between LAMTOR1 and the V₀ domain remains the same. V-ATPase proton pumping activity is required for the TOR complex to be recruited to the vacuole/lysosome membrane when amino acid levels are high [212]. In this way, the V-ATPase is upstream of the ragulator complex in amino acid sensing and plays an as of yet unclear role in the process.

Another proposed vacuolar amino acid sensor is SLC38A9 which is a transporter required for mTORC1 activation in response to arginine uptake in the vacuole. Overexpression of its N-terminal tail region 1–112 can activate mTORC1 regardless of amino acid levels. SLC38A9 activation of mTORC1 is independent of V-ATPase activity suggesting that it is an independent amino acid sensing mechanism [268]. SLC38A9 has multiple homologues in yeast, most notably Avt1, Avt2, and Avt3 which all possess a similar N-terminal tail that is seemingly important for Torc1 activation.

Lastly, the proton coupled histidine transporter SLC15A4, has been shown to affect lysosomal pH by the import of histidine into the lysosome due to its unique buffering capabilities as an amino acid. It was found that loss of SL15A4 caused an accumulation of histidine in the lysosome resulting in impaired lysosome acidification. Impaired lysosome acidification then affected V-ATPase activity and inhibited mTORC1 [269]. SLC15A4 does not seem to have a clear homologue or orthologue in yeast, however other histidine transporters on the vacuole membrane such as Ypq3 could possibly fulfil a similar function. The low levels of histidine in the vacuole in cells lacking *SOD1* could impact amino acid sensing resulting in aberrant amino acid levels in the cell. Ypq2 imports arginine into the vacuole lumen in exchange for histidine [270]

Figure 7.1.

In the future, measuring the expression levels of all of the amino acid transports on the vacuole and plasma membrane in WT and $\Delta sod1$ may help in understanding the perturbed amino acid levels in cells lacking *SOD1*. Furthermore, measuring of amino acid metabolite levels in the vacuoles and cytosolic fractions of the same WT and $\Delta sod1$ cells, with the same genetic background would allow for a direct comparison between vacuolar and cytosolic results.

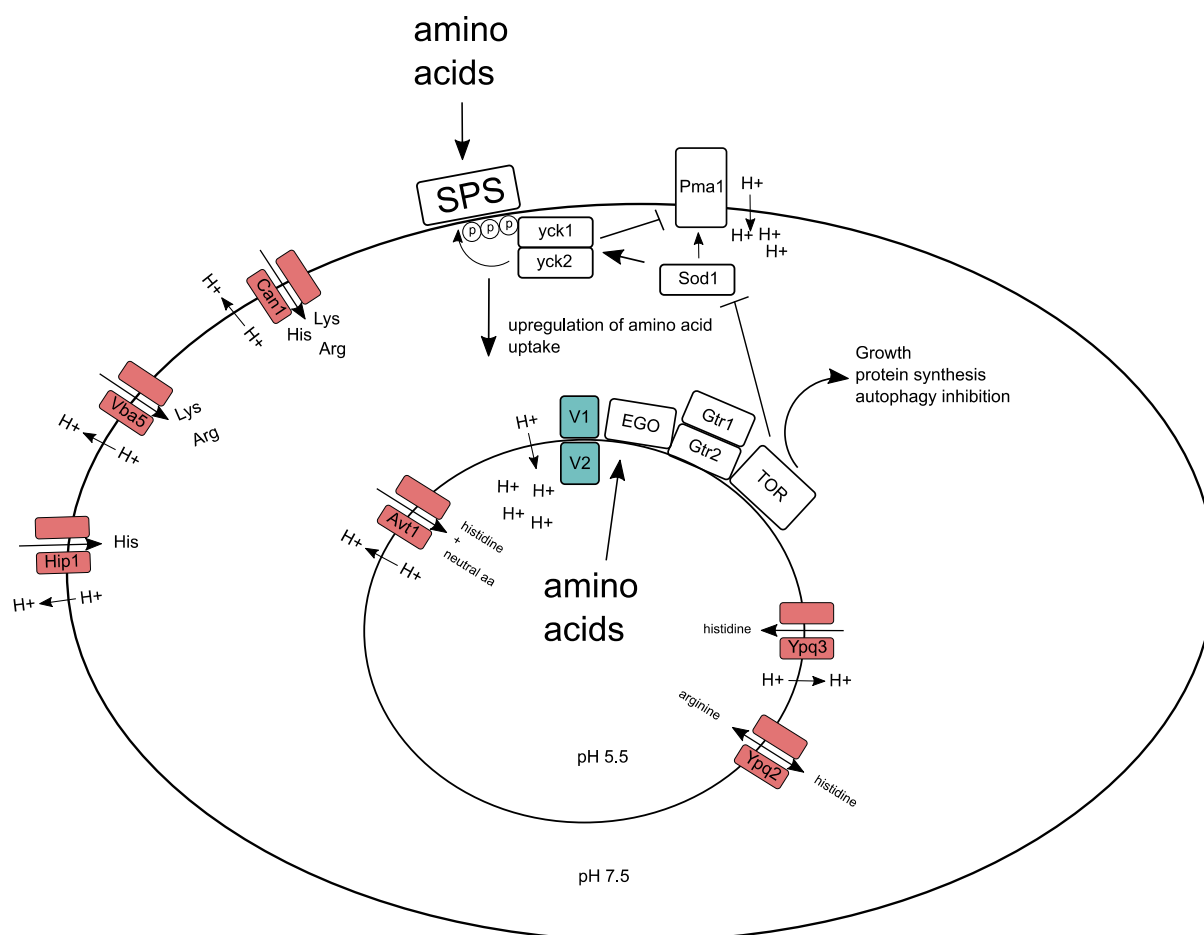


Figure 7.1 Amino acid homeostasis in yeast.

Schematic depicting the regulation of basic amino acid homeostasis in yeast. Amino acids are sensed from the extracellular environment by the SPS complex. Hyperphosphorylation of SPS by Yck1 and Yck2 results in activation of transcription factors that signal for upregulation of amino acid importers at the plasma membrane such as Can1, Vba5 and Hip1. These transporters are all reliant on the proton gradient generated by the cooperative action of Pma1, the P-ATPase on the plasma membrane and the V-ATPase found on the vacuole membrane. Pma1 is downregulated by Yck1 and Yck2 by phosphorylation in response to glucose signals. Sod1 directly binds to Yck1 and Yck2 and stabilises them due to the local production of H_2O_2 . Sod1 also has a positive effect on Pma1 as $\Delta sod1$ cells have attenuated Pma1 activity. The V-ATPase is thought to act between amino acid sensing and TOR activation, and it is thought to respond to arginine levels. Active V-ATPase is required for TOR activation at the vacuole membrane in response to increase amino acid levels in the vacuole lumen. Avt1 provides the bulk of histidine import into the vacuole, with Ypq3 understood to be a supplementary transporter. Ypq2 imports arginine into the vacuole uses the export of histidine to achieve this. Activation of TOR results in the upregulation of transcriptional programmes related to growth, protein synthesis, inhibition of autophagy and inhibition of Sod1.

7.3.3 Sod1 interacts with calcineurin in yeast and is required for its activation in response to increases in intracellular calcium

Calcineurin has long been understood to play an important role in ALS, specifically in the regulation of calcium homeostasis and pro-apoptotic pathways. Previous studies have identified an interaction between Sod1 and Calcineurin, with Sod1 playing a protective role in promoting calcineurin activity and stability. It has been suggested that mutant isoforms of Sod1 carry out this protective role less efficiently leading to reduced calcineurin signalling in MNs. The main downstream effects of reduced calcineurin signalling include an increase in intracellular calcium ions and inappropriate triggering of apoptosis.

In this study, it was shown that in *S. cerevisiae*, Sod1 is capable of interacting with the regulatory calcineurin subunit Cnb1 and the two redundant catalytic subunits Cna1 and Cmp2 in a DHFR-PCA assay, and that similar to previous results, the absence of Sod1 leads to a large reduction in calcineurin activity in response to calcium exposure. Overexpressed mutant isoforms or shorter fragments of Sod1 were not able to rescue calcineurin levels back to that when Sod1^{WT} is present. These results suggest that the interaction between Sod1 and calcineurin is conserved in *S. cerevisiae* and that the protective effects of Sod1 are mediated by a direct interaction with the calcineurin complex, rather than an indirect genetic effect.

One study demonstrated that Sod1 protects calcineurin activity by preventing the oxidation by superoxides of the Fe²⁺ into Fe³⁺ of the Fe²⁺/Zn²⁺ metal centre group that is crucial for calcineurin stability. The oxidized Fe³⁺/Zn²⁺ metal centre group is associated with a less stable form of calcineurin that is dependent on manganese to function [271]. Studies have also demonstrated that promotion of calcineurin activity by calmodulin can be inhibited by oxidation at a Met406 in the calmodulin binding domain. This has been suggested as a reversible PTM [272]. It could be that in the absence of Sod1, Met406 is more susceptible to oxidation due to the overall increase of endogenous oxidative stress in the $\Delta sod1$ mutant, leading to inability of calcineurin to be activated by calmodulin (Figure 7.2). Alternatively, Sod1 may even oxidatively modify the Met406 residue on the catalytic A subunit of calcineurin by the local production of H₂O₂.

This could also represent a process by which Sod1 could reversibly regulate the activity of calcineurin in response to different cellular signals. For example, when Sod1 is inhibited by activated Torc1, the oxidation state of the calcineurin Met406 residue may be affected resulting in an inhibition of calcineurin activation via calmodulin. Upon inhibition of Torc1 by growth in a nutrient poor environment, Sod1 activity would increase and calcineurin activity would then be

increased as well. The same study showed that, 42% of the identified proteins with calmodulin binding sites contain methionine residues in the binding sites. The regulation of calmodulin binding via methionine oxidation could be a more general PTM involving Sod1 by generating local bursts of H_2O_2 . Calmodulin activity is also reduced by oxidative modification due to a reduced stability of the protein by oxidation of methionine residues in its carboxyl tail region [273].

In the future, mutating candidate residues such as Met406. or other exposed residues that have the potential to be reversibly modified by redox signals in calcineurin may allow for the understanding of the direct mechanism by which Sod1 regulates the activity of calcineurin.

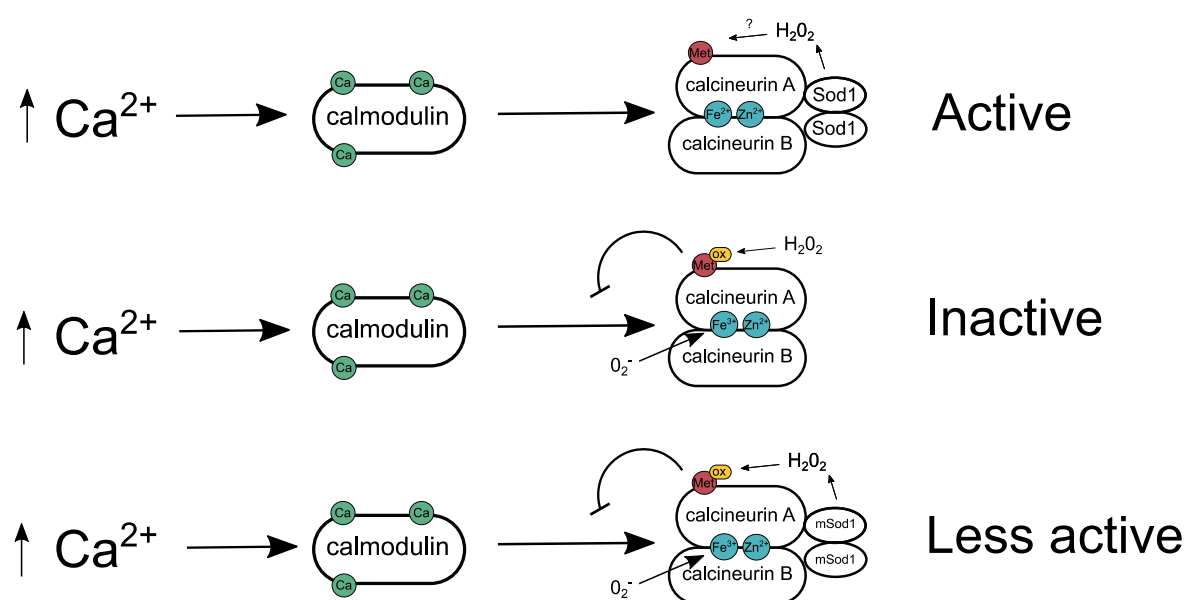


Figure 7.2 Redox control of calcineurin activity.

Schematic displaying what is currently understood about control of calcineurin activity by redox signalling. In the active scenario, as intracellular Ca^{2+} increases, calmodulin binds to calcineurin at the calmodulin binding domain and promotes its activity. Sod1 interacts with calcineurin and is known to promote its activity. In the inactive scenario, when Sod1 is not present, a number of oxidative modifications occur to calcineurin due to the overall increase in endogenous oxidative stress and the lack of Sod1 as a protective factor. Firstly, the $Fe^{2+}-Zn^{2+}$ metal cluster becomes $Fe^{3+}-Zn^{2+}$ which is associated with a loss of calcineurin activity. Secondly, met 406 becomes oxidised by H_2O_2 and inhibits calmodulin binding and activation of calcineurin in response to Ca^{2+} increases. Cells overexpressing ALS-linked Sod1 mutants have decreased calcineurin activity. The reduced activity of the ALS-linked mutants could result in less protection of calcineurin by Sod1. It could also be that mutant Sod1 isoforms could be disrupting calcineurin activity due to a toxic gain of function.

Calcineurin plays a crucial highly conserved role in regulating Ca^{2+} homeostasis in the cell. Over 90% of the Ca^{2+} in yeast is stored in the vacuole [274]. The vacuole is also the primary compartment with which cytosolic Ca^{2+} can be transferred to when levels are too high. The

sequestration of Ca^{2+} into the vacuole is mediated by Pmc1 and Vcx1. Vcx1 rapidly transports Ca^{2+} into the vacuole using the H^+ gradient established by the V-ATPase [275], whereas Pmc1 is a P-type ATPase that slowly transports Ca^{2+} into the vacuole, and also helps to establish the H^+ gradient in the vacuole lumen. Calcineurin upregulates Pmc1 via activation of the Crz1 transcription factor in a Ca^{2+} dependant fashion [224]. It has also been suggested that Calcineurin inhibits Vcx1 through an as of yet unidentified mechanism [275].

7.4 Implications for SOD1-associated Amyotrophic Lateral Sclerosis.

Lysosome dysfunction is becoming increasingly linked with ALS as a primary mechanism of the disease, rather than an endpoint defect due to protein aggregation. The interaction between Sod1 and the V-ATPase identified in this study and the fact that overexpression of ALS-linked mutant isoforms of Sod1 into Δsod1 causes vacuole defects suggests that vacuole / lysosomal dysfunction plays an important early role in the development of ALS. The knock-on effects of lysosomal dysfunction include an inability to store Ca^{2+} , impaired autophagic flux due to a reduction in Torc1 signalling an increase in protein aggregation and also mitochondrial defects. The understanding that vacuolar / lysosomal dysfunction may be an early factor in the development of ALS, may prove beneficial in the development of therapies that target lysosomal function such as targeted nano particles that can acidify the lysosomal compartment in the future [276].

This study suggests that in *S. cerevisiae*, Sod1 interacts with calcineurin and that it is required for the increase in calcineurin activity in response to increased levels intracellular Ca^{2+} . Calcineurin signalling is thought to play a crucial part in the development of cellular dysfunction in ALS. Human ALS patient's lymphocytes have markedly reduced levels of calcineurin activity [237]. The consequences of reduced calcineurin activity in motor neurons include an increase in intracellular Ca^{2+} levels, an increased in TDP-43 aggregation, ER stress and inappropriate triggering of apoptosis. Development of therapies that can restore calcineurin activity to normal levels could prove beneficial in treating ALS. (Figure 7.3)

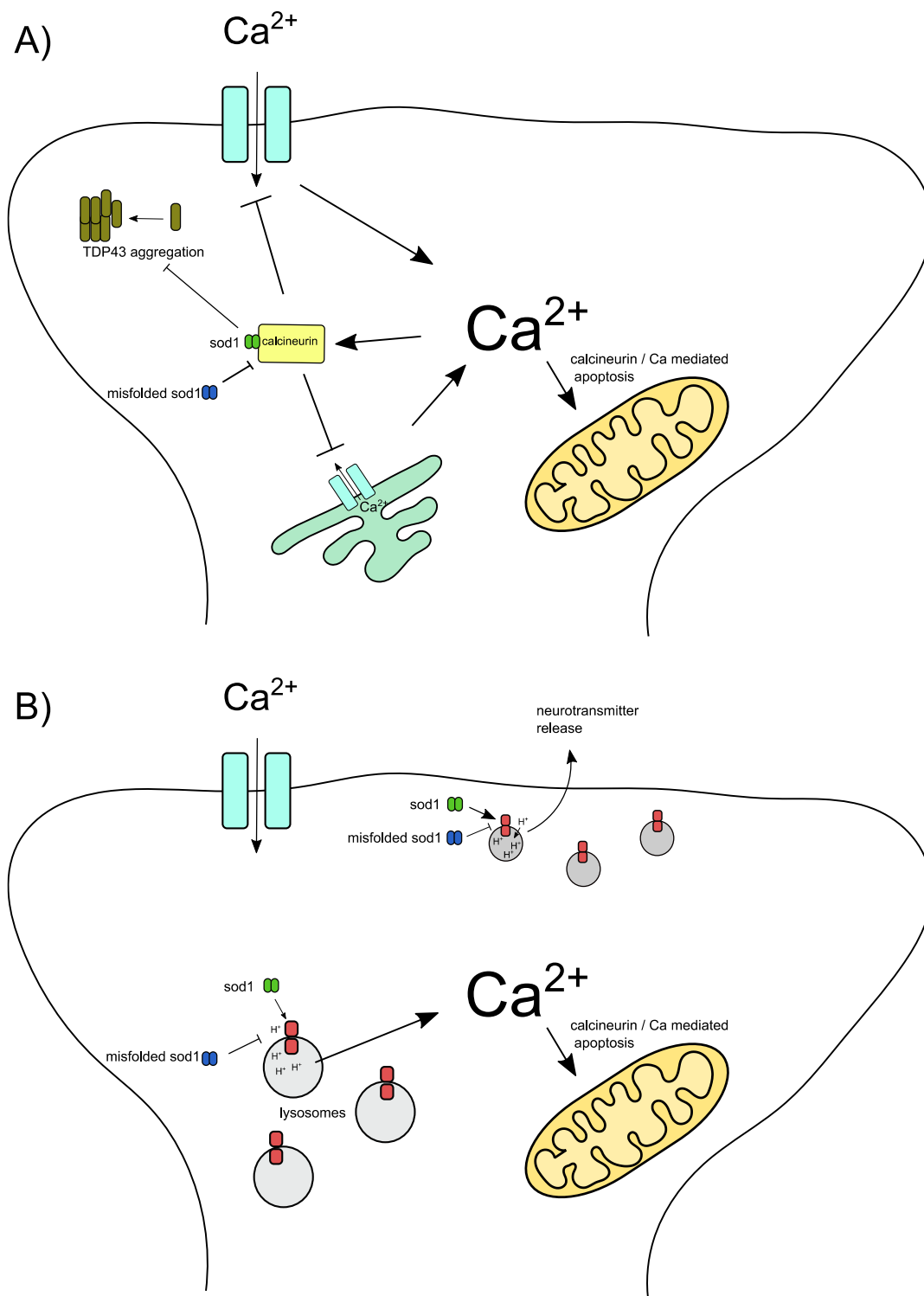


Figure 7.3 Implications for the Sod1 / V-ATPase & Sod1 / Calcineurin interactions in motor neurons.

A) Calcineurin signalling controls calcium homeostasis in MNs, in a number of different ways. Firstly, calcineurin controls the amount of calcium being imported into the cytoplasm via receptors at the synapse, ensuring that intracellular calcium levels don't become too elevated. Secondly, calcineurin represses calcium export from the ER. This ensures that as calcium levels increase in the cell, and calcineurin is subsequently activated, its activity will then repress calcium uptake in order to control calcium levels. Calcineurin also dephosphorylates TDP-43. Phosphorylation of TDP-43 causes its aggregation and

subsequent toxic effects on the cell. Calcineurin prevents the aggregation of TDP-43 by its dephosphorylation. In response to elevated calcium levels, calcium uptake into the mitochondria can trigger apoptosis via calcineurin dependant dephosphorylation of BAD. Misfolded / mutant Sod1 inhibits calcineurin activity and therefore should perturb all of the functions of calcineurin mentioned above, calcium homeostasis, prevention of TDP-43 aggregation and apoptosis via BAD. B) The V-ATPase acidifies the lumen of lysosomes in MNs. Proper acidification of the lysosomal compartment is crucial for the proper functioning of TOR signalling, amino acid storage and calcium storage. Mutant / misfolded Sod1 could perturb lysosome acidity thereby leading to defects in TOR signalling, amino acid, and calcium homeostasis. The V-ATPase mediated acidification of synaptic vesicles is required for the release of neurotransmitters into the synaptic junction. Mutated / misfolded Sod1 could inhibit acidification of synaptic vesicles in a similar way to that of lysosomes.

7.5 Conclusion.

Overall, the data from this study suggests that Sod1 plays an important role in central homeostatic processes in the cell, namely the functioning of the vacuole and calcineurin signalling. A model which illustrates where Sod1 fits into these processes is shown in Figure 7.3. This study also suggests that the degree to which ALS-linked mutant Sod1 isoforms are expressed into *S. cerevisiae* plays an important part in severity of phenotype that is observed.

Sod1 is not required for the maintenance of vacuole acidification, however cells that lack Sod1 have fragmented vacuoles. ALS-linked mutant isoforms of Sod1 cause cytotoxicity and a vacuole acidification defect when expressed from a 2 μ high-copy plasmid, however not when stably expressed from an integration vector. The development of single-copy stable models of ALS helped to uncover the rapamycin resistant phenotype of the Sod1^{A4V} mutant and potential synthetic growth defects with the deletions of *PMC1* and *EGO3*.

The results suggest that Sod1 interacts with Vma2 of the V-ATPase, however it does not appear to play any role in reversible disassembly of the enzyme. V-ATPase activity is decreased in vacuole extracts incubated with recombinant bovine Sod1 suggesting that an *in vitro* interaction between Sod1 and the V-ATPase is possible. As the V-ATPase has been suggested to play a role in sensing amino acids and the recruitment of Torc1 to the vacuole membrane it could be possible that Sod1 plays a part in this process. Sod1 is regulated by Torc1 and plays an important role in the yeast starvation response upon Torc1 inhibition. This is due to results that suggest that cells lacking *SOD1* have altered amino acid profiles, and possibly decreased levels of histidine and lysine in the vacuole. The results also suggest that in *S. cerevisiae*, Sod1 interacts with calcineurin, and that this interaction is important for activation of calcineurin in response to increase in intracellular calcium.

In this study a potentially novel loss-of function of the ALS-linked isoform Sod1A4V was identified due to its rapamycin resistance phenotype.

The findings in this study may help in developing an understanding into how fALS develops in patients that possess mutations in *SOD1*. If lysosomal dysfunction is an early defect in MNs from ALS patients, then perhaps it could be the focus for research and targeted therapies in the future.

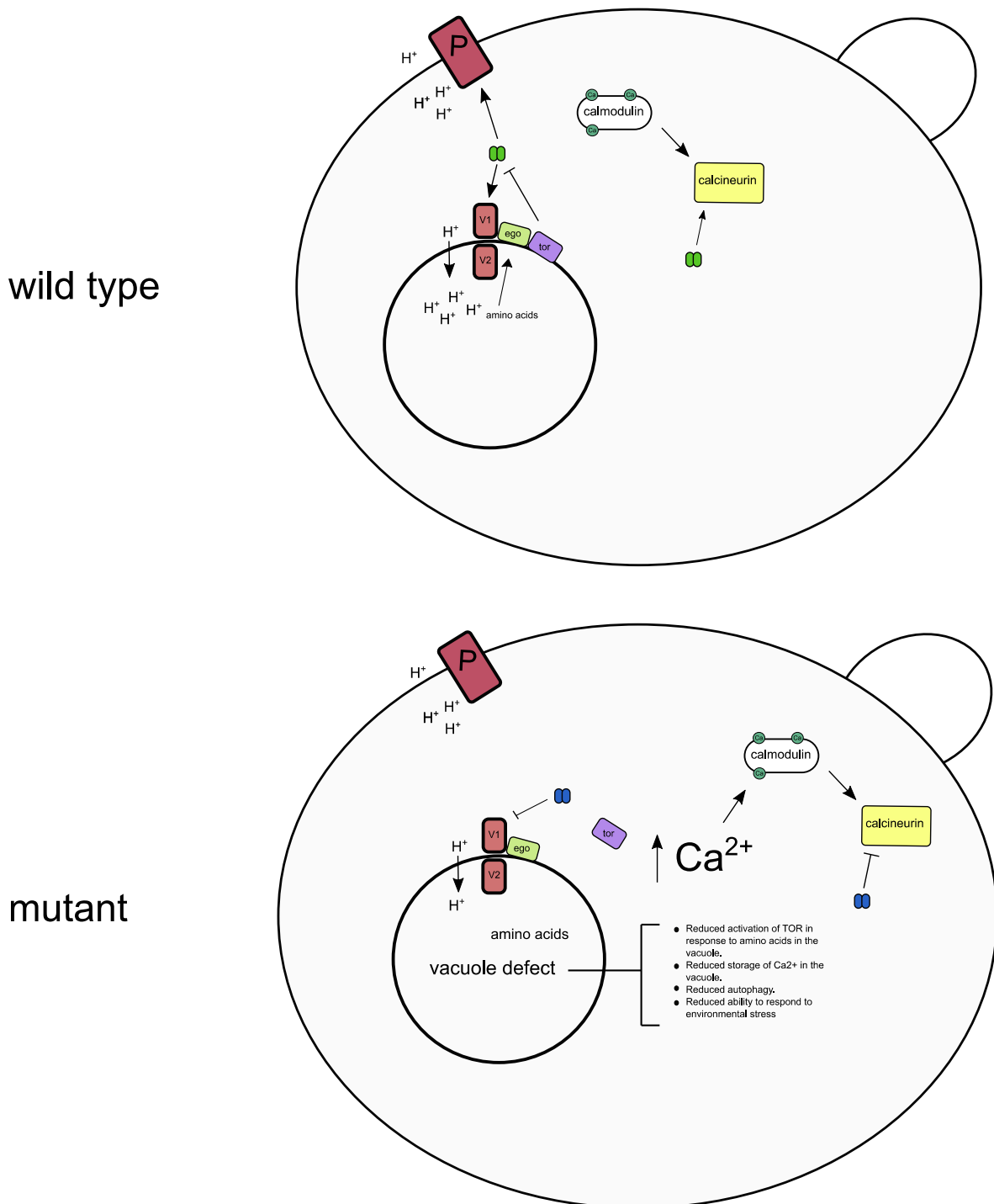


Figure 7.4 Implications for the Sod1 / V-ATPase and Sod1 / Calcineurin interactions in *S. cerevisiae*.

In *S. cerevisiae*, pH homeostasis is maintained by the coordinated action of the P-ATPase (Pma1) at the plasma membrane, and the V-ATPases that localise to the vacuole membrane. Sod1 has been previously shown to be a required for full activity of the P-ATPase through Yck1 / Yck2 signalling and also through protection against oxidative damage. It is also known that Sod1 is inhibited by TOR signalling due to phosphorylation at S39. The results from this study suggest that Sod1 interacts with the V-ATPase and the EGO complex in *S. cerevisiae*. This study also suggests that Sod1 directly interacts with calcineurin and promotes its activity. In mutant cells the phenotypes observed in this study suggest certain roles for Sod1 in its interaction between the V-ATPase and calcineurin in *S. cerevisiae*. Cells lacking *SOD1* have a loss in amino acid homeostasis, suggesting that either storage or sensing of amino acids is impaired in cells expressing mutant Sod1. The impact of ALS-linked mutant isoforms of Sod1 on the P-ATPase is yet to be explored. Mutant isoforms of Sod1 show decreased calcineurin activity in response to elevated calcium. Overall cells expressing ALS-linked Sod1 mutant isoforms are more vulnerable to environmental stresses and less able to control key homeostatic processes in the cell.

8 Appendix

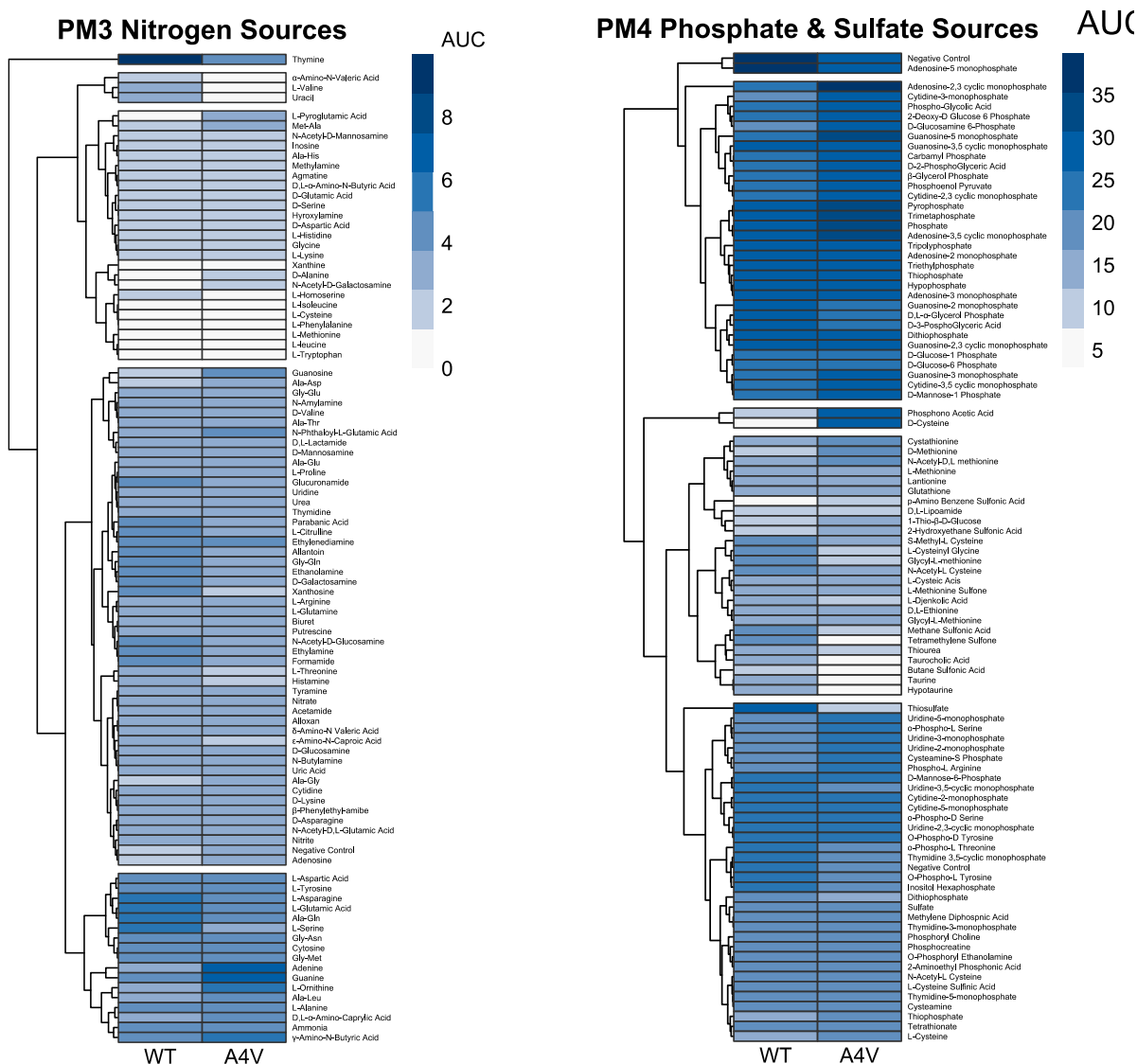


Figure 8.1 PM 3 and 4 AUC heatmap
 AUC values from growth curves of WT and A4V from the PM3 amino acid nitrogen source utilisation plate and PM4 phosphate and sulphate utilisation plate. Dendrograms represent hierarchical clustering of results with more similar AUC values clustered together. Higher and lower AUC values are represented by lighter and darker colours of blue respectively. N = 1.

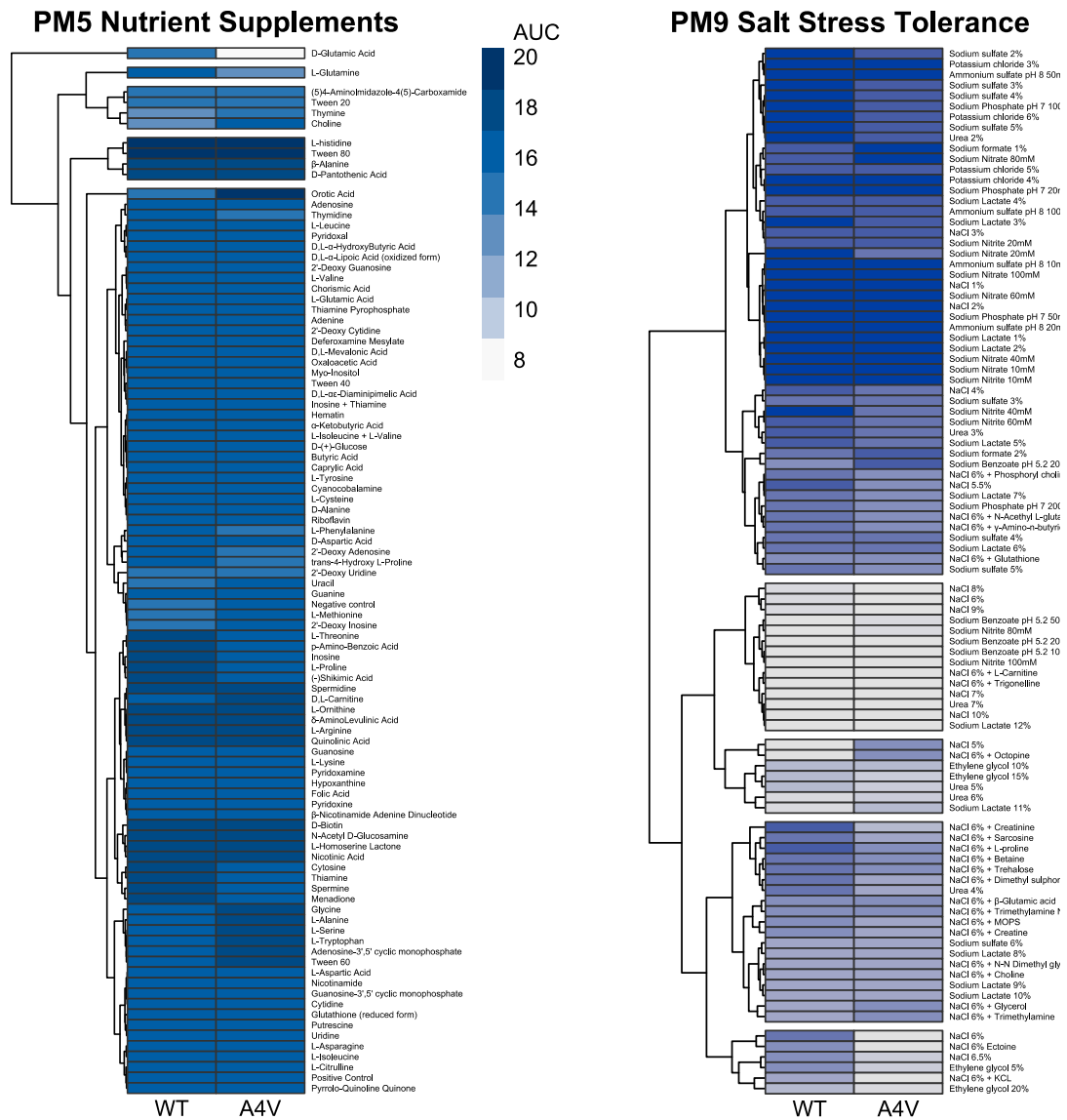


Figure 8.2 PM 5 and 9 AUC heatmaps
 AUC values from growth curves of WT and A4V from the PM5 nutrient supplements and PM9 salt stress plate. Dendrograms represent hierarchical clustering of results with more similar AUC values clustered together. Higher and lower AUC values are represented by lighter and darker colours of blue respectively. N = 1.

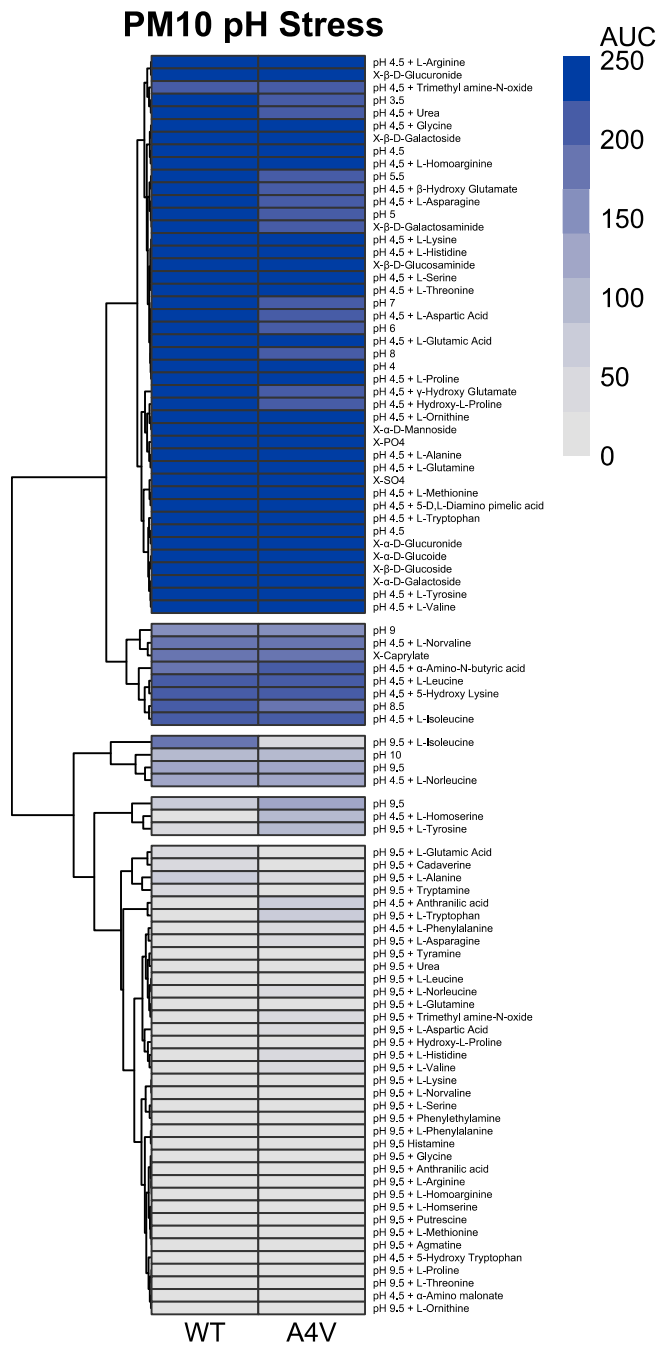


Figure 8.3 PM 10 AUC heatmap

AUC values from growth curves of WT and A4V from the PM10 pH stress plate. Dendrograms represent hierarchical clustering of results with more similar AUC values clustered together. Higher and lower AUC values are represented by lighter and darker colours of blue respectively. N = 1.

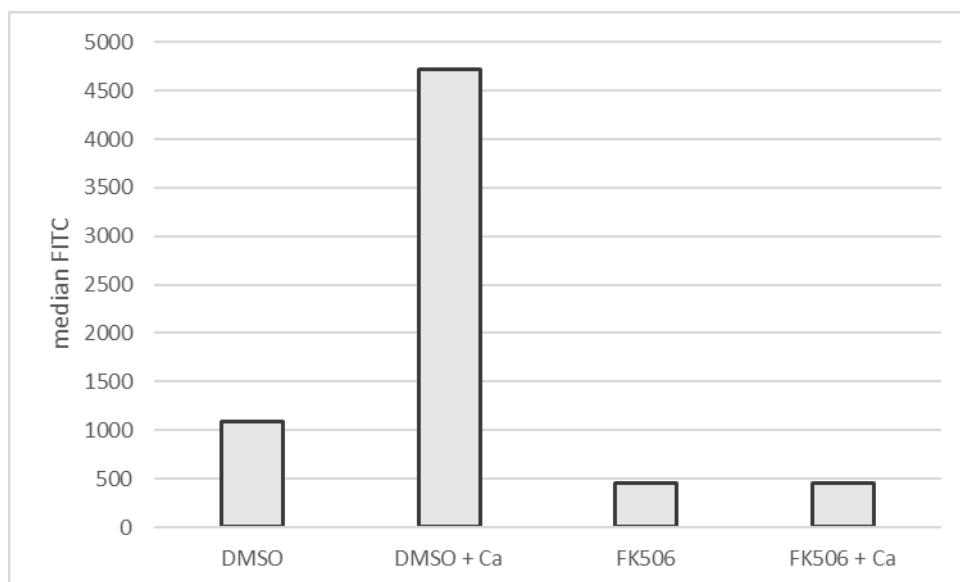


Figure 8.4 Calcineurin activity of WT cells in response to calcium with FK506
Quantification of the median FITC value from flow cytometry of WT cells containing the 4×-CDRE-GFP reporter treated 0.5 μ M FK506 or a DMSO control and with or without Ca^{2+} for 1 h. N = 1

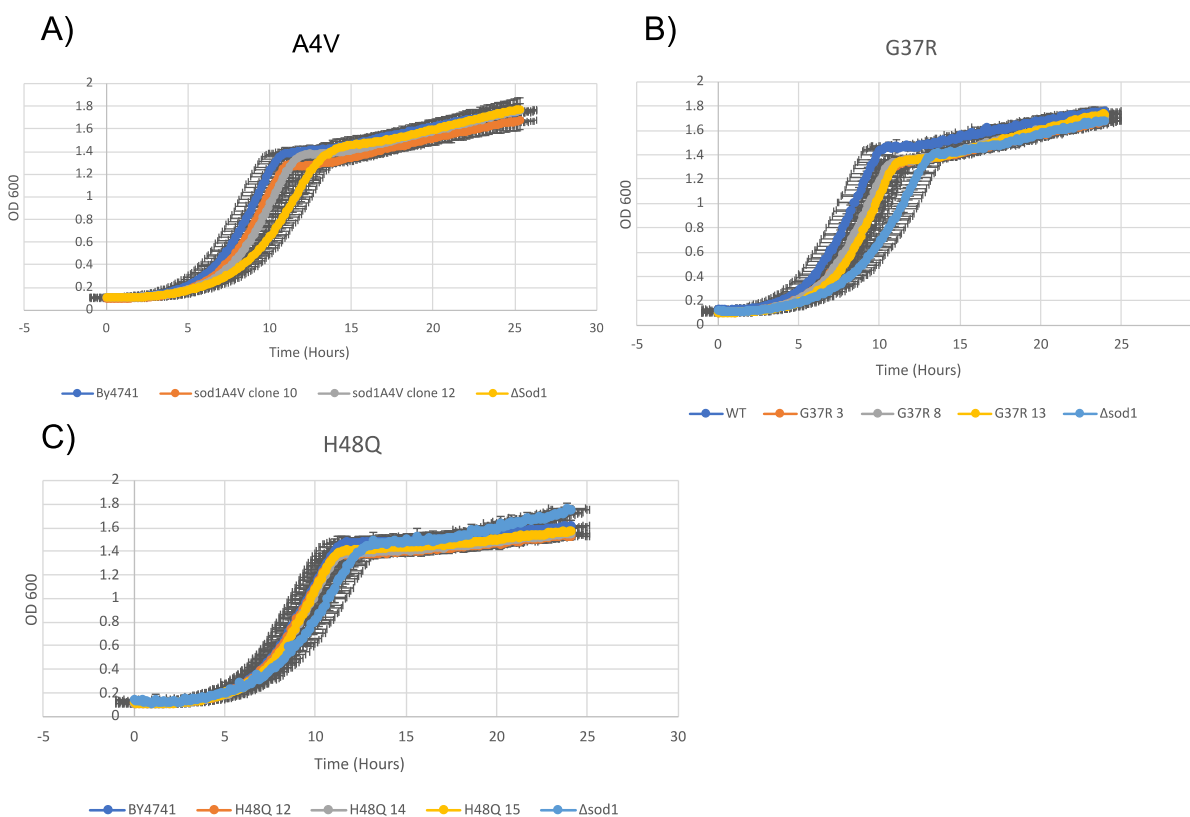


Figure 8.5 SOD1-ALS CRISPR strain liquid growth curves
A) The growth of BY4741, Sod1^{A4V} clone 10, Sod1^{A4V} clone 12, and Δsod1 in YPD media. B) The growth of BY4741, $\text{Sod1}^{\text{G37R}}$ clone 3, $\text{Sod1}^{\text{G37R}}$ clone 8, $\text{Sod1}^{\text{G37R}}$ clone 13, and Δsod1 in YPD media. C) The growth of BY4741, $\text{Sod1}^{\text{H48Q}}$ clone 12, $\text{Sod1}^{\text{H48Q}}$ clone 14, $\text{Sod1}^{\text{H48Q}}$ clone 15, and Δsod1 in YPD media. For all growth curves, the error bars represent the standard deviation of three technical replicates. N = 3.

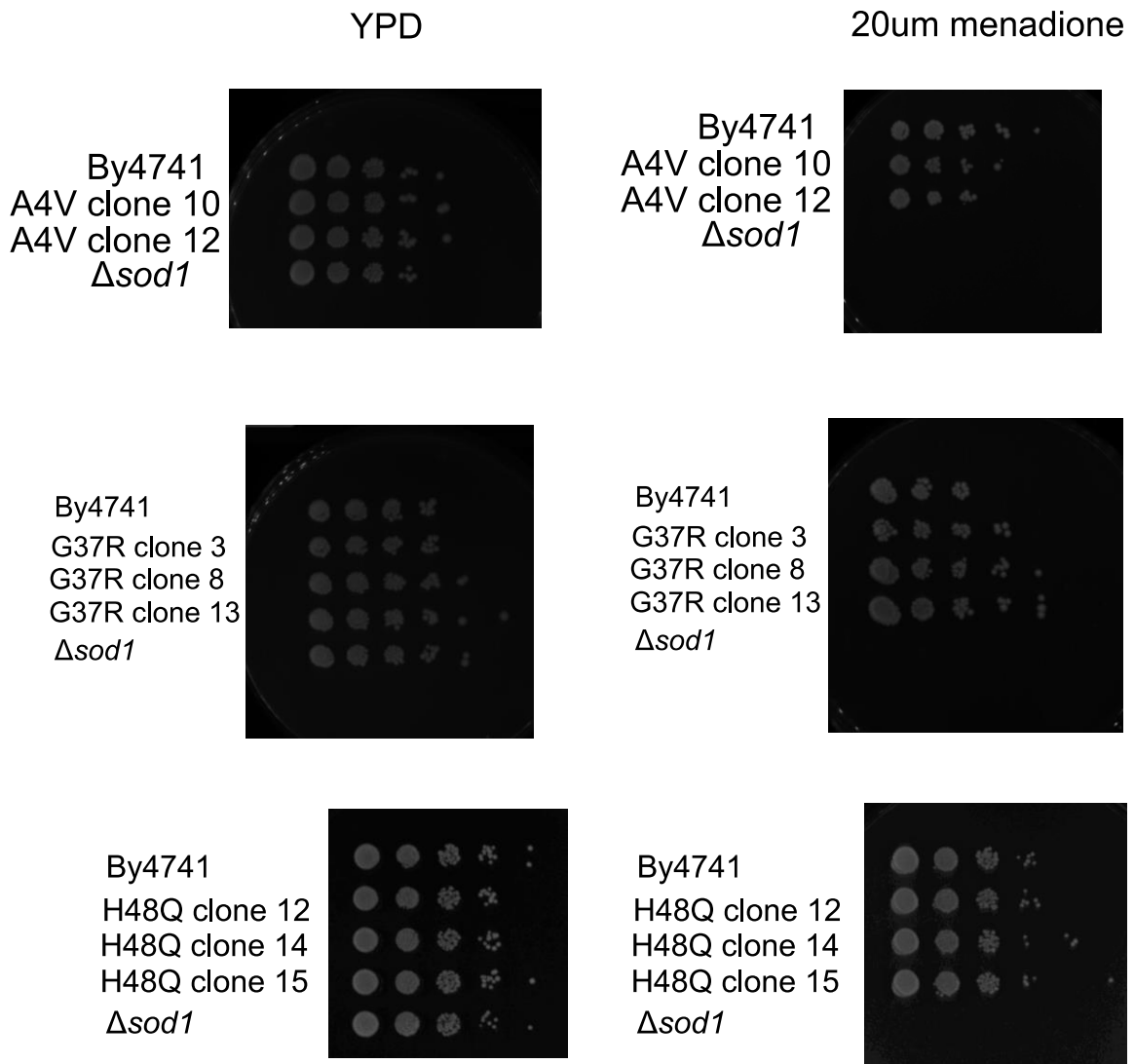


Figure 8.6 CRISPR *SOD1*-ALS model menadione sensitivity spotting assay

For all spotting assays shown above, *S. cerevisiae* cells were diluted to an OD_{600} of 1 and diluted ten-fold as follows (1, 0.1, 0.01, 0.001, 0.0001). Diluted cells were spotted onto either YPD or YPD supplemented with 20 μ M menadione.

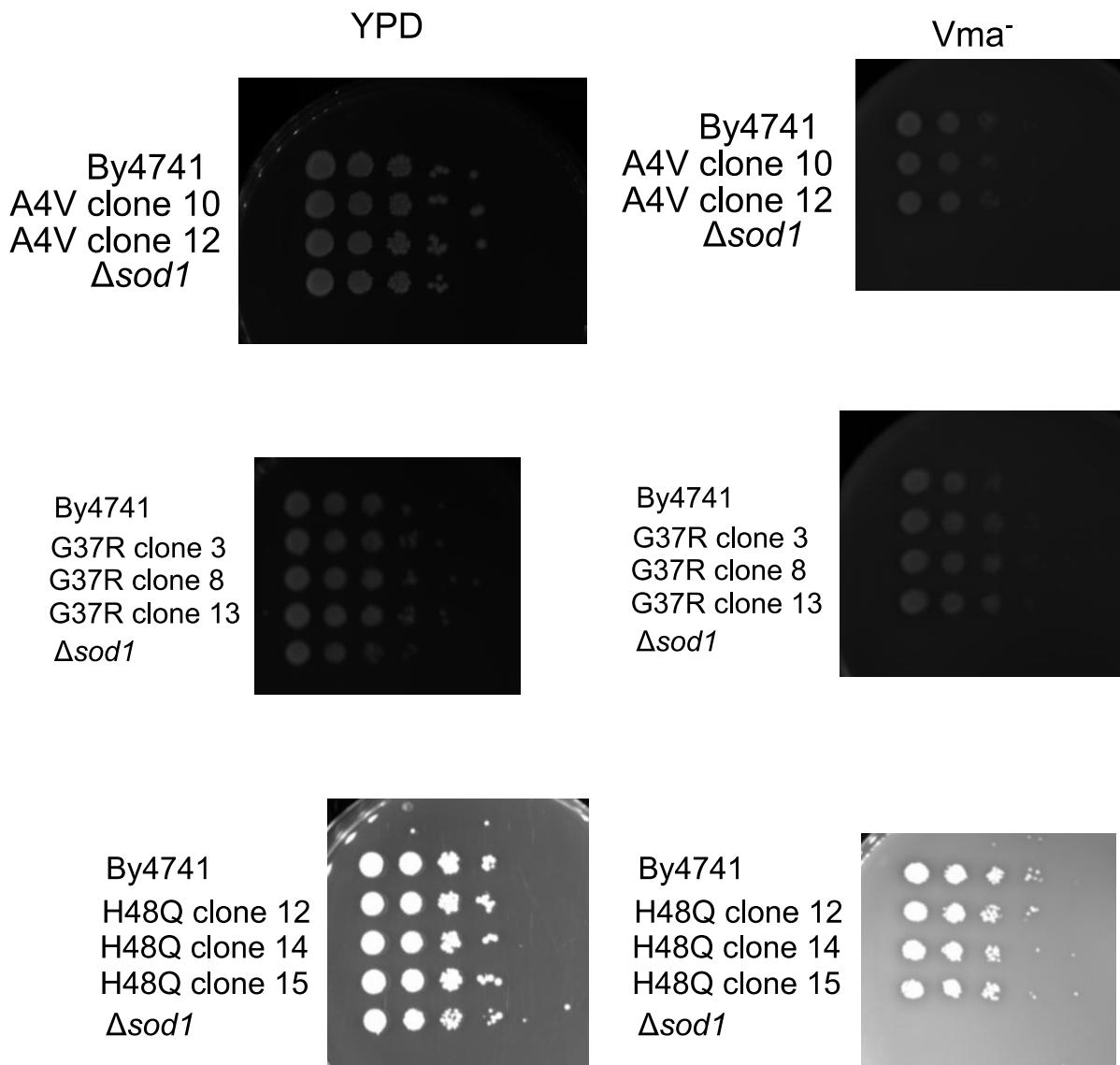


Figure 8.7 CRISPR SOD1-ALS model VMA spotting assay

For all spotting assays shown above, *S. cerevisiae* cells were diluted to an OD₆₀₀ of 1 and diluted ten-fold as follows (1, 0.1, 0.01, 0.001, 0.0001). Diluted cells were spotted onto either YPD or YPD supplemented with 20μM menadione.

Bibliography

- [1] G. Logroscino *et al.*, “Descriptive epidemiology of amyotrophic lateral sclerosis: New evidence and unsolved issues,” *J. Neurol. Neurosurg. Psychiatry*, vol. 79, no. 1, pp. 6–11, 2008.
- [2] P. Couratier, A. L. Leutenegger, P. M. Preux, and E. Beghi, “Clinical and demographic factors and outcome of amyotrophic lateral sclerosis in relation to population ancestral origin,” *Eur J Epidemiol*, vol. 31, no. 3, pp. 229–245, 2015.
- [3] P. Corcia *et al.*, “Causes of death in a post-mortem series of ALS patients,” *Amyotroph. Lateral Scler.*, vol. 9, no. 1, pp. 59–62, 2008.
- [4] L. Lacomblez, G. Bensimon, P. N. Leigh, P. Guillet, and V. Meininger, “Dose-ranging study of riluzole in amyotrophic lateral sclerosis,” *Lancet*, vol. 347, no. 9013, pp. 1425–1431, 1996.
- [5] K. Abe *et al.*, “Safety and efficacy of edaravone in well defined patients with amyotrophic lateral sclerosis: a randomised, double-blind, placebo-controlled trial,” *Lancet Neurol.*, vol. 16, no. 7, pp. 505–512, 2017.
- [6] J. Rooney *et al.*, “A multidisciplinary clinic approach improves survival in ALS : a comparative study of ALS in Ireland and Northern Ireland,” *Neuromuscular*, vol. 86, pp. 496–501, 2015.
- [7] L. Mazzini, S. D. Alfonso, and L. Corrado, “The multistep hypothesis of ALS revisited,” *Neurology*, vol. 91, no. 7, pp. 635–642, 2018.
- [8] A. Al-chalabi *et al.*, “Analysis of amyotrophic lateral sclerosis as a multistep process : a population-based modelling study,” *Lancet Neurol.*, vol. 13, no. 11, pp. 1108–1113, 2014.
- [9] H. X. Deng *et al.*, “Mutations in UBQLN2 cause dominant X-linked juvenile and adult-onset ALS and ALS/dementia,” *Nature*, vol. 477, no. 7363, pp. 211–215, 2011.
- [10] D. R. Rosen *et al.*, “Mutations in Cu/Zn superoxide dismutase gene are associated with familial amyotrophic lateral sclerosis,” *Nature*, vol. 362, no. 6415, pp. 59–62, 1993.
- [11] M. Dejesus-hernandez *et al.*, “Expanded GGGGCC hexanucleotide repeat in non-coding region of C9ORF72 causes chromosome 9p-linked frontotemporal dementia and amyotrophic lateral sclerosis,” *Neuron*, vol. 72, no. 2, pp. 245–256, 2012.
- [12] B. A. Hosler, P. Cortelli, P. J. De Jong, Y. Yoshinaga, and J. L. Haines, “Mutations in the FUS/TLS Gene on Chromosome 16 Cause Familial Amyotrophic Lateral Sclerosis,” *Science (80-.)*, vol. 547, no. February, pp. 1205–1209, 2009.
- [13] E. Kabashi *et al.*, “TARDBP mutations in individuals with sporadic and familial amyotrophic lateral sclerosis,” *Nat. Genet.*, vol. 40, no. 5, pp. 572–574, 2008.
- [14] A. C. Elden *et al.*, “Ataxin-2 intermediate-length polyglutamine expansions are associated with increased risk for ALS,” *Nature*, vol. 466, no. 7310, pp. 1069–1075, 2010.
- [15] B. N. Smith *et al.*, “Report Exome-wide Rare Variant Analysis Identifies TUBA4A Mutations Associated with Familial ALS,” *Neuron*, vol. 84, pp. 324–331, 2014.
- [16] B. N. Smith *et al.*, “Mutations in the vesicular trafficking protein annexin A11 are associated with amyotrophic lateral sclerosis,” *Sci. Transl. Med.*, vol. 9, pp. 1–16, 2017.
- [17] A. Nicolas *et al.*, “Genome-wide Analyses Identify KIF5A as a Novel ALS Gene,” *Neuron*, vol. 97, no. 6, pp. 1268–1283.e6, 2018.
- [18] M. A. Farg *et al.*, “C9ORF72 , implicated in amyotrophic lateral sclerosis and frontotemporal dementia , regulates endosomal trafficking” *Hum. Mol. Genet.*, vol. 23, no. 13, pp. 3579–3595, 2014.
- [19] J. Amick, A. Rocznik-ferguson, S. M. Ferguson, and J. Brill, “C9orf72 binds SMCR8 , localizes to lysosomes , and regulates mTORC1 signaling,” *Mol. Biol. Evol.*, vol. 72, pp.

Bibliography

- 2040–2051, 2016.
- [20] W. Wang *et al.*, “Interaction of FUS and HDAC1 Regulates DNA Damage Response and Repair in Neurons,” *Nat Neurosci*, vol. 16, no. 10, pp. 1383–1391, 2013.
- [21] H. An *et al.*, “ALS-linked FUS mutations confer loss and gain of function in the nucleus by promoting excessive formation of dysfunctional paraspeckles,” *Acta Neuropathol. Commun.*, vol. 7, no. 7, pp. 1–14, 2019.
- [22] J. R. Tollervey *et al.*, “Characterizing the RNA targets and position- dependent splicing regulation by TDP-43,” *Nat. Publ. Gr.*, vol. 14, no. 4, pp. 452–458, 2011.
- [23] B. S. Johnson, D. Snead, J. J. Lee, J. M. Mccaffery, J. Shorter, and A. D. Gitler, “TDP-43 Is Intrinsically Aggregation-prone , and Amyotrophic Lateral Sclerosis-linked Mutations Accelerate Aggregation and Increase Toxicity *,” *J. Biol. Chem.*, vol. 284, no. 30, pp. 20329–20339, 2009.
- [24] A. Russo *et al.*, “Increased cytoplasmic TDP-43 reduces global protein synthesis by interacting with RACK1 on polyribosomes,” *Hum. Mol. Genet.*, vol. 26, no. 8, pp. 1407–1418, 2017.
- [25] B. D. Freibaum, R. Chitta, A. A. High, and J. P. Taylor, “Global analysis of TDP-43 interacting proteins reveals strong association with RNA splicing and translation machinery,” *J Proteome Res*, vol. 9, no. 2, pp. 1104–1120, 2010.
- [26] S. Bannwarth *et al.*, “dementia and amyotrophic lateral sclerosis through CHCHD10 involvement,” *Brain*, vol. 137, pp. 2329–2345, 2014.
- [27] S. Hadano *et al.*, “A gene encoding a putative GTPase regulator is mutated in familial amyotrophic lateral sclerosis 2,” *Nat. Genet.*, vol. 29, no. october, pp. 166–173, 2001.
- [28] C. K. Hand *et al.*, “A Novel Locus for Familial Amyotrophic Lateral Sclerosis , on Chromosome 18q,” *Am. J. Hum. Genet.*, vol. 70, pp. 251–256, 2002.
- [29] Y. Chen *et al.*, “DNA / RNA Helicase Gene Mutations in a Form of Juvenile Amyotrophic Lateral Sclerosis (ALS4),” *Am. J. Hum. Genet.*, vol. 34, pp. 1128–1135, 2004.
- [30] A. Hentati and T. Siddique, “Linkage of recessive familial amyotrophic lateral sclerosis to chromosome 2q33-q35,” *Nature*, vol. 7, pp. 425–428, 1994.
- [31] P. C. Sapp *et al.*, “Identification of Two Novel Loci for Dominantly Inherited Familial Amyotrophic Lateral Sclerosis,” *Am. J. Hum. Genet.*, vol. 73, pp. 397–403, 2003.
- [32] A. L. Nishimura *et al.*, “A Mutation in the Vesicle-Trafficking Protein VAPB Causes Late-Onset Spinal Muscular Atrophy and Amyotrophic Lateral Sclerosis,” *Am. J. Hum. Genet.*, vol. 75, pp. 822–831, 2004.
- [33] M. J. Greenway *et al.*, “ANG mutations segregate with familial and ‘sporadic’ amyotrophic lateral sclerosis,” *Nat. Genet.*, vol. 38, no. 4, pp. 411–413, 2006.
- [34] C. Y. Chow *et al.*, “Deleterious Variants of FIG4 , a Phosphoinositide Phosphatase , in Patients with ALS,” *Am. J. Hum. Genet.*, vol. 84, pp. 85–88, 2009.
- [35] H. Maruyama *et al.*, “Mutations of optineurin in amyotrophic lateral sclerosis,” *Nature*, vol. 465, no. 7295, pp. 223–226, 2010.
- [36] J. O. Johnson *et al.*, “Exome Sequencing Reveals VCP Mutations as a Cause of Familial ALS,” *Neuron*, vol. 68, no. 5, pp. 857–864, 2010.
- [37] A. A. Luty *et al.*, “Sigma nonopioid intracellular receptor 1 mutations cause frontotemporal lobar degeneration-motor neuron disease,” *Ann. Neurol.*, vol. 68, no. 5, pp. 639–649, 2010.
- [38] N. Parkinson *et al.*, “ALS phenotypes with mutations in CHMP2B (charged multivesicular body protein 2B),” *Neurology*, vol. 67, no. 6, pp. 1074–1077, 2006.
- [39] C. H. Wu *et al.*, “Mutations in the profilin 1 gene cause familial amyotrophic lateral sclerosis,” *Nature*, vol. 488, no. 7412, pp. 499–503, 2012.
- [40] Y. Takahashi *et al.*, “Erbb4 mutations that disrupt the neuregulin-erbb4 pathway cause amyotrophic lateral sclerosis type 19,” *Am. J. Hum. Genet.*, vol. 93, no. 5, pp. 900–905,

Bibliography

- 2013.
- [41] H. J. Kim *et al.*, “Prion-like domain mutations in hnRNPs cause multisystem proteinopathy and ALS,” *Nature*, vol. 495, no. 7442, pp. 467–473, 2013.
- [42] J. O. Johnson *et al.*, “Mutations in the Matr3 gene cause familial amyotrophic lateral sclerosis performed laboratory-based experiments and data analysis, and revised the report; E HHS Public Access Author manuscript,” *Nat Neurosci*, vol. 17, no. 5, pp. 664–666, 2014.
- [43] K. P. Kenna and J. E. Landers, “NEK1 variants confer susceptibility to amyotrophic lateral sclerosis,” *Nat. Genet.*, vol. 48, no. 9, pp. 1037–1042, 2017.
- [44] F. Fecto and T. Siddique, “SQSTM1 Mutations in Familial and Sporadic Amyotrophic Lateral Sclerosis,” *Arch Neurol*, vol. 68, no. 11, pp. 1440–1446, 2011.
- [45] A. Freischmidt *et al.*, “Haploinsufficiency of TBK1 causes familial ALS and fronto-temporal dementia,” *Nat. Neurosci.*, vol. 18, no. 5, pp. 631–636, 2015.
- [46] A. M. Wang, J. Little, J. Gomes, and C. D. Krewski, “Identification of risk factors associated with onset and progression of amyotrophic lateral sclerosis using systematic review and meta-analysis,” *Neurotoxicology*, vol. 61, pp. 101–130, 2017.
- [47] J. M. McCord and I. Fridovich, “Superoxide Dismutase An enzymic function for erythrocyte (hemocuprein,” *J. Biol. Chem.*, vol. 244, no. 22, pp. 6049–6055, 1969.
- [48] A. J. Lambert and M. D. Brand, “Superoxide production by NADH : ubiquinone oxidoreductase (complex I) depends on the pH gradient across the mitochondrial inner membrane,” *Biochem J*, vol. 517, pp. 511–517, 2004.
- [49] C. L. Quinlan, A. L. Orr, I. V. Perevoshchikova, J. R. Treberg, B. A. Ackrell, and M. D. Brand, “Mitochondrial Complex II Can Generate Reactive Oxygen Species at High Rates in Both the Forward and Reverse,” *J. Biol. Chem.*, vol. 287, no. 32, pp. 27255–27264, 2012.
- [50] C. Montllor-albalade, H. Kim, A. E. Thompson, A. P. Jonke, and M. P. Torres, “Sod1 integrates oxygen availability to redox regulate NADPH production and the thiol redoxome,” *PNAS*, vol. 119, no. 1, 2022.
- [51] R. W. Strange, S. V. Antonyuk, M. A. Hough, P. A. Doucette, J. Selverstone, and S. S. Hasnain, “Variable Metallation of Human Superoxide Dismutase : Atomic Resolution Crystal Structures of Cu – Zn , Zn – Zn and As-isolated Wild-type Enzymes,” *J Mol Bio*, vol. 356, pp. 1152–1162, 2006.
- [52] A. S. Rose, A. R. Bradley, Y. Valasatava, P. W. Rose, J. M. Duarte, and A. Prli, “Structural bioinformatics NGL viewer : web-based molecular graphics for large complexes,” *Bioinformatics*, vol. 34, no. May, pp. 3755–3758, 2018.
- [53] N. Mesecke *et al.*, “A Disulfide Relay System in the Intermembrane Space of Mitochondria that Mediates Protein Import,” *Cell*, vol. 121, pp. 1059–1069, 2005.
- [54] R. Lepock, L. E. E. D. Arnold, B. H. Torrie, and B. Andrews, “Structural Analyses of Various Cu²⁺ , Zn²⁺ -Superoxide Dismutases Differential Scanning Calorimetry and Raman Spectroscopy,” *Arch. Biochem. Biophys.*, vol. 241, no. 1, pp. 243–251, 1985.
- [55] R. M. Culik, A. Sekhar, J. Nagesh, H. Deol, and J. A. O. Rumpf, “Effects of maturation on the conformational free-energy landscape of SOD1,” *PNAS*, vol. 115, no. 11, pp. E2546–E2555, 2018.
- [56] C. Montllor-Albalade *et al.*, “Extra-mitochondrial Cu/Zn superoxide dismutase (Sod1) is dispensable for protection against oxidative stress but mediates peroxide signaling in *Saccharomyces cerevisiae*,” *Redox Biol.*, vol. 21, no. August 2018, p. 101064, 2019.
- [57] C. A. Pardo, Z. Xut, D. R. Borchelt, D. L. Price, S. S. Sisodia, and D. O. N. W. Clevelandt, “Superoxide dismutase is an abundant component in cell bodies , dendrites , and axons of motor neurons and in a subset of other neurons,” *Proc. Natl. Acad. Sci. U. S. A.*, vol. 92, no. February, pp. 954–958, 1995.
- [58] C. K. wa. Tsang, Y. Liu, J. Thomas, Y. Zhang, and X. F. S. Zheng, “Superoxide dismutase 1 acts as a nuclear transcription factor to regulate oxidative stress resistance,” *Nat.*

Bibliography

- Commun.*, vol. 5, p. 3446, 2014.
- [59] E. P. Marin and W. C. Sessa, “Endothelial cell palmitoylproteomics identifies novel lipid modified targets and potential substrates for protein acyl transferases Ethan,” *Circ Res*, vol. 110, no. 10, pp. 1336–1344, 2012.
- [60] M. M. Harraz *et al.*, “SOD1 mutations disrupt redox-sensitive Rac regulation of NADPH oxidase in a familial ALS model,” *J. Clin. Invest.*, vol. 118, no. 2, pp. 659–670, 2008.
- [61] A. R. Reddi and V. C. Culotta, “SOD1 Integrates Signals from Oxygen and Glucose to Repress Respiration,” *Cell*, vol. 152, no. 1–2, pp. 224–235, 2013.
- [62] C. K. Tsang and X. F. S. Zheng, “SOD1 Phosphorylation by mTORC1 Couples Nutrient Sensing and Redox Regulation,” *Mol. Cell*, vol. 70, no. 3, pp. 502–515, 2018.
- [63] M. E. Gurney *et al.*, “Motor neuron degeneration in mice that express a human Cu,Zn superoxide dismutase mutation,” *Science (80-.)*, vol. 264, no. 5166, pp. 1772–1775, 1994.
- [64] J. A. Rodriguez *et al.*, “Destabilization of apoprotein is insufficient to explain Cu , Zn-superoxide dismutase-linked ALS pathogenesis,” *PNAS*, vol. 102, no. 30, pp. 10516–10521, 2005.
- [65] J. Wang *et al.*, “Copper-binding-site-null SOD1 causes ALS in transgenic mice : aggregates of non-native SOD1 delineate a common feature,” *Hum. Mol. Genet.*, vol. 12, no. 21, pp. 2753–2764, 2003.
- [66] R. Rakhit *et al.*, “Oxidation-induced Misfolding and Aggregation of Superoxide Dismutase and Its Implications for Amyotrophic Lateral Sclerosis *,” *J. Biol. Chem.*, vol. 277, no. 49, pp. 47551–47556, 2002.
- [67] H. R. Broom, J. A. O. Rumfeldt, K. A. Vassall, and E. M. Meiering, “Destabilization of the dimer interface is a common consequence of diverse ALS- associated mutations in metal free SOD1,” *Protein Sci.*, vol. 24, pp. 2081–2089, 2015.
- [68] P. A. Doucette *et al.*, “Dissociation of Human Copper-Zinc Superoxide Dismutase Dimers Using Chaotrope and Reductant,” *J. Biol. Chem.*, vol. 279, no. 52, pp. 54558–54566, 2004.
- [69] C. K. Tsang *et al.*, “SOD1 Phosphorylation by mTORC1 Couples Nutrient Sensing and Redox Regulation,” *Mol. Cell*, vol. 70, no. 3, pp. 502-515.e8, 2018.
- [70] C. J. Banks and J. L. Andersen, “Mechanisms of SOD1 regulation by post-translational modifications,” *Redox Biol.*, vol. 26, no. May, p. 101270, 2019.
- [71] V. K. Mulligan, A. Kerman, R. C. Laister, P. R. Sharda, P. E. Arslan, and A. Chakrabartty, “Early Steps in Oxidation-Induced SOD1 Misfolding : Implications for Non-Amyloid Protein Aggregation in Familial ALS,” *J. Mol. Biol.*, vol. 421, no. 4–5, pp. 631–652, 2012.
- [72] D. Petrov, X. Daura, and B. Zagrovic, “Effect of Oxidative Damage on the Stability and Dimerization of Superoxide Dismutase 1,” *Biophysj*, vol. 110, no. 7, pp. 1499–1509, 2016.
- [73] N. D. Schmitt, J. N. Agar, and B. Analysis, “Parsing Disease-relevant Protein Modifications from Epiphenomena: Perspective on the Structural Basis of SOD1-Mediated ALS,” *J Mass Spectrom*, vol. 52, no. 7, pp. 480–491, 2018.
- [74] A. G. Reaume *et al.*, “Motor neurons in Cu/Zn superoxide dismutase-deficient mice develop normally but exhibit enhanced cell death after axonal injury,” *Nat. Genet.*, vol. 13, no. 1, pp. 43–47, 1996.
- [75] D. R. Borchelt *et al.*, “Superoxide dismutase 1 with mutations linked to familial amyotrophic lateral sclerosis possesses significant activity,” *Proc. Natl. Acad. Sci. U. S. A.*, vol. 91, no. August, pp. 8292–8296, 1994.
- [76] P. B. Stathopoulos *et al.*, “Cu Zn superoxide dismutase mutants associated with amyotrophic lateral sclerosis show enhanced formation of aggregates in vitro,” *PNAS*, vol. 100, no. 12, pp. 7021–7026, 2003.
- [77] L. J. Hayward *et al.*, “Decreased Metallation and Activity in Subsets of Mutant Superoxide Dismutases Associated with Familial Amyotrophic Lateral Sclerosis , Supplemental material : Decreased Metallation and Activity in Subsets of Mutant Superoxi,” vol. 277,

Bibliography

- no. 18, pp. 15923–15931, 2002.
- [78] M. Wiedau-pazos *et al.*, “Altered Reactivity of Superoxide Dismutase in Familial Amyotrophic Lateral Sclerosis,” vol. 271, no. 1976, pp. 5–8, 1996.
- [79] J. P. Crow, B. Sampson, J. Thompson, and S. Beckman, “Decreased Zinc Affinity of Amyotrophic Lateral Sclerosis- Associated Superoxide Dismutase Mutants Leads to Enhanced Catalysis of Tyrosine Nitration by Peroxynitrite,” 1997.
- [80] F. L. Muller *et al.*, “Absence of CuZn superoxide dismutase leads to elevated oxidative stress and acceleration of age-dependent skeletal muscle atrophy,” *Free Radic. Biol. Med.*, vol. 40, pp. 1993–2004, 2006.
- [81] J. D. Glass and L. R. Fischer, “Oxidative stress induced by loss of Cu,Zn-superoxide dismutase (SOD1) or superoxide-generating herbicides causes axonal degeneration in mouse DRG cultures,” *Acta Neuropathol.*, vol. 119, no. 2, pp. 249–259, 2010.
- [82] D. A. Bosco *et al.*, “Wild-type and mutant SOD1 share an aberrant conformation and a common pathogenic pathway in ALS,” vol. 13, no. 11, pp. 1396–1403, 2011.
- [83] T. Bonifacino *et al.*, “Nearly 30 Years of Animal Models to Study Amyotrophic Lateral Sclerosis : A Historical Overview and Future Perspectives,” *Int. J. Mol. Sci.*, vol. 22, no. 12236, pp. 1–40, 2021.
- [84] J. Wang *et al.*, “An ALS-linked mutant SOD1 produces a locomotor defect associated with aggregation and synaptic dysfunction when expressed in neurons of *Caenorhabditis elegans*,” *PLoS Genet.*, vol. 5, no. 1, 2009.
- [85] J. Li, T. Li, X. Zhang, Y. Tang, J. Yang, and W. Le, “Human superoxide dismutase 1 overexpression in motor neurons of *Caenorhabditis elegans* causes axon guidance defect and neurodegeneration,” *Neurobiol. Aging*, vol. 35, no. 4, pp. 837–846, 2014.
- [86] S. N. Baskoylu *et al.*, “Single copy/knock-in models of ALS SOD1 in *C. elegans* suggest loss and gain of function have different contributions to cholinergic and glutamatergic neurodegeneration,” *PLoS Genet.*, vol. 14, no. 10, pp. 1–28, 2018.
- [87] A. H. Brand and N. Perrimon, “Targeted gene expression as a means of altering cell fates and generating dominant phenotypes,” *Development*, vol. 415, pp. 401–415, 1993.
- [88] R. J. Mockett, S. N. Radyuk, J. J. Benes, W. C. Orr, and R. S. Sohal, “Phenotypic effects of familial amyotrophic lateral sclerosis mutant Sod alleles in transgenic *Drosophila*,” *PNAS*, vol. 100, no. 1, pp. 301–306, 2003.
- [89] M. R. Watson, R. D. Lagow, K. Xu, B. Zhang, and N. M. Bonini, “A *Drosophila* model for amyotrophic lateral sclerosis reveals motor neuron damage by human SOD1,” *J. Biol. Chem.*, vol. 283, no. 36, pp. 24972–24981, Sep. 2008.
- [90] A. Şahin *et al.*, “Human SOD1 ALS mutations in a *Drosophila* knock-in model cause severe phenotypes and reveal dosage-sensitive gain- and loss-of-function components,” *Genetics*, vol. 205, no. 2, pp. 707–723, 2017.
- [91] J. B. Phillips and M. Westerfield, “Zebrafish models in translational research : tipping the scales toward advancements in human health,” *Dis. Model. Mech.*, vol. 7, pp. 739–743, 2014.
- [92] R. Lemmens *et al.*, “Overexpression of mutant superoxide dismutase 1 causes a motor axonopathy in the zebrafish,” *Hum. Mol. Genet.*, vol. 16, no. 19, pp. 2359–2365, 2007.
- [93] M. M. J. Da Costa, C. E. Allen, A. Higginbottom, T. Ramesh, P. J. Shaw, and C. J. McDermott, “A new zebrafish model produced by TILLING of SOD1-related amyotrophic lateral sclerosis replicates key features of the disease and represents a tool for in vivo therapeutic screening,” *DMM Dis. Model. Mech.*, vol. 7, no. 1, pp. 73–81, 2014.
- [94] I. Keskin *et al.*, “Effects of Cellular Pathway Disturbances on Misfolded Superoxide Dismutase-1 in Fibroblasts Derived from ALS Patients,” *PLoS One*, vol. 11, no. 2, pp. 1–15, 2016.
- [95] H. Chen *et al.*, “Modeling ALS with iPSCs Reveals that Mutant SOD1 Misregulates Neurofilament Balance in Motor Neurons,” *Cell Stem Cell*, vol. 14, no. 6, pp. 796–809,

Bibliography

- 2014.
- [96] M. Crisp and T. M. Miller, “Canine Degenerative Myelopathy: Biochemical characterization of superoxide dismutase 1 in the first naturally occurring non-human amyotrophic lateral sclerosis model,” *Exp Neurol*, vol. 248, pp. 1–9, 2013.
- [97] M. N. Chieppa *et al.*, “Modeling Amyotrophic Lateral Sclerosis in hSOD1 G93A Transgenic Swine,” *Neurodegener Dis*, vol. 13, pp. 246–254, 2014.
- [98] P. Crociara *et al.*, “Motor neuron degeneration, severe myopathy and TDP-43 increase in a transgenic pig model of SOD1-linked familial ALS,” *Neurobiol. Dis.*, p. #pagerange#, 2018.
- [99] A. Uchida *et al.*, “Non-human primate model of amyotrophic lateral sclerosis with cytoplasmic mislocalization of TDP-43,” *Brain*, vol. 135, pp. 833–846, 2012.
- [100] F. Borel *et al.*, “Therapeutic rAAVrh10 Mediated SOD1 Silencing in Adult SOD1 G93A Mice and Nonhuman Primates,” *Hum. Gene Ther.*, vol. 27, no. 1, pp. 19–31, 2016.
- [101] S. Shimizu, M. Narita, and Y. Tsujimoto, “Bcl-2 family proteins regulate the release of apoptogenic cytochrome c by the mitochondrial channel VDAC,” *Nature*, vol. 66, no. 1992, pp. 1–5, 1999.
- [102] C. Vande Velde, T. M. Miller, N. R. Cashman, and D. W. Cleveland, “Selective association of misfolded ALS-linked mutant SOD1 with the cytoplasmic face of mitochondria,” *PNAS*, vol. 105, no. 10, pp. 1–6, 2008.
- [103] S. Pedrini *et al.*, “ALS-linked mutant SOD1 damages mitochondria by promoting conformational changes in Bcl-2,” vol. 19, no. 15, pp. 2974–2986, 2010.
- [104] P. C. Wong *et al.*, “An adverse property of a familial ALS-linked SOD1 mutation causes motor neuron disease characterized by vacuolar degeneration of mitochondria,” *Neuron*, vol. 14, no. 6, pp. 1105–1116, 1995.
- [105] S. E. Browne, A. Bowling, M. J. Baik, H. Brown, and M. F. Beal, “Metabolic Dysfunction in Familial , but Not Sporadic , Amyotrophic Lateral Sclerosis,” *J. Neurochem.*, vol. 71, no. 1, pp. 281–287, 1998.
- [106] C. Münch, J. O’Brien, and A. Bertolotti, “Prion-like propagation of mutant superoxide dismutase-1 misfolding in neuronal cells,” *Proc. Natl. Acad. Sci. U. S. A.*, vol. 108, no. 9, pp. 3548–3553, 2011.
- [107] J. Wang *et al.*, “Progressive aggregation despite chaperone associations of a mutant SOD1-YFP in transgenic mice that develop ALS,” *PNAS*, vol. 106, no. 5, pp. 1392–1397, 2009.
- [108] D. A. Bosco *et al.*, “Wild-type and mutant SOD1 share an aberrant conformation and a common pathogenic pathway in ALS,” *Nat. Neurosci.*, vol. 13, no. 11, pp. 1396–1403, 2010.
- [109] F. Fulceri, M. Ferrucci, G. Lazzeri, S. Paparelli, and A. Bartalucci, “Autophagy activation in glutamate-induced motor neuron loss,” *Arch. Ital. Biol.*, vol. 149, pp. 101–111, 2011.
- [110] Y. Tashiro *et al.*, “Motor Neuron-specific Disruption of Proteasomes , but Not Autophagy , Replicates Amyotrophic Lateral Sclerosis * □,” *J. Biol. Chem.*, vol. 287, no. 51, pp. 42984–42994, 2012.
- [111] X. Zhang *et al.*, “MTOR-independent, autophagic enhancer trehalose prolongs motor neuron survival and ameliorates the autophagic flux defect in a mouse model of amyotrophic lateral sclerosis,” *Autophagy*, vol. 10, no. 4, pp. 588–602, 2014.
- [112] F. Fornai *et al.*, “Lithium delays progression of amyotrophic lateral sclerosis,” *PNAS*, vol. 105, no. 6, pp. 2052–2057, 2008.
- [113] X. Zhang *et al.*, “Rapamycin treatment augments motor neuron degeneration in SOD1 G93A mouse model of amyotrophic lateral sclerosis,” *Autophagy*, vol. 7, no. 4, pp. 412–425, 2011.
- [114] K. A. Staats *et al.*, “Rapamycin increases survival in ALS mice lacking mature lymphocytes,” *Mol. Neurodegener.*, vol. 8, no. 31, pp. 2–6, 2013.
- [115] E. L. Bastow *et al.*, “New links between SOD1 and metabolic dysfunction from a yeast

Bibliography

- model of amyotrophic lateral sclerosis,” *J. Cell Sci.*, vol. 129, no. 21, pp. 4118–4129, 2016.
- [116] J. N. Keller, W. R. Marquesbery, S. Appel, R. G. Smith, E. Kasarskis, and M. P. Mattson, “Protein Modification by the Lipid Peroxidation Product 4-Hydroxynonenal in the Spinal Cords of Amyotrophic Lateral Sclerosis Patients,” *Ann. Neurol.*, vol. 44, no. 5, pp. 819–824, 1998.
- [117] P. K. Andrus, T. J. Fleck, M. E. Gurney, and E. D. Hall, “Protein Oxidative Damage in a Transgenic Mouse Model of Familial Amyotrophic Lateral Sclerosis,” *J. Neurochem.*, vol. 71, pp. 2041–2048, 1998.
- [118] M. Arundine and M. Tymianski, “Molecular mechanisms of calcium-dependent neurodegeneration in excitotoxicity,” *Cell Calcium*, vol. 34, no. 4–5, pp. 325–337, 2003.
- [119] L. Siklős, J. I. Engelhardt, M. E. Alexianu, M. E. Gurney, T. Siddique, and S. H. Appel, “Intracellular calcium parallels motoneuron degeneration in SOD-1 mutant mice,” *J. Neuropathol. Exp. Neurol.*, vol. 57, no. 6, pp. 571–587, 1998.
- [120] D. S. Howland *et al.*, “Focal loss of the glutamate transporter EAAT2 in a transgenic rat model of SOD1 mutant-mediated amyotrophic lateral sclerosis (ALS),” *Proc. Natl. Acad. Sci. U. S. A.*, vol. 99, no. 3, pp. 1604–1609, 2002.
- [121] M. Tateno *et al.*, “Calcium-permeable AMPA receptors promote misfolding of mutant SOD1 protein and development of amyotrophic lateral sclerosis in a transgenic mouse model,” *Hum. Mol. Genet.*, vol. 13, no. 19, pp. 2183–2196, 2004.
- [122] E. A. Winzeler *et al.*, “Functional characterization of the *S. cerevisiae* genome by gene deletion and parallel analysis,” *Science (80-.)*, vol. 285, no. 5429, pp. 901–906, 1999.
- [123] S. Mnaimneh *et al.*, “Exploration of essential gene functions via titratable promoter alleles,” *Cell*, vol. 118, no. 1, pp. 31–44, 2004.
- [124] W. K. Huh *et al.*, “Global analysis of protein localization in budding yeast,” *Nature*, vol. 425, no. 6959, pp. 686–691, 2003.
- [125] K. Tarassov *et al.*, “An in vivo map of the yeast protein interactome,” *Science (80-.)*, vol. 320, no. 5882, pp. 1465–1470, 2008.
- [126] Z. T. Monahan, S. N. Rhoads, D. S. Yee, and F. P. Shewmaker, “Yeast Models of Prion-Like Proteins That Cause Amyotrophic Lateral Sclerosis Reveal Pathogenic Mechanisms,” *Front. Mol. Neurosci.*, vol. 11, no. December, pp. 1–11, 2018.
- [127] T. F. Outeiro and S. Lindquist, “Yeast Cells Provide Insight into Alpha-Synuclein Biology and Pathobiology,” *Science (80-.)*, vol. 302, no. 5651, pp. 1772–1775, 2003.
- [128] D. F. Tardiff, M. L. Tucci, K. A. Caldwell, G. A. Caldwell, and S. Lindquist, “Different 8-hydroxyquinolines protect models of TDP-43 protein, α -synuclein, and polyglutamine proteotoxicity through distinct mechanisms,” *J. Biol. Chem.*, vol. 287, no. 6, pp. 4107–4120, 2012.
- [129] L. J. Su *et al.*, “Compounds from an unbiased chemical screen reverse both ER-to-Golgi trafficking defects and mitochondrial dysfunction in Parkinson’s disease models,” *DMM Dis. Model. Mech.*, vol. 3, no. 3–4, pp. 194–208, 2010.
- [130] C. Y. Chung and S. Lindquist, “Identification and Rescue of α -Synuclein Toxicity in Parkinson Patient-Derived Neurons,” *Science (80-.)*, vol. 342, no. 6161, pp. 983–987, 2013.
- [131] D. F. Tardiff *et al.*, “Yeast reveal a ‘druggable’ Rsp5 / Nedd4 Network that Ameliorates α – Synuclein Toxicity in Neurons,” *Science (80-.)*, vol. 342, no. 6161, pp. 979–983, 2013.
- [132] D. Harold *et al.*, “Genome-wide association study identifies variants at CLU and PICALM associated with Alzheimer’s disease, and shows evidence for additional susceptibility genes,” *Nat. Genet.*, vol. 41, no. 10, pp. 1088–1093, 2010.
- [133] C. Pereira, C. Bessa, J. Soares, M. Leo, and L. Saraiva, “Contribution of yeast models to neurodegeneration research,” *J. Biomed. Biotechnol.*, vol. 2012, pp. 1–12, 2012.
- [134] K. Fushimi, C. Long, N. Jayaram, X. Chen, L. Li, and J. Y. Wu, “Expression of human FUS / TLS in yeast leads to protein aggregation and cytotoxicity, recapitulating key

Bibliography

- features of FUS proteinopathy,” *Protein Cell*, vol. 2, no. 2, pp. 141–149, 2011.
- [135] Z. Sun *et al.*, “Molecular Determinants and Genetic Modifiers of Aggregation and Toxicity for the ALS Disease Protein FUS / TLS,” *Plos Biol.*, vol. 9, no. 4, p. e100614, 2011.
- [136] S. Ju *et al.*, “A Yeast Model of FUS / TLS-Dependent Cytotoxicity,” *Plos Biol.*, vol. 9, no. 4, p. e1001052, 2011.
- [137] Y. M. Ayala *et al.*, “Structural determinants of the cellular localization and shuttling of TDP-43,” *J. Cell Sci.*, vol. 121, no. 22, pp. 3778–3785, 2008.
- [138] B. S. Johnson, J. M. Mccaffery, S. Lindquist, and A. D. Gitler, “A yeast TDP-43 proteinopathy model : Exploring the molecular determinants of TDP-43 aggregation and cellular toxicity,” *PNAS*, vol. 105, no. 17, pp. 6439–6444, 2008.
- [139] S. M. Cascarina, K. R. Paul, S. Machihara, and E. D. Ross, “Sequence features governing aggregation or degradation of prion-like proteins,” *PLoS Genet.*, vol. 14, no. 7, p. e1007517, 2018.
- [140] J. Couthouis, M. P. Hart, J. Shorter, M. Dejesus-hernandez, R. Erion, and R. Oristano, “A yeast functional screen predicts new candidate ALS disease genes,” *PNAS*, vol. 108, no. 52, pp. 20881–20890, 2011.
- [141] J. Couthouis *et al.*, “Evaluating the role of the FUS / TLS -related gene EWSR1 in amyotrophic lateral sclerosis,” *Hum. Mol. Genet.*, vol. 21, no. 13, pp. 2899–2911, 2012.
- [142] A. Jovic *et al.*, “Modifiers of C9orf72 dipeptide nucleocytoplasmic transport defects to FTD / ALS,” *Nat. Neurosci.*, vol. 18, no. 9, pp. 1226–1231, 2015.
- [143] S. Rabizadeh *et al.*, “Mutations associated with amyotrophic lateral sclerosis convert superoxide dismutase from an antiapoptotic gene to a proapoptotic gene: Studies in yeast and neural cells,” *Proc. Natl. Acad. Sci. U. S. A.*, vol. 92, no. 7, pp. 3024–3028, 1995.
- [144] A. L. Hughes, D. E. Gottschling, and F. Hutchinson, “An Early-Age Increase in Vacuolar pH Limits Mitochondrial Function and Lifespan in Yeast,” *Nature*, vol. 492, no. 7428, pp. 261–265, 2012.
- [145] C. B. Brachmann, A. Davies, G. J. Cost, and E. Caputo, “Designer Deletion Strains derived from *Saccharomyces cerevisiae* S288C : a Useful set of Strains and Plasmids for PCR-mediated Gene Disruption and Other Applications,” *Yeast*, vol. 132, pp. 115–132, 1998.
- [146] M. F. Laughery *et al.*, “New Vectors for Simple and Streamlined CRISPR-Cas9 Genome Editing in *Saccharomyces cerevisiae*,” *Yeast*, vol. 32, no. 12, pp. 711–720, 2015.
- [147] J. Diessl, A. Nandy, C. Schug, L. Habernig, and S. Büttner, “Stable and destabilized GFP reporters to monitor calcineurin activity in *Saccharomyces cerevisiae*,” *Microb. Cell*, vol. 7, no. 4, pp. 106–114, 2020.
- [148] M. S. Longtine, A. M. K. Iii, D. J. Demarini, and N. G. Shah, “Additional Modules for Versatile and Economical PCR-based Gene Deletion and Modification in *Saccharomyces cerevisiae*,” *Yeast*, vol. 961, no. December 1997, pp. 953–961, 1998.
- [149] U. Gueldener, J. Heinisch, G. J. Koehler, D. Voss, and J. H. Hegemann, “A second set of loxP marker cassettes for Cre-mediated multiple gene knockouts in budding yeast,” *Nucleic Acids Res.*, vol. 30, no. 6, pp. 1–8, 2002.
- [150] C. W. Gourlay and K. R. Ayscough, “Actin-Induced Hyperactivation of the Ras Signaling Pathway Leads to Apoptosis in *Saccharomyces cerevisiae*,” *Mol. Cell. Biol.*, vol. 26, no. 17, pp. 6487–6501, 2006.
- [151] R. D. Gietz and R. H. Schiestl, “High-efficiency yeast transformation using the LiAc/SS carrier DNA/PEG method,” *Nat. Protoc.*, vol. 2, no. 1, pp. 31–34, 2007.
- [152] D. C. Chen, B. C. Yang, and T. T. Kuo, “One-step transformation of yeast in stationary phase,” *Curr. Genet.*, vol. 21, no. 1, pp. 83–84, 1992.
- [153] M. Looke, “EXTRACTION OF GENOMIC DNA FROM YEASTS FOR PCR-BASED APPLICATIONS,” *Biotechniques*, vol. 50, no. 5, pp. 325–328, 2011.
- [154] T. Von Der Haar *et al.*, “The control of translational accuracy is a determinant of healthy

Bibliography

- ageing in yeast,” *Open Biol*, vol. 7, no. 16029, pp. 1–12, 2017.
- [155] M. Cabrera and C. Ungermann, *Purification and in vitro analysis of yeast vacuoles.*, 1st ed., vol. 451, no. 08. Elsevier Inc., 2009.
- [156] K. Tabke and H. Wiczorek, “Reversible disassembly of the yeast V-ATPase revisited under in vivo conditions,” *Biochem J*, vol. 197, pp. 185–197, 2014.
- [157] C. S. Rule, M. Patrick, and M. Sandkvist, “Measuring in vitro ATPase activity for enzymatic characterization,” *J. Vis. Exp.*, vol. 2016, no. 114, p. e54305, 2016.
- [158] P. Van Damme, W. Robberecht, and L. Van Den Bosch, “Modelling amyotrophic lateral sclerosis: Progress and possibilities,” *DMM Dis. Model. Mech.*, vol. 10, no. 5, pp. 537–549, 2017.
- [159] H. Mitsumoto, B. R. Brooks, and V. Silani, “Clinical trials in amyotrophic lateral sclerosis: Why so many negative trials and how can trials be improved?,” *Lancet Neurol.*, vol. 13, no. 11, pp. 1127–1138, 2014.
- [160] K. S. Graffmo *et al.*, “Expression of wild-type human superoxide dismutase-1 in mice causes amyotrophic lateral sclerosis,” *Hum. Mol. Genet.*, vol. 22, no. 1, pp. 51–60, Jan. 2013.
- [161] P. I. Joyce *et al.*, “A novel SOD1-ALS mutation separates central and peripheral effects of mutant SOD1 toxicity,” *Hum. Mol. Genet.*, vol. 24, no. 7, pp. 1883–1897, Apr. 2014.
- [162] R. A. Preston, “Assay of vacuolar pH in yeast and identification of acidification-defective mutants,” *Proc. Natl. Acad. Sci. U. S. A.*, vol. 86, no. September, pp. 7027–7031, 1989.
- [163] K. Powis, T. Zhang, N. Panchaud, R. Wang, C. De Virgilio, and J. Ding, “Crystal structure of the Ego1-Ego2-Ego3 complex and its role in promoting Rag GTPase-dependent TORC1 signaling,” *Cell Res.*, vol. 25, no. 9, pp. 1043–1059, Sep. 2015.
- [164] K. W. Cunningham and G. R. Fink, “Calcineurin-dependent growth control in *Saccharomyces cerevisiae* mutants lacking PMC1, a homolog of plasma membrane Ca²⁺ ATPases,” *J. Cell Biol.*, vol. 124, no. 3, pp. 351–363, 1994.
- [165] S. D. Khare, M. Caplow, and N. V Dokholyan, “FALS mutations in Cu, Zn superoxide dismutase destabilize the dimer and increase dimer dissociation propensity: A large-scale thermodynamic analysis,” *Amyloid*, vol. 13, no. December, pp. 226–235, 2006.
- [166] C. A. Smith, G. A. Tillinghast, and A. L. O. Neil, “Free energy calculations of ALS-causing SOD1 mutants reveal common perturbations to stability and dynamics along the maturation pathway,” *Protein Sci.*, vol. 1, no. January, pp. 1804–1817, 2021.
- [167] N. Bokna, P. M. Andersen, M. Oliveberg, M. J. Lindberg, and R. Bystro, “Systematically perturbed folding patterns of amyotrophic lateral sclerosis (ALS)-associated SOD1 mutants,” *PNAS*, no. Track II, 2005.
- [168] B. R. Bochner, “New technologies to assess genotype-phenotype relationships,” *Nat. Rev. Genet.*, vol. 4, no. 4, pp. 309–314, 2003.
- [169] O. R. Homann, H. Cai, J. M. Becker, and S. L. Lindquist, “Harnessing natural diversity to probe metabolic pathways,” *PLoS Genet.*, vol. 1, no. 6, pp. 0715–0729, 2005.
- [170] K. Kogan, E. D. Spear, C. A. Kaiser, and D. Fass, “Structural conservation of components in the amino acid sensing branch of the TOR pathway in yeast and mammals,” *J. Mol. Biol.*, vol. 402, no. 2, pp. 388–398, 2010.
- [171] L. Bar-Peled, L. D. Schweitzer, R. Zoncu, and D. M. Sabatini, “Ragulator is a GEF for the rag GTPases that signal amino acid levels to mTORC1,” *Cell*, vol. 150, no. 6, pp. 1196–1208, 2012.
- [172] T. Zhang, M. P. Péli-Gulli, H. Yang, C. De Virgilio, and J. Ding, “Ego3 functions as a homodimer to mediate the interaction between Gtr1-Gtr2 and Ego1 in the EGO complex to activate TORC1,” *Structure*, vol. 20, no. 12, pp. 2151–2160, 2012.
- [173] T. L. Orr-Weaver, J. W. Szostak, and R. J. Rothstein, “Yeast transformation: A model system for the study of recombination,” *Proc. Natl. Acad. Sci. U. S. A.*, vol. 78, no. 10 I, pp. 6354–6358, 1981.

Bibliography

- [174] A. Wach, A. Brachat, R. Pöhlmann, and P. Philippsen, “New heterologous modules for classical or PCR-based gene disruptions in *Saccharomyces cerevisiae*,” *Yeast*, vol. 10, no. 13, pp. 1793–1808, 1994.
- [175] S. Ghaemmaghami *et al.*, “Global analysis of protein expression in yeast,” *Nature*, vol. 425, no. 6959, pp. 737–741, 2003.
- [176] K. A. S, K. Curran, and H. Alper, “Characterization of plasmid burden and copy number in *Saccharomyces cerevisiae* for optimization of metabolic engineering applications,” *FEMS Yeast Res.*, vol. 13, no. 1, pp. 1–17, 2013.
- [177] U. Güldener *et al.*, “A new efficient gene disruption cassette for repeated use in budding yeast,” *Nucleic Acids Res.*, vol. 24, no. 13, pp. 2519–2524, 1996.
- [178] J. C. Miller *et al.*, “An improved zinc-finger nuclease architecture for highly specific genome editing,” *Nat. Biotechnol.*, vol. 25, no. 7, pp. 778–785, 2007.
- [179] M. Aouida, M. J. Piatek, D. K. Bangarusamy, and M. M. Mahfouz, “Activities and specificities of homodimeric TALENs in *Saccharomyces cerevisiae*,” *Curr. Genet.*, vol. 60, no. 2, pp. 61–74, 2014.
- [180] Y. Ishino, H. Shinagawa, K. Makino, M. Amemura, and A. Nakamura, “Nucleotide sequence of the *iap* gene, responsible for alkaline phosphatase isoenzyme conversion in *Escherichia coli*, and identification of the gene product,” *J. Bacteriol.*, vol. 169, no. 12, pp. 5429–5433, 1987.
- [181] R. Barrangou *et al.*, “CRISPR provides acquired resistance against viruses in prokaryotes,” *Science (80-.)*, vol. 315, no. 5819, pp. 1709–1712, 2007.
- [182] M. Jinek, K. Chylinski, I. Fonfara, M. Hauer, J. A. Doudna, and E. Charpentier, “A programmable dual-RNA-guided DNA endonuclease in adaptive bacterial immunity,” *Science (80-.)*, vol. 337, no. 6096, pp. 816–821, 2012.
- [183] Y. Ahn and Y. Jun, “Measurement of pain-like response to various NICU stimulants for high-risk infants,” *Early Hum. Dev.*, vol. 83, no. 4, pp. 255–262, 2007.
- [184] J. E. Dicarolo, J. E. Norville, P. Mali, X. Rios, J. Aach, and G. M. Church, “Genome engineering in *Saccharomyces cerevisiae* using CRISPR-Cas systems,” *Nucleic Acids Res.*, vol. 41, no. 7, pp. 4336–4343, 2013.
- [185] G. A. Martínez-Muñoz and P. Kane, “Vacuolar and plasma membrane proton pumps collaborate to achieve cytosolic pH homeostasis in yeast,” *J. Biol. Chem.*, vol. 283, no. 29, pp. 20309–20319, 2008.
- [186] S. C. Li and P. M. Kane, “The yeast lysosome-like vacuole: Endpoint and crossroads,” *Biochim. Biophys. Acta - Mol. Cell Res.*, vol. 1793, no. 4, pp. 650–663, 2009.
- [187] E. Zinser, C. D. M. Sperka-Gottlieb, E. V. Fasch, S. D. Kohlwein, F. Paltauf, and G. Daum, “Phospholipid synthesis and lipid composition of subcellular membranes in the unicellular eukaryote *Saccharomyces cerevisiae*,” *J. Bacteriol.*, vol. 173, no. 6, pp. 2026–2034, 1991.
- [188] M. Sambade, M. Alba, A. M. Smardon, R. W. West, and P. M. Kane, “A genomic screen for yeast vacuolar membrane ATPase mutants,” *Genetics*, vol. 170, no. 4, pp. 1539–1551, 2005.
- [189] E. Milgrom, H. Diab, F. Middleton, and P. M. Kane, “Loss of vacuolar proton-translocating ATPase activity in yeast results in chronic oxidative stress,” *J. Biol. Chem.*, vol. 282, no. 10, pp. 7125–7136, 2007.
- [190] H. Nelson and N. Nelson, “Disruption of genes encoding subunits of yeast vacuolar H⁺-ATPase causes conditional lethality,” vol. 87, no. May, pp. 3503–3507, 1990.
- [191] H. Imamura *et al.*, “Evidence for rotation of V1-ATPase,” *Proc. Natl. Acad. Sci. U. S. A.*, vol. 100, no. 5, pp. 2312–2315, 2003.
- [192] S. Kawasaki-nishi, T. Nishi, and M. Forgac, “Yeast V-ATPase Complexes Containing Different Isoforms of the 100-kDa α -subunit Differ in Coupling Efficiency and in Vivo Dissociation *,” *J. Biol. Chem.*, vol. 276, no. 21, pp. 17941–17948, 2001.

Bibliography

- [193] K. C. Miranda, F. E. Karet, and D. Brown, "An Extended Nomenclature for Mammalian V-ATPase Subunit Genes and Splice Variants," *PLoS One*, vol. 5, no. 3, pp. 1–5, 2010.
- [194] T. Toyomura, T. Oka, C. Yamaguchi, Y. Wada, and M. Futai, "Three Subunit a Isoforms of Mouse Vacuolar H⁺-ATPase," *J. Biol. Chem.*, vol. 275, no. 12, pp. 8760–8765, 2000.
- [195] N. Morel, J. Dedieu, and J. Philippe, "Specific sorting of the a1 isoform of the V-H⁺ ATPase a subunit to nerve terminals where it associates with both synaptic vesicles and the presynaptic plasma membrane," *J. Cell Sci.*, vol. 116, pp. 4751–4761, 2003.
- [196] A. Hurtado-lorenzo *et al.*, "V-ATPase interacts with ARNO and Arf6 in early endosomes and regulates the protein degradative pathway," *Nat. Cell Biol.*, vol. 8, no. 2, 2006.
- [197] T. Oka *et al.*, "a4, a Unique Kidney-specific Isoform of Mouse Vacuolar H⁺-ATPase Subunit a," *J. Biol. Chem.*, vol. 276, no. 43, pp. 40050–40054, 2001.
- [198] J. H. Seol, A. Shevchenko, A. Shevchenko, and R. J. Deshaies, "Skp1 forms multiple protein complexes, including RAVE, a regulator of V-ATPase assembly," *Nat. Cell Biol.*, vol. 3, no. April, pp. 384–391, 2001.
- [199] A. M. Smardon, M. Tarsio, and P. M. Kane, "The RAVE complex is essential for stable assembly of the yeast V-ATPase," *J. Biol. Chem.*, vol. 277, no. 16, pp. 13831–13839, 2002.
- [200] P. M. Kane, "Disassembly and reassembly of the yeast vacuolar H⁺-ATPase in vivo," *J. Biol. Chem.*, vol. 270, no. 28, pp. 17025–17032, 1995.
- [201] Y. Feng and M. Forgac, "Cysteine 254 of the 73-kDa a subunit is responsible for inhibition of the coated vesicle (H⁺)-ATPase upon modification by sulfhydryl reagents," *J. Biol. Chem.*, vol. 267, no. 9, pp. 5817–5822, 1992.
- [202] Y. Feng and M. Forgac, "A novel mechanism for regulation of vacuolar acidification," *J. Biol. Chem.*, vol. 267, no. 28, pp. 19769–19772, 1992.
- [203] Y. E. Oluwatosin and P. M. Kane, "Mutations in the CYS4 gene provide evidence for regulation of the yeast vacuolar H⁺-ATPase by oxidation and reduction in vivo," *J. Biol. Chem.*, vol. 272, no. 44, pp. 28149–28157, 1997.
- [204] L. B. Corson, J. Folmer, J. J. Strain, V. C. Culotta, and D. W. Cleveland, "Oxidative stress and iron are implicated in fragmenting vacuoles of *Saccharomyces cerevisiae* lacking Cu,Zn-superoxide dismutase," *J. Biol. Chem.*, vol. 274, no. 39, pp. 27590–27596, 1999.
- [205] R. J. Sanchez *et al.*, "Exogenous manganous ion at millimolar levels rescues all known dioxygen-sensitive phenotypes of yeast lacking CuZnSOD," *J. Biol. Inorg. Chem.*, vol. 10, no. 8, pp. 913–923, 2005.
- [206] M. Mülleder *et al.*, "Functional Metabolomics Describes the Yeast Biosynthetic Regulome," *Cell*, vol. 167, no. 2, pp. 553–565.e12, 2016.
- [207] S. Bond and M. Forgac, "The Ras/cAMP/protein kinase A pathway regulates glucose-dependent assembly of the vacuolar (H⁺)-ATPase in yeast," *J. Biol. Chem.*, vol. 283, no. 52, pp. 36513–36521, 2008.
- [208] P. Ma, S. Wera, P. Van Dijck, and J. M. Thevelein, "The PDE1-encoded low-affinity phosphodiesterase in the yeast *Saccharomyces cerevisiae* has a specific function in controlling agonist-induced cAMP signaling," *Mol. Biol. Cell*, vol. 10, no. 1, pp. 91–104, 1999.
- [209] N. Perzov, V. Padler-Karavani, H. Nelson, and N. Nelson, "Characterization of yeast V-ATPase mutants lacking Vph1p or Stv1p and the effect on endocytosis," *J. Exp. Biol.*, vol. 205, no. 9, pp. 1209–1219, 2002.
- [210] R. L. Cross and V. Müller, "The evolution of A-, F-, and V-type ATP synthases and ATPases: Reversals in function and changes in the H⁺/ATP coupling ratio," *FEBS Lett.*, vol. 576, no. 1–2, pp. 1–4, 2004.
- [211] L. Y. Chang, J. W. Slot, H. J. Geuze, and J. D. Crapo, "Molecular immunocytochemistry of the CuZn superoxide dismutase in rat hepatocytes," *J. Cell Biol.*, vol. 107, no. 6 I, pp. 2169–2179, 1988.
- [212] R. Zoncu, L. Bar-Peled, A. Efeyan, S. Wang, Y. Sancak, and D. M. Sabatini, "mTORC1

Bibliography

- senses lysosomal amino acids through an inside-out mechanism that requires the vacuolar H⁺-ATPase,” *Science* (80-.), vol. 334, no. 6056, pp. 678–683, 2011.
- [213] T. Wilms *et al.*, “The yeast protein kinase Sch9 adjusts V-ATPase assembly/disassembly to control pH homeostasis and longevity in response to glucose availability,” *PLoS Genet.*, vol. 13, no. 6, pp. 1–30, 2017.
- [214] A. Kumar, K. Nakamura, J. Parkinson, and M. Babu, “A Map of Human Mitochondrial Protein Interactions Linked to Neurodegeneration Reveals New Mechanisms Article A Map of Human Mitochondrial Protein Interactions Linked to Neurodegeneration Reveals New Mechanisms of Redox Homeostasis and NF- k B Sign,” *Cell Syst.*, vol. 5, no. 6, pp. 564-577.e12, 2017.
- [215] P. M. Kane, M. Tarsio, and J. Liu, “Early Steps in Assembly of the Yeast Vacuolar H⁺-ATPase,” *J. Biol. Chem.*, vol. 274, no. 24, pp. 17275–17283, 1999.
- [216] J. J. Tomashek, L. A. Graham, M. U. Hutchins, T. H. Stevens, and D. J. Klionsky, “V 1 -situated Stalk Subunits of the Yeast Vacuolar Proton-translocating ATPase *,” *J. Biol. Chem.*, vol. 272, no. 42, pp. 26787–26793, 1997.
- [217] A. M. Smardon, N. D. Nasab, M. Tarsio, T. T. Diakov, and P. M. Kane, “Molecular Interactions and Cellular Itinerary of the Yeast RAVE (Regulator of the H ⁺ -ATPase of Vacuolar and Endosomal Membranes) Complex *,” *J. Biol. Chem.*, vol. 290, no. 46, pp. 27511–27523, 2015.
- [218] B. C. B. Klee, G. F. Draetta, and M. J. Hubbard, “CALCINEURIN,” *Adv. Enzymol. relates areas Mol. Biol.*, vol. 61, pp. 149–200, 1988.
- [219] K. Dolinski, S. Muir, M. Cardenas, and J. Heitman, “All cyclophilins and FK506 binding proteins are, individually and collectively, dispensable for viability in *Saccharomyces cerevisiae*,” *Proc. Natl. Acad. Sci. U. S. A.*, vol. 94, no. 24, pp. 13093–13098, 1997.
- [220] M. S. Cyert, R. Kunisawa, D. Kaim, and J. Thorner, “Yeast has homologs (CNA1 and CNA2 gene products) of mammalian calcineurin, a calmodulin-regulated phosphoprotein phosphatase,” *Proc. Natl. Acad. Sci. U. S. A.*, vol. 88, no. 16, pp. 7376–7380, 1991.
- [221] T. Nakamura *et al.*, “Protein phosphatase type 2B (calcineurin)-mediated, FK506-sensitive regulation of intracellular ions in yeast is an important determinant for adaptation to high salt stress conditions,” *EMBO J.*, vol. 12, no. 11, pp. 4063–4071, 1993.
- [222] I. C. Farcasanu, D. Hirata, E. Tsuchiya, F. Nishiyama, and T. Miyakawa, “Protein Phosphatase 2B of *Saccharomyces Cerevisiae* is Required for Tolerance to Manganese, in Blocking the Entry of ions into the Cells,” *Eur. J. Biochem.*, vol. 232, no. 3, pp. 712–717, 1995.
- [223] H. Iida and Y. Anraku, “Essential Role for Induced Ca²⁺ + Influx Followed by [Ca²⁺]_i Rise in Maintaining Viability of Yeast Cells Late in the Mating Pheromone Response Pathway,” *J.*, vol. 265, no. 22, pp. 13391–13399, 1990.
- [224] A. M. Stathopoulos and M. S. Cyert, “Calcineurin acts through the CRZ1/TCN1-encoded transcription factor to regulate gene expression in yeast,” *Genes Dev.*, pp. 3432–3444, 1997.
- [225] M. Paidhungat and S. Garrett, “A homolog of mammalian, voltage-gated calcium channels mediates yeast pheromone-stimulated Ca²⁺ uptake and exacerbates the *cdc1*(Ts) growth defect,” *Mol. Cell. Biol.*, vol. 17, no. 11, pp. 6339–6347, 1997.
- [226] H. Iida, H. Nakamura, T. Ono, M. S. Okumura, and Y. Anraku, “MID1, a novel *Saccharomyces cerevisiae* gene encoding a plasma membrane protein, is required for Ca²⁺ influx and mating,” *Mol. Cell. Biol.*, vol. 14, no. 12, pp. 8259–8271, 1994.
- [227] C. P. Palmer, X. L. Zhou, J. Lin, S. H. Loukin, C. Kung, and Y. Saimi, “A TRP homolog in *Saccharomyces cerevisiae* forms an intracellular Ca²⁺-permeable channel in the yeast vacuolar membrane,” *Proc. Natl. Acad. Sci. U. S. A.*, vol. 98, no. 14, pp. 7801–7805, 2001.
- [228] M. E. Alexianu, B. -K Ho, A. H. Mohamed, V. La Bella, R. G. Smith, and S. H. Appel, “The role of calcium-binding proteins in selective motoneuron vulnerability in amyotrophic lateral sclerosis,” *Ann. Neurol.*, vol. 36, no. 6, pp. 846–858, 1994.

Bibliography

- [229] T. L. Williams, N. C. Day, P. G. Ince, R. K. Kamboj, and P. J. Shaw, "Calcium-permeable α -amino-3-hydroxy-5-methyl-4-isoxazole propionic acid receptors: A molecular determinant of selective vulnerability in amyotrophic lateral sclerosis," *Ann. Neurol.*, vol. 42, no. 2, pp. 200–207, 1997.
- [230] H. G. Wang *et al.*, "Ca²⁺-Induced Apoptosis Through Calcineurin Dephosphorylation of BAD," *Science (80-.)*, vol. 284, no. 5412, pp. 339–343, 1999.
- [231] S. Leal, I. Cardoso, J. S. Valentine, and M. Gomes, "Calcium Ions Promote Superoxide Dismutase 1 (SOD1) Aggregation into Non-fibrillar Amyloid," *J. Biol. Chem.*, vol. 288, no. 35, pp. 25219–25228, 2013.
- [232] A. Israelson *et al.*, "Misfolded mutant SOD1 directly inhibits VDAC1 conductance in a mouse model of inherited ALS," *Neuron*, vol. 67, no. 4, pp. 575–587, 2010.
- [233] S. F. Oliveria, P. J. Dittmer, D. Youn, M. L. D. Acqua, W. A. Sather, and V. A. C. V., "Localized Calcineurin Confers Ca²⁺-Dependent Inactivation on Neuronal L-Type Ca²⁺-Channels," *J. Neurosci.*, vol. 32, no. 44, pp. 15328–15337, 2012.
- [234] J. J. Krupp, B. Vissel, C. G. Thomas, S. F. Heinemann, and G. L. Westbrook, "Calcineurin acts via the C-terminus of NR2A to modulate desensitization of NMDA receptors," *Neuropharmacology*, vol. 42, no. 2002, pp. 593–602, 2002.
- [235] H. Lee, K. Kameyama, R. L. Huganir, M. F. Bear, and H. Hughes, "NMDA Induces Long-Term Synaptic Depression and Dephosphorylation of the GluR1 Subunit of AMPA Receptors in Hippocampus," *Neuron*, vol. 21, no. November, pp. 1151–1162, 1998.
- [236] M. J. Kipanyula, W. H. Kimaro, and P. F. S. Etet, "The Emerging Roles of the Calcineurin-Nuclear Factor of Activated T-Lymphocytes Pathway in Nervous System Functions and Diseases," *J. Aging Res.*, vol. 2016, pp. 1–20, 2016.
- [237] A. Ferri *et al.*, "Activity of protein phosphatase calcineurin is decreased in sporadic and familial amyotrophic lateral sclerosis patients," *J. Neurochem.*, vol. 90, no. 5, pp. 1237–1242, 2004.
- [238] X. Wang, V. C. Culotta, and C. B. Klee, "Superoxide dismutase protects calcineurin from inactivation," *Nature*, vol. 383, no. 6599, pp. 434–437, 1996.
- [239] S. D. Boyd *et al.*, "The yeast copper chaperone for copper-zinc superoxide dismutase (CCS1) is a multifunctional chaperone promoting all levels of SOD1 maturation," *J. Biol. Chem.*, vol. 294, no. 6, pp. 1956–1966, 2019.
- [240] A. B. Parsons *et al.*, "Integration of chemical-genetic and genetic interaction data links bioactive compounds to cellular target pathways," *Nat. Biotechnol.*, vol. 22, no. 1, pp. 62–69, 2004.
- [241] Y. Feng and N. G. Davis, "Akr1p and the Type I Casein Kinases Act prior to the Ubiquitination Step of Yeast Endocytosis: Akr1p Is Required for Kinase Localization to the Plasma Membrane," *Mol. Cell. Biol.*, vol. 20, no. 14, pp. 5350–5359, 2000.
- [242] S. S. Leal and C. M. Gomes, "Calcium dysregulation links ALS defective proteins and motor neuron selective vulnerability," *Front. Cell. Neurosci.*, vol. 9, no. June, pp. 1–6, 2015.
- [243] G. D. Ghadge *et al.*, "Truncated wild-type SOD1 and FALS-linked mutant SOD1 cause neural cell death in the chick embryo spinal cord," *Neurobiol. Dis.*, vol. 21, no. 1, pp. 194–205, 2006.
- [244] I. Tanida, A. Hasegawa, H. Iida, Y. Ohya, and Y. Anraku, "Cooperation of calcineurin and vacuolar H⁺-ATPase in intracellular Ca²⁺ homeostasis of yeast cells," *J. Biol. Chem.*, vol. 270, no. 17, pp. 10113–10119, 1995.
- [245] A. Agbas, D. Hui, X. Wang, V. Tek, A. Zaidi, and E. K. Michaelis, "Activation of brain calcineurin (Cn) by Cu-Zn superoxide dismutase (SOD1) depends on direct SOD1-Cn protein interactions occurring in vitro and in vivo," *Biochem. J.*, vol. 405, no. 1, pp. 51–59, 2007.
- [246] H. Volkel *et al.*, "Superoxide dismutase mutations of familial amyotrophic lateral sclerosis and the oxidative inactivation of calcineurin," *FEBS Lett.*, vol. 503, no. 2–3, pp. 201–205,

Bibliography

- 2001.
- [247] J. Wang *et al.*, “Fibrillar inclusions and motor neuron degeneration in transgenic mice expressing superoxide dismutase 1 with a disrupted copper-binding site,” *Neurobiol. Dis.*, vol. 10, no. 2, pp. 128–138, 2002.
- [248] I. Jahan and S. M. Nayeem, “Conformational dynamics of superoxide dismutase (SOD1) in osmolytes: A molecular dynamics simulation study,” *RSC Adv.*, vol. 10, no. 46, pp. 27598–27614, 2020.
- [249] J. M. Kim *et al.*, “Impaired Cu–Zn Superoxide Dismutase (SOD1) and Calcineurin (Cn) Interaction in ALS: A Presumed Consequence for TDP-43 and Zinc Aggregation in Tg SOD1 G93A Rodent Spinal Cord Tissue,” *Neurochem. Res.*, vol. 44, no. 1, pp. 228–233, 2019.
- [250] B. Stanger, E. Kim, and B. Seedt, “RIP : A Novel Protein Containing a Death Domain That Interacts with FadAPO-1 (CD95) in Yeast and Causes Cell Death,” *Cell*, vol. 81, no. May, pp. 513–523, 1995.
- [251] I. Faizan and T. Ahmad, “Mitochondrion Altered mitochondrial calcium handling and cell death by necroptosis : An emerging paradigm,” *Mitochondrion*, vol. 57, no. December 2020, pp. 47–62, 2021.
- [252] F. Bassermann and R. Eichner, “The ubiquitin proteasome system – Implications for cell cycle control and the targeted treatment of cancer,” *Biochim Biophys Acta*, vol. 1843, no. 1, pp. 1–29, 2014.
- [253] H. Wang, Z. Ying, and G. Wang, “Ataxin-3 regulates aggresome formation of copper-zinc superoxide dismutase (SOD1) by editing K63-linked polyubiquitin chains,” *J. Biol. Chem.*, vol. 287, no. 34, pp. 28576–28585, 2012.
- [254] O. Soetens, J. De Craene, and B. Andre, “Ubiquitin Is Required for Sorting to the Vacuole of the Yeast General Amino Acid Permease , Gap1 *,” *J. Biol. Chem.*, vol. 276, no. 47, pp. 43949–43957, 2001.
- [255] L. Wang, H. Deng, G. Grisotti, H. Zhai, T. Siddique, and R. P. Roos, “Wild-type SOD1 overexpression accelerates disease onset of a G85R SOD1 mouse,” *Hum. Mol. Genet.*, vol. 18, no. 9, pp. 1642–1651, 2009.
- [256] D. Jaarsma *et al.*, “Human Cu/Zn superoxide dismutase (SOD1) overexpression in mice causes mitochondrial vacuolization, axonal degeneration, and premature motoneuron death and accelerates motoneuron disease in mice expressing a familial amyotrophic lateral sclerosis mutant SO,” *Neurobiol. Dis.*, vol. 7, no. 6, pp. 623–643, 2000.
- [257] A. De Araújo, M. Dias, C. De Carvalho, E. Gerhardt, and D. Dias, “Characterization of the activity , aggregation , and toxicity of heterodimers of WT and ALS-associated mutant Sod1,” *PNAS*, vol. 116, no. 51, pp. 25991–26000, 2019.
- [258] N. Pujol-Carrion, M. I. Petkova, L. Serrano, and M. A. de la Torre-Ruiz, “The MAP kinase Slt2 is involved in vacuolar function and actin remodeling in *Saccharomyces cerevisiae* mutants affected by endogenous oxidative stress,” *Appl. Environ. Microbiol.*, vol. 79, no. 20, pp. 6459–6471, 2013.
- [259] T. Seidel *et al.*, “Regulation of the V-type ATPase by redox modulation,” *Biochem. J.*, vol. 448, no. 2, pp. 243–251, Dec. 2012.
- [260] V. Jonckheere *et al.*, “Redox Proteomics of Protein-bound Methionine Oxidation * □,” *Mol. Cell. Proteomics* 10.5, vol. 10, pp. 1–12, 2011.
- [261] E. J. Walker, J. Q. Bettinger, K. A. Welle, J. R. Hryhorenko, and S. Ghaemmaghami, “Global analysis of methionine oxidation provides a census of folding stabilities for the human proteome,” *PNAS*, vol. 116, no. 13, pp. 6081–6090, 2019.
- [262] V. C. Culotta and J. A. Baron, “Cu/Zn Superoxide Dismutase and the Proton ATPase Pma1p of *Saccharomyces cerevisiae*,” *Biochem. Biophys. Res. Commun.*, vol. 462, no. 3, pp. 251–256, 2015.
- [263] K. Manabe, M. Kawano-Kawada, K. Ikeda, T. Sekito, and Y. Kakinuma, “Ypq3p-

Bibliography

- dependent histidine uptake by the vacuolar membrane vesicles of *Saccharomyces cerevisiae*,” *Biosci. Biotechnol. Biochem.*, vol. 80, no. 6, pp. 1125–1130, 2016.
- [264] E. Llinares, A. O. Barry, and B. André, “The AP-3 adaptor complex mediates sorting of yeast and mammalian PQ-loop-family basic amino acid transporters to the vacuolar/lysosomal membrane,” *Sci. Rep.*, vol. 5, no. October, pp. 1–15, 2015.
- [265] A. Jézégou, E. Llinares, C. Anne, S. Kieffer-jaquinod, S. O. Regan, and J. Aupetit, “Heptahelical protein PQLC2 is a lysosomal cationic amino acid exporter underlying the action of cysteamine in cystinosis therapy,” *PNAS*, vol. 109, no. 50, pp. E3434–E3443, 2012.
- [266] M. I. Shimoto, N. S. Ugimoto, T. S. Ekito, M. K. A. Awada, and Y. K. Akinuma, “ATP-Dependent Export of Neutral Amino Acids by Vacuolar Membrane Vesicles of *Saccharomyces cerevisiae*,” *Biosci Biotechnol Biochem*, vol. 76, no. 9, pp. 1802–1804, 2012.
- [267] M. Rubio-texeira and C. A. Kaiser, “Amino Acids Regulate Retrieval of the Yeast General Amino Acid Permease from the Vacuolar Targeting Pathway,” *Mol. Biol. Cell*, vol. 17, no. July, pp. 3031–3050, 2006.
- [268] M. Rebsamen *et al.*, “SLC38A9 is a component of the lysosomal amino acid-sensing machinery that controls mTORC1,” *Nature*, vol. 519, no. 7544, pp. 477–481, 2015.
- [269] T. Kobayashi *et al.*, “The Histidine Transporter SLC15A4 Coordinates mTOR-Dependent Inflammatory Responses and Pathogenic Antibody Production,” *Immunity*, vol. 41, no. 3, pp. 375–388, 2014.
- [270] M. Kawano-Kawada *et al.*, “A PQ-loop protein Ypq2 is involved in the exchange of arginine and histidine across the vacuolar membrane of *Saccharomyces cerevisiae*,” *Sci. Rep.*, vol. 9, no. 1, pp. 3–5, 2019.
- [271] D. Namgaladze, H. W. Hofer, and V. Ullrich, “Redox control of calcineurin by targeting the binuclear Fe²⁺-Zn²⁺ center at the enzyme active site,” *J. Biol. Chem.*, vol. 277, no. 8, pp. 5962–5969, 2002.
- [272] N. J. Carruthers and P. M. Stemmer, “Methionine Oxidation in the Calmodulin-Binding Domain of Calcineurin Disrupts Calmodulin Binding and Calcineurin Activation,” *Biochemistry*, vol. 47, pp. 3085–3095, 2008.
- [273] J. Gao *et al.*, “Loss of Conformational Stability in Calmodulin upon Methionine Oxidation,” *Biophys. J.*, vol. 74, no. March, pp. 1115–1134, 1998.
- [274] T. Dunns, K. Gable, and T. Beeler, “Regulation of Cellular Ca²⁺ by Yeast Vacuoles,” *J. Biol. Chem.*, vol. 269, no. 10, pp. 7273–7278, 1994.
- [275] K. W. Cunningham and G. R. Fink, “Calcineurin Inhibits VCX1-Dependent H⁺ / Ca²⁺ Exchange and Induces Ca²⁺ ATPases in *Saccharomyces cerevisiae*,” *Mol. Cell. Biol.*, vol. 16, no. 5, pp. 2226–2237, 1996.
- [276] G. C. Baltazar *et al.*, “Acidic Nanoparticles Are Trafficked to Lysosomes and Restore an Acidic Lysosomal pH and Degradative Function to Compromised ARPE-19 Cells,” *PLoS One*, vol. 7, no. 12, pp. 1–10, 2012.